



NEUTRONS
FOR SOCIETY

INSTITUT LAUE-LANGEVIN

THE EUROPEAN NEUTRON SOURCE



Annual Report 20**20**



Contents

Publishing information

Editors:

Giovanna Cicognani and Mark Johnson

Production team:

Giovanna Cicognani, Virginie Guerard

Scientific advisors:

Markus Appel, Laura Cañadillas-Delgado,
Kim Yung Hee, Lukas Helfen,
Ursula Bengaard Hansen, Armando Maestro,
Olga Matsarskaia, Sylvain Prevost,
Jacques Ollivier, Thomas Saerbeck,
Alberto Rodriguez Velamazán

Design:

Morton Ward Limited

Photography:

Serge Claisse – ILL (unless otherwise specified,
and C. Tresca for ILL's Directors' portraits)

Further copies can be obtained from:

Institut Laue-Langevin
Communication Unit
CS 20156, F-38042 Grenoble Cedex 9
communication@ill.eu
www.ill.eu

FOREWORD	4
WHAT IS THE ILL	
About the ILL	7
Why neutron scattering is useful	7
THE ILL IN THE PRESS	8
SCIENTIFIC HIGHLIGHTS	10
College introductions	12
Magnetism	14
Materials science	26
Soft condensed matter	40
Biology and health	48
Spectroscopy	56
Nuclear and particle physics	60
Theory	66
MODERNISATION PROGRAMME AND TECHNICAL DEVELOPMENTS	70
Modernisation programme and instrument upgrades	72
Technical and methods developments	80
INDUSTRIAL ACTIVITIES	88
EXPERIMENTAL AND USER PROGRAMME	
User programme	93
User and beamtime statistics	94
Instrument list	98
REACTOR OPERATION	100
MORE THAN SIMPLY NEUTRONS	104
Scientific support laboratories	106
Training and outreach	109
European programmes	110
WORKSHOPS AND EVENTS	114
Chronicle	115
Scientific events	116
FACTS AND FIGURES	118
Facts and figures	119
Publications	121
Organisation chart	122

FIND US ON:   



2020 was a year dominated by COVID, a pandemic that has affected the whole world, bringing to the fore questions about how we work together, enjoy time off work and ensure the health of a diverse population.

After the initial COVID impact, which meant a lockdown of two months in spring in Europe, attention was focused on getting back to work while adapting to new health guidelines. At the ILL this meant progressing with the Endurance upgrade programme, a particularly relevant project being the installation and commissioning of a second protein crystallography station on which COVID-related experiments will be performed in 2021. It also meant running a second cycle in 2020 with a much reduced (35 %) user presence and therefore enhanced remote access to the instruments, which constitutes a major step forward in the digital transformation of the way we work.

The unique ILL reactor also passed two major milestones during this challenging period. One was the 10-year safety evaluation, which is a rolling process of preparation, evaluation and work to be done—the next application to the Nuclear Safety Authority will be in 2027. In addition, the reactor vessel itself was requalified for use until 2031.

The ILL has shown that it can both adapt to the present and prepare for a future in which the need for neutrons to address societal challenges like health and clean energy is clearer than ever. This was highlighted once again during the second ILL-ESS user meeting, which took place virtually in September and attracted almost 800 participants to its plenary sessions.

Major funding is of course required to operate the ILL and significant progress was made by the Associates of the ILL (France, Germany and the UK) on the next operating period under the 6th protocol. The Scientific Members, which now include Slovenia, make a critical contribution to the ILL and we look forward to working closely with them in the future.

To end, I would like to sincerely thank ILL staff for their commitment and efforts in confronting the COVID challenge in 2020 so that we can look forward, in 2021, to an exciting scientific programme and to emerging from COVID into a new normal of work, leisure and, above all, good health.

Grahame Blair
ILL Steering Committee Chair



2020 will certainly be remembered, if only for reminding us of our vulnerability to disaster despite the prodigious progress our societies have made. At the same time, however, it has confirmed what we know: our best defence against disaster is scientific knowledge transformed into technological know-how. The techniques we have developed over decades of progress have helped us understand the mechanisms of life at microscopic level; they have helped us identify the virus, track down its whereabouts and block its progress with sophisticated vaccines. If today we are ready for the challenge, it is thanks to the investments made in the past in our science and scientific infrastructure. And it is our current investments that will ensure resilience in the future.

The ILL is proud to be part of today's scientific network of excellence. We strive constantly to ensure that our research remains world-class, on our many different fronts. For we are well aware that the next crisis could be completely different, and that it is often the quest for the fundamentally unknown that pushes us to the highest levels of inventiveness.

I hope that you will enjoy as much as I do the examples of outstanding scientific achievements in this year's report.

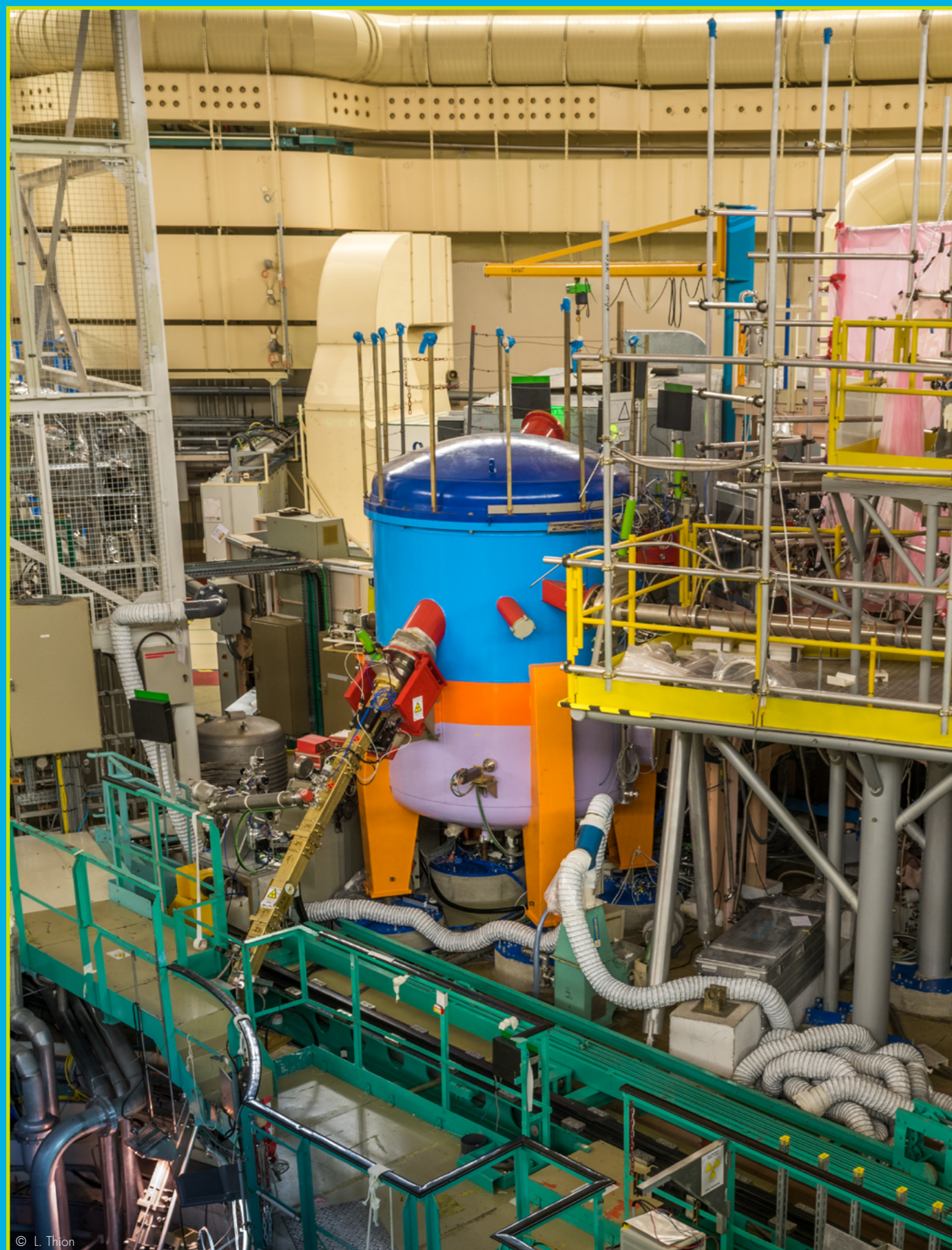
The excellence of our science depends crucially on the quality of our tools. For this reason, the ILL has spared no effort to ensure that both its neutron source and the instruments used for scientific investigation remain at the cutting edge of performance. The year 2020 was no exception, despite its many difficulties. Not only did we perform two successful reactor cycles but we did so despite severe travel restrictions on our users; this clearly highlights the importance of the investments we have made in the remote control of experiments. In parallel with the reactor operations, we successfully installed new instruments and upgraded others. And, last but not least, we were able to successfully demonstrate, via the compulsory 10-year safety evaluation, that our neutron source is compliant with today's extremely strict standards. The excellent health of our installations was further confirmed by the successful decennial examination of our reactor vessel.

This impressive list of achievements is the fruit of the competence and commitment of the ILL's staff, combined with the excellence of the ILL's scientific community. Our Associates and Scientific Members honour this performance by securing the resources required to ensure future operations and development. In this context, the imminent conclusion of negotiations on the 6th intergovernmental protocol is extremely good news for the whole scientific community. This international agreement will lay the legal foundations for a further decade of exciting science to be generated by the ILL's outstanding infrastructure.

Given all these achievements, you will certainly share my conviction that 2020 has been another highly successful year for the ILL. This should not, of course, blind us to the fact that we are all suffering to various degrees from the pandemic. It is my hope that this suffering will not be in vain, and that the lessons learned from fighting it will re-orient our path towards the most important targets for research; and investment in the future of our children—and in a healthy planet for them all—is certainly one of those targets. The ILL will be on that path.

Helmut Schober
ILL Director





© L. Thion

About the ILL

The Institut Laue Langevin (ILL) is an international research centre providing world-leading facilities in neutron science and technology. Neutrons are used at the ILL to probe the microscopic structure and dynamics of a broad range of materials at molecular, atomic and nuclear level.

The ILL operates the most intense neutron source in the world, a 58.3 MW nuclear reactor designed for high brightness. The reactor normally functions round-the-clock for four 50-day cycles per year, supplying neutrons to a suite of 40 high-performance instruments constantly maintained at the highest state of the art.

The ILL is owned by the three founding countries — France, Germany and the United Kingdom. These three Associate countries contributed some 68 M€ to the Institute in 2020, a sum enhanced by significant contributions from the ILL's Scientific Member countries — Austria, Belgium, the Czech Republic, Denmark, Italy, Poland, Slovakia, Spain, Sweden, Switzerland and recently Slovenia. The ILL's overall budget in 2020 amounted to around 102 M€.

As a service institute, the ILL makes its facilities and expertise available to visiting scientists. It has a global user community of around 2 000 researchers from almost 40 countries who come to work at the ILL every year. The 850 experiments they perform annually are pre-selected by a scientific review committee. Between 550 and 600 scientific papers are published annually, following the treatment and interpretation of data obtained from the use of our facilities. Of these articles, 163 were published in high-impact journals in 2020.

NEUTRONS AND SOCIETY

The scope of the research carried out at the ILL is very broad, embracing condensed matter physics, chemistry, biology, materials and earth sciences, engineering, and nuclear and particle physics. Much of it impacts on many of the challenges facing society today, from sustainable sources of energy, better healthcare and a cleaner environment, to new materials for information and computer technology.

PREPARING FOR THE FUTURE

To maintain its status as leader in neutron science, the Institute has constantly upgraded its instruments, infrastructure and scientific equipment over the last 50 years. The latest modernisation exercise — the Endurance programme — will continue to develop instrumentation and support services with a view to maintaining the Institute's world-leading position for another decade at least. Endurance phase I (2016–2019) has now been completed, with the second, current, phase anticipated to run between 2020 and 2023.

Why neutron scattering is useful

When used to probe small samples of materials, neutron beams have the power to reveal what is invisible using other forms of radiation. Neutrons can appear to behave as particles, waves or microscopic magnetic dipoles; with these very specific properties they can provide information that is often impossible to obtain using other techniques. Below are a few of the special characteristics of neutrons.

WAVELENGTHS OF TENTHS OF NANOMETRES

Neutrons have wavelengths varying from 0.01 to 100 nanometres. This makes them an ideal probe of atomic and molecular structures, whether composed of single-atom species or complex biopolymers.

ENERGIES OF MILLI-ELECTRONVOLTS

The milli-electronvolt energies associated with neutrons are of the same magnitude as the diffusive motions of atoms and molecules in solids and liquids, the coherent waves in single crystals (phonons and magnons) and the vibrational modes in molecules. Any energy exchange, therefore, of between 1 μ eV (or even 1 neV with neutron spin-echo techniques) and 1 eV between the incoming neutron and the sample is easy to detect.

MICROSCOPICALLY MAGNETIC

Neutrons possess a magnetic dipole moment that makes them sensitive to the magnetic fields generated by unpaired electrons in materials. They therefore play an important role in investigations of the magnetic behaviour of materials at the atomic level. In addition, as the neutron scattering effect of the atomic nuclei in a sample depends on the orientation of the spin of both the neutron and the atomic nuclei, neutron scattering techniques are ideal for detecting nuclear spin order.

ELECTRICALLY NEUTRAL

As neutrons are electrically neutral they can penetrate far into matter without doing damage. They are therefore precious allies in research into biological samples or engineering components under extreme conditions of pressure, temperature or magnetic field, or within chemical-reaction vessels.

HIGH SENSITIVITY AND SELECTIVITY

The scattering from nucleus to nucleus in a sample varies in a quasi-random manner, even for different isotopes of the same atom. This means that light atoms remain visible in the presence of heavy atoms, and atoms close to each other in the periodic table can be clearly distinguished. This makes it possible to use isotopic substitution in order to vary the contrast in certain samples and thus highlight specific structural features.

Neutrons are also particularly sensitive to hydrogen atoms and are therefore essential for research into hydrogen-storage materials, organic molecular materials and biomolecular samples or polymers.

1. Published in *PhysicsWorld* on 30 September 2020
2. Published in *ResearchProfessional News* on 18 August 2020
3. Published in *Pro-Physik* on 28 July 2020
4. Published in *CERN COURIER* on 7 July 2020

More articles at <https://www.ill.eu/news-press-events/press-corner/ill-in-the-media/>

1. **physicsworld**

PROJECTS AND FACILITIES | INTERVIEW

Continuous upgrades keep Institut Laue-Langevin at the heart of Europe's neutron community

30 Sep 2020 *Hannah Johnston*

Taken from the 2020 Physics World Big Science Briefing. You can enjoy the full issue via the [Physics World app](#) from 1 October.

Helmut Schober is director of the Institut Laue-Langevin (ILL) neutron research facility in Grenoble, France. As a physicist, his research has focused on fullerenes; the dynamics of liquids and glasses; and neutron instrumentation. He spoke to *Physics World* about how ILL strives to provide the best possible research environment for its user community.



Blue glow Cherenkov radiation in the reactor pool at ILL. (Courtesy: B Lehn)

ILL has been upgraded continuously since 2000. What enhancements have been made and how are they currently being exploited by researchers?

Our Millennium upgrade programme ran from 2000 to 2016 and had a budget €100m. To put this into context, we were spending close to 10% of our overall budget every year on

2. **ResearchProfessional News**

K Europe USA Australia & NZ Africa World Opinion Funding Insight Co

2020 18 AUG 2020

Slovenia gains member access to European neutron source

By Ben Upson



Membership of the Institut Laue-Langevin will open up access to Slovenian academia and companies. Researchers in Slovenia have gained access to the world's most powerful neutron source—used to probe the structure of matter—at the Institut Laue-Langevin in Grenoble, France, after the country became the eleventh member country of the facility.

Slovenia's National Institute of Chemistry will act as the official partner until 2023, coordinating the

3. **pro-physik.de**

Forschung

Variable Struktur magnetischer Nanoteilchen

28.07.2020 - In einem externen Magnetfeld vergrößert sich das Kernvolumen deutlich.

Wenden ultrakleine magnetische Partikel einem ausser einwirkenden Magnetfeld ausgesetzt, wächst ihr magnetischer Kern in bisher unerwarteter Weise. Das hat eine Forschergruppe an der Universität Köln, des Forschungszentrums Jülich und des Instituts Laue-Langevin in Grenoble, Frankreich, durch Untersuchungen mit Neutronenstreuung gezeigt. Die Studie ermöglicht ein genaueres Verständnis von Struktur und Verhalten der magnetischen Nanoteilchen in einem Magnetfeld, was für zahlreiche Anwendungen von Bedeutung ist.

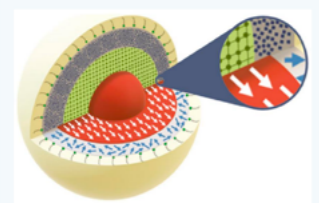


Abb. Die innere Struktur eines magnetischen Nanoteilchens verändert sich unter Einfluss eines äußeren Magnetfelds. (Bild: © Zakaria et al., APS / 10.1103/PhysRevX.10.031019)

So können magnetische Nanoteilchen zum Beispiel gezielt an bestimmte Stellen des menschlichen Körpers gesteuert und dort für eine Wärmetherapie bei der Krebsbehandlung eingesetzt werden. Magnetische Nanoteilchen werden zudem in chemischen Prozessen als Katalysator eingesetzt und spielen eine Rolle für die Entwicklung neuer Batterietechnologien. Magnetische Nanoteilchen beispielsweise aus Eisen, Nickel oder Kobalt verhalten sich wie kleine Magnete. Man findet sie natürlich gewachsen in Gesteinen, aber auch in einigen Lebewesen, wie Bakterien, wo die Mini-Magnete bei der Orientierung der Bewegung eine Rolle spielen. Von technologischer Bedeutung sind sie für magnetische Flüssigkeiten,

4. **CERN COURIER** Reporting on international high-energy physics

Physics • Technology • Community • In focus • Magazine

APPLICATIONS | FEATURES

Neutron sources join the fight against COVID-19

7 Jul 2020

Advanced neutron facilities such as the Institut Laue-Langevin are gearing up to enable a deeper understanding of the structural workings of SARS-CoV-2.



An eye for structure The LADI instrument at the ILL, a quasi-Laser neutron diffractometer used for single-crystal studies of biological macromolecules at high resolution. Neutron Laser diffraction patterns are recorded on a cylindrical detector, allowing the determination of protein structures including the locations of hydrogen/deuterium atoms. Credits: B Cubitt

The global scientific community has mobilised at an unprecedented rate in response to the COVID-19 pandemic, beyond just pharmaceutical and medical researchers. The world's most powerful analytical tools, including neutron sources, harbour the unique ability to reveal the invisible, structural workings of the virus – which will be essential to developing effective treatments. Since the outbreak of the pandemic, researchers worldwide have been using large-scale research infrastructures such as synchrotron


5. **nature**

NEWS FEATURE 05 JUNE 2020

The pandemic mixed up what scientists mixed up – and some won't go back

Thousands of researchers have jumped into studying coronavirus and many want to continue: part 8 in a series on science after the pandemic.

Illustration: Sherry



Rose Valenti typically spends her days using quantum physics to understand exotic states of matter. But last month she turned her modelling skills to a very different problem – simulating the evolution of the coronavirus pandemic. "Our normal day's things had

7. **laboratory news** Field Sector Digi

Home > Physics > Bridging the neutron gap


Bridging the neutron gap

3 Mar 2020

So much more than the quiet neighbour of the sub-atomic world, neutrons hold the key to so many breakthroughs – from the origin of the universe to novel medicines. Which is why it is such a worry that three neutron science reactors in Europe have stopped operating in the last year. We spoke to Helmut Schober about the 'neutron gap'...

So, the 'neutron gap' – that sounds very dramatic. How has this come about?

In 2019, three of Europe's neutron facilities closed: BER-II in Berlin, Orphée in Paris and JEEP II outside Oslo. The former two especially supported large communities of scientists that have made important contributions to the methods of neutron science. Europe has always held a leading position in the global 'big science' community, however if we want this advantage in neutron science to be maintained and developed further, then the impact of these closures



6. **CERN COURIER** Reporting on international high-energy physics

POLICY | OPINION

Bridging Europe's neutron gap

24 April 2020

The recent closure of reactors means making the most of existing facilities while preparing accelerator-based sources, says Helmut Schober.



Reactor neutrons The Institut Laue-Langevin in Grenoble. Credit: ILL

8. **The Telegraph** Coronavirus News Politics Sport Business Money Opinion Tech Life


UK News • World news • Blogs • Health • Defence • Science • Education • Environment • Investigations • Gossip

Museums warned cleaning products are irreversibly damaging great masterpieces

Restoration watchdog describes scientists' findings as 'truly shocking' and 'politically explosive'

By Delya Alberger

14 March 2020 - 8:00pm



9. **Materials World**

HOME FEATURES BLOG BACK ISSUES MEDIA INFORMATION ABOUT

COVID-19 News / Seeing how batteries degrade

SEEING HOW BATTERIES DEGRADE

Carl James

Materials World magazine, 4 Mar 2020

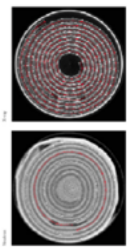
Combining imaging techniques has helped researchers see exactly how working battery cells for the first time, reveals carbon footprint manufacturing. Carl James reports.

Existing imaging techniques have been combined to provide a picture of what happens inside a lithium battery while it is working. Normally, batteries are cut open after being discharged and examined to understand how they function and degrade. But this new technique allows them to be observed while operating to better understand the processes involved.

The technology tools and instruments were used to determine the structure of a lithium-ion battery cell. The team, led by Professor Carl James at the Australian Synchrotron, explained that while X-ray images are used to determine the structure of a battery, neutron imaging reveals what is going on inside the battery and its components. He said that using these highly complementary imaging tools to see how the battery works is a real breakthrough in the history of battery research, which could improve their design and, therefore, safety.

IMAGES

The neutron information regards the lithium, specifically, the movement of the anions within the battery, while the X-rays are predominantly about variations in density, and structural changes in some cases.



5. Published in *nature* on 5 June 2020
6. Published in *CERN COURIER* on 24 April 2020
7. Published in *laboratory news* on 3 March 2020
8. Published in *The Telegraph* on 14 March 2020
9. Published in *Materials World* on 4 March 2020

SCIENTIFIC HIGHLIGHTS

The scientific highlights presented in this annual report demonstrate how research with neutrons continues to push back the frontiers of science.

- 12 COLLEGE INTRODUCTIONS
- 14 MAGNETISM
- 26 MATERIALS SCIENCE
- 40 SOFT CONDENSED MATTER
- 48 BIOLOGY AND HEALTH
- 56 SPECTROSCOPY
- 60 NUCLEAR AND PARTICLE PHYSICS
- 66 THEORY



KEEP **UP-TO-DATE:**

-  facebook.com/ILLGrenoble
-  twitter.com/ILLGrenoble
-  linkedin.com/company/institut-laue-langevin

FIND US ON:   



549
ILL PUBLICATIONS
RECORDED IN 2019
OF WHICH **163** PUBLISHED
IN HIGH-IMPACT JOURNALS

 **17**
PRESS
RELEASES

WERE PRODUCED IN 2020
LEADING TO
36 ARTICLES
IN THE GENERAL PRESS

COVID dominated

2020 in a multitude of ways. Depending on the type of people we are, such disruptive situations are seen as crises, problems, challenges or even opportunities. While the suffering health-wise and economically of significant parts of the population is a crisis, COVID is proving to be an opportunity to demonstrate the role of scientific research in a knowledge-based society and to pursue the digital transformation of our society.

After the initial lockdown, the first 20 or so scientists and technicians from the Life Sciences, Large-Scale Structures and Spectroscopy groups in the Science Division that came back to work were part of a taskforce pursuing, along with our collaborators, COVID-related research using neutrons. This initiative took full advantage of expertise developed over many years in sample preparation (e.g. macromolecular deuteration) and neutron scattering experiments (e.g. reflectometry, SANS and quasi-elastic scattering). In addition, on the EPN campus the Partnerships for Structural Biology (PSB) and Soft Condensed Matter (PSCM) have played a major role in the campus-wide response. About 10 experiments were performed during the cycle in August–September using Director's Discretionary Time (DDT), and a dozen or so proposals for further work were received in the autumn proposal round.

In the coming months, neutron protein crystallography will be used on COVID protein crystals, with experiments being performed on LADI and on DALI, a second measuring station that will ultimately increase our capacity in this technique by a factor of ~5. DALI was one of the Endurance projects that we were determined to finish in 2020 despite COVID.

COVID is changing the way we live and work, often requiring digital solutions. About one-third of our users were able to come for experiments in the second cycle of 2020. Nevertheless, building on developments that were already underway at the ILL—and accelerated by work in the Photon and Neutron Open Science Cloud (<https://www.panosc.eu/>)—we were able to offer remote access for instrument control and data treatment to the majority of our users. We depend on users for a great deal of the work that is carried out during experiments, but some gains in efficiency were possible from, e.g. reduced travelling, receiving samples in advance and being able to mix experiments and thereby minimise configuration changes. As the vaccination programme is rolled out across the world and restoring some semblance of normality can be hoped for during 2021, we must fully integrate the flexible operations that were essential in 2020—including remote access, DDT and EASY access—into future operations, while preserving the close scientific collaboration that we have with ILL users.

COVID is a major, societal challenge and the scientific response at the ILL has clearly benefitted from the considerable support infrastructure available on the EPN campus. As we look forward to funding projects in the future, in Horizon Europe and national programmes, the question arises as to how best to tackle societal challenges at large-scale facilities. To date, we depend on a bottom-up, excellence-based approach to beam time, which must be preserved; but can space also be made for programmatic research? A lively discussion on this question is underway with the Scientific Council at the ILL. The initial focus is on battery research given, we are very pleased to say, that we are part of the BIG-MAP project (<https://www.big-map.eu/>), which started in September 2020.

The wide range of scientific highlights that follow do not yet include an article on COVID research, but there are a number of articles closely related to societal challenges. It is, however, crucial to fully support fundamental research, since this is the true foundation of a knowledge-based society and underpins the disruptive technology of the future. The next generation of high performance computers will not be the result of improving silicon-based technology, which is one very good reason for studying quantum materials now.

Mark R. Johnson
Associate Director,
Head of Science Division

COLLEGE INTRODUCTIONS

FIND US ON:   **COLLEGE 1 – APPLIED MATERIALS SCIENCE, INSTRUMENTATION AND TECHNIQUES**

L. Helfen (College 1 secretary)

College 1 traditionally deals with applied physics, materials science and new instrumentation techniques in neutron scattering. The main areas covered are typically metallurgy, applied neutron scattering, cultural heritage, novel neutron scattering techniques, instrumentation and scientific computing. This college therefore hosts proposals from a very diverse user community.

In 2020, the neutron-imaging instrument NeXT became available to the general ILL user community and a dedicated imaging section was therefore added to College 1. This has led to an increase of around 50 % in the proposals submitted to the College. Energy-related research and geoscience are hot topics. Neutron strain characterisations on SALSA accounted for about 30 % of the proposals submitted. Thanks to major technical improvements made to SALSA (such as a redesigned beam optics support structure), the user community can be given more beam time than originally planned. Metal additive manufacturing continued to be the focus of much research in 2020. Where SANS and reflectometry instruments are concerned, the main difference between the proposals submitted to College 1 and those submitted to other Colleges is that College 1 proposals involve applied and industry-related research.

COLLEGE 2 – THEORY

E. Rebolini (College 2 secretary)

College 2 deals with the theoretical aspects of a variety of subjects within the fields of soft matter, electronic structure and magnetism. It works in synergy with the ILL's core missions, benefitting from collaborations between theoreticians and experimentalists both inside and outside the Institute. Although the College's tradition of hosting visiting scientists has been hampered over the past year by the COVID-19 pandemic, remote collaborations have continued to flourish. A number of members of the group have been actively involved in neutron experiments at the ILL, providing theoretical input either ahead of an experiment to help with its design or after the experiment to assist with the interpretation of experimental data.

The year 2020 saw the arrival of four new postdoctoral fellows: Maria Weseloh and Geetanjali Giri, who are working on magnetic excitations and multiferroic compounds; Tatiana Morozova, who is investigating the influence of the sequence of amino acids on intrinsically disordered proteins; and Willian Natori, who is studying models to describe Mott insulators that retain both spin and orbital degrees of freedom.

COLLEGE 3 – NUCLEAR AND PARTICLE PHYSICS

Y.H. Kim (College 3 secretary)

College 3 is dedicated to nuclear and particle physics research. In 2020, PN1/LOHENGRIN pushed into the unexplored regions of extremely asymmetric fission and revealed subtle fine structures in the kinetic energy distribution of fission fragments. At PF1B, by diffracting cold neutrons at a perfect silicon crystal, a seven orders of magnitude enhancement of the Stern–Gerlach effect for neutrons was observed, opening up the possibility of new kinds of experiments to study the fundamental properties of the neutron. STEREO published its phase-II data, providing the most accurate result to date on the reactor neutrino deficit from ^{235}U reactors and increasing the parameter space in which oscillations to a sterile neutrino are excluded. The instrument was dismantled at the end of 2020. The VCN beamline PF2 was

used to demonstrate the properties of nanodiamond-dispersed, nanocomposite holographic gratings. This extensive study paves the way for slow-neutron optics applications. The commissioning phase of SuperSUN is ongoing and the first ultracold neutrons are due to be delivered in 2021. At FIPPS, spectroscopy after (n,g) reactions on very rare radioactive targets has been performed to explore new nuclear structure phenomena. And finally, the GAMS spectrometer was shut down due to the unavailability of the H6/H7 beam tube.

COLLEGE 4 – MAGNETIC EXCITATIONS

U. Bengaard Hansen (College 4 secretary)

College 4 is dedicated to the study of magnetic excitations in ordered and disordered magnets, superconductors and frustrated systems. Superconductor research continues to be a core activity of College 4 and in particular research into unconventional superconductors, in which spin fluctuations are believed to play an important role in the superconducting pairing. There has also been continued strong interest in low-dimensional magnetism, where exotic collective ground states and excitations are found. The increasing complexity of the experiments proposed is due not only to small samples and small magnetic moments but also to growing demand for complex sample environments: low temperatures, high magnetic fields and high pressures. A few proposals even required a combination of all three.

The thermal time-of-flight spectrometer PANTHER had its first user experiment in 2020. Installation and commissioning of the copper monochromator, the single-crystal mode and the new background choppers will take place in 2021. In addition, the new wide-angle, XYZ-polarisation analysis device PASTIS-3 is now available to the user community on the thermal triple-axis instrument IN20.

COLLEGE 5A – CRYSTALLOGRAPHY

L. Cañadillas-Delgado (College 5A secretary)

College 5A focuses on crystallographic studies aimed at investigating the relationships between the structure and properties of materials. These studies are performed on single-crystal and powder samples and mainly on diffraction instruments. Neutron diffraction is a powerful tool for determining crystalline structures and is often used in combination with other types of radiation from which complementary information can be obtained.

The College 5A user community is made up of groups of experienced scientists from the fields of chemistry and solid-state and condensed-matter physics. These research groups are from the ILL member countries, although many also involve international collaborations with other non-member countries. The materials investigated in 2020 included, among others, perovskites, zeolites, organic/inorganic hybrid materials, minerals, inorganic materials and pure organic compounds. Among the topics covered were accurate structural models and studies of co-crystals and the thermal behaviour of minerals. However, there has also been increasing interest in more applied studies: for example, on gas-storage materials, solar-cell materials including perovskites for photovoltaic applications, ionic conductors, *in situ* and/or *in operando* measurements on battery materials and superconducting materials.

COLLEGE 5B – MAGNETIC STRUCTURES

A. Velamazán (College 5B secretary) and T. Saerbeck (focus group secretary)

College 5b focuses on the study of magnetic structures using polarised and unpolarised neutron powder and single-crystal diffraction, small-angle neutron scattering (SANS) and neutron reflectometry. Over the past year, frustrated magnetism has continued to be one of the key topics, with an increasing number of researchers looking at structures and topologies other than the pyrochlore lattice. Studies on low-dimensional magnetism and quantum critical points have also continued to attract interest. Experiments involving multiferroics, aimed at controlling the magnetic and electric order parameters or establishing the relation between crystallographic and magnetic chirality, remain popular too. Other topics investigated in 2020 include molecular magnets, superconductors, topological materials (Weyl semimetals) and multipolar orders.

On the SANS instruments, studies focusing on Skyrmion hosting and superconducting systems remained prominent, although an increase in studies to determine the magnetic structure of shape-memory alloys, magnetocaloric compounds and nanoparticle assemblies has also been noted. Reflectometry experiments attempt to utilise and modify the magnetic and electronic structure of materials through proximity effects in heterostructures. The material combinations investigated in 2020 ranged from metallic layers and multiferroics to layered van der Waals and topological materials. In addition, several teams examined the lateral arrangement of magnetic moments in patterned structures, using off-specular neutron scattering.

COLLEGE 6 – STRUCTURE AND DYNAMICS OF DISORDERED SYSTEMS

M. Appel (College 6 secretary)

Bulk and confined water, electrolytes and ionic liquids, and polymeric and 'simple' glasses are the principal topics of interest investigated in College 6. For all these disordered systems, our users see a well-balanced need to study structural features using diffraction instruments (mainly D3, D4, D16 and D11/22/33) and dynamical features using spectroscopy (mainly on IN5, IN16B and WASP). After large fluctuations in the number of proposals submitted in previous years, we observed a more stable situation in the two subcommittee meetings in 2020. While around two-thirds of the proposals aim to shed light on problems of fundamental science, about one-third have direct relevance for energy and battery research. The intriguing topic of water, and in particular water in soft and hard confinement, continues to thrive and was the subject of a sizeable proportion of proposals.

COLLEGE 7 – SPECTROSCOPY IN SOLID STATE PHYSICS AND CHEMISTRY

J. Ollivier (College 7 secretary)

College 7 encompasses a broad variety of topics in solid-state physics, ranging from fundamental research to applied studies with societal relevance focusing on environmental, energy-related or life-science subjects. Such studies are well served by the ILL's inelastic instrument suite. In the past year, there has been sustained demand from scientists wishing to investigate interactions between structural and magnetic excitations. Understanding these interactions is extremely important, for example for spintronic devices or for learning more about magnetisation relaxation in molecular nanomagnets. There has also been strong demand for beam time

for studying materials for the production of cleaner energy. Although a large share of the demand was for phonon studies of thermoelectric materials, the flood of proposals aimed at characterising the properties of organometallic perovskite solar cells has not yet abated. More recently, we have noted a growing trend concerning materials for solid-electrolyte batteries. In addition to requiring structural studies (not covered by College 7), these materials need to be characterised, to determine the mobility of the charge carriers, for example—a task well suited to neutron spectroscopy.

COLLEGE 8 – STRUCTURE AND DYNAMICS OF BIOLOGICAL SYSTEMS

O. Matsarskaia (College 8 secretary)

College 8 uses a diverse array of techniques to elucidate the molecular structures, functionality and dynamics of biomolecules. Over the past year, our biological expertise has also been applied to studies of SARS-CoV-2 and COVID-19. With its unique capability for locating hydrogen atoms, neutron crystallography (D19, IADI and DALI) is a vital tool for investigating biological catalysis and structures, including viruses. Solution studies are performed using our unique set of SANS instruments (D11, D22 and D33). Selective deuteration—often carried out in collaboration with the ILL's Deuteration Laboratory (D-lab)—and contrast-matching are crucial for analysing biomolecular complexes. Reflectometers (Figaro, D17) and the diffractometer D16 are used to investigate model lipids and their interaction with biomolecules. This is of particular interest for studies of the infection cycle of SARS-CoV-2. The spectrometers IN15, IN13 and IN11 provide insight into the dynamics of biological systems over a large range of time and Q. A wide variety of complementary techniques to further characterise samples is available through the EMBL, the PSB platform and the PSCM.

COLLEGE 9 – STRUCTURE AND DYNAMICS OF SOFT CONDENSED MATTER

S. Prevost (College 9 secretary) and A. Maestro (focus group secretary)

College 9 studies large-scale structures at nm to μm scales and their related dynamics. Proposals involving bio-related molecules are becoming dominant (35 %), with an increasing number of experiments using natural lipids extracted in the PSCM labs. The SANS/SAXS combination has been successfully used on D22 and *in situ* dynamic light scattering (DLS) has been tested on D11. On FIGARO, the unique liquid-liquid set-up and the continuously developed model membrane capabilities have been attracting more and more users. Thanks to a new Langmuir trough, automatic feedback between pressure and reflectometry measurements is now possible. Many instruments are currently benefitting from upgrades, including new choppers for D17 and new detectors for D11 and D22, more than doubling the solid angle covered. Our users can take advantage of the Chemistry Laboratory (now managed by Martina Sandroni) and support from the PSCM (with Leonardo Chiappisi as the new Scientific Co-ordinator). This platform offers techniques essential for sample preparation and optimisation, helping scientists to exploit the full potential of neutron beam time. A new 3D-DLS developed under a BMBF grant at HZB is on loan from Prof. Hellweg (Bielefeld University). Finally, four ILL soft matter students successfully completed their PhDs in 2020 and five students began their thesis work, four of whom were recruited through the InnoXN programme.

More information on the support facilities cited can be found on p.106.

**Romain Sibille.** French

Laboratory for Neutron Scattering and Imaging,
Paul Scherrer Institute, Switzerland

'After completing a PhD in chemistry, I joined
PSI as a postdoc. Since 2016, I have been a
scientist on the thermal neutron diffractometer,
Zebra. My main research interests are the

preparation, crystal chemistry and fundamental properties of magnetic
materials with strong fluctuations, especially rare-earth pyrochlores.'

Neutron scattering by magnetic octupoles of a quantum liquid

Time-of-flight spectrometer IN5,
diffractometers D20 and D7

HRPT diffractometer at the Paul Scherrer Institute

MAPS spectrometer at STFC Rutherford

Appleton Laboratory

Spin liquids are known as highly correlated yet disordered states of magnetic dipoles [1]. We show that $\text{Ce}_2\text{Sn}_2\text{O}_7$ evades long-range magnetic order for one such state that is instead based on magnetic octupoles. Correlations in this system cause the electronic wavefunction to become essentially octupolar below 1 K, and the defining signatures of this state are visible in the form of a liquid-like signal at high scattering vectors. The discovery of such a new type of quantum spin liquid is remarkable, especially because these topological states of matter are notoriously difficult to detect.

AUTHORS

R. Sibille and V. Porée (PSI, Villigen, Switzerland)
S. Petit (LLB, CEA, CNRS, Université Paris-Saclay, France)
N. Gauthier (SLAC National Accelerator Laboratory and
Stanford University, California, USA)
E. Lhotel (Institut Néel, CNRS–Université Grenoble Alpes, France)
T. Hansen, J. Ollivier, C. Ritter and A. Wildes (ILL)

ARTICLE FROM

Nat. Phys. (2020) — doi:10.1038/s41567-020-0827-7

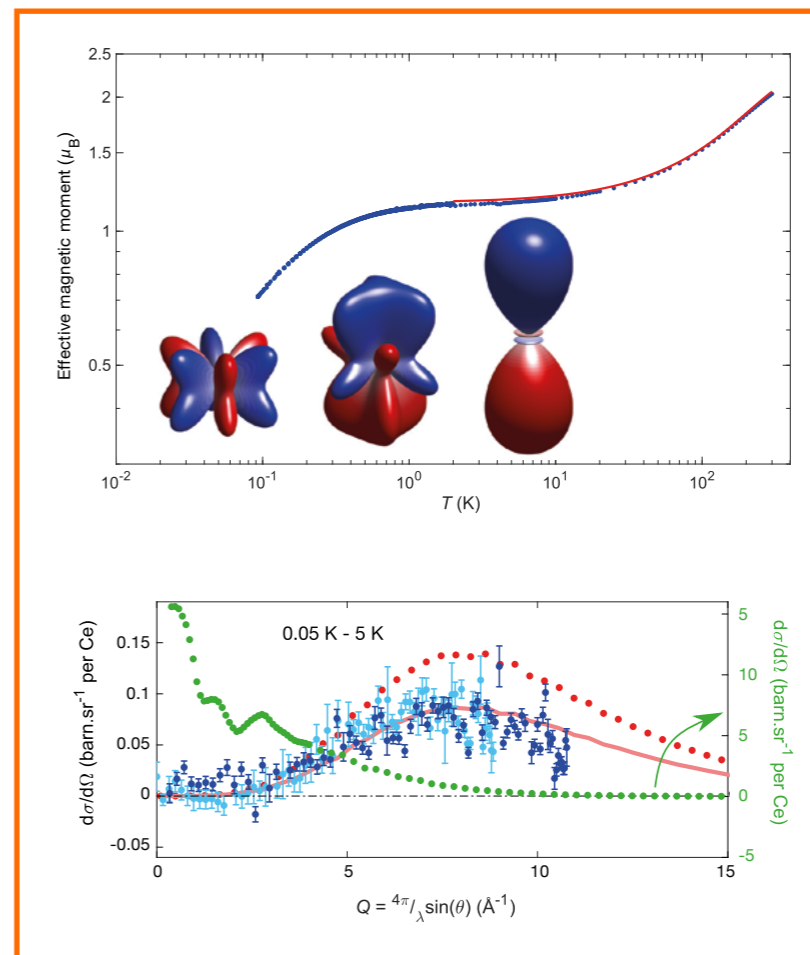
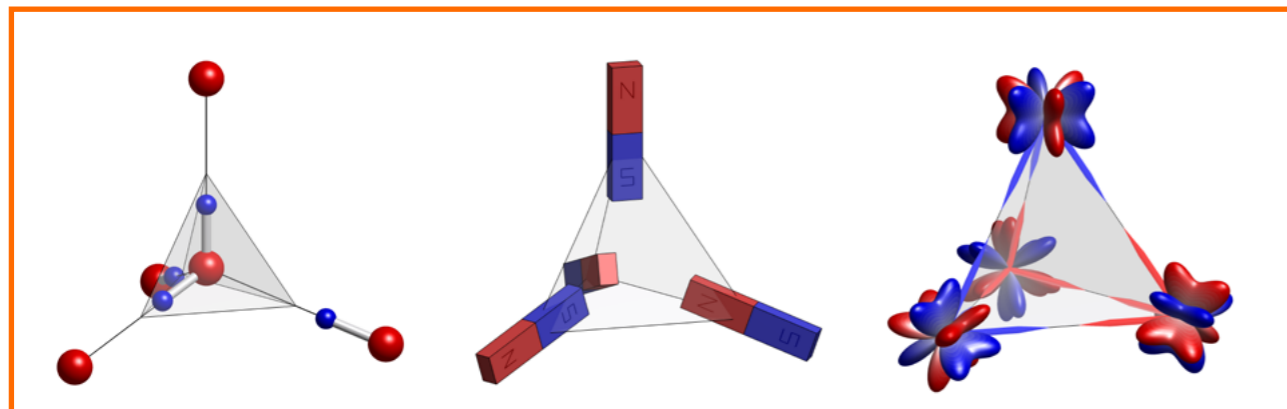
REFERENCES

- [1] L. Balents, Nature 464 (2010) 199
- [2] M.J.P. Gingras and P.A. McClarty, Rep. Prog. Phys. 77 (2014) 056501
- [3] Y.-D. Li and G. Chen, Phys. Rev. B 95 (2017) 041106
- [4] Y.-P. Huang, G. Chen and M. Hermele, Phys. Rev. Lett. 112 (2014) 167203

Spin ice is an intriguing state of matter. If magnetic moments are suitably arranged in a crystal structure—most famously, in rare-earth pyrochlore oxides—they can be subject to frustrated interactions that obey the so-called 'two-in, two-out' ice rule on each of the corner-sharing tetrahedra of the lattice. As a consequence, the ground state can remain disordered though highly correlated, in direct analogy to the residual entropy seen in water ice due to proton disorder (figure 1). In a quantum spin ice, this manifold of ice states is at the basis of a quantum-entangled phase in which fluctuations lead to emergent electrodynamics [2]. Here, we report an example of one such quantum spin liquid formed not by dipoles but by higher-rank degrees of freedom, magnetic octupoles. This exotic state of matter forms in a cerium pyrochlore and constitutes a rare example of a phase in which higher multipolar interactions define the phase behaviour.

Figure 1

Icy states of matter. In water ice (left), the four hydrogen atoms around each oxygen atom are arranged randomly, but always such that two of them are close and two far apart. In spin ice (centre), the magnetic dipole moments obey the same 'two-in, two-out' rule. In the octupole ice, the corners of the tetrahedron are occupied by magnetic octupoles (right). Their magnetic charge distribution is constrained by an analogous ice rule (the two different magnetisation directions are emphasised by the arrows in red and in blue along the edges).

**Figure 2**

Degrees of freedom and correlations in cerium stannate. The effective dipole moment obtained from bulk susceptibility measurements (upper panel) decreases at high temperature ($T < 10$ K) due to crystal field effects, to reach a plateau ($1 \text{ K} < T < 10 \text{ K}$) corresponding to the ground-state doublet. Its wavefunction has a 'dipole–octupole' character and can become essentially octupolar under the effect of dominant octupole–octupole interactions, which further reduces the dipole moment at temperatures below 1 K. Magnetic octupoles constrained by an ice rule on the pyrochlore lattice avoid long-range order and give rise to a liquid-like hump in neutron diffraction. This signal increases in intensity upon cooling in the correlated regime and is only observed at high-momentum transfer due to the form factor associated with degrees of freedom having a complex magnetisation density (bottom panel). Blue data points with error bars are neutron data and refer to the low-intensity scale on the left. Red and green colours are Monte Carlo simulations for the octupole ice (low-intensity scale) and a spin ice of magnetic dipoles (high-intensity scale on the right), respectively. The solid curve in red is the octupole ice simulation (red dots) scaled onto the finite-temperature neutron data ($\times 0.625$).

In $\text{Ce}_2\text{Sn}_2\text{O}_7$ —a clean realisation of a pyrochlore lattice of Ce^{3+} ions—magnetisation and muon-spin relaxation measurements suggest an unusual ground state with signatures of a quantum spin liquid. The spin–orbital entanglement of the electron spin $S = 1/2$ and orbital angular momentum $L = 3$ result in a $J = 5/2$ manifold, which is split by the crystal–electric field into three Kramers doublets. We show, using inelastic neutron spectroscopy, that the ground-state doublet $|\pm\rangle$ is a linear combination of $|m_J = \pm 3/2\rangle$ states, which defines a composite object carrying both a magnetic dipole and a magnetic octupole [3]. Bulk susceptibility measures the dipole component separately and shows that the constant moment value found in the temperature range between approximately 1 and 10 K, corresponding to the uncorrelated ground-state doublet, is further reduced upon cooling below 1 K (figure 2). As an alternative to the intuitive interpretation of antiferromagnetic correlations, this simple observation can be understood as the evolution of the mixing of the wavefunction. In particular, dominant octupole–octupole couplings can lead the octupole moment to strengthen at the expense of the dipole moment in order to minimise the energy of the system. This yields a specific signature in energy-integrated neutron scattering where a signal is

observed at high-momentum transfers due to the complex magnetisation density of the octupoles, whose magnitude increases when the temperature decreases in the correlated regime.

The octupolar scattering in $\text{Ce}_2\text{Sn}_2\text{O}_7$ remains diffuse down to the lowest temperatures (figure 2), which together with its magnitude indicates dominant ferro–octupolar interactions leading to a degenerate manifold of octupole ice states. In addition, fits of the bulk properties, using the relevant Hamiltonian for dipole–octupole doublets on the pyrochlore lattice [4], corroborate this interpretation and indicate that weak transverse interactions endow the system with quantum dynamics. The resulting state is characterised by a continuum of spin excitations, whose main features (onset, peak and extent) agree with theoretical predictions for the expected spinons, thus further confirming the octupolar quantum spin ice scenario.

The findings reported here bring together the intriguing world of multipoles—a field of growing relevance in explaining a number of phenomena in condensed matter—with that of frustrated magnetism and quantum spin liquids in general—phases that go beyond the symmetry-breaking paradigm and therefore challenge our understanding of correlated matter.



Jennifer Graham. British
The ILL and University of Birmingham (UK)
*'I am a second-year chemistry PhD student.
In my research, I employ diffuse neutron
scattering techniques to explore the interplay
between chemical disorder and magnetic
frustration in materials.'*

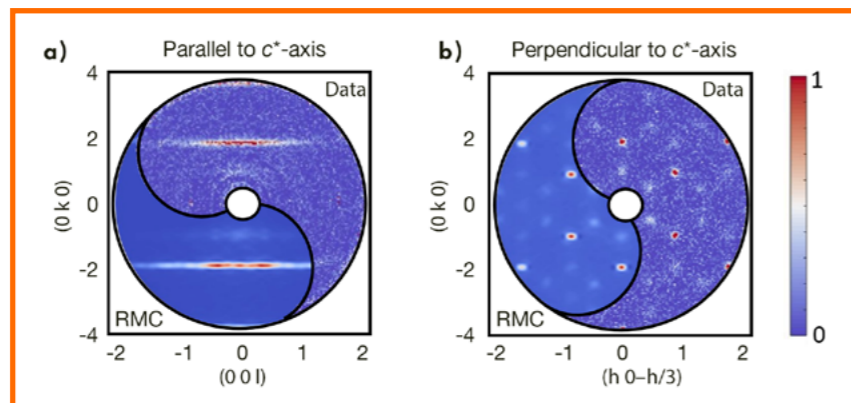
Local nuclear and magnetic order in the two-dimensional spin glass $\text{Mn}_{0.5}\text{Fe}_{0.5}\text{PS}_3$

*High-resolution, two-axis diffractometer D2B
and diffuse-scattering diffractometer D7*

In this study we investigated the nuclear and magnetic correlations in the spin glass, $\text{Mn}_{0.5}\text{Fe}_{0.5}\text{PS}_3$. Our analysis shows that $\text{Mn}_{0.5}\text{Fe}_{0.5}\text{PS}_3$ is a near-ideal example of a two-dimensional magnetic material, and that the spin glass state is constructed from a mixture of satisfied and unsatisfied correlations between magnetic moments within the honeycomb planes.

Figure 1

Magnetic component of single-crystal neutron scattering data measured at 1.5 K on D7 compared against the RMC SPINVERT model. Data were measured **a)** parallel and **b)** perpendicular to the c^* -axis. The intensity of these data has been normalised arbitrarily, as indicated by the colour bar.



AUTHORS

J. Graham (ILL and University of Birmingham, UK)
L. Clark (University of Birmingham, UK)
E. Suard and A. Wildes (ILL)
M. Coak (University of Warwick, UK)
J.-G. Park and S. Son (Seoul National University, Republic of Korea)

ARTICLE FROM

Phys. Rev. Materials (2020) - doi: 10.1103/PhysRevMaterials.4.084401

REFERENCES

- [1] J.A. Mydosh, Rep. Prog. Phys. 78 (2015) 052501
- [2] G. Ouvard *et al.*, Mater. Res. Bull. 20 (1985) 1181
- [3] T. Masubuchi *et al.*, J. Alloys Compd. 460 (2008) 668
- [4] J.A.M. Paddison *et al.*, J. Phys.: Condens. Matter 25 (2013) 454220

Unconventional magnetism encompasses a broad spectrum of modern materials research. Of particular interest to our group are materials that display magnetic frustration, a phenomenon that arises when magnetic moments are unable to orientate themselves in an energetically favourable arrangement. This can be due to geometry, competing exchange interactions or spin-orbit interactions. The addition of site disorder to frustrated systems often leads to a spin glass state. In a spin glass, randomised moments interact in such a way that a classical phase transition occurs at a distinctive temperature, known as the glass transition, T_g [1]. Once in the spin glass state, moments are frozen into place, with no long-range correlated order, and are readily characterised by bulk magnetisation measurements through the observation of frequency-dependent features.

The MPS_3 compounds represent a diverse family of honeycomb-layered van der Waals materials, where the physical properties are heavily reliant on the choice of transition-metal ion (M) [2]. MnPS_3 and FePS_3 have both been well characterised in earlier studies and are quasi-two-dimensional antiferromagnets. However, differences in their respective magnetic structures, originating from the nature of their nearest-neighbour interactions and spin anisotropies, mean that frustration is generated within the mixed $\text{Mn}_{0.5}\text{Fe}_{0.5}\text{PS}_3$ compound.

Whilst a spin glass phase was known to exist in $\text{Mn}_{0.5}\text{Fe}_{0.5}\text{PS}_3$ [3], we investigated the nature of its local nuclear and magnetic correlations through a series of magnetisation and neutron scattering measurements.

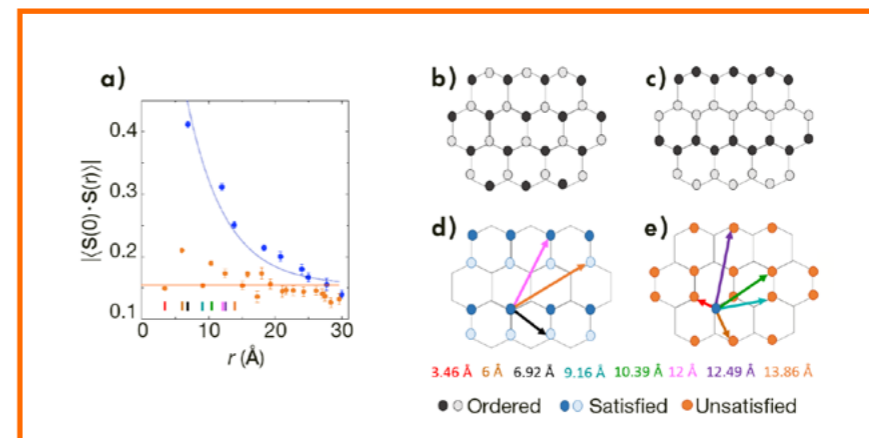


Figure 2

a) Magnitude of intraplanar correlations, $|S(0) \cdot S(r)|$ at 1.5 K. Blue and orange points, corresponding to neighbours with entirely satisfied correlations or at least one unsatisfied correlation, have been fitted with exponential and linear functions, respectively. In-plane magnetic structures of **b)** MnPS_3 and **c)** FePS_3 have conventional long-ranged ordered states. Moment orientations that are **d)** common to and **e)** different between the structures give rise to satisfied and unsatisfied correlations, respectively. The first eight correlations are shown by arrows in **d)** and **e)** and links to a corresponding coloured tick mark in 2a.

To explore the nuclear order, we used the high-resolution D2B diffractometer at the ILL. What was interesting to us about these data was not the peaks but actually the background—or lack thereof! In a diffraction experiment such as this, any nuclear short-range order should be clearly visible given that the neutron scattering lengths of Mn and Fe yield excellent contrast. The absence of any diffuse structure within the background indicates a lack of short-range order between Mn and Fe, and therefore shows that the magnetic ions are essentially randomly distributed within the honeycomb lattice.

We chose the diffuse-scattering diffractometer, D7, to study the magnetic order as it enabled us to use xyz-polarisation analysis, a technique that separates the nuclear and magnetic contributions of the signal. This is particularly appealing for the study of disordered magnets, as diffuse features tend to be broad in Q and weak in intensity and are therefore easy to miss in other experiments. We measured both powder and single-crystal samples on D7. Our powder data show a mixture of broad and sharp features at low temperatures that are reminiscent of the parent compounds. We fitted these data using reverse Monte Carlo (RMC) methods on the program SPINVERT [4]. Our model assumes that moments lie parallel or anti-parallel to the c^* -axis, an assumption that is supported by the orientation of ordered moments in the parent compounds. Using our analysis of the powder data, we were able to reconstruct single-crystal diffraction patterns on the program SCATTY and as shown in **figure 1** are in excellent agreement with our measured data: we see rod-like structures, which reflect the two-dimensional

nature of our compound, appearing parallel to the c^* -axis; whereas, perpendicular to the c^* -axis we observe strong magnetic intensity, which corresponds to the expected magnetic Bragg positions for ordered MnPS_3 , with additional weaker intensity observed at positions consistent with the in-plane magnetic structure for FePS_3 .

Our analysis of the in-plane spin correlations is shown in **figure 2a** and has a physical analogy arising from relationships between the magnetic structures of MnPS_3 and FePS_3 (**figures 2b** and **2c**, respectively). We split our intraplanar correlations into two groups: satisfied correlations, as shown in **figure 2d**, between moment orientations that are common between the two structures; and unsatisfied correlations, as shown in **figure 2e**, where moments at equivalent distances have at least one pair that differs between the structures. The competition resulting from these satisfied and unsatisfied correlations gives rise to some very localised magnetic order and the glassy behaviour, respectively.

In summary, we investigated the local correlations that make up the spin glass phase in $\text{Mn}_{0.5}\text{Fe}_{0.5}\text{PS}_3$. Spin glasses have three main ingredients: randomness, frustration and competing exchange interactions. We verified the randomness from observing little structure in the background of our D2B diffraction data, and the frustration from our analysis of the spin correlations. A combination of these effects leads to competing exchange interactions between the transition-metal ions within the honeycomb network, resulting in a spin glass state.

Please note that J. Graham and L. Clark are no longer affiliated with the University of Liverpool, which is different from the paper.



Morten Ring Eskildsen. Danish and American University of Notre Dame, Indiana, USA
 ‘My work focuses on large-scale magnetic structures such as vortices in type-II superconductors and skyrmions in chiral magnets. Recently, I have been interested in how to achieve metastable states and how we can use them to probe fundamental properties of vortex-/skyrmion-hosting materials.’

Broken time-reversal symmetry in the topological superconductor UPt_3

Small-angle scattering instrument D33

Unconventional superconductors that break time-reversal symmetry are of great interest, as the superconducting state is protected topologically and vortices can host Majorana fermions with potential use in quantum computing. We used small-angle neutron scattering to demonstrate that vortices in UPt_3 possess an internal degree of freedom. This provides direct evidence of broken time-reversal symmetry in this material, something that has previously been difficult to establish in the bulk.

AUTHORS

K.E. Avers, W.P. Halperin and J.A. Sauls (Northwestern University, Illinois, USA)
 W.J. Gannon (University of Kentucky, Kentucky, USA)
 M.R. Eskildsen (University of Notre Dame, Indiana, USA)

ARTICLE FROM

Nat. Phys. (2020) — doi:10.1038/s41567-020-0822-z

REFERENCES

- [1] X.-L. Qi and S.-C. Zhang, Rev. Mod. Phys. 83 (2011) 1057
- [2] R. Joynt and L. Taillefer, Rev. Mod. Phys. 74 (2002) 235
- [3] S. Mühlbauer *et al.*, Rev. Mod. Phys. 91 (2019) 015004
- [4] J.A. Sauls and M. Eschrig, New J. Phys. 11 (2009) 075008

Superconductors that break time-reversal symmetry are relatively rare [1]. The heavy-fermion superconductor UPt_3 represents one of the most prominent candidates. In this material, one of the three superconducting phases—the so-called B-phase—is predicted to exhibit broken time-reversal symmetry [2]. To test this prediction we performed small-angle neutron scattering studies (SANS) of the vortex lattice (VL) [3], using the vortices to probe the nature of the superconducting state.

Due to the broken time-reversal symmetry the superconducting order parameter has an associated axis of chiral symmetry, with a direction that is determined by the magnetic field along the *c*-axis on entering the B-phase. Once the chiral direction is established, there is an energy barrier to its reversal even if the applied field is reduced to zero and then reapplied with the opposite polarity. It is therefore possible to have the chiral direction either parallel or anti-parallel to the field. This is illustrated in the schematic in **figure 1a**, where the field-reduced (also denoted ++ or --) and field-reversed (+- or -+) configurations correspond to equilibrium and metastable states, respectively.

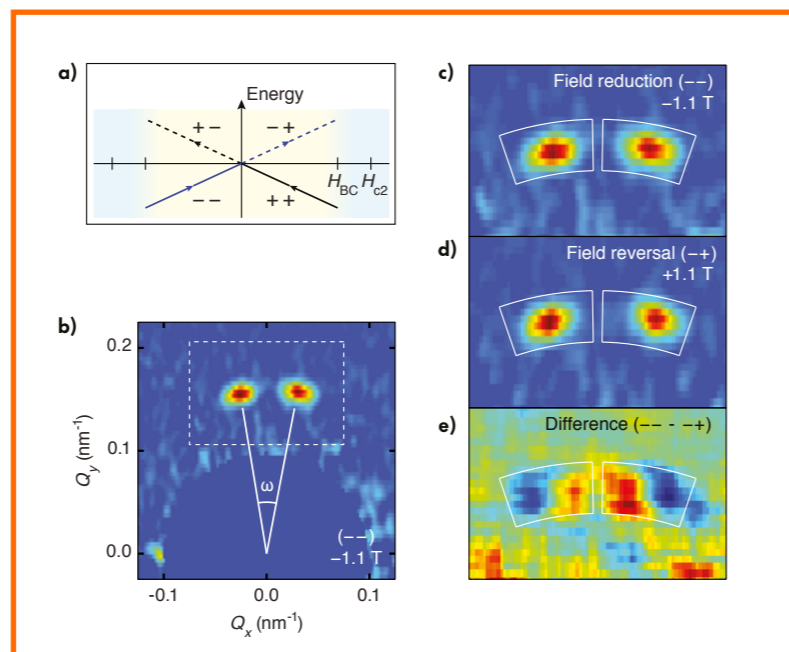


Figure 1

- Energy of the superconducting condensate as a function of field history: for a field reduction (++) or --) the system is in the ground state (solid lines) and for a field reversal (+- or -+) it is in a metastable state (dashed lines).
- Diffraction pattern indicating the VL domain splitting (ω) following a field reduction. Only one pair of Bragg peaks (out of six) was imaged to make efficient use of the SANS beam time.
- An expanded view of the portion of reciprocal space.
- Same as (c) but for a field reversal.
- Difference between field-reduced and field-reversed diffraction patterns. The blue (red) colours indicate negative (positive) values. Sector boxes show the regions relevant for the subtraction.

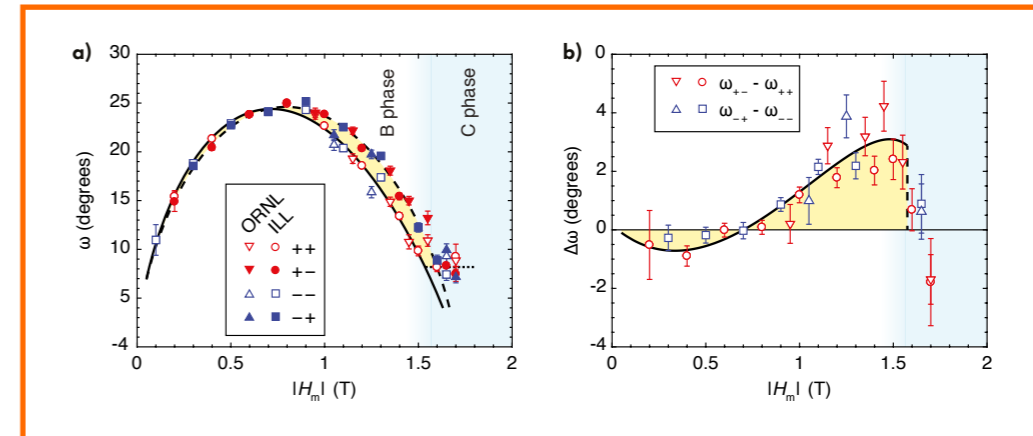


Figure 2

- Field dependence of the VL split angle, ω .
- The split difference, $\Delta\omega$, between the field reversed and field reduced.

The order parameter in the vortex cores is sensitive to the superconducting state of the host material. This is manifested in the VL symmetry and orientation relative to the crystalline axes, as these are determined by the anisotropy of the screening current in the plane perpendicular to the applied field which effects the vortex–vortex interactions. In UPt_3 in the B-phase this gives rise to a rotation of the VL as the field, and hence the vortex density, is changed. This causes the VL to split into domains that are rotated either clockwise or counter-clockwise around the field, giving rise to a splitting of the VL Bragg peaks as seen in **figure 1b**. The peak splitting (ω) first increases and then decreases as the applied field is increased, as shown in **figure 2a**. The decrease at high fields indicates an increasing effect of the cores as the vortices become more tightly packed.

Our main result is illustrated in **figures 1c–e**, which show a difference in the VL splitting for the two different field histories used. This is most readily seen as an intensity ‘dipole’ centered on each peak position in the subtraction of the two diffraction patterns shown in **figure 1e**. The field dependence of ω as well as the difference in the peak splitting between the two field histories ($\Delta\omega = \omega_{+-} - \omega_{++}$ or $\omega_{-+} - \omega_{--}$) are shown in **figure 2**. At low fields $\Delta\omega$ is small and negative, changing sign and increasing in magnitude as we approach the transition between the B- and C-phases at roughly 1.5 T. Once inside the C-phase, ω ceases

to change with the field and $\Delta\omega$ approaches zero, although errors bars are large due to the rapidly vanishing scattered intensity. We note that there is no difference between measurements whether the field-reduced or field-reversed state originated in the normal state or in the intermediate C-phase, as one would expect when the C-phase (like the normal state) is expected to be time-reversal invariant.

The non-zero $\Delta\omega$ is direct evidence that vortices in the B-phase in UPt_3 possess an internal degree of freedom, from which we infer both that the time-reversal symmetry is indeed broken and that the *c*-axis is a chiral symmetry axis. The difference in the splitting between the two field histories is attributed to different vortex core structures [4], which will have the greatest impact at high vortex densities, in accordance with the results in **figure 2b**.

In closing, we note that SANS studies of the UPt_3 VL are challenging due to the long penetration depth and the corresponding weak scattering, and are only possible at a powerful neutron facility such as the ILL. The high intensity available at D33, together with the high quality of the UPt_3 single crystal used for the measurements, allowed us to extend the magnetic field along the chiral *c*-axis by an order of magnitude compared with that used in previous SANS studies of this material. This is critical as it allowed us to explore the high-field part of the phase diagram where the VL is most sensitive to changes in the superconducting state and especially the vortex-core structure.



Dalila Bounoua. Algerian
Laboratoire Léon Brillouin, CEA-Saclay
'After being awarded a PhD at the
Université Paris-Saclay (2017) for the study of
low-dimensional spin liquids, my postdoctoral
research focuses on the study of new
magnetolectric quantum states of matter

such as magnetolectric multipoles and loop current-like magnetism in strongly correlated electron systems, using neutron scattering and resonant X-ray diffraction.'

Loop currents in two-leg ladder cuprates

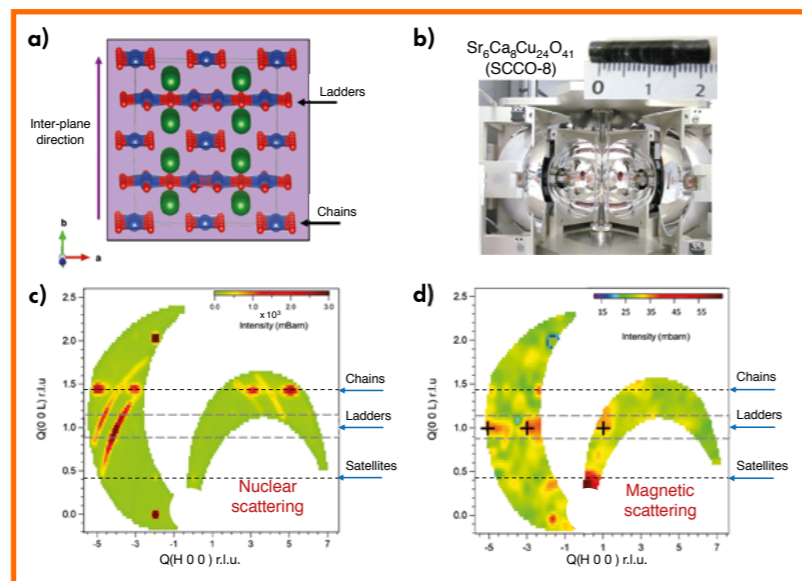
Diffuse-scattering diffractometer D7

Three-axis spectrometer 4F1 at LLB-Orphée

Quantum materials with strong electronic correlations are at the heart of modern physics. Within these systems, as a growing number of experimental studies are uncovering, are unconventional quantum states of matter where the electronic degrees of freedom intimately couple to form novel, exotic quantum entities such as orbital loop currents or magnetolectric multipoles [1–3]. Such objects are of great fundamental interest as they are thought to be essential to our understanding of superconductivity and multiferroicity, both of which have a key role in meeting the societal challenges of tomorrow. Our discovery shows, for the first time, a loop current-like magnetism in a one-dimensional quasi-1D spin chains and ladders cuprate $(\text{Sr,Ca})_{1-x}\text{Cu}_{2x}\text{O}_{4-1}$ (SCCO- x).

Figure 1

a) Crystal structure of SCCO- x (Cu in blue, O in red and Sr in green).
b) Single crystal of SCCO-8 obtained using the travelling solvent floating zone technique. Momentum space mapping (in r.l.u.), obtained on D7, by: **c)** nuclear scattering; and **d)** magnetic scattering deduced from XYZ-polarisation analysis.



AUTHORS

D. Bounoua, Y. Sidis and P. Bourges (LLB, CEA-Saclay, France)
L. Mangin-Thro (ILL)
R. Saint-Martin and L. Pinsard-Gaudart (ICMMO, Université Paris-Saclay, France)
J. Jeong (Institute for Basic Science, Korea)

ARTICLE FROM

Commun. Phys. (2020) — <https://doi.org/10.5291/ILL-DATA.5-53-279>

REFERENCES

- [1] C. Varma, Phys. Rev. B 73 (2006) 155113
- [2] S.W. Lovesey and D.D. Khalyavin, J. Phys. Condens. Matter 29 (2017) 215603
- [3] M.S. Scheurer and S. Sachdev, Phys. Rev. B 98 (2018) 235126
- [4] Deng, G. *et al.*, Phys. Rev. B 88 (2013) 174424

We revealed this new magnetic phase using polarised neutron diffraction (PND) on the D7 multi-detector diffractometer at the ILL and the triple-axis spectrometer 4F1 at LLB-Orphée. Owing to the highly stable and reliable neutron polarisation, the high signal-to-noise ratio and the access to longitudinal XYZ-polarisation analysis (XYZ-PA) provided by both instruments, as well as the large, accessible Q -range offered by D7, we succeeded in detecting the weak magnetic moment ($\sim 0.05\mu_B$) and precisely determining the structure factor of this novel magnetism. Longitudinal XYZ-PA was a particularly powerful asset in this work. Indeed, combining measurements with the neutron polarisation within (X,Y) or perpendicular to (Z), the scattering plane allowed a detailed description of the observed magnetic signal.

SCCO- x crystallises in an incommensurate nuclear structure consisting of an alternating stack of CuO_2 chains and Cu_2O_3 ladders along the b -axis (**figure 1a**). In this system, the chains are intrinsically hole-doped for $x = 0$. Doping Ca on the Sr site results in a transfer of the holes from the chains to the ladders and leads to a rich electronic phase diagram within the ladders. This further triggers the emergence of superconductivity, at high Ca (hole)-doping. This feature has placed SCCO- x under the spotlight of numerous in-depth investigations reported in the literature in recent years.

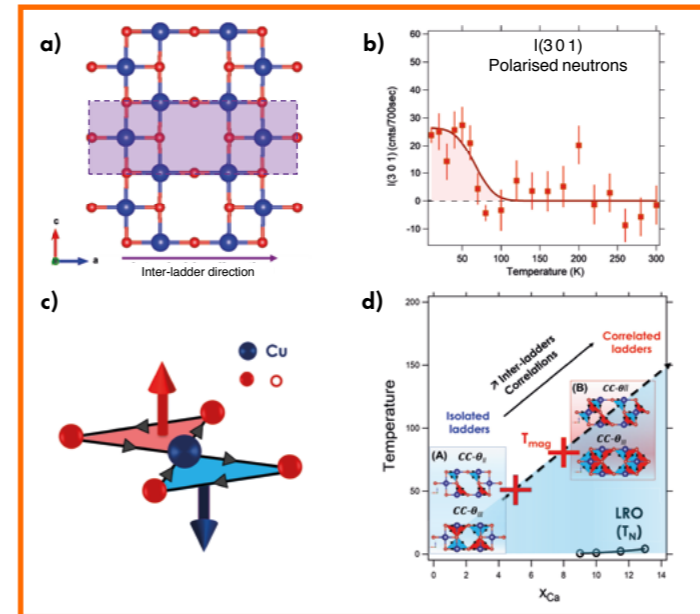


Figure 2

a) $[a,c]$ plane projection of the ladders subsystem. The highlighted area corresponds to one ladder unit cell.
b) Temperature dependence of the magnetic signal in SCCO-8 (4F1).
c) Two staggered Cu–O LCs per Cu site flowing clockwise (red triangles) and anticlockwise (blue triangles) and giving rise to two magnetic moments per Cu site perpendicular to the Cu–O plane.
d) Schematic phase diagram of SCCO- x showing the evolution of the LCs pattern as a function of the Ca content (x_{Ca}). At large doping, magnetic correlations develop between ladders at the onset temperature T_{mag} (red crosses). The insets show two different models of LCs considered in this work, with uncorrelated (A) and correlated (B) cases described within the ladders unit cell.

We performed the measurements in two different, high-quality, centimetric-size single crystals of SCCO- x (with $x = 5$ and 8) belonging to the gapped spin liquid-state region of the phase diagram (a state with exponentially decaying spin–spin correlations). We grew the crystals using the travelling solvent floating zone technique in a four-mirror image furnace at the *Institut de Chimie Moléculaire et des Matériaux d'Orsay* (**figure 1b**).

PND measurements on D7 (SCCO-8) allowed us to map out the reciprocal space spanning the $(H,0,0)/(0,0,1)$ ladders scattering plane (r.l.u.). Our investigations revealed the occurrence of a translationally invariant magnetism at integer (Bragg) Q -positions along the $(H,0,1)$ ladders scattering ridge, where no nuclear scattering was observed in accordance with the crystallographic space group selection rules (**figures 1c** and **1d**).

This magnetism is short-ranged (correlation lengths: $\xi_a \sim 6\text{Å}$, along the inter-ladder direction, $\xi_c \sim 11\text{Å}$ along the ladder legs; see **figure 2a**). It originates exclusively from the ladders subsystem and can be viewed as magnetic clusters confined within the ladders with no correlation along the stacking direction (b -axis). The temperature dependence of the magnetic scattering gives $T_{\text{mag}} \sim 80\text{K}$ (**figure 2b**) as the onset temperature for magnetic correlations, which does not correspond to any reported magnetic or electronic instability within the phase diagram of SCCO- x ladders. Upon decreasing the Ca(hole) content to $x = 5$ our results further highlight the loss of inter-ladder correlations resulting in uncorrelated ladders, and a weaker $T_{\text{mag}} \sim 50\text{K}$.

Interestingly, classical copper spin or magnetic moments on oxygen sites models fail to reproduce the peculiar structure factor of this novel phase. Thus, relying on theoretical predictions [1, 3] we considered magnetic structures involving new quantum states of matter as building blocks for this novel magnetism. These microscopic loop currents (LCs) models were proposed in the framework of hole-doped cuprates and spin liquid systems [1, 3], considering currents flowing between the Cu and O sites (**figure 2c**) and between O sites only, respectively. Remarkably, the models reproduced our experimental data for both weakly correlated and uncorrelated cases.

Additionally, this novel LCs-like phase gives rise to scattering at the same Q -positions as those expected from an intriguing magnetic long-range ordered state (LRO), developing at higher Ca-doping and much lower temperature (**figure 2d**) [4]. This raises the question of the quintessential nature of the LRO state and makes it tempting to propose that an LCs-like phase could further act as a pre-emptive state triggering the LRO, as the Ca-doping evolution of the correlations suggests [3]. Indeed, while the proposed LRO spin models require very complex spin magnetic structures involving several unit cells, an intra-unit cell LCs model successfully reproduced the measured magnetic structure factor (insets **A** and **B**, **figure 2d**). The nature of the link between both phases has yet to be established through the study of samples with higher Ca-doping.

Our study demonstrates, for the first time, the ability of LCs-like patterns to emerge in quasi-1D spin liquids as confined ribbons due to dimensionality.

**Navid Qureshi**, French

The ILL

'After finishing my PhD thesis at the ILL in 2008, I returned as an "instrument responsible" in 2014. My main research fields are frustrated magnetism, multiferroic materials and chiral structures, which I investigate using polarised neutrons and spherical neutron polarimetry in particular.'

Absolute crystal and magnetic chiralities in the langasite compound $\text{Ba}_3\text{NbFe}_3\text{Si}_2\text{O}_{14}$

Spin-polarised diffractometer D3

We present a combination of polarised neutron scattering techniques on an enantiopure langasite single crystal, aimed at determining its absolute structural and magnetic chiralities and the coupling between them. The use of polarised neutrons and the consistent use of scattering theory conventions were essential to this study and reveal that magnetic handedness is pinned by structural handedness. Simple considerations of the energy balance in the magnetic Hamiltonian reveal that the local single-ion anisotropy on a triangular plaquette plays a key role in stabilising one of the two magnetic helices.

AUTHORS

N. Qureshi and E. Lelièvre-Berna (ILL)
A. Bombardi and L.C. Chapon (Diamond Light Source, UK)
P. Barone (CNR, Istituto SPIN, Italy)
S.-W. Cheong (Rutgers Center for Emergent Materials and Department of Physics and Astronomy, USA)

ARTICLE FROM

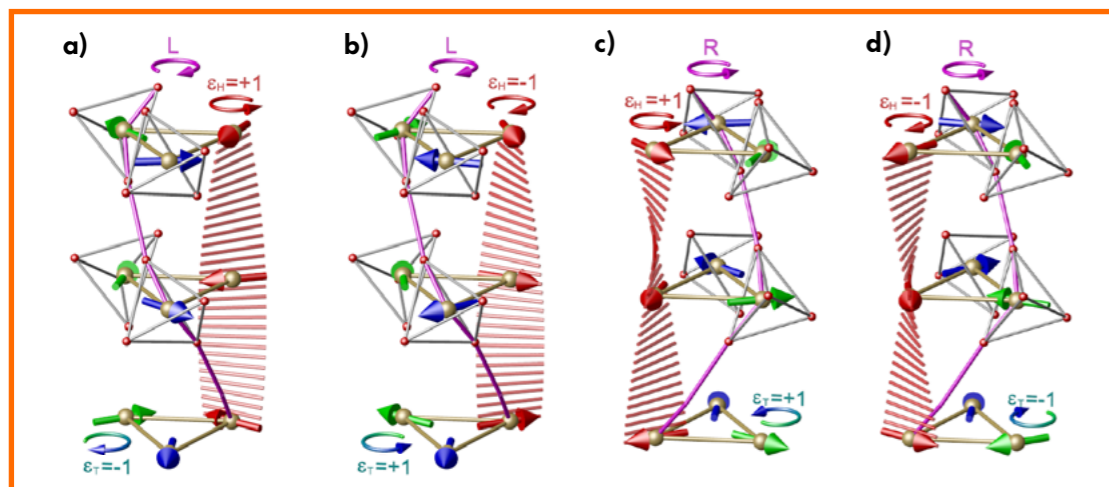
Phys. Rev. B (2020) — doi:10.1103/PhysRevB.102.054417

REFERENCES

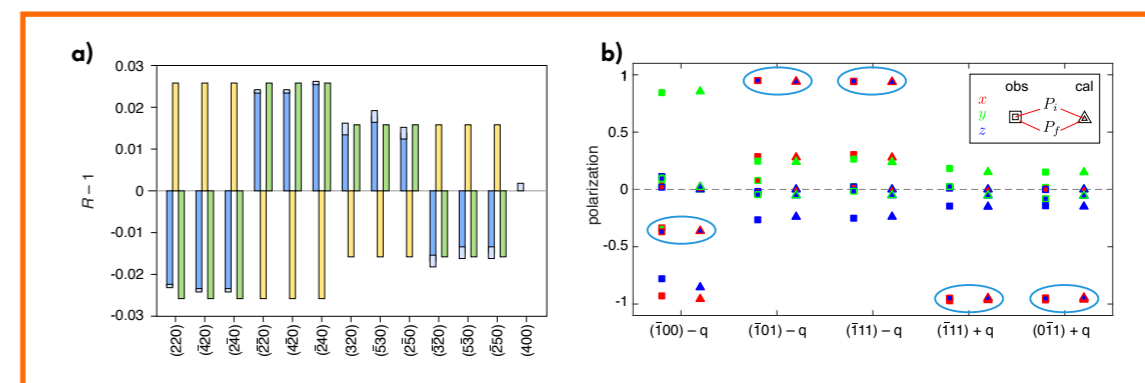
- [1] S. Mühlbauer *et al.*, *Science* 323 (2009) 5916
- [2] S.-W. Cheong and M. Mostovoy, *Nat. Mater.* 6 (2007) 13
- [3] N. Qureshi, *J. Appl. Cryst.* 52 (2019) 175
- [4] L. Chaix *et al.*, *Phys. Rev. B* 93 (2016) 214419

Structural and magnetic chirality is at the heart of various physical phenomena that have attracted enormous attention in condensed matter physics, e.g. skyrmions [1] develop as complex magnetic structures under an applied magnetic field in chiral crystals such as MnSi and promise new alternatives to data storage applications. Certain chiral magnetic structures are able to break the inversion symmetry of the underlying crystal structure and can therefore induce an electric polarisation that is intimately coupled to the magnetic properties of the material. These materials, known as multiferroics [2], reveal exciting possibilities such as switching magnetic domains using an electric field. Recently, electromagnons, hybridised excitations of nuclear and magnetic nature, have been observed in a pure enantiomer crystal of the langasite compound $\text{Ba}_3\text{NbFe}_3\text{Si}_2\text{O}_{14}$. This system possesses a chiral crystal structure (space group $P321$) and develops a spiral magnetic ordering with a 120° spin configuration on a triangular plaquette below $T_N = 27$ K (**figure 1**).

In all these systems there is a direct interplay between the structural and the magnetic chiralities that is expressed by antisymmetric terms in the Hamiltonian. It is a complex task to determine these properties of a crystal. Structural chiralities are routinely measured by X-rays via the anomalous form factor, but their magnetic counterparts require bright and polarised synchrotron radiation. With neutrons, the absolute magnetic chirality can easily be determined by measuring the chiral components of the so-called polarisation matrix within a spherical neutron polarisation (SNP) experiment. However, with the incident neutron energies usually employed being far from high-resonance energies, anomalous scattering cannot be used to determine the

**Figure 1**

Four different configurations that all yield the same nuclear and magnetic structure factors and are therefore indistinguishable using unpolarised neutrons.

**Figure 2**

a) Asymmetry $R-1$ of observed flipping ratios R (blue) of different nuclear Bragg reflections compared with calculated values for a left-handed (yellow) and a right-handed (green) structure.

b) Observed (squares) and calculated (triangles) polarisation matrix elements of five different magnetic Bragg reflections. The chiral elements are emphasised by ellipses. Calculations and fits were done using the Mag2Pol program [3].

structural chirality. The only way to extract this information is to measure a very weak scattering asymmetry, depending on the initial neutron polarisation direction, which is induced by relativistic spin-orbit scattering (also called Schwinger scattering), i.e. a coupling of the neutron polarisation to the magnetic field generated (in the neutron reference frame) by the distribution of electric charges in the chiral crystal. Its experimental realisation is analogous to the classic flipping ratio method familiar to the magnetisation density community. However, in order to detect the weak Schwinger flipping ratios, the sample needs to be kept inside a zero-field chamber (Cryopad) in order to suppress the conventional nuclear-magnetic interference scattering.

In this study, we demonstrate that structural and magnetic chiralities can be determined simultaneously by employing a single experimental set-up and a single specimen without sample cuts or reorientations. By measuring integrated intensities with unpolarised neutrons only, one cannot distinguish between the four configurations shown in **figure 1a–d**, which differ with respect to their structural chirality (left-handed or right-handed, $L/R = \pm 1$), their helical chirality $\epsilon_H = \pm 1$ and their triangular chirality $\epsilon_T = \pm 1$. Only the invariant $L/R \cdot \epsilon_H \cdot \epsilon_T$ is accessible. The use of polarised neutrons is therefore essential.

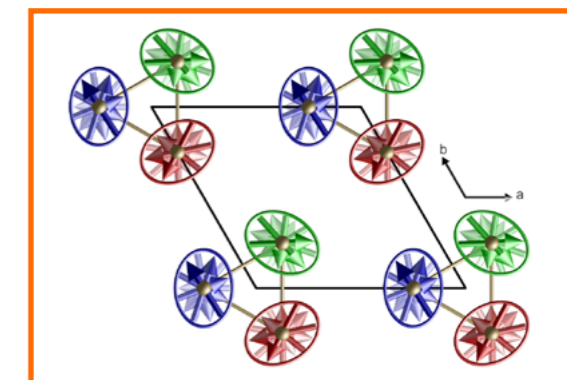
The experiment was carried out on the hot-neutron, polarised diffractometer D3 using the Cryopad/Cryocradle set-up, with a ^3He neutron spin filter for the SNP part.

Figure 2a shows the asymmetry of the flipping ratios $R-1$, together with calculated values for a left- and a right-handed sample; **figure 2b** depicts the observed polarisation matrix elements, focusing on the chiral elements calculated for a right-handed ($\epsilon_H = 1$) helix (note that those elements would reveal an inverted sign for $\epsilon_H = -1$). The beauty of the techniques employed is that in spite of their complexity—both theoretically and experimentally—there is no ambiguity in the interpretation of the results. The data clearly show that magnetic handedness is pinned by structural handedness, with the investigated sample corresponding to the configuration shown in **figure 1c**.

The absolute chirality $\epsilon_H \cdot \epsilon_T$ is dictated by the exchange parameters along the c -axis of the crystal structure, which in turn are fixed by the structural chirality. However, so-called antisymmetric exchange parameters, such as the Dzyaloshinskii-Moriya interaction (DMI), between two

triangles along c do not allow us to distinguish between the two helical configurations with fixed absolute chirality. On the other hand, the DMI within a single triangle and the single-ion anisotropy impose a fixed value of ϵ_T , which, on its own, is experimentally inaccessible. However, detailed analysis of the SNP data reveals a slight ellipticity of the spin envelope, as shown (exaggerated by a factor of three) in **Figure 3**, which implies that it is energetically favourable for a spin to align perpendicular to the diad axes of the triangular plaquette. Such directional preference is a consequence of the single-ion anisotropy, and only the $\epsilon_T = 1$ configuration can explain the onset of an elliptical spiral since the easy and hard axes rotate by 120° between each triangle vertex.

Our work shows that integrated intensities, SNP and Schwinger scattering can determine the absolute structural, magnetic helical and magnetic triangular handedness of one and the same sample in the same experiment. The results are in perfect agreement with reported helical bunching [4], i.e. the rotation angle between successive spins along the c -axis is smaller when the spins are parallel to the easy axis in order to minimise the energy. Since a minus sign at any stage of the employed formalism would lead to the opposite result, the use of consistent scattering conventions is mandatory, something we have validated using optical methods on a certified quartz sample.

**Figure 3**

The envelope of the spin modulation along the c -axis is elliptical.

**Ketty Beauvois.** French
The ILL

'After finishing my PhD thesis on quantum fluids at the ILL in 2016, I moved to frustrated magnetism and started a post-doc as "instrument co-responsible" for the CRG's single-crystal diffractometer, D23. Since 2019, I have been co-responsible for the ILL's single-crystal diffractometer, D10.'

Dimer physics in the frustrated Cairo pentagonal antiferromagnet $\text{Bi}_2\text{Fe}_4\text{O}_9$

Two-axis, single-crystal diffractometer D23
in its polarised neutron mode
Three-axis spectrometer IN22

The research field of magnetic frustration is dominated by triangle-based lattices, but exotic phenomena can also be observed in pentagonal networks such as the well-known Cairo lattice. We demonstrate it here with the prototypical $\text{Bi}_2\text{Fe}_4\text{O}_9$ material. Thanks to a neutron scattering investigation we unveil various facets of its unconventional magnetism, including a rationalisation of its non-collinear magnetic order, exotic magnetic excitations and dimer physics.

AUTHORS

K. Beauvois (ILL)
V. Simonet, J. Robert and R. Ballou (Néel Institut, CNRS and Grenoble University UGA, France)
S. Petit (Léon Brillouin Laboratory, CEA-CNRS, Paris-Saclay University, France)
F. Bourdarot and E. Ressouche (Grenoble University UGA and CEA, Grenoble, France)

ARTICLE FROM

Phys. Rev. Lett. (2020) — doi:10.1103/PhysRevLett.124.127202

REFERENCES

- [1] E. Ressouche, V. Simonet, B. Canals, M. Gospodinov and V. Skumryev, Phys. Rev. Lett. 103 (2009) 267204
- [2] I. Rousochatzakis, A.M. Läuchli and R. Moessner, Phys. Rev. B 85 (2012) 104415

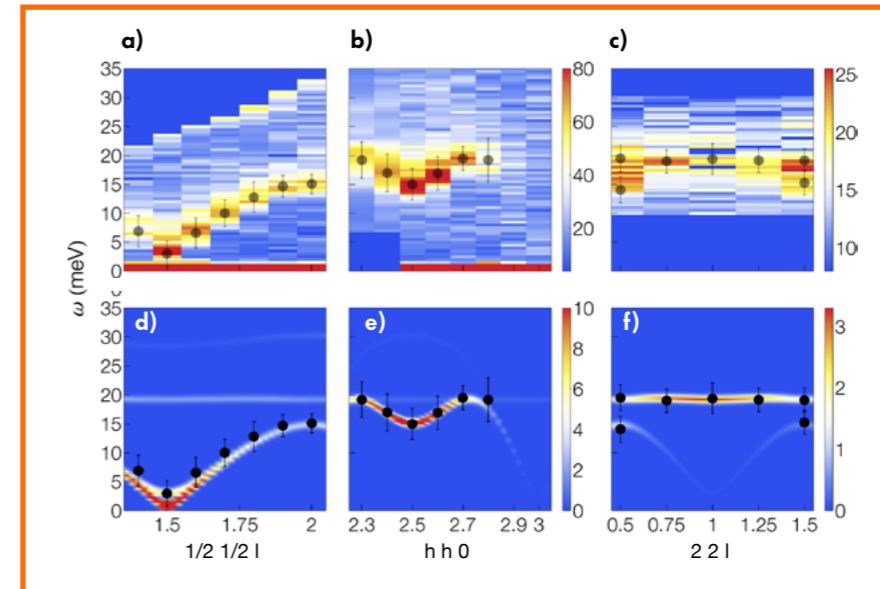
In $\text{Bi}_2\text{Fe}_4\text{O}_9$, the Fe^{3+} ions form a magnetic Cairo pentagonal lattice. With the odd number of bonds per pentagon the lattice is prone to geometric frustration, which results in competition between spin-pair interactions. It also has complex connectivity with three- and four-fold connected Fe_1 and Fe_2 sites, in contrast to the simpler, triangle-based lattices. This results in an unconventional ground state consisting of an orthogonal arrangement of the magnetic moments below the ordering temperature $T_N \sim 240$ K [1] (see **figure 1a**). This classical ground state was also obtained theoretically [2]. However, before our study no experimental determination of the microscopic ingredients at the origin of this peculiar order had been reported.

In the present study we show our measurements, using inelastic neutron scattering, of the rich excitation spectrum of $\text{Bi}_2\text{Fe}_4\text{O}_9$ reflecting the co-existence of local and collective motions of spins due to the complex geometry of the magnetic lattice.

Indeed, we observe a peculiar non-dispersive excitation located at a constant energy for all scattering vectors (see **figure 2c**). This is related to a local precession of a pair of Fe_2 spins (see **figure 1b**). In addition to this, expected dispersive spin waves, arising from a collective precession

**Figure 1**

a) Magnetic arrangement of the Fe_1 (in blue) and Fe_2 (in orange) on the pentagonal lattice. Blue ellipses emphasise strongly coupled antiferromagnetic Fe_1 spins.
b) Schematic description of the local motion of two Fe_2 spins responsible for the flat mode observed at 19 meV in the inelastic spectrum.

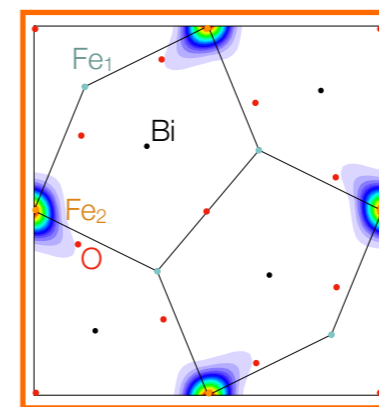
**Figure 2**

Measured **a-c** and calculated **d-f** dynamic structure factor $S(\mathbf{Q},\omega)$. The empty (filled) black points on top of the measured (calculated) $S(\mathbf{Q},\omega)$ give the fitted energy positions of the experimental spin wave dispersion. The flat mode is present at the energy of 19 meV.

of the magnetic moments around their equilibrium position, are visible (shown in **figures 2a-c**). These allow us to determine quantitatively the complex magnetic interactions in $\text{Bi}_2\text{Fe}_4\text{O}_9$ through comparison with spin wave calculations (displayed in **figures 2d-f**). Five isotropic, antiferromagnetic super-exchange interactions account for the magnetic order and the associated excitations, including the peculiar flat mode. Strikingly, there is a hierarchy in the strength of these interactions that results in a lattice with dominant pairs of antiferromagnetically coupled Fe_1 spins on almost orthogonal bonds (see **figure 1a**).

We investigated the fingerprint of these Fe_1 dimers in the paramagnetic state by measuring the magnetisation distribution induced by a magnetic field above T_N (see **figure 3**). We found that the induced magnetisation on site Fe_1 is vanishingly small, whereas the Fe_2 ions carry a non-negligible induced magnetic moment aligned along the field. The different responses of these two Fe types to the magnetic field confirms that even at a temperature where the thermal fluctuations are expected to prevent magnetic ordering, strong antiferromagnetic correlations persist between the Fe_1 pairs. They form an array of dimers in a sea of fluctuating Fe_2 spins.

Our study reveals, beyond the canonical examples of frustrated systems, novel behaviours that should be more generally observed in materials where the frustration is interlocked with complex connectivity and hierarchal interactions.

**Figure 3**

Magnetisation distribution projected along the c -axis measured with polarised neutrons (flipping ratio method) under a magnetic field $\mu_0H = 6$ T applied along $a-b$ at $T = 250$ K.



Ralf F. Ziesche, German
Diamond Light Source & The Faraday Institution
(UK)

'I regularly use neutron and X-ray computed tomography as unique, complementary tools to explore the dynamic processes of lithium diffusion, electrolyte usage and structural evolution in lithium batteries in three dimensions, over time.'

Correlative neutron/X-ray computed tomography of lithium batteries

Imaging instrument NeXT

Lithium batteries are one of the most promising candidates for powering future mobility and storing energy from renewable energy sources, as a result of their high-power density and cycle life. The investigation of internal processes in three dimensions (3D), such as structural changes in electrodes, is classically conducted using *in situ/operando* X-ray computed tomography (CT). Due to the nature of X-rays, light elements such as lithium and hydrogen (used in the battery electrolyte) are invisible. In contrast, neutron CT techniques are sensitive to such elements and provide information about the electrochemical changes during (dis-)charging.

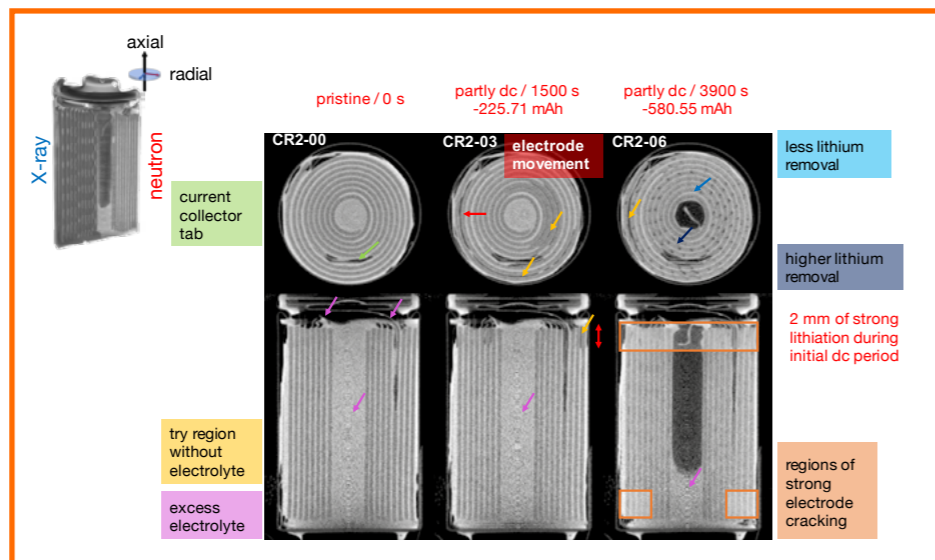


Figure 1

Reconstructed, 3D, *in situ* neutron CTs show vertical and horizontal orthogonal slices of a CR2 cell captured during the discharging (dc) process over a 4.7 Ω resistor. Here we can see the consumption of the excess electrolyte at the centre of the radial electrode, lithium diffusion and stronger cell activity in the upper section during the initial discharge period [3].

AUTHORS

R.F. Ziesche (UCL, Diamond Light Source and The Faraday Institution, UK)
A. Tengattini (ILL)

ARTICLE FROM

Nat. Commun. (2020) — doi:10.1038/s41467-019-13943-3/
J. Electrochem. Soc. (2020) — doi:10.1149/1945-7111/abfd9

REFERENCES

- [1] T.M.M. Heenan *et al.*, Mater. Today 31 (2019) 69
- [2] A. Tengattini *et al.*, Nucl. Instrum. Methods Phys. Res. A: Accel. Spectrometers, Defect. Assoc. Equip. 968 (2020) 1
- [3] R.F. Ziesche *et al.*, Nat. Commun. 11 (2020) 777
- [4] R.F. Ziesche *et al.*, J. Electrochem. Soc. 167 (2020) 140509

During the life span of lithium batteries the cells undergo several hundreds of charging cycles, during which Li-ions are transported between the positive and negative electrodes. A loss of capacity is caused by degradation processes of the active material which can be invoked by nano-cracking and which reduce the electrical and ion conductivity inside the micro-metre-sized, active particles. Such structural changes are commonly investigated by X-ray CT [1]. However, when using X-ray techniques, lithium diffusion or intercalation in the electrodes can only be detected indirectly by the swelling of the electrodes and the wetting of the electrodes by the electrolyte. Neutron CT enables this to be directly investigated through the high sensitivity to the natural lithium mixture of ^6Li and ^7Li and ^1H used in the electrolyte, which guarantees a high imaging contrast. This makes neutron CT the perfect complementary imaging technique to X-ray CT.

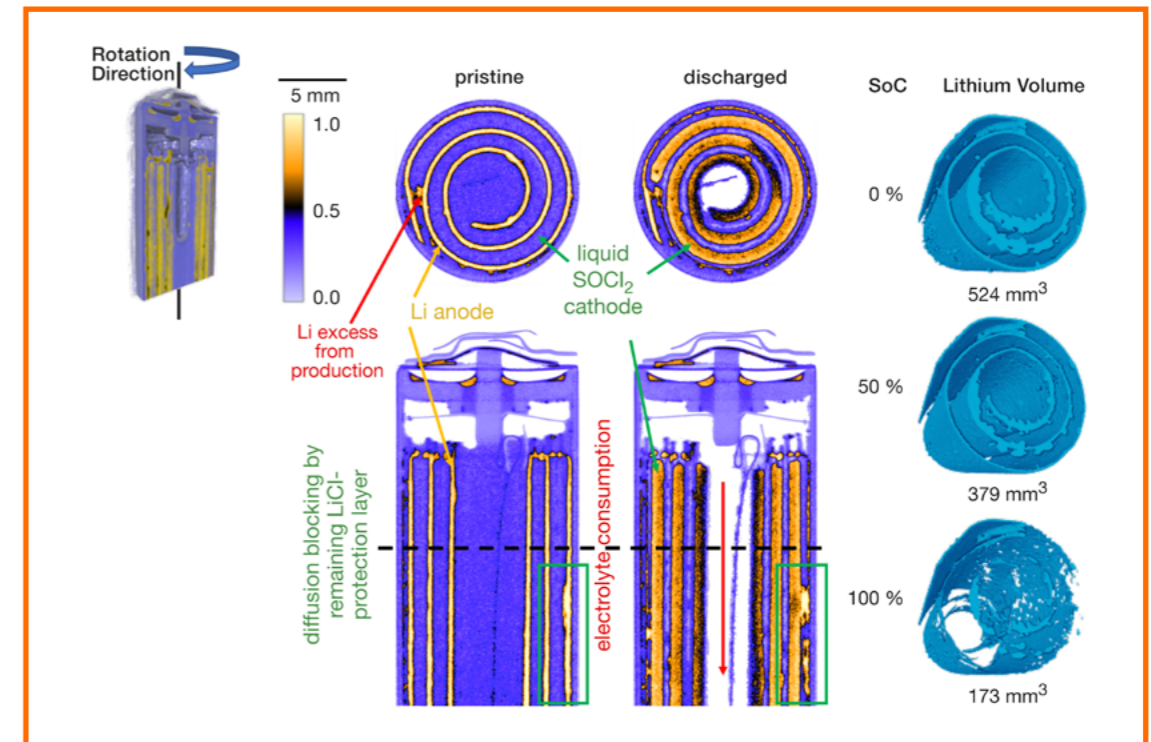


Figure 2

Reconstructed, 3D, orthogonal slices and the visualised lithium volume of an ER14505M thionyl chloride battery cell discharged with 100 mA. The removal of lithium from the lithium anode is quantitatively measured and intercalation in the cathode becomes visible, as does the electrolyte consumption at the centre of the axial cell [4].

Recent developments in neutron-imaging facilities have made a big step forward in spatial and temporal resolution. This is due to the development of more efficient detector systems and the installation of new neutron-imaging beamlines on high-flux neutron sources, such as the NeXT instrument at the ILL [2], which allow simultaneous neutron and X-ray imaging.

Figure 1 illustrates the 3D-rendered CT of a CR2 primary cell, where the left side of the electrode ensemble shows structural electrode features such as the active MnO_2 cathode permeated by a nickel mesh current collector. The right side and the orthogonal slices illustrate the discharging process, with the electrochemical changes imaged using neutron CT. Besides the consumption of the electrolyte, the cell shows high activity during the first discharge period in the upper axial section of the cell where the lithium anode and the electrolyte are fully consumed [3].

The high neutron flux of the NeXT instrument allows for four-dimensional imaging—3D spatially and 1D time-resolved—of the lithium diffusion and the electrolyte consumption of the battery cells, with a time resolution of 7.5 mins per CT. **Figure 2** shows orthogonal slices of a pristine and discharged SOCl_2/Li cell with the 3D-rendered and quantified volume change of the lithium electrode. The neutron data yield detailed information

about the Li-ion diffusion and blocking by the remaining LiCl from the protection layer, valuable information for future battery design and cell engineering [4]. Whilst here we have applied the techniques to primary, non-rechargeable cells, the methodology can be directly translated to rechargeable batteries, such as those found in electric vehicles, to study the degradation processes occurring over their long-term operation.

Neutron imaging opens up a wide range of possibilities for optimising the electrochemical processes in commercial lithium battery cells, offering the potential to improve cell capacity and performance and thereby reduce the amount of active material and help to reduce weight and costs. However, the investigation of dynamic processes is not limited to commercial cells; with higher spatially-resolved neutron CTs, below 4 μm , the study of the electrochemistry inside single secondary particles will be possible. Further, the use of different attenuating hydrogen ions in the electrolyte—high or low attenuating ^1H or ^2D —makes the investigation of lithium intercalation possible. Achieving a higher lithium contrast is possible using the higher-absorbing ^6Li as the working ion. The combination of neutron and X-ray imaging techniques allows for observations that are hidden to a single technique, thus providing a platform for unique findings and developments.



Leonardo del Rosso, Italian CNR, Istituto di Fisica Applicata 'Nello Carrara', Italy

'I am an experimental physicist interested in condensed matter. Currently, I'm enrolled as a scientist in the development of innovative neutron instrumentation for ESS. I have recently

investigated high-pressure gas hydrate compounds and ice, with a particular focus on their crystalline structure and dynamic properties.'

Transformation of ice XVII produces the cleanest cubic ice Ic

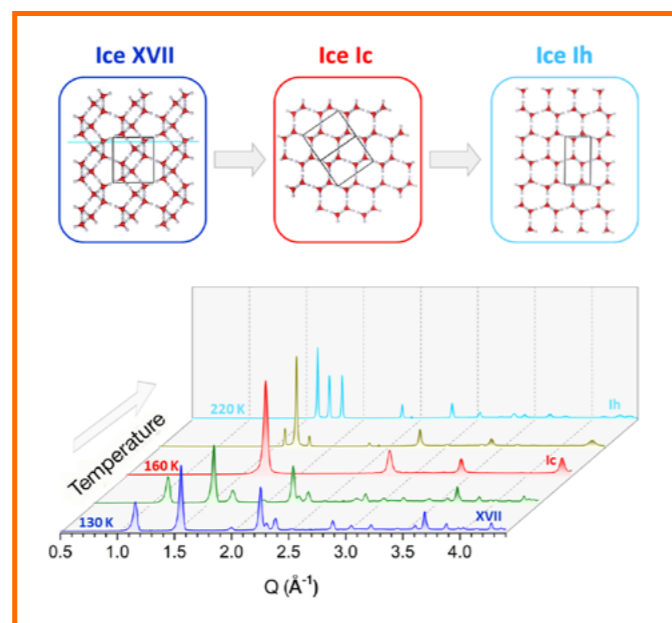
High-intensity two-axis diffractometer with variable resolution D20

HRPD diffractometer at ISIS

None of the samples of 'cubic ice' discovered so far has a fully cubic crystal structure. Instead, they are stacking-disordered forms of ice I (namely, ice I_{sd}), which contain both hexagonal and cubic stacking sequences of hydrogen-bonded water molecules. We have developed a method to obtain large quantities of cubic ice Ic, starting from a powder sample of D₂O ice XVII. Thanks to the high-resolution diffraction measurements performed on D20 we demonstrate its high structural purity, opening up the route for further investigations of this metastable ice form.

Figure 1

D20 neutron diffractograms of the ice powder sample during heating from 130 to 220 K and the consequent change in its crystalline structure. In the upper boxes, the three schematic figures represent the arrangement of the water molecules in the different types of ice investigated in this study: ice XVII, ice Ic (cubic) and ice Ih (hexagonal).



AUTHORS

L. del Rosso, M. Celli, F. Grazzi and L. Ulivi (IFAC-CNR, Italy)
M. Catti (University of Milano Bicocca, Italy)
T.C. Hansen (ILL)
A.D. Fortes (ISIS, UK)

ARTICLE FROM

Nat. Mater. (2020) — doi:10.1038/s41563-020-0606-y

REFERENCES

- [1] C.G. Salzmann, J. Chem. Phys. 150 (2019) 060901
- [2] L. del Rosso, M. Celli and L. Ulivi, Nat. Commun. 7 (2016) 13394
- [3] M. Catti, L. del Rosso, L. Ulivi, M. Celli, F. Grazzi and T.C. Hansen, Phys. Chem. Chem. Phys. 21 (2019) 14671
- [4] K. Komatsu, S. Machida, F. Noritake, T. Hattori, A. Sano-Furukawa, R. Yamane, K. Yamashita and H. Kagi, Nat. Commun. 11 (2020) 464
- [5] J. Amaya *et al.*, J. Chem. Phys. Lett. 8 (2017) 3216
- [6] T.L. Malkin *et al.*, Phys. Chem. Chem. Phys. 17 (2015) 60

Ice has always aroused considerable interest in science and technology, particularly because of the close link it has with the biosphere and, more generally, with anthropic activities. Although under standard conditions ice is a material of common experience, numerous studies have identified many different phases of it. To date, 19 of these are known, all of which are stable or metastable at different pressure and temperature conditions and different because of their crystalline structure.

Common ice, called ice Ih, has a hexagonal symmetry structure. In principle, a form of ice with cubic symmetry should also exist (ice Ic), but up to now no structurally pure cubic ice has ever been produced [1]. In fact, since the middle of the last century the numerous attempts pursued using different synthesis strategies—such as, for example, the freezing of ice from steam or the freezing of nano-drops of water—have always led to a form of cubic ice with a significant number of defects. This is usually called ice I_{sd} (stacking-disordered) and contains both hexagonal and cubic stacking sequences of hydrogen-bonded water molecules.

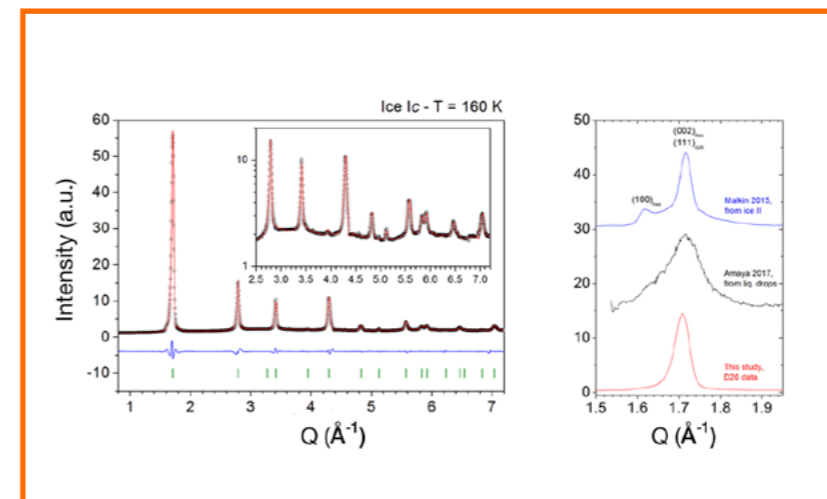


Figure 2

Left panel Rietveld fits (red line) with a single-phase model, *i.e.* $Fd\bar{3}m$ structure, of the D20 diffraction patterns (black circles) recorded for ice Ic at 160 K. The blue line and the green bars represent the residuals and the positions of the ice Ic reflections, respectively.

Right panel D20 neutron data (160 K, red curve) compared with an X-ray diffraction measurement of ice I_{sd} at 213 K (black curve), obtained from liquid nano-drops, with a cubicity of about 80 % [5]; and of ice I_{sd} at about 160 K (blue curve), obtained from a recrystallisation of ice II, with a cubicity of 73 % [6]. Data were adjusted and renormalised to facilitate the comparison.

Our team has finally identified a successful route to obtain the cubic phase of ice I with high structural purity, starting from ice XVII. This is a new form of ice, obtained from the C₀ hydrogen hydrate by releasing the hydrogen gas trapped inside the water skeleton [2]. Ice XVII has a very low density and is highly porous, capable of absorbing and desorbing gas repeatedly [3]. Probably because of these peculiarities, ice XVII has turned out to be a valid precursor of ice Ic. Indeed, by studying ice XVII under vacuum and subjecting it to slow heating we observed the transition to the pure form of cubic ice Ic at 140 K, verifying the metastability of this structure for temperatures below 180 K; above this the sample slowly turns into the common hexagonal ice Ih.

It is thanks only to an accurate structural analysis of ice XVII during its transformation (see **figure 1**), conducted with the advanced neutron instrumentation of the D20 instrument at the ILL (together with a further measurement campaign using the HRPD diffractometer at ISIS), that confirmation of the high level of purity of the cubic structure obtained with our procedure has been possible. This has subsequently been verified by the good quality of the Rietveld refinement of our data using a single-phase model, *i.e.* $Fd\bar{3}m$ structure, reported in the left panel of **figure 2**. Moreover, by comparing our raw experimental data for ice Ic with

instances of ice I_{sd} with some of the highest degrees of cubicity (*i.e.* the highest proportion of cubic stacking sequences) obtained to date (see **figure 2, right panel**), it is easy to observe the purity of our cubic structure. The D20 pattern (red curve) presents the only single and narrow $(111)_{\text{cub}}$ reflection, while the presence of a second reflection (blue curve) and the broadness of the main reflection (black curve) in the other cases demonstrate their lower degree of cubicity with respect to our case.

This study, together with a concomitant describing a similar result obtained by degassing a C₂ hydrogen hydrate [4], represents a milestone in the field of ice physics. In future, thanks to the large amount of cubic ice sample obtained by means of our route, scientists can fully characterise it from a structural and thermodynamical point of view—clarifying, for example, whether a temperature region of negative thermal expansion similar to hexagonal ice is present; or resolving the issue of the relative stability of the two polytypes of ice I present at ambient pressure, since the free energy difference is too low to be easily calculated using available computational methods. However, the reason why ice XVII is the precursor of ice Ic remains an open point of considerable physical interest that the whole scientific community is called upon to face.



Alexis Grimaud, French Collège de France, Paris
 'My research focuses on charge-transfer phenomena occurring at electrochemical interfaces for applications such as water electrolysis and batteries.'

Proton insertion to control the reactivity of water-splitting catalysts in acidic conditions

High-intensity powder diffractometer D20

The integrity of oxygen evolution reaction (OER) electrocatalysts, which are necessary to achieve good performance in the electrolysis of water and the evolution of hydrogen, suffers from the highly oxidising and acidic conditions in which the electrocatalysts operate. Only iridium-based oxides are believed to be stable enough to be used in practical electrolyzers, which, owing to the scarcity of iridium, greatly hampers their large-scale deployment. Furthermore, while more stable than 3d transition metal oxides, iridium oxides still suffer from dissolution and reconstruction upon use in acidic conditions. Developing new avenues to limit the dissolution of iridium-based catalysts and ensure their stability, as well as their strong performance, under prolonged operation is therefore fundamental to making hydrogen a viable energy carrier.

AUTHORS

P.E. Pearce, G. Rousse, J.-M. Tarascon and A. Grimaud
 (Collège de France, Paris, France)
 A. Iadecola (SOLEIL, France)
 J. Rodriguez-Carvajal (ILL)

ARTICLE FROM

Chem. Mater. (2019) — doi:10.1021/acs.chemmater.9b01976

REFERENCES

- [1] M.-F. Lagadec and A. Grimaud, Nat. Mater. 19 (2020) 1140
 [2] R. Zhang, P.E. Pearce, Y. Duan, N. Dubouis, T. Marchandier and A. Grimaud, Chem. Mater. 31 (2019) 8248

Controlling the reactivity and stability of active sites is of prime importance in the development of water-splitting electrocatalysts. This is especially true for the oxygen evolution reaction (OER), the half reaction of water splitting that oxidises water to produce oxygen as well as the electrons and protons necessary for the production of hydrogen. For this reaction, iridium-based oxides are the only catalysts stable enough to tolerate the strongly acidic conditions encountered in the so-called Proton Exchange Membrane Water Electrolyser (PEMWE), which is currently the technology of choice for producing hydrogen by electrolysis on a large scale [1]. Nevertheless, despite their relative stability compared with cheaper and more abundant 3d transition metal oxides, numerous studies continue to point to the reactivity of iridium oxides with water [2].

Figure 1

- a)** Online mass spectrometry for $\beta\text{-IrO}_3$ upon chemical exposure to 1 M H_2SO_4 .
b) Rietveld refinement of synchrotron XRD data for $\beta\text{-H}_2\text{IrO}_3$.
c) Thermogravimetric analysis with mass spectrometry data during THA showing the evolution of $m/z = 18$ and 32, corresponding to H_2O and O_2 .

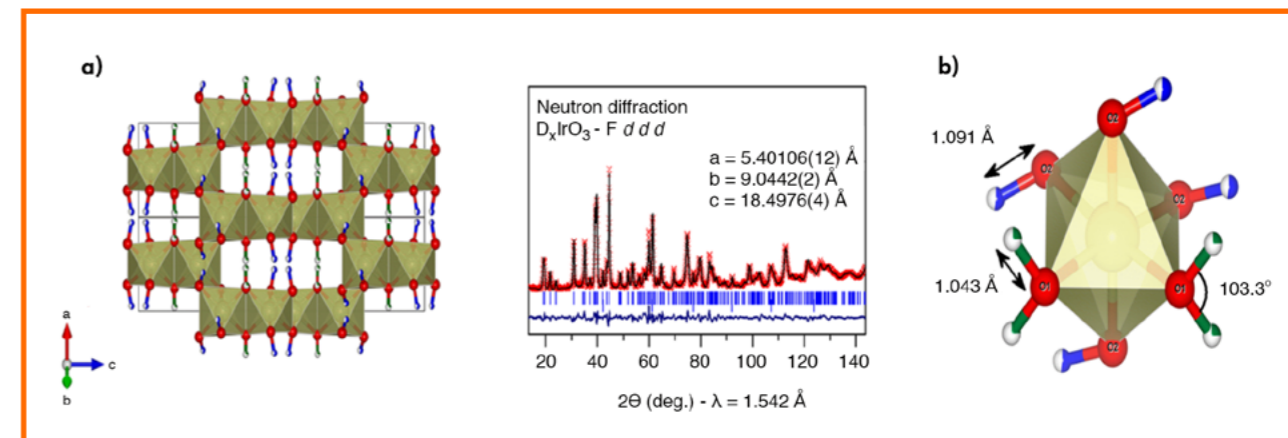
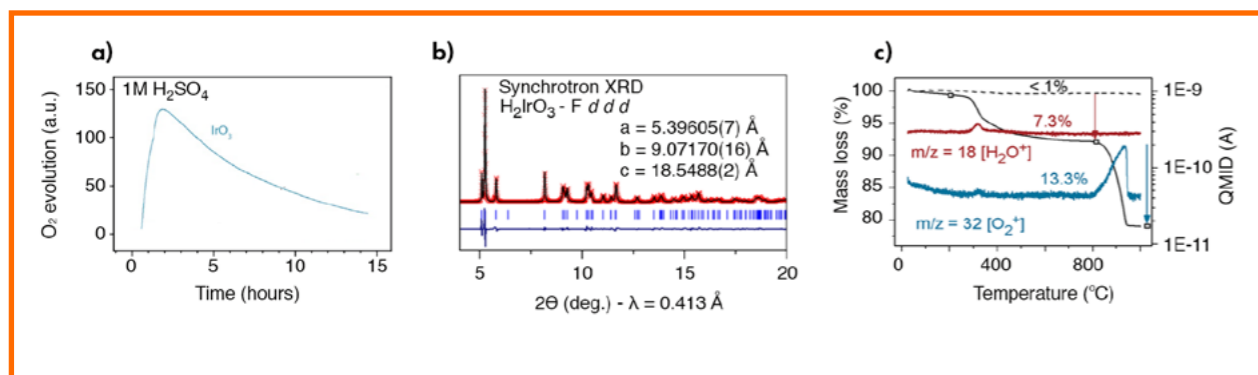


Figure 2

- a)** View of the $\beta\text{-H}_2\text{IrO}_3$ structure along the $[110]$ axis and Rietveld refinement of the neutron powder diffraction data for $\beta\text{-H}_2\text{IrO}_3$.
b) A close-up view of the IrO_6 octahedra with two proton positions (H1 in blue and H2 in green).

In this study, we first stabilised the high-valence iridium trioxide $\beta\text{-IrO}_3$ by delithiation of the $\beta\text{-Li}_2\text{IrO}_3$ phase. We then exposed this phase to H_2SO_4 solutions and studied its reactivity using mass spectrometry (**figure 1a**). We found that contact with the acidic solution generated a copious amount of gaseous oxygen. We then combined this observation with *ex situ* synchrotron X-ray diffraction to show not only that the water becomes oxidised to generate $\text{O}_{2(\text{g})}$, but also that the $\beta\text{-IrO}_3$ catalyst undergoes bulk transformation (**figure 1b**). In order to understand this bulk transformation, thermogravimetric analysis was carried out to detect the dehydration of the phase and the loss of protons, starting at around 300 °C (**figure 1c**). In this way we were able to demonstrate that the high-valence $\beta\text{-IrO}_3$ phase chemically reacts with water according to the equation: $\beta\text{-IrO}_3 + \text{H}_2\text{O} \rightarrow \beta\text{-H}_2\text{IrO}_3 + \frac{1}{2} \text{O}_2$.

Following on from this observation, the phase was then reacted in deuterated water in order to prepare the $\beta\text{-D}_2\text{IrO}_3$ phase. Neutron powder diffraction was performed on D20, the neutron diffractometer at the ILL, to refine the positions of structural protons using the Rietveld method (**figure 2a**). Two different positions were found: one forming hydroxyl groups with an O-H bond length of 1.091(6) Å; the second forming H_2O groups with an O-H bond length of 1.043(11) Å and an H-O-H angle of 103.3(6)°, this value being close to that for free water (**figure 2b**).

Highlighting this chemical reactivity is crucial to our understanding of the chemical reactivity of such Ir-based catalysts upon exposure to acidic conditions. Combining this post-mortem analysis with *operando* laboratory XRD and *operando* X-ray absorption spectroscopy at the Ir L-edge, we were able to demonstrate that the high-valence IrO_3 intermediate is constantly regenerated by electrochemical oxidation/deprotonation during water oxidation. Furthermore, the bulk insertion of protons stabilises the phase and prevents the dissolution of iridium that is normally encountered with such catalysts but which is largely reduced for this one, as demonstrated by our inductively coupled plasma (ICP) measurements. Thus, the ability to control the bulk insertion of protons will be core to developing new and stable, iridium-based OER catalysts.



Peter Zalden, German
European X-ray Free Electron Laser
'I work as an instrument scientist at the
Femtosecond X-ray Experiments (FXE) endstation
on the development of instrumentation for
single-shot X-ray scattering and other techniques.'

My scientific interest lies in glass formation in
fragile liquids, such as those formed by chalcogenides, and their
application in phase-change electronic memory.'

How phase-change materials form a stable yet rapidly crystallisable glass in memory devices

Disordered materials diffractometer D4

Phase-change materials (PCMs) such
as $\text{Ge}_{15}\text{Sb}_{85}$ and $\text{Ag}_4\text{In}_3\text{Sb}_{67}\text{Te}_{26}$
(AIST) are used in non-volatile random
access memory (NVRAM). Their glassy
(amorphous) and crystalline states provide
the property contrast needed to recover
stored information. While the archival
lifetime of this memory relies on the stability
of the glass against crystallisation, the
writing process requires fast crystallisation.
PCMs fulfil both requirements and
can be crystallised in less than a
nanosecond at elevated temperatures.

AUTHORS

P. Zalden (European XFEL, Germany)
H.E. Fischer (ILL)
K. Sokolowski-Tinten (University of Duisburg-Essen, Germany)

ARTICLE FROM

Science (2019) — doi:10.1126/science.aaw1773

REFERENCES

- [1] J. Orava, H. Weber, I. Kaban and A.I. Greer, *J. Chem. Phys.* 144 (2016) 194503
- [2] M. Salinga, E. Carria, A. Kaldenbach, M. Bornhöff, J. Benke, J. Mayer and M. Wuttig, *Nat. Commun.* 4 (2013) 2371
- [3] P. Zalden, A. von Hoegen, P. Landreman, M. Wuttig and A.M. Lindenberg, *Chem. Mater.* 27 (2015) 5641
- [4] C. Steimer, V. Coulet, W. Welnic, H. Dieker, R. Detemple, C. Bichara, B. Beuneu, J.P. Gaspard and M. Wuttig, *Adv. Mater.* 20 (2008) 4535
- [5] A.V. Kolobov, P. Fons, A.I. Frenkel, A.L. Ankudinov, J. Tominaga and T. Uruga, *Nat. Mater.* 3 (2004) 703

The crystallisation speed, *i.e.* the rate of the underlying nucleation and growth processes, is most dominantly controlled by the diffusivity D of atoms in the respective glass or supercooled liquid. Therefore, the temperature dependence of atomic diffusivity (or viscosity) has been the subject of several prior studies, which found that PCMs such as AIST show remarkably different behaviour from that of good glass formers such as SiO_2 (see **figure 1a**) [1–3]. This deviation from Arrhenius behaviour in the supercooled liquid regime is quantified in terms of fragility and has been reported, mostly to lesser degrees, in other materials. Because atomic diffusivity varies by many orders of magnitude between glass transition and melting temperatures, we refer instead to its activation energy,

$$E_A = k_B \times \frac{\partial \ln(D_0/D)}{\partial(1/T)}$$

In the case of PCMs, this activation energy strongly decreases when approaching the melting temperature upon heating. The aim of this study was to search for changes in the microscopic bonding mechanism that might be responsible for the change in kinetic properties.

Figure 1

a) While the temperature dependence of diffusivity follows Arrhenius behaviour with constant activation energy in the case of SiO_2 and slightly non-Arrhenius behaviour in the case of Se, one observes a pronounced change in the slope when comparing (supercooled) liquid AIST (points and triangles) with glassy/amorphous AIST (squares and circles). The point where these regimes merge is marked by a vertical dotted line.

b) Upon laser-induced heating, changes from the initial structure (obtained by neutron scattering) are observed in AIST by femtosecond X-ray scattering that indicate more than a simple increase in disorder.

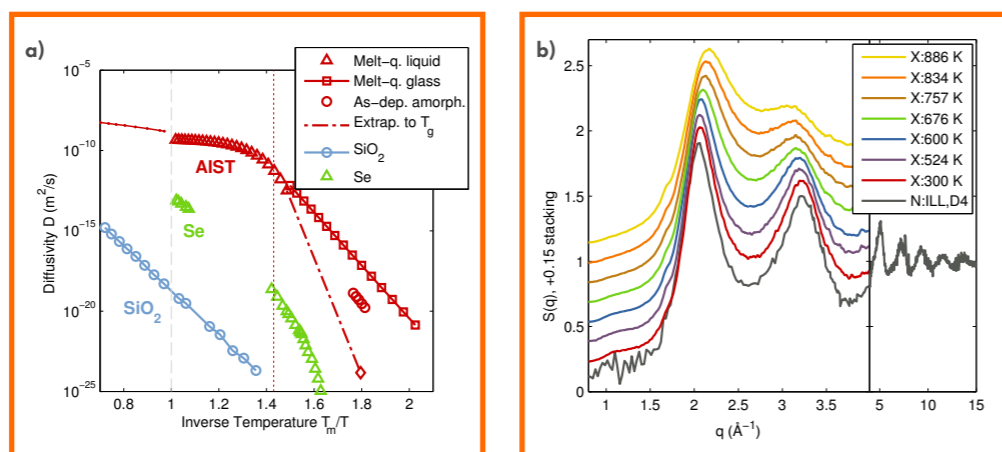


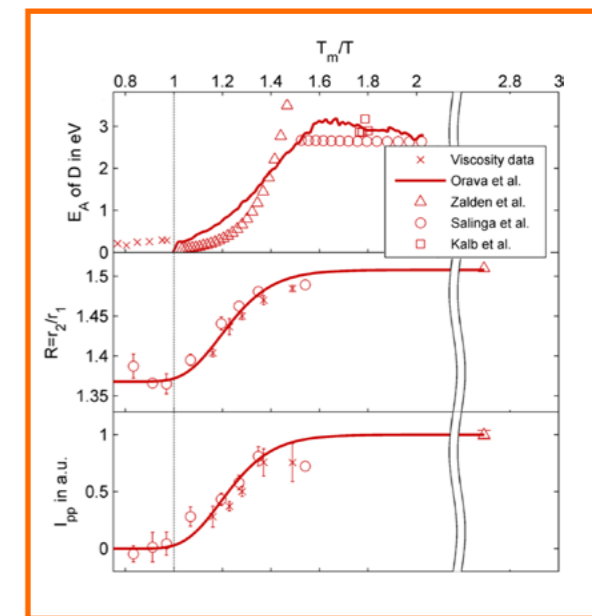
Figure 2

The pre-peak intensity and the ratio of interatomic correlation shell distances are shown for the PCM AIST as a function of temperature. Both structural parameters scale with the activation energy of diffusivity E_A , obtained from the data shown in figure 1a. The correlation reveals a structural contribution to the change in kinetics.

Investigations of the local atomic structure using total neutron scattering have already established that the equilibrium liquid of PCMs deviates from that of the amorphous (glassy) state [4, 5]. The large q -range accessible on the instrument D4 at the ILL enabled us to precisely measure the structure of amorphous AIST (**figure 1b**) and revealed a significant shortening of the first co-ordination shell, as compared with the liquid state. However, the structure of the 'intermediate' supercooled liquid state, from which the PCM crystallises during memory operation, could not be determined using conventional neutron or X-ray scattering techniques because it can be probed only for nanoseconds until crystallisation sets in. Due to further limitations in repeatedly performing the melt-quenching, femtosecond pulses of hard X-rays generated by the Linac Coherent Light Source (LCLS) at the Stanford Linear Accelerator Centre (SLAC) were used in this study. The initial amorphous state was heated by femtosecond optical pulses, and after a time delay of 100 to 300 ps the atomic structure was probed by X-ray pulses of 9.5 keV photon energy. Delay scans, performed by probing a fresh spot of material with every pulse, showed that during this time window the structure of the PCM did not change. Furthermore, effects caused by incomplete equilibration were ruled out. The experiments were performed in a transmission geometry with a 2D area detector recording the diffraction patterns produced by single pulses of X-rays interacting with a 50 nm film of PCM on a Si_3N_4 membrane.

The diffraction patterns shown in **figure 1b** are obtained after excitation of the sample with increasing laser fluence. The resulting temperature is calculated from the energy deposited into the film by the laser pulse and can be verified against diffraction data obtained at later delays (not shown here). Most importantly, the initial atomic structure at 300 K is found to be consistent with total neutron scattering measurements performed under static, ambient conditions on D4 at the ILL. In the case of AIST, the ratio of scattering cross sections of the dominant elements Sb and Te differs by only 6% for X-rays as compared to the ratio for neutrons, allowing direct comparison of the structure factors. At temperatures above 600 K, however, the first peak in $S(q)$ shifts to higher momentum transfer, whereas the second peak reduces significantly in intensity and shifts to lower momentum transfer.

Figure 2 shows structural parameters derived from the $S(q)$'s. In ambient conditions there is a pre-peak with intensity I_{pp} , centred at $q = 1.05 \text{ Å}^{-1}$, exactly half the momentum transfer of the strongest peak. Its intensity is associated with the presence of an additional spatial correlation with twice the interatomic spacing,



characteristic of a Peierls distortion. This distortion is found to decrease above 600 K and disappears before the temperature reaches the equilibrium melting point. The same behaviour is found for the ratio R of the radius of the second to the first co-ordination shells obtained from a transformation of $S(q)$ into real space. This transformation is strongly affected by the limited q -range available at this photon energy and could be used to extract co-ordination shell distances only because comparison with high- q neutron scattering data up to 20 Å^{-1} confirmed the assignment of co-ordination shells.

A qualitatively identical trend is observed in the PCM $\text{Ge}_{15}\text{Sb}_{85}$, and the temperature dependence of both structural parameters is in good agreement with the reduction in activation energy E_A upon heating (**figure 1a**). The correlation shows that the change in kinetic properties is probably caused by the structural transition, namely the disappearance of the Peierls distortion. This mechanism is plausible because the Peierls mechanism opens a band gap, localises electronic charge and thereby makes the chemical bonds more covalent. *Ab initio* molecular dynamics simulations performed to simulate the cooling process, starting from the liquid materials, confirm the trend of an increasing Peierls distortion and the opening of a band gap. This mechanism strengthens angular bonding constraints as compared with the (presumably) metallic, undistorted liquid at higher temperatures and makes the low-temperature state more rigid. The onset temperature of this structural transition upon heating coincides with the loss of the activation energy of the diffusivity when merging various data sets. Following the structural transition at different pump-probe delays we find no temperature dependence of the transition and therefore refer to the process as a liquid-liquid phase transition. This enables PCMs to reliably form a glass at low temperature and rapidly crystallise due to high atomic diffusivity over a wide range of elevated temperatures.



Finian Allen, English
Department of Chemistry,
University of Cambridge, UK
'I am in the final stages of my PhD in Physical
Chemistry at Cambridge and will soon be taking
up a postdoctoral position at the ISIS Neutron
Source. My work has focused on the adsorption

and interaction of organic species at mineral surfaces, using
techniques including neutron reflectometry. I will be moving on
to study adsorption under high shear and high pressure.'

Neutron reflectometry used to study transiently bound cation-bridged layers

Vertical reflectometer D17

The binding of negatively charged organic species to negatively charged clay mineral surfaces, which can be facilitated by specific inorganic cations in solution, is thought to be key to a number of processes including enhanced oil recovery. Neutron reflectivity provides an opportunity to characterise the molecular layers forming, without perturbing the delicate interactions occurring. Significantly, the present study revealed the nature of the cations that can facilitate adsorption, changing our previous understanding of the binding effect, and the nuances of reversibility and cation competition.

Figure 1

Neutron reflectivity data from mica exposed to AOT with different cations added, showing different profiles in each case. Reprinted with permission from [3]. Copyright 2019, American Chemical Society.

AUTHORS

F.J. Allen, C.L. Truscott and S.M. Clarke (University of Cambridge, UK)
P. Gutfreund (ILL)
R.J.L. Welbourn (ISIS, UK)

ARTICLE FROM

Langmuir (2019) — doi:10.1021/acs.langmuir.9b00533.

REFERENCES

- [1] L.R. Griffin *et al.*, Langmuir 32 (2016) 13054
- [2] J. Eastoe *et al.*, J. Chem. Soc., Faraday Trans 88 (1992) 461
- [3] F.J. Allen *et al.*, Langmuir 35 (2019) 5753

Adsorption of anionic species to anionic surfaces seems unlikely due to the repulsive electrostatics but has been observed to occur in the presence of specific cations. This has previously been described as 'divalent cation-bridging'. It is thought that this effect takes place between polar components in crude-oil and clay mineral surfaces in sandstone reservoirs. Understanding the nature and interactions of cation bridging may enable methods that efficiently liberate additional oil from existing reservoirs, limiting the need to develop new reservoirs as part of the energy transition away from fossil fuels.

The study of 'buried' interfaces, such as the solid-liquid interface under investigation here, is experimentally challenging. This is particularly true when the system under study is only weakly or transiently bound and when external probes may perturb the behaviour. Neutron reflectometry on instruments such as D17 and FIGARO at the ILL provides a non-invasive but highly sensitive tool for interfacial studies.

We have studied the adsorption of the anionic surfactant AOT on the clay mineral of muscovite mica, a popular substrate as the crystal can be cleaved to give atomically flat surfaces. Neutron reflectometry experiments on mica are non-trivial and require the use of a complex substrate consisting of a mica sheet supported by a highly polished silicon wafer. The sodium salt of the AOT anion, which has a sulfonate headgroup, has been shown not to adsorb to mica although adsorption in the presence of calcium has been reported [1]. AOT has been used in many studies of cation behaviour as the counter-ion may be exchanged for alternative species [2].

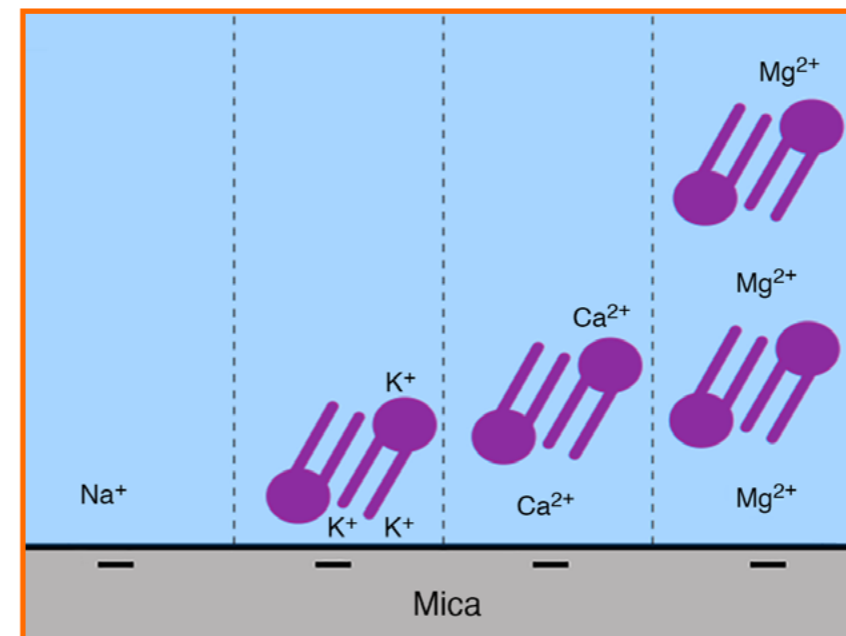
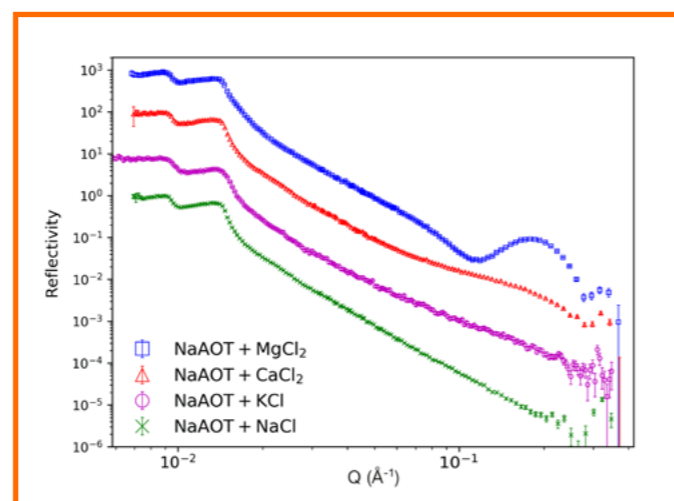


Figure 2

A schematic of the different structures fitted to AOT adsorbed to a mica surface in solutions with different inorganic salts present. Reprinted with permission from [3]. Copyright 2019, American Chemical Society.

Rather than exchanging the counter-ion, we have more closely replicated a real-world system by utilising the sodium salt and including additional cations in solution. In this way there will be multiple cations present that can compete for the surface and for the organic-solution species. In a series of experiments, we investigated the effect of adding sodium, potassium, calcium and magnesium ions. These are the most common cations in sea water, which is often used for water flooding in oil recovery. As ionic strength can affect the adsorption characteristics of ionic species, all solutions were buffered to the same ionic strength using sodium chloride.

The results of these experiments are shown in **figure 1**. No adsorption was seen for the sodium case, the reflectivity data being the same as those recorded for mica in pure water. Surprisingly, we did see adsorption for all the other added salts tested, with different structures evident in each case as seen in the different reflectivity profiles. It is particularly interesting that potassium ions can lead to a bridging interaction, as often treatment of flooding water focuses on the removal of divalent ions specifically.

Fits to the reflectivity data suggested single layers of AOT on the mica for the potassium and calcium cases but two layers with an intervening water layer when magnesium was added. A schematic of the fitted structure is given in **figure 2**. We further probed the relative concentrations at which the calcium ions in solution were still able to out-compete sodium and lead to adsorption of the organic. Even at concentration ratios of greater than 100:1 in favour of sodium, the same reflectivity data were recorded. This has potential consequences for flooding water design.

This contribution represents part of wider intense activity to understand mineral surfaces and their interaction with organic species in aqueous and non-aqueous solvents. It is evident that the unique insight made possible by neutron reflection at the ILL is a key facet of this work.



Christophe Candolfi. French Institut Jean Lamour, Université de Lorraine, Nancy, France
‘After completing a PhD in solid-state chemistry in 2008, I was a post-doctoral fellow at the Max Planck Institut in Dresden. I am currently associate professor at the École des Mines de

Nancy. My research activities, performed in the Institut Jean Lamour in Nancy, focus on optimising the thermoelectric properties of novel materials and understanding their lattice dynamics.’

Inelastic neutron scattering sheds light on the role played by strong disorder on the thermal transport of semiconducting sulphide materials for energy applications

Time-of-flight spectrometer IN6-SHARP

Order–disorder phenomena observed in copper-based chalcogenides are of interest for their impact on physical properties. Important parameters, such as band gap, charge carrier concentration and mobility, and phonon scattering, can be modified for a wide range of applications (photovoltaics, thermoelectrics, etc.). Recently, significant advances have been made in these fields as a result of a better understanding of the relationship between atomic disorder and transport properties in several well-known Cu-Sn-S-based materials, such as mohite Cu_2SnS_3 , colusite $\text{Cu}_{26}\text{V}_2\text{Sn}_6\text{S}_{32}$ and kesterite $\text{Cu}_2\text{ZnSnS}_4$. Compared with other sulphides, colusites exhibit high thermoelectric performance owing to their heavily-doped semiconducting behaviour coupled with extremely low lattice thermal conductivity. We show that the substantial lowering of lattice thermal conductivity originates from a disorder-driven process, thereby opening up new avenues for modifying the heat transport in thermoelectric chalcogenides.

AUTHORS

C. Candolfi and B. Malaman (Institut Jean Lamour, Nancy, France)
G. Guélou and E. Guilmeau (CRISMAT, Caen, France)
P. Lemoine (Université de Rennes, Rennes, France)
J.-M. Zanotti (LLB, CEA, Saclay, ILL-CRG, IN6-SHARP, Grenoble, France)

ARTICLE FROM

Phys. Rev. Mater. (2020) — doi:10.1103/PhysRevMaterials.4.025404

REFERENCES

- [1] G. Tan, L.D. Zhao and M.G. Kanatzidis, Chem. Rev. 116 (2016) 12123
- [2] V. Pavan Kumar, A.R. Supka, P. Lemoine, O.I. Lebedev, B. Raveau, K. Suekuni, V. Nassif, R. Al Rahal Al Orabi, M. Fornari and E. Guilmeau, Adv. Energy Mater. 9 (2019) 1803249
- [3] C. Bourges, Y. Bouyrie, A.R. Supka, R. Al Rahal Al Orabi, P. Lemoine, O.I. Lebedev, M. Ohta, K. Suekuni, V. Nassif, V. Hardy, R. Daou, Y. Miyazaki, M. Fornari and E. Guilmeau, J. Am. Chem. Soc. 140 (2018) 2186
- [4] V. Pavan Kumar, G. Guélou, P. Lemoine, B. Raveau, A.R. Supka, R. Al Rahal Al Orabi, M. Fornari, K. Suekuni and E. Guilmeau, Angew. Chem. Int. Ed. 58 (2019) 15455

Understanding the role played by atomic disorder in materials on their physical properties is of paramount importance for designing the next generation of compounds for energy-harvesting applications [1]. Physical parameters such as charge carrier mobility and phonon heat transport are often key parameters that determine the conversion efficiency of the resulting devices. Most of these parameters are, however, greatly impacted by the degree of disorder, increases in which usually lower their values. For thermoelectric applications, optimising the thermoelectric performance of doped semiconductors requires heat transport to be minimised and high carrier mobility concomitantly to be maintained [1]. In this field, disorder is thus as eagerly sought after as it is a source of worry. Achieving a compromise between these two properties in a compound necessitates enhancing its atomic disorder while preserving its electrically-conductive network.

In addition to being low-cost and environmentally-friendly materials, copper-based sulphides represent a particularly promising area of research when it comes to designing thermoelectric materials with highly conductive frameworks that can nevertheless accommodate sufficient structural disorder to disrupt the propagative, heat-carrying acoustic phonons [2–4]. Varying the synthesis conditions—an experimental dial, as it were—offers an effective strategy for modifying the structural disorder [3]. A particularly illuminating example of such behaviour is provided by colusites (**figure 1a**) that feature an electrically-conductive ‘ $\text{Cu}_{26}\text{S}_{32}$ ’ network, while significant disorder can be induced in the cationic tetrahedra through mixed occupancies by increasing the temperature of the consolidation process from 873 to 1023 K [3]. The stronger structural disorder that emerges leads to a spectacular reduction in lattice thermal conductivity κ_L , which then exhibits a temperature dependence that mimics that observed in amorphous compounds (**figure 1b**).

We used Mössbauer spectroscopy and powder inelastic neutron scattering experiments (**figure 2**) to investigate high-purity polycrystalline samples, in order to shed further light on the main driving mechanism. While the former technique can finely probe the atomic environment of the Sn atoms

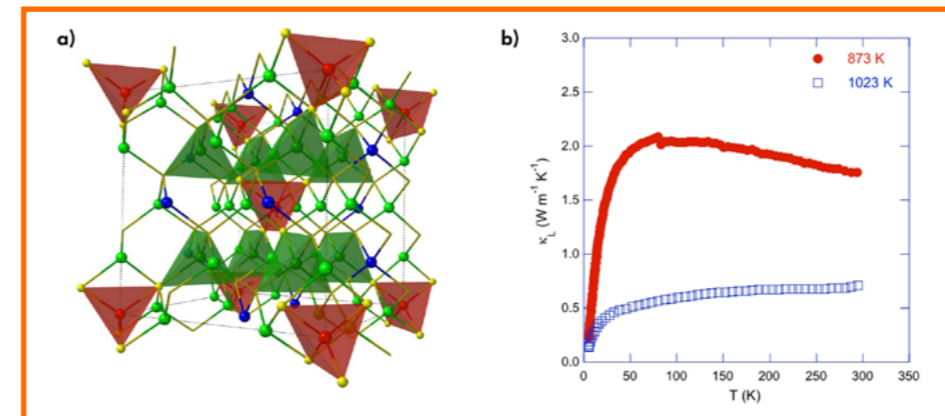


Figure 1

a) Perspective view of the cubic unit cell of colusites of general chemical formula $\text{Cu}_{26}\text{V}_2\text{Sn}_6\text{S}_{32}$.
b) Temperature dependence of the lattice thermal conductivity κ_L of polycrystalline samples of $\text{Cu}_{26}\text{V}_2\text{Sn}_6\text{S}_{32}$ consolidated at 873 and 1023 K. The high sintering temperature induces a drastic lowering of κ_L , which exhibits a glass-like temperature dependence.

as well as weak distortions from their ideal tetrahedral symmetry, the latter is a powerful tool for measuring the generalised vibrational density of states (GVDOS) and their evolution upon cooling or warming, thus providing important information on lattice anharmonicity. Comparison of the Mössbauer spectra (**figure 2a**) collected on one sample consolidated at 873 K and another at 1023 K revealed a significant broadening of the line shape in the latter sample. Further refinement of the two spectra, using a sharpening procedure that makes fine differences more visible, confirms the presence of disorder in both samples. However, the degree of disorder is clearly enhanced in the sample consolidated at 1023 K as shown by the two peaks, attributed to a doublet and a singlet respectively, characteristic of the site symmetry. These results show that only a small fraction of the Sn atoms (35 %) is located on the high symmetry site while the remaining fraction is on the lower symmetry site.

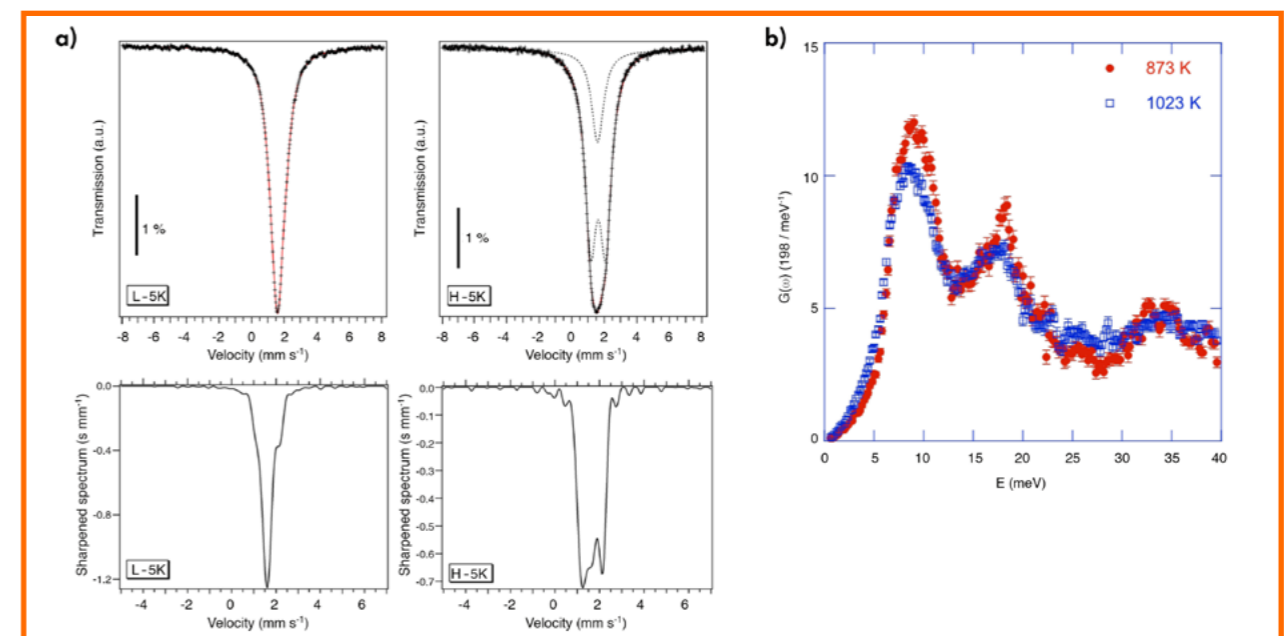
Overall, this analysis demonstrates the higher degree of disorder achieved in the sample consolidated at 1023 K.

This conclusion is supported by comparing the GVDOS measured on both samples at 300 K (**figure 2b**). These measurements show a smearing tendency of the main features of the GVDOS in the most disordered sample, supporting the idea that increasing the temperature of the consolidation process significantly increases the level of disorder in the unit cell. Further measurements, performed at 100 K and 500 K, revealed no anomalous temperature shifts that would correspond to anharmonicity beyond that associated with unit cell expansion.

The combined results from these spectroscopic tools clearly highlight the role played by disorder in driving heat transport in colusites to a level that mimics that encountered in amorphous compounds, which ultimately leads to enhanced thermoelectric performance.

Figure 2

a) Mössbauer spectroscopy performed at 5 K on the samples consolidated at 873 K (**left panels**) and 1023 K (**right panels**). The upper panels show the measured data while the lower panels have been obtained by a sharpening procedure to highlight the difference in the disorder of the unit cell between the two samples.
b) Generalised phonon density of states measured at 300 K on the time-of-flight spectrometer IN6-SHARP for two $\text{Cu}_{26}\text{V}_2\text{Sn}_6\text{S}_{32}$ samples consolidated at 823 and 1023 K.





Eleonora Vottero, Italian
Department of Chemistry, NIS Centre and
INSTM, University of Turin, Italy.
*'I am at the end of my PhD, carried out under
the co-tutorship of the ILL and the University of
Turin. In collaboration with the company
Chimet, I am working on the characterisation*

*of precious metal nanoparticle catalysts and their activated carbons
supports, using neutron and infrared spectroscopies in parallel with
computational simulations.'*

How do the graphenic domains terminate in activated carbons and carbon-supported metal catalysts?

Three-axis spectrometer LAGRANGE

Activated carbons are large surface area, carbonaceous materials, widely employed as adsorbent or storage materials as supports in heterogeneous catalysis or as catalysts in their own right [1]. Their textural, morphological and surface properties are greatly affected by both the nature of the starting precursor and the activation procedure and have dramatic effects on their catalytic performance [2]. A detailed understanding of the microscopic structure of activated carbons is therefore essential for optimising their performance in catalysis.

AUTHORS

E. Vottero, E. Groppo and M. Carosso (University of Turin, Italy)
R. Pellegrini (Chimet SpA Catalyst Division, Viciomaggio Arezzo, Italy)
A. Piovano and M. Jimenez-Ruiz (ILL)

ARTICLE FROM

Carbon 169 (2020) — doi: <https://doi.org/10.1016/j.carbon.2020.07.033>

REFERENCES

- [1] F. Rodríguez-Reinoso, Handbook of Porous Solids (2002) 1766
- [2] B.S. Girgis, S.S. Yunis and A.M. Soliman, Mater. Lett. 57 (2002) 164
- [3] P. Yan, B. Zhang, K.-H. Wu, D. Su and W. Qi, Carbon 143 (2019) 915

Among the numerous techniques that can be employed to characterise activated carbons [3], Inelastic Neutron Scattering (INS) spectroscopy stands out as one of the most powerful for determining the nature of the C-H terminations of the graphenic domains. The technique is in principle characterised by the absence of selection rules and by strong sensitivity to the vibrational modes involving the displacement of hydrogen atoms, providing information not accessible via the most commonly employed FTIR and Raman spectroscopies. We have provided evidence of its potential in chemical research by showing its application in supported Pt- and Pd-based (5 % wt load) industrial catalysts for hydrogenation reactions.

INS spectroscopy provided details of the interaction between the metal nanoparticles and the carbon support. **Figure 1a** shows the INS spectra of one Pt- and two Pd-based catalysts and of the corresponding carbon support (of wood origin, Cw), measured on the LAGRANGE spectrometer at the ILL. The deposition of the metal nanoparticles results in a decrease in the spectral intensity, which indicates a reduction in the number of C-H terminations in the support. The central band is the

Figure 1

- a)** Comparison between the experimental INS spectrum of the activated carbon support (Cw) and of the corresponding three catalysts (Pt(R)/Cw, Pd(NR)/Cw and Pd(R)/Cw).
b) Fit of the INS spectrum of the activated carbon Cw using a linear combination of the contribution of regular and defective C-H terminations (Z1D, D-all, Disordered Z1, Isolated Z1 and Single Vacancy). We report an example of the geometry of each contribution, for clarity.

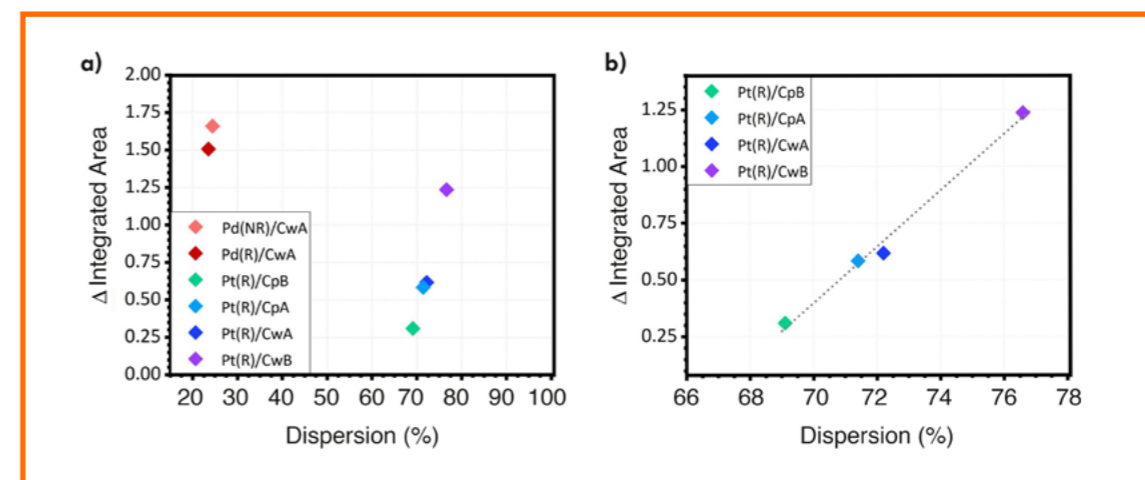
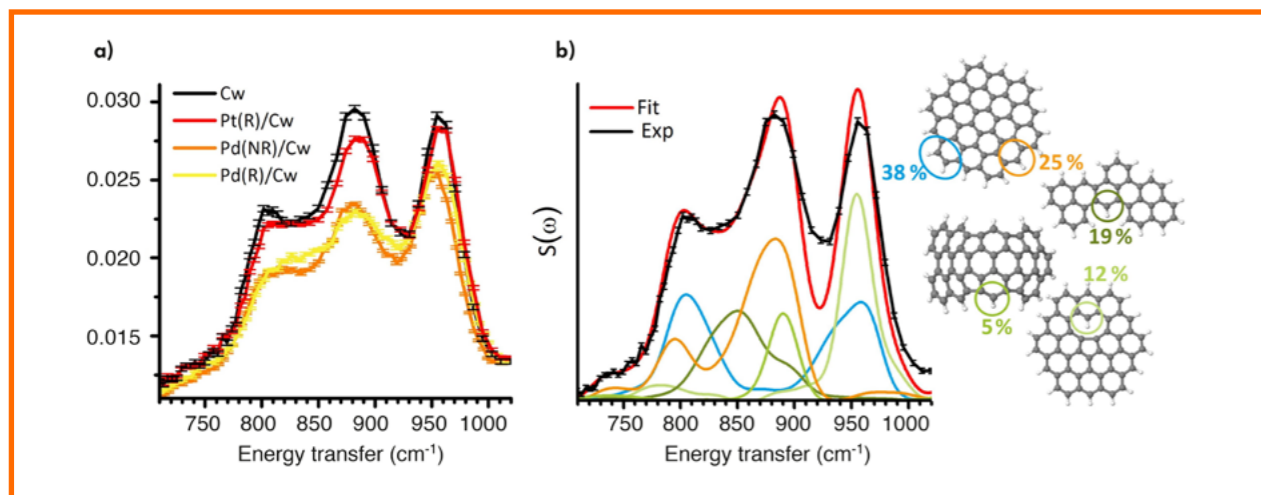


Figure 2

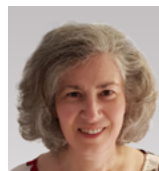
- a)** Difference in the integrated area in the 690–1020 cm^{-1} region between the activated carbon support and the corresponding catalysts, plotted against the metal nanoparticles' dispersion.
b) Detail of the supported Pt catalysts values showing a linear trend.

most affected, meaning that not all the terminations are perturbed by the nanoparticles to the same extent. We compared the experimental spectra with the results of DFT simulations on a very large number of aromatic models that reproduced the INS fingerprints of regular and defective C-H terminations in activated carbons. By fitting the experimental spectra with a linear combination of the simulated ones (**figure 1b**) we found that the species most affected by the deposition of the metal nanoparticles are benzene rings exposing a single C-H group, indicating that the metal nanoparticles preferentially interact with these sites.

We used the integrated area of the spectra in the out-of-plane bending region (690–1020 cm^{-1}) to evaluate the H concentration in each of the samples. For this, we plotted in **figure 2** the variation in the integrated area of the spectra for all the catalysts with respect to the bare carbon support against the metal nanoparticles' dispersion. For the Pt catalysts, the decrease in the

integrated area (*i.e.* of H concentration) is directly proportional to the dispersion of the metal nanoparticles (**figure 2b**). This observation suggests that the smaller the nanoparticles, the higher their interaction with the borders of the graphenic platelets. The two Pd catalysts exhibit larger variations in H content despite their low dispersion (**figure 2a**), suggesting that Pd nanoparticles interact more than Pt ones with the C-H terminations.

In conclusion, this study focused on determining the most likely border morphologies in the H-terminated graphenic domains that constitute activated carbons used as supports for metal nanoparticle catalysts. We were able to quantify the concentration of each terminal C-H species in the samples and to identify the species most affected by the metal nanoparticles' deposition. Specific benzene rings exposing a single C-H group appear to have a decisive role in their interaction with the metal nanoparticles and their deposition procedure.



Christine M. Papadakis, German Physics Department of the Technical University of Munich, Germany
‘I study self-assembling and (multi-)responsive polymer systems, polymers of complex architecture, polymers for medical applications and block co-polymer thin films.’

For this, scattering methods at large facilities are widely used. In situ, high-pressure experiments allow us to gain new insight into the interactions between polymers and solvents.’

Pressure dependence of the co-non-solvency effect in aqueous poly(*N*-isopropylacrylamide) solutions

Small-angle neutron scattering instrument D11

Co-solvents are essential in many contexts, e.g. pharmaceutical formulations. In biological systems, small organic molecules acting as co-solvents can alter the folding/unfolding equilibrium of proteins or facilitate the dissolution of hydrophobic molecules. In responsive polymers in mixed solvents, the striking phenomenon of co-non-solvency has been observed: while the polymers are readily soluble in water and in an organic solvent, they become insoluble at certain compositions of the mixture. High pressure reverses this effect, leading to a hugely expanded solubility range. We use small-angle neutron scattering (SANS) to reveal the pressure-dependent interactions between the polymer and the solvent mixture that are associated with this intriguing phenomenon.

Figure 1

a) Coexistence lines $T_{cp}(p)$ of the 3 wt% PNIPAM solutions in pure D_2O (dashed blue line) and in 80:20 v/v D_2O/CD_3OD (full red line).
b) Representative SANS data from a temperature scan at 265 MPa below $T_{cp}(p)$ (symbols). Black lines are model fits.

AUTHORS

B.-J. Niebuur, C.-H. Ko, X. Zhang, K.-L. Claude and C.M. Papadakis (Technical University of Munich, Germany)
A. Schulte (University of Central Florida, Orlando, USA)
L. Chiappisi (ILL and Technische Universität Berlin)

ARTICLE FROM

Macromolecules (2020) — doi:10.1021/acs.macromol.0c00489

REFERENCES

- [1] M. Shibayama, K. Isono, S. Okabe, T. Karino and M. Nagao, *Macromolecules* 37 (2004) 2909
- [2] G. Yuan, X. Wang, C.C. Han and C. Wu, *Macromolecules* 39 (2006) 3642
- [3] T. Norisuye, N. Masui, Y. Kida, D. Ikuta, E. Kokufuta, S. Ito, S. Panyukov and M. Shibayama, *Polymer* 43 (2002) 5289
- [4] A. Pica and G. Graziano, *Biophys. Chem.* 231 (2017) 34

To answer why the temperature- and pressure-dependent phase behaviour of poly(*N*-isopropyl acrylamide) (PNIPAM) is so strongly affected by the addition of methanol, we used SANS, which allows us to elucidate the effect of methanol on the chain conformation of the polymer. A 3 wt% solution of PNIPAM in a water-methanol mixture (80:20 v/v) was studied as a function of temperature at different pressures. At elevated pressures, the presence of a co-solvent significantly increases the single-phase region in the temperature–pressure frame (**figure 1a**): the elliptic coexistence line formed by the pressure-dependent cloud points $T_{cp}(p)$ (determined by turbidimetry) is much broader than that for PNIPAM in pure D_2O [1].

SANS temperature scans were carried out at pressures between atmospheric pressure (0.1 MPa) and 265 MPa; this is 2.5 times the pressure found at the bottom of the Mariana Trench, the deepest oceanic trench on Earth.

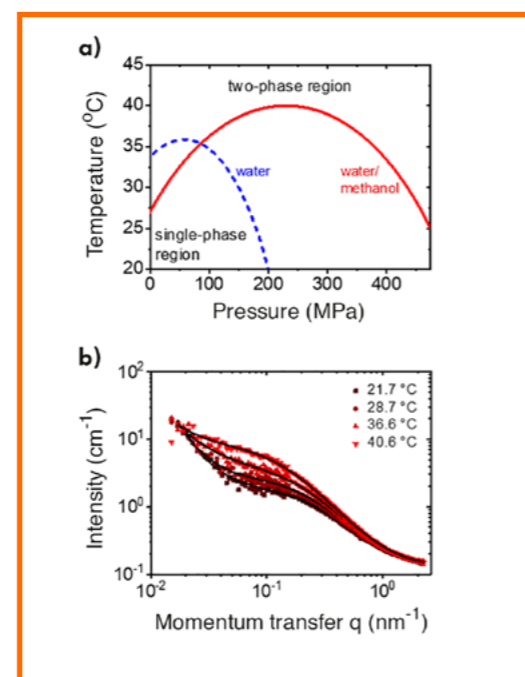


Figure 2

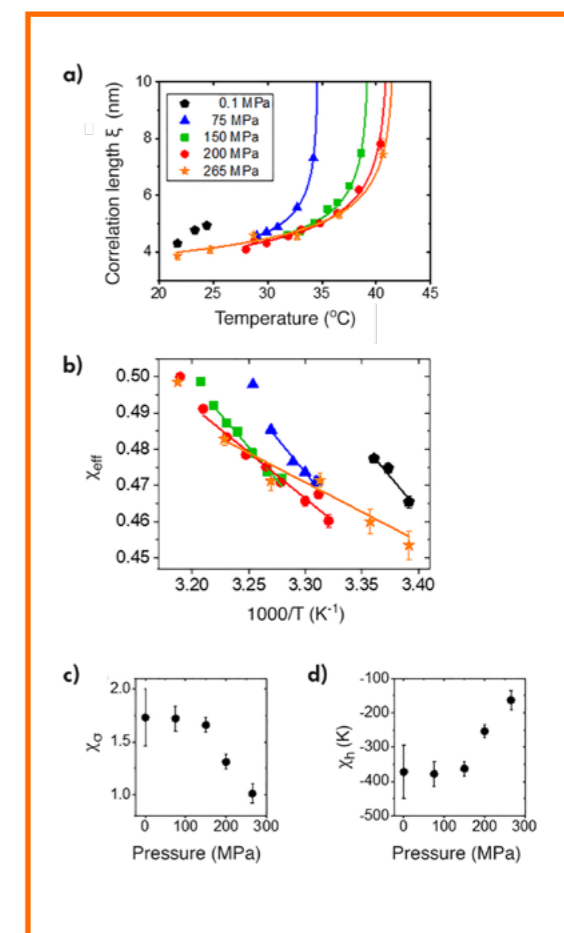
a) Correlation length of concentration fluctuations, ξ , as a function of temperature in the single-phase state at the pressures given in the graph. The lines are fits of power laws.
b) Effective polymer–solvent interaction parameter χ_{eff} as a function of inverse temperature. Same symbols as in (a). The lines are fits of equation 1.
c, d) Entropic and enthalpic components of the polymer–solvent interaction parameters χ_σ and χ_h , as a function of pressure.

Figure 1b shows representative scattering curves below T_{cp} at 265 MPa measured on D11, the 40 m-long SANS machine at the ILL. A shoulder at $q \approx 0.2 \text{ nm}^{-1}$ is observed, which is caused by concentration fluctuations of the polymer solution at length scales in the nanometre range. In addition, weak forward scattering at $q < 0.05 \text{ nm}^{-1}$ is present, pointing to large-scale inhomogeneities. To extract quantitative structural information, the scattering curves are modelled using the Ornstein–Zernike structure factor, which yields the correlation length of the concentration fluctuations, ξ , and an additional term accounting for scattering by large-scale inhomogeneities. In the single-phase state, ξ can be assigned to the distance between overlap points in the semi-dilute solution [2] and is therefore related to the chain conformation. Excellent fits are obtained. We have summarised the results of the fits in **figure 2**. In the single-phase state, the correlation length ξ increases with temperature at all pressures, diverging near $T_{cp}(p)$. Thus, with increasing temperature the chains shrink, which increases the distance between overlap points between the chains.

From the correlation length ξ [3] obtained from the neutron scattering data, the effective Flory–Huggins interaction parameter, χ_{eff} , can be extracted. It describes the interaction strength between the polymer segments and the solvent mixture. At all pressures, χ_{eff} is ~ 0.45 – 0.47 at the lowest measured temperatures and increases with temperature (**figure 2b**). Thus, at all pressures, the solvent mixture changes from being a good solvent far below $T_{cp}(p)$ to being a theta solvent for PNIPAM near the cloud point. Both local entropic and enthalpic effects contribute to the polymer–solvent interaction parameter χ_{eff} . In the commonly used expression

$$\chi_{eff} = \chi_\sigma + \frac{\chi_h}{T}, \quad (1)$$

these contributions are described by the parameters χ_σ and χ_h , respectively. Fits of equation 1 above to the data (**figure 2b**) allow us to examine the pressure dependence of both contributions individually, as shown in **figure 2c** and **d**. χ_σ may originate from the hydrophobic effect, which favours de-mixing. The decrease in this parameter with pressure indicates that



the hydrophobic effect is weakened at high pressures. This may be due to the release of methanol from the PNIPAM chains at high pressures [4], which leads to an enrichment of the solvent phase with methanol. This weakens the hydrophobic effect and stabilises the single-phase region. The observed decrease in the magnitude of χ_h with pressure suggests that the tendency to mix on enthalpic grounds becomes weaker, possibly due to a lower number of hydrogen bonds between the polymer chains and water at high pressure. The resulting reduction in overall chain solvation may therefore lead to weaker enthalpic polymer–solvent interactions, which is consistent with the contraction of the chain conformation in the single-phase state at high pressures (**figure 2a**).

In conclusion, high-pressure SANS measurements in the single-phase state of PNIPAM in water/methanol reveal the pressure-dependent chain conformation. Analysis of the effective Flory–Huggins interaction parameter indicates that the enthalpic polymer–solvent interactions and the hydrophobic effect are weakened at high pressure, which may be related to the contracted chain conformation. These changes in interactions may be related to the largely expanded solubility region in the temperature–pressure phase diagram in the water/methanol mixture compared with pure water.



Vincenzo Calabrese, Italian
Department of Chemistry, University of Bath, UK
Twitter: @vincenz67878664
'I am a postdoctoral scholar at OIST (JP). My research focuses on the structure-property relationship of colloidal rods under flow.'

Filler size effect in an attractive fibrillated network: a structural and rheological perspective

Small-angle scattering instrument D22

The formulation of hydrogels with tuneable rheological properties is of pivotal importance for process optimisation and for creating products that appeal to consumers. We show that by adding colloidal fillers to a fibrillated hydrogel composed of cellulose nanofibrils, the rheological properties can be easily controlled. Contrast-matched, small-angle neutron scattering (SANS) experiments allowed us to determine the architecture of the fibrillar network and thus to establish a relationship between the filler size and the mesh size of the network. These results will aid the rational design of soft materials for specific rheological responses.

Figure 1
a) SANS patterns of the 1 wt% OCNF-based gels. The lines describe the fitting of a model of non-interacting flexible cylinders with an elliptical cross section.
b) Residual plot from the fits in (a). Reproduced from [1].

AUTHORS

V. Calabrese (Department of Chemistry, University of Bath, UK)
K.J. Edler (Department of Chemistry, University of Bath, UK)
L. Porcar (ILL)

ARTICLE FROM

Soft Matter (2020) — doi:10.1039/C9SM02175B.

REFERENCES

[1] V. Calabrese, M.A. da Silva, L. Porcar, J. Bryant, K.M. Zakir Hossain, J.L. Scott and K.J. Edler, *Soft Matter* 16 (2020) 3303

Hydrogels composed of networks of fibres are industrially relevant materials due to their deformation-dependent rheological properties. This property makes fibrillated hydrogels especially suitable for applications in personal care and food products, where a large deformation range is required for processing operations and to generate the flow and sensory properties expected by customers.

In this study we investigate how the addition of colloidal fillers, in the form of silica nanoparticles (SiNp), affects the structural and rheological properties of a fibrillated hydrogel composed of partially oxidised cellulose nanofibrils (OCNF). Such fillers can be employed to tune mechanical properties of the materials such as structural breakage (yielding), flow, structural recoverability and plasticity, while remaining environmentally benign.

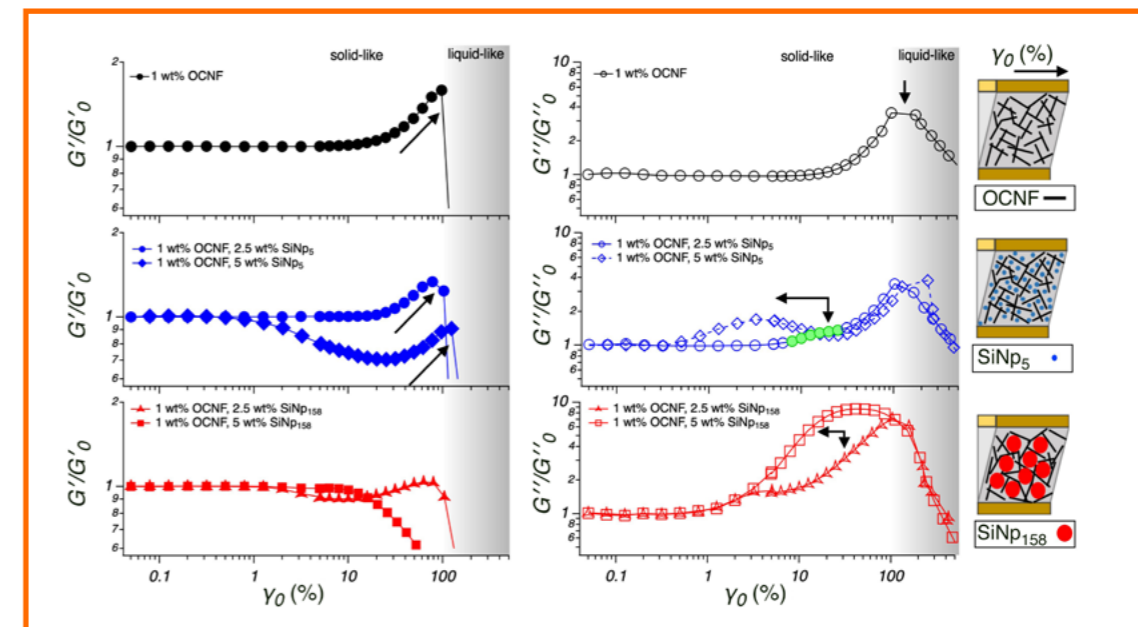
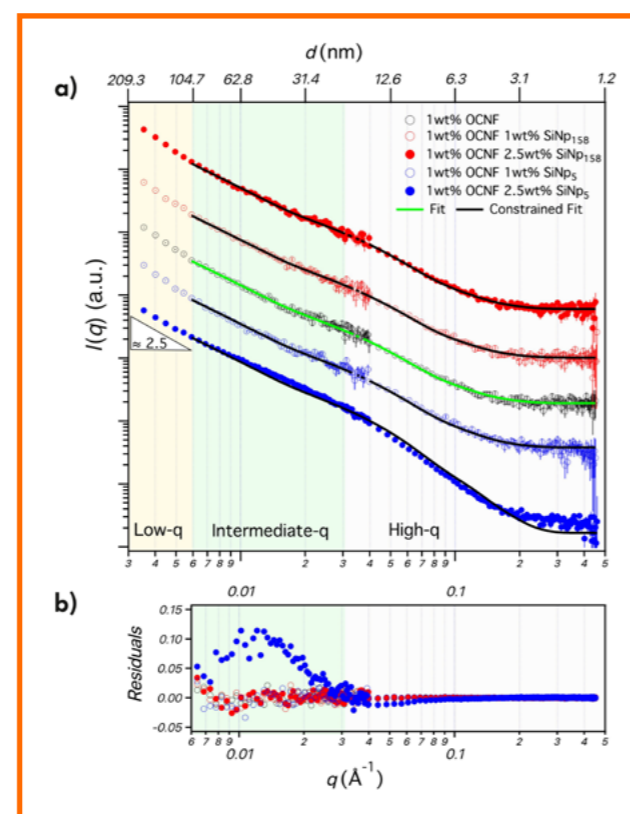


Figure 2
Strain sweep for the OCNF-based hydrogels. Normalised values of the elastic and viscous moduli, G' and G'' , respectively, as a function of strain (γ_0). On the right are schematics of the OCNF-based hydrogels upon deformation. Adapted from [1].

Specifically, we use silica nanoparticles with an average dimension of 5 nm (SiNp_5) and 158 nm (SiNp_{158}), which are, respectively, of a similar size to the mesh size of the OCNF network and ca. five times larger than the mesh size of the network. These impart distinctly different properties to the resulting gels.

As filler-network compatibility must be carefully considered in order to avoid undesired phenomena during a product's shelf-life, the effect of SiNp_5 and SiNp_{158} on the structural properties of the OCNF network was revealed by contrast-matched SANS experiments (figure 1). SANS experiments conducted using the small-angle scattering diffractometer D22 (ILL) allowed us to explore the structural properties of the network at nm-length scales. Data from the OCNF hydrogel were fitted, in the q region where interfibrillar interactions are not detectable (high- q and intermediate- q range), to a model of non-interacting flexible cylinders with an elliptical cross section. The SiNp -OCNF mixtures could also be well modelled as OCNF alone, indicating that the network architecture is unaffected by the presence of the fillers.

The structural insights provided by the SANS experiment are essential to understanding the rheological response of the hydrogels upon large deformations (figure 2). The OCNF hydrogel undergoing an increasing oscillatory shear displayed characteristic overshoots of the elastic and viscous moduli (G' and G'' , respectively). The addition of SiNp_5 kept the elastic fingerprint unperturbed while generating a second viscous overshoot. Conversely, the addition of SiNp_{158} smoothed the elastic overshoot but enhanced the viscous contribution.

The difference in the behaviour of the SiNp_5 and the SiNp_{158} gels is associated with the ability of SiNp_5 to fit within the mesh size of the OCNF gel network without altering the dynamics of the network upon large amplitude oscillatory shear (see schematic in figure 2). In contrast, the presence of the larger filler, SiNp_{158} , resulted in a gradual structural breakage as the SiNp_{158} could actively dislodge the junctions of the network. The fundamental understanding arising from this study has implications for industrially relevant formulations where the efficacy of additives in primary matrixes is of chief importance in the on-demand tuneability of specific structural and mechanical properties.

**Philipp Gutfreund**, German
The ILL

'I am an instrument scientist at the ILL, responsible for the FIGARO reflectometer. My main research interest is focused on the microscopic structure and dynamics of polymeric liquids in out-of-equilibrium or in confinement. I mainly use neutron scattering techniques in my investigations, with an emphasis on the in situ combination of shear/rheology and neutron scattering. I also work on the development of the reflectometry technique.'

Using neutrons to protect our works of art

Horizontal reflectometer FIGARO

Artwork does not last forever. This is particularly true of paintings, which are appreciated for their visual appearance but which inevitably deteriorate through physical processes such as the deposition of airborne dust and soot, oxidation and attack by free radicals. As a result, after 50 to 100 years a once-colourful painting that has been exposed to city air and relative humidity may become uniformly brown or white, and its protective varnish, opaque, cracked and irregular.

AUTHORS

B. Cabane (ESPCI, Paris, France)
Y. Rharbi (Université Grenoble Alpes -UGA, France)
Ph. Gutfreund (ILL)
A. Castel (Université Grenoble Alpes -UGA, France and ILL)

ARTICLE FROM

Soft Matter 2020 — doi:10.1039/C9SM01976F

REFERENCES

- [1] E. Caretti *et al.*, *Acc. Chem. Res.* 43 (2010) 751
[2] A. Castel *et al.*, *Soft Matter* 16 (2020) 1485

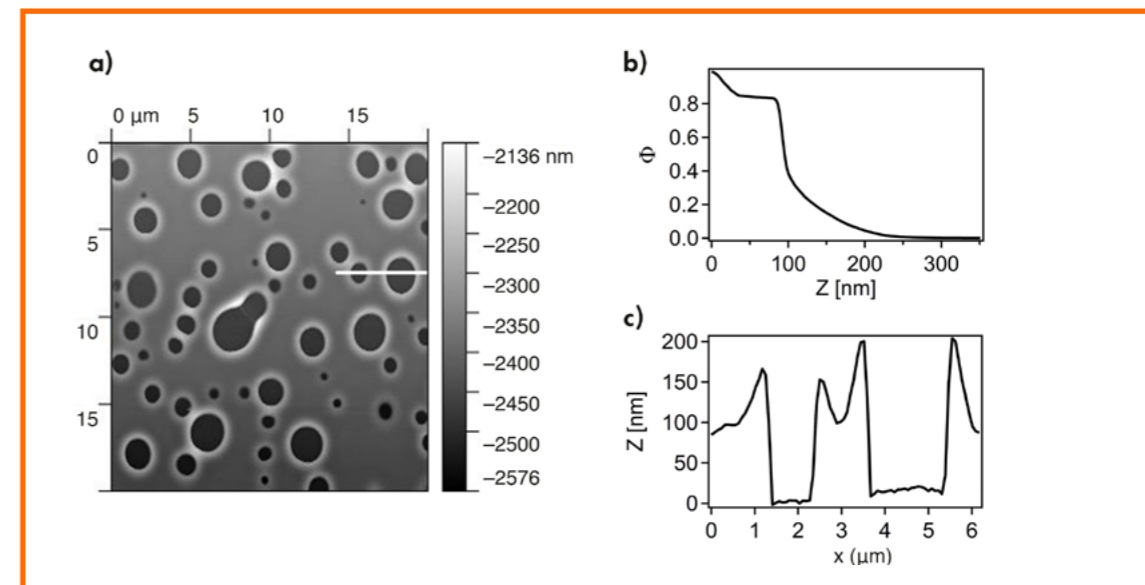
In order to mitigate these effects, antique paintings are periodically 'restored' (**figure 1**). The restoration is a major transformation: it aims to re-establish the appearance of the original painting through the dissolution and replacement of most of the varnish covering the paint layer, replacement of part of the pigment layer, extraction of 'dirt' that may have been deposited near the surface of the varnish layer and the filling of cavities that may have materialised during accidental exposure to water.

It is often said that the 20th century was the century during which the largest number of paintings were damaged, not through war or natural disasters but through deliberate restoration operations. To mitigate this destruction, there is an urgent need for a deeper understanding of the processes employed in both restoration operations and those that take place later as a consequence of such operations.

A critical task in restoration consists of removing the damaged or opaque outer part of the varnish film and replacing it with fresh, transparent and resistant varnish. Commonly, the restorer will use a swab soaked with solvent to transfer the solution to the painting's film and remove the outer part of the old varnish using minimal shear.

**Figure 1**

Successive stages in the removal of polluted layers from a varnish [2].

**Figure 2**

a) An atomic force microscopy (AFM) image of a varnish layer after prolonged exposure to water containing 0.3 % benzyl alcohol.

b) Vertical density profile of the AFM image.

c) Horizontal cut along the white line shown in (a).

The painting is at high risk of damage from the transfer of excessive solvent as it may infiltrate the paint layer. Once inside, it can reduce the cohesion of the composite, enter cracks and create capillary bridges that exert stresses on the material.

An apparently 'mild' alternative to using pure solvents has recently been proposed, namely, diluting the good solvent in a bad solvent, usually water [1]. This proposed method was critically examined in the study presented here [2].

We studied the removal of varnish layers on model solid supports by organic solvents used in the restoration of easel paintings. We observed that the de-wetting of all the varnish (rather than controlled dissolution) can occur above a critical solvent concentration, due to the presence of water (**figure 2**). This would be catastrophic for the painting as it would expose the pigment layer to the cleaning liquid. We hypothesise that this effect is due to the polar moieties of the solvent screening the stabilising polar interactions of the varnish at higher concentrations, catalysing the de-wetting of the hydrophobic polymer film from the hydrophilic substrate and exposing it to the water matrix.

The central part of the project involved the use of neutron reflectometry on FIGARO to determine the depth profile of solvent concentration in the film of varnish (Laropal A81), which was sandwiched between a bulk layer of water and solvent (benzyl alcohol) and a single-crystal silicon substrate. The varnish layer thickness was ~100 nm, and was prepared using spin-coating. Complementary measurements were carried out using atomic force microscopy.

By examining this commonly used system of art restoration, this study demonstrated that higher concentrations of solvent and prolonged exposure to it cause water-filled cavities to appear and grow. This leads to the break-up of the varnish, in contrast to the usual molecular dissolution. Consequently, commonly held expectations in the cultural heritage sphere regarding the behavior of solvent mixtures in the restoration of easel paintings should be revised.

The findings of this study can contribute to safer restoration processes by encouraging closer examination of the polarity of the solvents used *vis-a-vis* the polar groups present in the protective layer of a painting.

**Barbara Gold**, German.

Federal Ministry of Education and Research (BMBF), Germany

'Before I changed my path to the field of research policy, I mainly studied complex polymeric systems using a multi-methods approach. Therefore, I combined laboratory methods with various experimental set-ups—especially neutron-scattering techniques—at large-scale facilities to gain deeper insight into the microscopic properties of soft materials such as gels, melts and elastomers and relate them to their macroscopic behaviour.

Direct assessment of tube dilation in entangled polymers

Spin-echo spectrometer IN 15

Polymeric materials have become integral parts of our daily life. Their processing properties, mechanical characteristics and thermal behaviour depend mainly on the dynamics of their macromolecular building blocks. Thus, a fundamental understanding of how these units move and interact with each other in the material is a basic requirement for building even smarter materials with enhanced performance.

AUTHORS

B.J. Gold and D. Richter (FZ Jülich, Germany)
D. Vlassopoulos (FORTH, Greece)
I. Hoffmann (ILL)

ARTICLE FROM

Phys. Rev. Lett. (2019) — doi:10.1103/PhysRevLett.122.088001

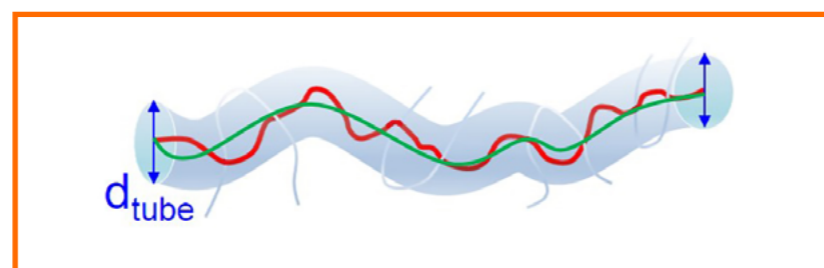
REFERENCES

- [1] T. McLeish, Adv. Phys. 51 (2002) 1379
- [2] M. Kapnistos, G. Koutalas, N. Hadjichristidis, J. Roovers, D.J. Lohse and D. Vlassopoulos, Rheol. Acta 46 (2006) 273
- [3] R.H. Colby and M. Rubinstein, Macromolecules 23 (1990) 2753

High-molecular-weight polymer melts and solutions exhibit unique rheological properties, such as viscoelasticity with rubber-like behaviour at intermediate times and very long terminal relaxation times accompanied by high viscosities, shear thinning, strain hardening and hierarchical relaxation of branched polymers. They originate from topological constraints imposed by the mutually interpenetrating chains. These constraints, or entanglements, lead to preferred motion in the direction of the chain contour. Much progress in our understanding of polymer-chain dynamics has been achieved in terms of tube models based on the reptation mechanism [1].

The tube in such models is characterised by its diameter d and its contour length L (figure 1). In theories focusing on the relaxation behaviour of entangled polymers, a key ingredient is the way in which the topological constraints of an entangled chain are lifted by unconstrained segments, *i.e.* how the constraining tube is dilated. Dynamic tube dilation [1, 2] widens the initial tube diameter d_0 over time $d(t)$ both by dilution with short non-entangled chains (concentration: $1 - c$, with c being the volume concentration of long matrix chains) and by dynamic dilation, where $\phi(t)$ is the fraction of initial constraints that survived at time t : $d(t) = d_0[c\phi(t)]^{-a/2}$

Thus, the (dynamic) dilution exponent a is a fundamental quantity in tube concepts. However, its proper value is highly controversial, the most frequently reported values in the literature being $a = 1$, $a = 4/3$ or $a = 2$. This controversy is even more important, since the exponent a relates to the question of what an entanglement is all about.

**Figure 1**

Schematic representation of the microscopic view inside polymeric bulk material. The macromolecular building blocks ('polymer chains') topologically constrain each other in space by entanglements. Thus, a model chain (red) can only relax on its contour length (green line) within a tube-like volume built up by the surrounding chains.

We addressed this open question by directly measuring the tube diameter d of highly entangled polymers using neutron spin-echo spectroscopy (NSE) (figure 2), which provides an unambiguous determination of the dilution exponent a on the spatial and temporal scale of the tube. To underpin the experimental outcome, in parallel the dilution effect on the plateau modulus G_N^0 was investigated rheologically using SAOS measurements.

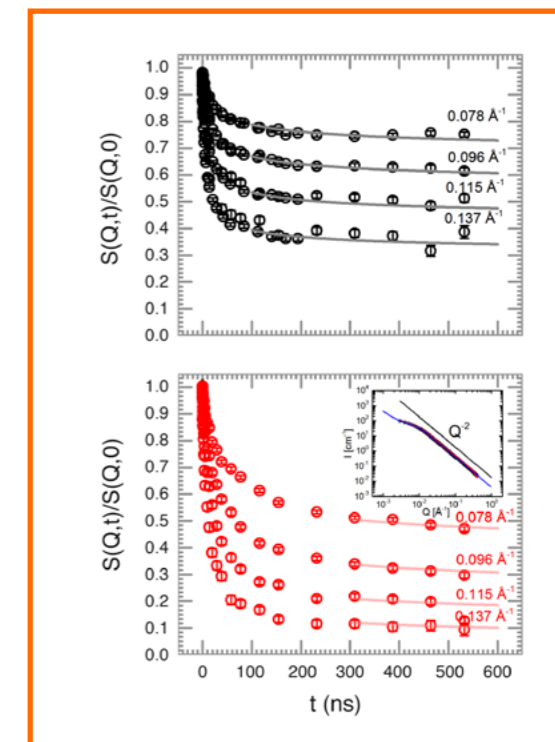
The NSE measurements at IN15 (ILL), as well as the SAOS investigations on a series of high-molecular-weight PEO chains diluted by different amounts of oligomers by up to 50 vol% (resulting in at least 38 entanglements), revealed a concentration dependence $d \propto c^{a/2}$ and $G_N^0 \propto c^{1+a}$ with a well-defined dilution exponent $a = 1.34 \pm 0.04$ (figure 3). This result allows clear discrimination between different theoretical models and imposes ancillary conditions on rheological theories.

Thus, we have replaced the indirect conclusions arrived at by adapting theories to the rheological properties of polymer melts, with a direct measurement of dynamic tube dilution. Furthermore, the microscopic result provides us with the means to select between various models of entanglement formation. It clearly favours the Colby–Rubinstein picture [3]: in order to form an entanglement, a given universal number of binary contacts has to occur within a volume set by the cube of the tube diameter. This requirement determines the size of the tube diameter d and predicts $a = 4/3$. A parallel investigation of G_N^0 on the same samples resulted in a dilution exponent compatible with the microscopic result. The findings resolve the protracted controversy concerning the effect of tube dilution and confirm the entanglement model of Colby and Rubinstein.

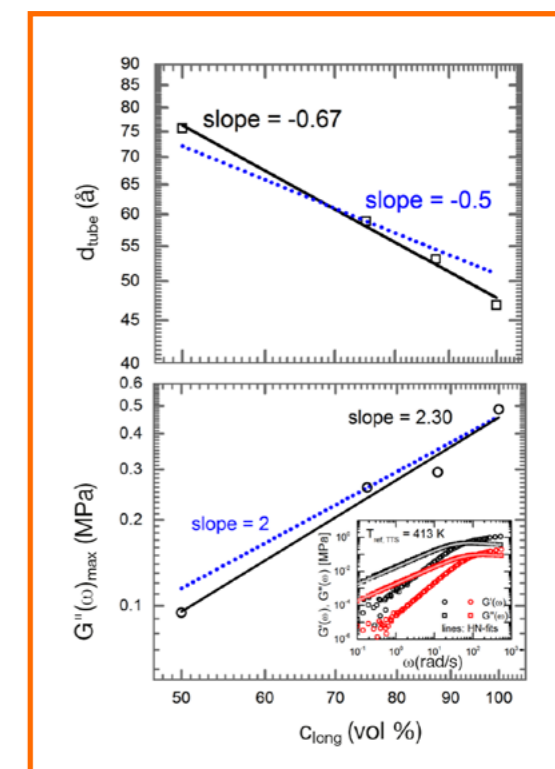
Figure 3

Top) Double logarithmic representation of the tube diameter as a function of oligomeric dilution (symbols). The slope of the fitted power law exponent amounts to -0.67 , revealing a dynamic dilution exponent of $a = 1.34$ (black line), close to $a = 4/3$.

Bottom) Double logarithmic presentation of the plateau modulus G_N^0 as a function of the matrix chain concentration at $T_{ref} = 413$ K. The slope of the power law amounts to 2.30, revealing a dynamic dilution exponent of $a = 1.30$. For comparison, a slope of 2 corresponding to $a = 1$ (blue dotted line) is shown. The inset in the lower part shows the SAOS measurements of the undiluted reference sample (black symbols) and the most diluted sample ($c = 50$ vol%) (red symbols) at $T_{ref} = 413$ K.

**Figure 2**

NSE spectra from the undiluted reference sample (black symbols) and the most diluted sample ($c = 50$ vol%) (red symbols) at $T = 413$ K. Lines represent fits of the coherent single chain dynamic structure factor as given by de Gennes to determine the tube diameter d . The inset in the lower part shows SANS data for both samples.





Alycia Yee, British Keele University (UK) and the ILL 'This work formed an important part of my PhD, which focused on the molecular mechanisms underlying the fatal condition of ATTR amyloidosis, which causes restrictive cardiomyopathy and polyneuropathy. My project homed in on clues from mutagenesis work, combined with structural techniques including neutron and X-ray crystallography, macromolecular deuteration, mass spectrometry and molecular modelling. Crucially, it made use of the infrastructures of the Partnership for Structural Biology (PSB)'

Molecular mechanisms underlying fatal restrictive amyloid cardiomyopathy and polyneuropathy: neutron structural studies and consequences for drug design

Macromolecular crystallography instrument LADI, Deuteration Laboratory (D-Lab), Partnership for Structural Biology (PSB)

An advanced analysis of a blood hormone transporter protein called transthyretin was carried out using neutron diffraction, mass spectrometry, molecular modelling and X-ray diffraction [1]. The results reveal a molecular mechanism underlying fatal cardiomyopathic and polyneuropathic diseases associated with the misfolding of this protein, with implications for the development of new, more effective, drugs.

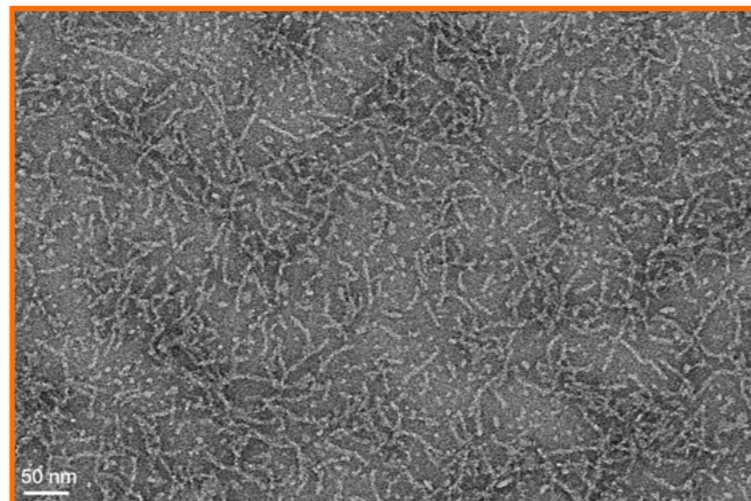


Figure 1

Electron micrograph of amyloid fibrils that have assembled from misfolded TTR molecules. Image acquired by M. Oliva, A. Minns, C. De'Ath (ILL) and D. Fennel (IBS) using the PSB/IBS electron microscopy platform.

AUTHORS

A.W. Yee and V.T. Forsyth (Keele University, UK and ILL)
M. Aldeghi and B.L. de Groot (MPI, Göttingen, Germany)
M.P. Blakeley (ILL)
M. Moulin and M. Haertlein (ILL)

ARTICLE FROM

Nat. Comms. (2019) — doi:10.1038/s41467-019-08609-z

REFERENCES

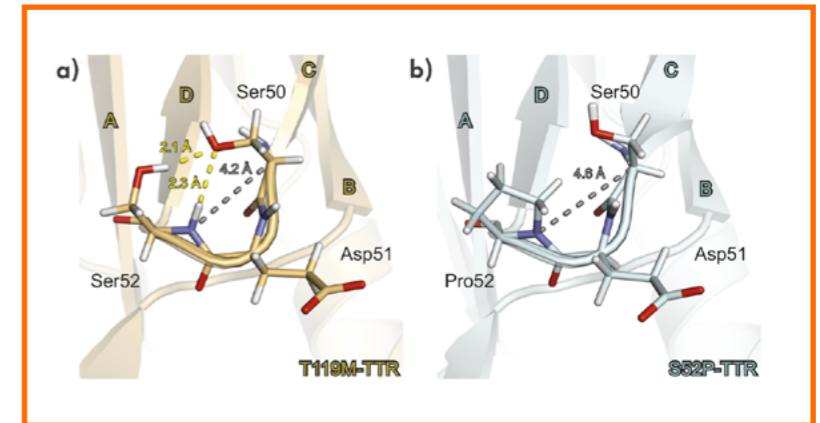
- [1] A.W. Yee *et al.*, Nat. Commun. 10 (2019) 925
- [2] M. Haertlein *et al.*, Methods Enzymol. 566 (2016) 113

ATTR amyloidosis. Transthyretin amyloidosis is a devastating progressive condition associated with misfolded forms of a protein that normally transports the hormone thyroxine and vitamin A in the blood and in the cerebrospinal fluid. Transthyretin (TTR) is an inherently unstable protein molecule that tends to fall apart and misassemble as extended filaments (amyloid fibrils, see **figure 1**) in various parts of the body, including the heart and the nervous system. Specific mutations of TTR (often point mutations) may cause the early onset of these pathologies and are often associated with amyloidosis in specific tissues. However, it is notable that some mutations are protective against TTR amyloidosis.

Medically relevant transthyretin mutations—a way into the problem. Normal human TTR was studied alongside two variants of the protein (mutants that are found in different parts of the population). One of these (the T119M or 'stable' mutant) imparts remarkable stability to TTR and is strongly protective against the formation of amyloid fibrils. However, the other (the S52P or 'unstable' mutant) results in a very aggressive form of hereditary amyloidosis. These mutant forms of the protein (in both hydrogenated and perdeuterated forms) were produced using recombinant methods and compared using biophysical techniques. Given the very marked differences in the behaviour of the mutants, the goal was to understand at a structural level the reasons for this molecular pathology.

Figure 2

The C-D loop in TTR is tight in the crystal structure of the stable T119M mutant (protective against amyloidosis), determined using neutron diffraction. However, the same loop at the mutation site of the S52P mutant (associated with the most aggressive form of transthyretin amyloidosis) is loosened by an absent hydrogen bond, causing degradation of the protein and misfolding into damaging amyloid fibrillary deposits.



Multi-technique approaches. Both TTR mutants were studied using neutron and X-ray crystallography, along with mass spectrometry and computer modelling. Crucially, the project was able to exploit the technologies available within the Deuteration Laboratory (D-Lab) platform of the ILL's Life Sciences Group [2], as well as other platforms available within the Partnership for Structural Biology (PSB) (see p. 106). These investigations showed how the loss of a single hydrogen bond arising from a mutated amino acid causes instability in the C-D loop of the protein and renders the entire TTR molecule susceptible to amyloid fibrillogenesis (**figure 2**). This is confirmed by molecular dynamics calculations that highlight this part of the structure as being at the origin of the instability (**figure 3**).

Drugs that stabilise TTR. This investigation has revealed a molecular mechanism by which TTR forms amyloid fibrils through a parallel equilibrium of partially unfolded protein forms. TTR has a complex hierarchical structure of four subunits (monomers). This instability renders the whole protein more susceptible to degradation effects, enhancing the rate of amyloid fibril formation. The nature of this instability has led to intense interest in drugs that could be used to stabilise the molecule and impede progress of the disease. TTR has two binding sites to which some ('monovalent') drugs bind individually. In this study, we found that one commercially available monovalent drug stabilises the normally folded protein in a way that is closely analogous to that for highly stable protein mutants such as the T119M mutant (**figure 4**).

Bridging the gap between biophysics and clinical application. Current work is homing in on other medically important mutants that can be investigated to further probe TTR amyloidosis. There is also considerable interest in obtaining detailed information on other drugs that might be more effective in stabilising the protein—in particular, bivalent drugs that extend over both binding pockets of the molecule. There is also major interest in relating these results to those from TTR purified from the blood plasma of patients having the same TTR mutations. These developments are currently underway as part of a scientific collaboration between the ILL and researchers at the UCL Centre for Amyloidosis and Acute Phase Proteins located at the Royal Free Hospital (CAAPP) in London.

Figure 3

Molecular dynamics calculations reveal the instability of the C-D loop (seen in red, yellow and green) of the TTR structure, consistent with the neutron crystallographic results.

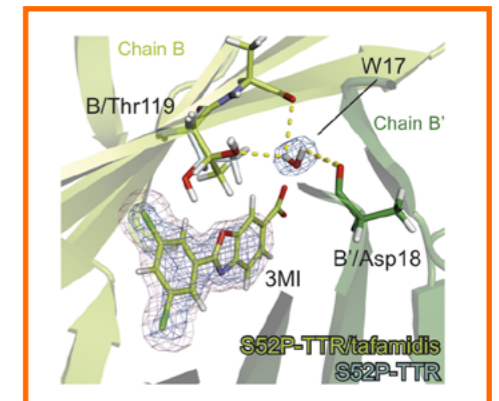
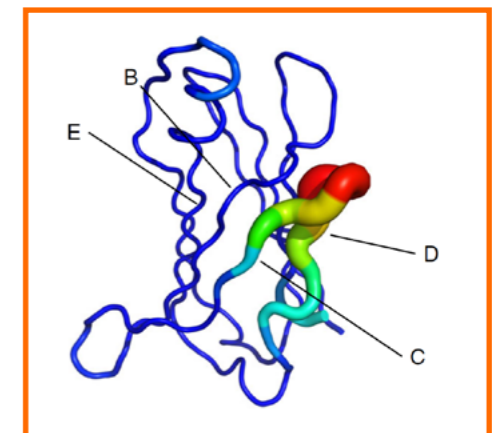


Figure 4

The drug tafamidis (shown in neutron map density) binds to TTR, causing a 180° flip of the Thr119 side-chain (cyan, before binding; green, after binding), resulting in the recruitment of a water molecule that bridges and stabilises the two dimers via an asparagine residue.



Charlotte Beddoes, English Leiden Academic Centre for Drug Research, Netherlands
'I am a postdoc working at the LACDR. I am studying the structure of the lipid matrix of the skin and how this effects the barrier function.'

Arrangement of ceramides in the skin: Sphingosine chains localise at a single position in stratum corneum lipid matrix models

High-resolution diffractometer D16

The skin's barrier is controlled by the lipid matrix located in the stratum corneum (the skin's outer layer). The barrier is essential for terrestrial life, and alterations in the composition and arrangement of the lipids can be observed as inflammatory skin diseases. It is important to understand the lipid arrangement in this layer, since skin diseases are one of the most common health problems and the fourth leading cause of non-fatal disease burden when considering both dermatological and socioeconomic factors [1].

AUTHORS

C.M. Beddoes, J. Bouwstra and G.S. Gorris (Leiden Academic Centre for Drug Research, Netherlands)
 D.J. Barlow (Pharmaceutical Science Division, King's College London, UK)
 J. Lawrence (Division of Pharmacy and Optometry, Manchester University, UK)

ARTICLE FROM

Langmuir (2020) — doi:10.1021/acs.langmuir.0c01992

REFERENCES

- [1] D. Seth, K. Cheldize, D. Brown and E.F. Freeman, *Curr. Dermatol. Rep.* 6 (2017) 204
- [2] E.H. Mojumdar, G.S. Gorris, D.J. Barlow, M.J. Lawrence, B. Deme and J.A. Bouwstra, *Biophys. J.* 108 (2015) 2670
- [3] E.H. Mojumdar, G.S. Gorris, D. Groen, D.J. Barlow, M.J. Lawrence, B. Demé and J.A. Bouwstra, *Biochim. Biophys. Acta, Biomembr.* 1858 (2016) 1926
- [4] J. Gonthier, M.A. Barrett, O. Aguetz, S. Baudoin, E. Bourgeat-Lami, B. Demé, N. Grimm, T. Hauß, K. Kiefer, E. Lelièvre-Berna, A. Perkins and D.J. Wallacher, *Neutron Res.* 21 (2019) 65

The lipid matrix within the stratum corneum (SC) controls the physical barrier's ability to prevent both the penetration of external materials and desiccation from the body. As a result, to understand the skin barrier it is essential to study the lipid matrix. Using prepared models of the lipid matrix on D16, the small-angle diffractometer at the ILL, we identified the arrangement of the lipids needed for a strong, healthy barrier.

Within the SC, the lipid matrix consists of twin chain ceramides (CER), single-chain fatty acids and cholesterol. These form a 13 nm trilayer long-periodicity phase (LPP), a unique structure that is essential for the barrier function. We are able to prepare lipid models that mimic the lamellar structure, packing density and barrier abilities of the native SC lipid matrix, using synthetic lipids. These models can vary by either mimicking the composition found in SC or consisting of just CER EOS and NS as the CER component (structures are presented in **figure 1c**). Previous experiments on the high-resolution diffractometer D16 revealed that different lipids occupy specific locations within the trilayer structure (**figure 1a**) [2, 3].

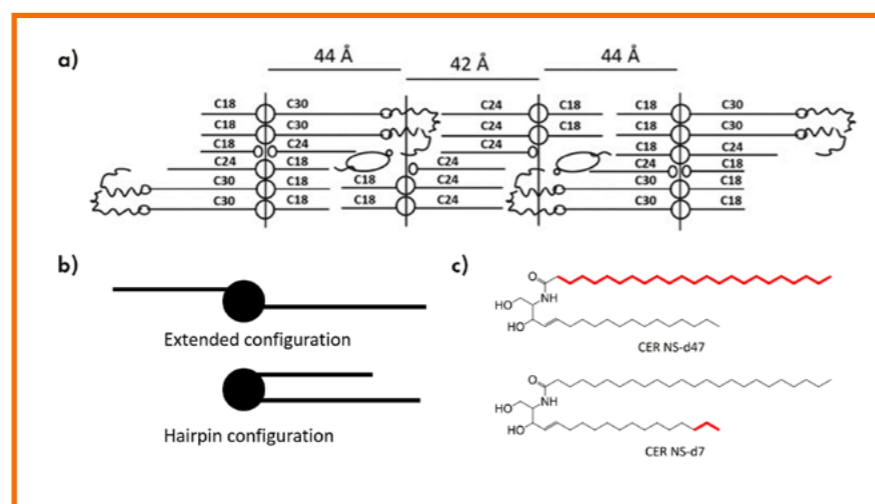


Figure 1

a) Schematic diagram of the lipid arrangement within the LPP. The general position of each lipid class is indicated in the three layers. Image from [3].
b) Possible configurations of CER NS.
c) Structure of CER NS. The deuterium labelled carbons are highlighted in red. The location of the deuterium are used to determine the position of either the acyl chain (CER NS-d47); and the sphingosine chain (CER NS-d7).

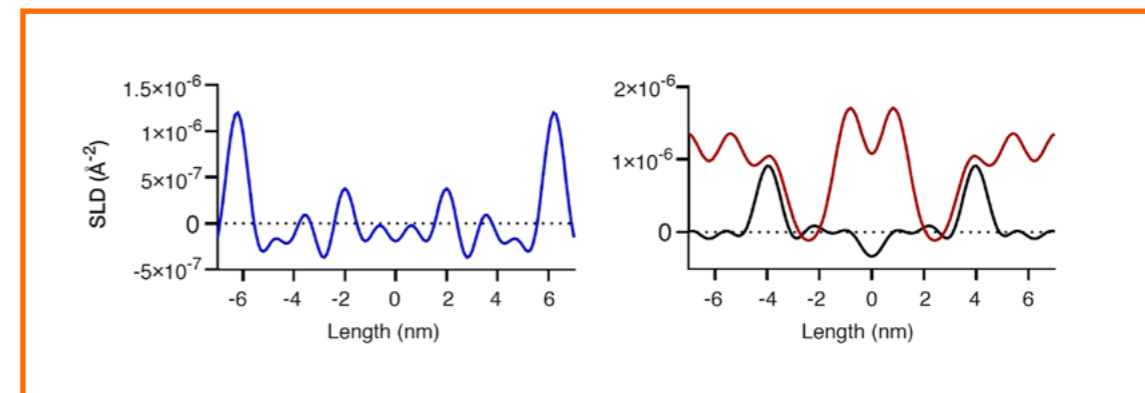


Figure 2

SLD profile of the water (blue), where the four areas of greater scattering length density signify the water regions and a trilayer structure. The position of the individual CER NS carbon chains shows that CER NS acyl chains (red) are located in both the inner and outer layers of the LPP, while the sphingosine chain (black) extends beyond the inner water region and is located exclusively in the outer layers.

The configuration of twin chained CERs is also important: CERs can adopt either an extended or a hairpin conformation (**figure 1b**), which can determine how the separate layers interact with each other. This is important for better comprehension of the barrier function.

In the present study, we focused on the CER NS configuration within the LPP and its relation to the connectivity between the layers. CER NS headgroups are located primarily at the inner water layers of the unit cell (**figure 1a**). By partially deuterating either the sphingosine (CER NS-d7) or the acyl (CER NS-d47) chains (**figure 1c**), their location could be identified using contrast variation measurements. Samples were hydrated in 100, 50 and 8 % D₂O, then the scattering length density (SLD) profiles for each hydration condition were calculated.

The position of the deuterated moiety was determined after subtracting the fully protiated SLD profile from the deuterated SLD profile, while the water profile was determined subtracting 8 % from the 100 % D₂O measurement of the protiated model. For the highest quality SLD profiles a higher number of orders are required. Hence, these measurements were performed on D16, due to the wide q-range available which enables measurements up to the 10th order, combined with the relative humidity control available with the BerILL cells to simulate the highly humid environment experienced within the skin [4].

From the SLD profiles we could observe the water profile, which shows the characteristic three-layer structure (**figure 2, blue line**) with an inner water layer located $\sim\pm 2$ nm from the cell centre. When CER NS-d47 was substituted into the model, most of it could be seen located in the central layer while a smaller proportion was located at the outer parts of the outer layer (**figure 2, red line**). In contrast, when the CER NS-d7 was substituted in, it was localised in the centre of the outer layers only, $\sim\pm 4$ nm from the unit centre (**figure 2, black line**).

From these results we can conclude that the majority of the CERs are arranged in an extended conformation, physically linking the three layers together. This crossover between the layers by the extended CERs and the extra-long CER EOS affords several advantages for a stronger barrier, including a reduced area of permeable boundaries, reduced swelling capability, greater packing densities of lipids and reduced packing strain, and thus lower permeability of materials.

In conclusion, the present study provides evidence that CER NS adopts a linear conformation in the centre, while also being located to a lesser extent in the outermost region, of the LPP. The results of this study highlight a new aspect of the lipid arrangement, namely, that the lipid configuration needs to be considered when assessing alterations observed between healthy and diseased SC and its impact on the skin barrier function.



Nataliya Danilenko, Russian Structural Biochemistry group, Freie Universität Berlin, Germany
 'I am a structural biologist focusing on the characterisation of protein complexes by hybrid methods. During my PhD in the Carlomagno group, I employed SANS and NMR data to solve the structure of histone modification machinery. Now, I am interested in applying this integrative approach to bacterial transcription systems.'

A combined NMR and SANS approach reveals the molecular mechanism of histone tail acetylation

Small-angle scattering instrument D22

Small-angle scattering instrument at FRM2

Eukaryotic DNA is packaged into chromatin, a highly structured assembly consisting mainly of DNA and histone proteins. Chemical modifications of histones control gene expression as well as the recruitment of chromatin-associated proteins. We applied a combination of NMR and SANS to determine the structure of a multi-protein enzyme that modifies histone H3 by adding an acetyl group to its unstructured tail. Our results reveal a new mechanism for promoting chemical reactions of unstructured protein tails.

AUTHORS

N. Danilenko (Structural Biochemistry group, Freie Universität Berlin, Germany)
 T. Carlomagno (Leibniz University Hannover and Helmholtz Centre for Infection Research, Braunschweig, Germany)
 F. Gabel (ILL and IBS, Grenoble)

ARTICLE FROM

Nat. Commun. (2019) — doi:10.1038/s41467-019-11410-7

REFERENCES

- [1] P. Zhang, K. Torres, X. Liu, C.G. Liu and R.E. Pollock, *Curr. Protein Pept. Sci.* 17 (2016) 401
 [2] S. D'Arcy and K. Luger, *Curr. Opin. Struct. Biol.* 21(6) (2011) 728-34

The genome of eukaryotic cells displays a hierarchy of structures that generate a tightly packed arrangement called chromatin. At the smallest scale, DNA molecules wind around protein complexes known as histone octamers to form nucleosomes (figure 1). These nucleosomes are then tightly packed in regular chromatin fibre arrangements which in turn fold to give rise to the overall structure of chromosomes.

This variability in chromatin packing provides the cells with unique mechanisms for regulating gene expression, i.e. for producing proteins selectively and specifically as needed. For example, genes in certain DNA regions can be selectively 'turned off' by the dense packing of the local chromatin structure, or activated through the unwinding of chromatin fibres.

Histone proteins are key players in the regulation of DNA condensation. There are only four major histone types; however, histones can acquire diversity through an extensive array of site-specific modifications, including acetylation, methylation and phosphorylation. The modification sites are mostly located in the histone tails (unstructured terminal domains) and modulate DNA-histone interactions as well as the recruitment of additional proteins to the DNA [1]. The set of histone modifications makes up the so-called 'histone code', in which certain modification patterns are associated with gene activation or silencing.

Figure 1

Scheme of the eukaryotic DNA condensation.

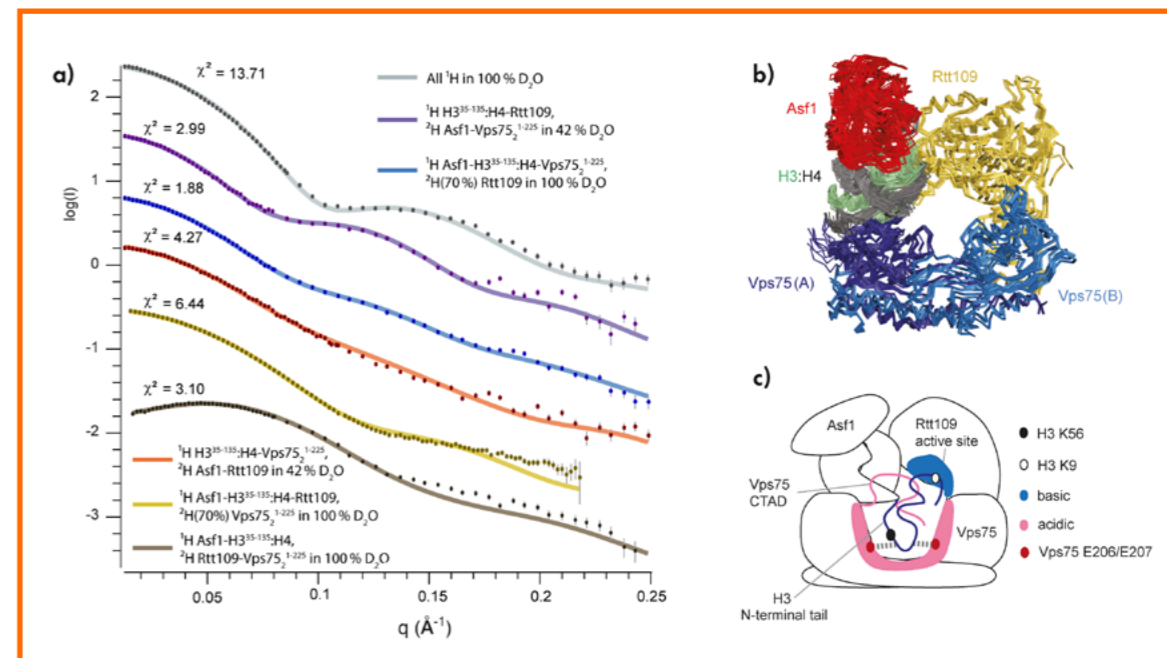
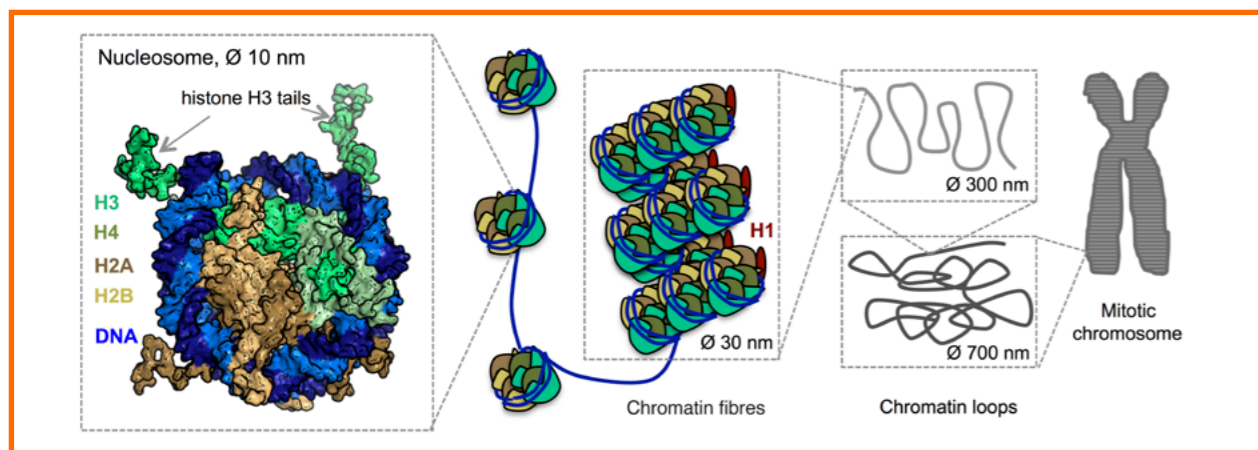


Figure 2

- a) SANS curves of six different contrast variation experiments for complexes containing protonated (^1H), deuterated (^2H) and 70 %deuterated ($^2\text{H}(70\%)$) proteins in solutions of varying $\text{H}_2\text{O}/\text{D}_2\text{O}$ ratio. The solid lines correspond to fits to the atomic model of the complex (PDB 6O22).
 b) Overlay of the 10 best atomic models (average pairwise backbone RMSD, 2 Å).
 c) Schematic model of the catalytic complex, including the disordered tails.

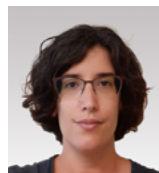
Despite their importance, structural and functional details of the chemical modifications of histone tails are poorly understood.

In this study we examined how Rtt109, a fungal-specific enzyme, places acetyl modifications at multiple sites on histone H3. H3 acetylation is essential for nucleosome assembly in fungi; consequently, Rtt109 is considered a potential target for anti-fungal infection therapy. Biochemical data have pointed to a unique regulation mechanism of Rtt109, which owes its specificity and efficiency to an association with the two histone chaperones, Asf1 and Vps75 [2].

To understand the mechanism behind the function and regulation of Rtt109, we determined the structure of the 160 kDa Asf1-H3:H4-Rtt109-Vps75 complex using a combination of complementary techniques: nuclear magnetic resonance spectroscopy (NMR) and small-angle neutron scattering (SANS). SANS curves were measured at KWS-1 (FRM2, Garching) and D22 (ILL, Grenoble), using the neutron-specific contrast-matching technique, for 12 complexes reconstituted with differently labelled proteins in 0, 42 and 100 % D_2O (figure 2a). With these data we were able

to determine the arrangement of the subunits within the complex, as well as probe its overall shape and stoichiometry. The combination of this information with NMR data, which provided protein-protein distance restraints in the short- to medium-distance range, was essential for determining the structure of the complex.

The structure of Asf1-H3:H4-Rtt109-Vps75 complex (figure 2b) revealed that all proteins contribute to the assembly of a doughnut-like complex where the central cavity, which includes the Rtt109 catalytic pocket, accommodates the histone H3 tail. The combination of SANS and NMR in solution with molecular dynamics simulations offered unique insights into the mechanism of activity and regulation of the complex: the negatively charged C-terminal domain of Vps75 acts as a specificity switcher, attracting the dynamic, positively charged histone H3 tail to the enzyme's active centre and thereby promoting the acetylation of amino acids in the N-terminal end of the H3 tail (figure 2c). Such fuzzy electrostatic interactions allow localising disordered substrates with minimal entropy loss and may represent a general mechanism for supporting enzymatic reactions acting on highly unfolded substrates.



Marta Salvador Castell. Spanish University of California San Diego, USA 'I obtained my PhD from the University of Lyon and today I am a postdoctoral researcher at the University of California, San Diego. I am interested in cell biophysics, specifically in understanding how cells work at a molecular level, with a focus on cell membrane structure and dynamics.'

The first study on the impact of osmolytes on entire cells of thermophilic micro-organisms

Time-of-flight spectrometer IN5
Backscattering spectrometer IN13

Osmolytes are molecules that help to stabilise macromolecular structures by enhancing water structure. Such molecules are synthesised by micro-organisms to tolerate non-optimal environmental conditions. For example, the piezophilic (*i.e.* requiring high pressures) *Thermococcus barophilus* accumulates the osmolyte mannosylglycerate (MG) in the cytoplasm to counteract the stress induced by pressures lower than the bacterium's pressure optimum ('low-pressure stress').

AUTHORS

M. Salvador-Castell and P. Oger (University of Lyon and CNRS, France)
M. Golub and N. Martinez (ILL and University of Grenoble Alpes UGA, CNRS and CEA, IBS, Grenoble, France)
J. Ollivier (ILL)
J. Peters (ILL and University of Grenoble Alpes, France)

ARTICLE FROM

Soft Matter (2019) — doi:10.1039/C9SM01196J

The effect of osmolytes has mostly been studied by considering only selected parts of cells, *e.g.* proteins. Therefore, important effects resulting from the interplay of different molecules or the crowding of the cellular environment might not have been considered. Accordingly, we studied here the impact of osmolytes on entire, intact living cells. We exploited the accumulation of osmolytes by *T. barophilus* under low-pressure stress to test the impact of the presence of such molecules under a relevant cellular context. We compared the dynamics of *T. barophilus* cells grown under low-pressure stress (0.1 MPa), which synthesises MG (here named Tba_MG), and *T. barophilus* cells grown at optimal pressure (40 MPa), which does not synthesise MG (here named Tba_Ø).

We used incoherent neutron scattering to directly determine the water and proteome dynamics inside living *T. barophilus* cells, *in vivo*. We studied the cells with two different neutron techniques: elastic incoherent neutron scattering (EINS), to obtain an overall overview of cell dynamics; and quasi-elastic neutron scattering (QENS), with which we could discriminate between the molecular dynamics of cellular constituents and water. The broad time window range of the ILL instruments allowed us to use two instruments with a possible similar timescale (100 ps): IN13 for EINS and IN5 for QENS. For both instruments, we studied the cells under temperature and pressure values up to the cells' optimal range, *i.e.* between 0.1 and 40 MPa and between 293 and 358 K.

The EINS results showed some temperature-dependent differences in the overall dynamics of the systems probed, as reflected in their summed intensities (**figure 1**). Up to

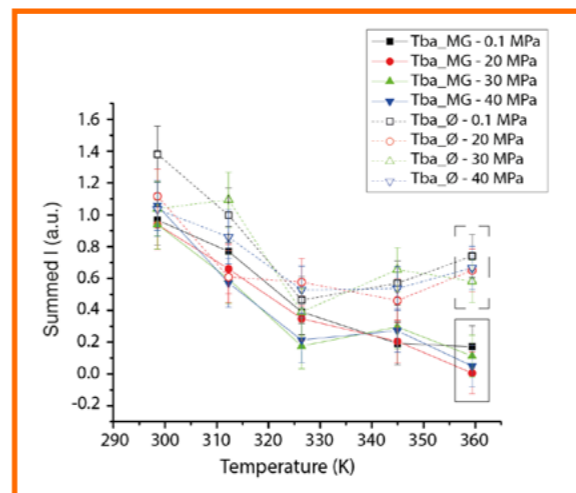


Figure 1 Summed incoherent intensities plotted against temperature for Tba_MG (filled symbols) and Tba_Ø (empty symbols) at different pressures (0.1 MPa (black squares), 20 MPa (red circles), 30 MPa (green triangles pointing up) and 40 MPa (blue triangles pointing down)). The frames around the last data points are only to guide the eye.

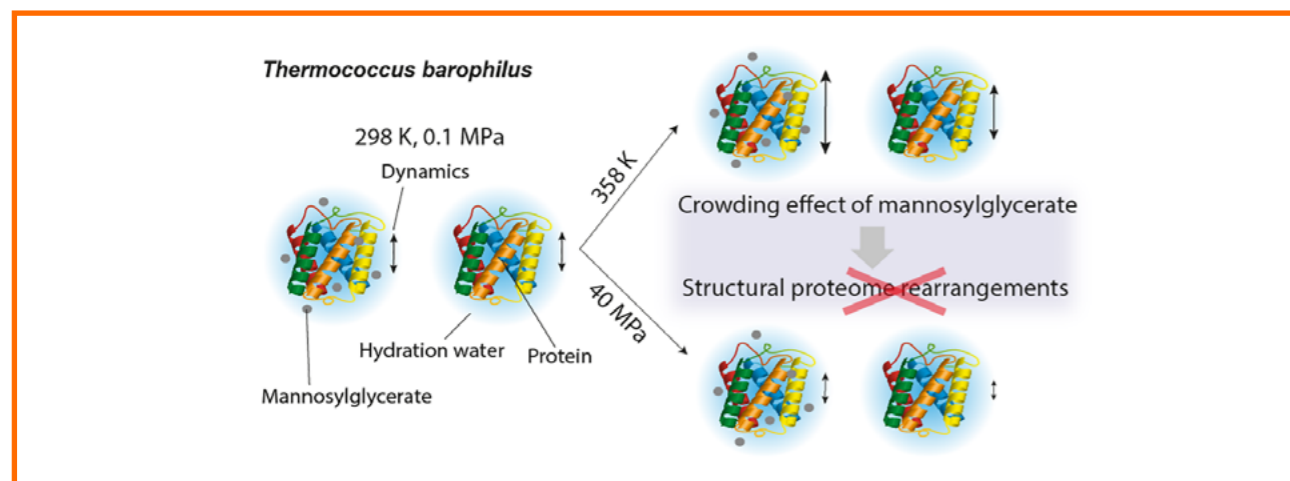
325 K, the summed intensities decrease with increasing temperature in both Tba_MG and Tba_Ø. Thus, the dynamics of both systems increase as expected from a temperature increase. Interestingly, the intensity-temperature curves of both samples display two different regimes with a change of slope at 325 K, this temperature being close to the minimal growth temperature of *T. barophilus* (321 K). For the sample grown under optimal conditions without MG (Tba_Ø), the summed incoherent intensities increase only slightly above 325 K, indicating that cell molecular dynamics are stabilised when the cells approach their optimal growth temperature (358 K). In contrast, samples grown under low-pressure stress (Tba_MG; accumulates MG) have summed intensities that further decrease (*i.e.* the internal overall cell dynamics increases). This change in cell dynamics is indicative of structural rearrangements of cellular macromolecules, which correspond mostly to

proteins in the current set-up. These findings suggest that the proteome of this species is in a destabilised and partially non-functional form at temperatures below 325 K, which might explain its inability to grow below this temperature. The presence of MG in the Tba_MG sample seems to inhibit the extent of the structural rearrangements of the proteome, which is expected since osmolytes may rigidify and stabilise the proteome.

The QENS data was fitted with four functions corresponding to elastic contribution, bulk water, hydration water and proteome. The half width at half maximum of the translational component of hydration and bulk water plotted against Q^2 curves represents the typical signature of jump-diffusional motions. The best fit values along with errors obtained through error propagation are given in **table 1**. QENS data established the importance of crowding on cell dynamics. At 298 K, the translational diffusion coefficient for hydration water, $D_{\text{Hydration}}$, is decreased due to high hydrostatic pressure (HHP) as well as a lower crowding degree. The pressure-induced decrease in $D_{\text{Hydration}}$ is more pronounced for the less crowded sample, Tba_Ø, probably because MG protects the proteome against structural changes. At 358 K, the presence of osmolytes in sample Tba_MG limits the temperature-induced increase in the translational diffusion coefficient for bulk water, D_{Bulk} , indicating that crowding impacts bulk water motion as well.

Interestingly, at high temperature $D_{\text{Hydration}}$ decreases when pressure is increased, as observed at 298 K, though the temperature does not increase $D_{\text{Hydration}}$. Indeed, Tba_Ø shows lower $D_{\text{Hydration}}$ at 358 K than at 298 K. The lower $D_{\text{Hydration}}$ found in Tba_Ø may reflect the structural adaptation of the *T. barophilus* proteome to high temperatures, as observed by EINS—this is a structural proteome rearrangement of which Tba_MG is deprived due to the presence of osmolytes.

Here, we studied intact, live cells and show that the accumulation of osmolytes significantly impacts intracellular crowding, and that the osmolyte mannosylglycerate acts by rigidifying proteins indirectly through a crowding effect—possibly at the hydration shell level. This work further builds on previous observations that the main hydrostatic high-pressure adaptive mechanisms of piezophiles include a decrease in hydration water diffusion.



298K	Tba_MG		Tba_Ø	
	0.1 MPa	40 MPa	0.1 MPa	40 MPa
P_{elastic}	0.01 ± 0.01	0.01 ± 0.01	0.01 ± 0.01	0.01 ± 0.01
$P_{\text{hydration}}$	0.11 ± 0.02	0.11 ± 0.02	0.10 ± 0.02	0.11 ± 0.02
P_{bulk}	0.65 ± 0.03	0.65 ± 0.03	0.66 ± 0.03	0.65 ± 0.03
P_{proteome}	0.25 ± 0.03	0.25 ± 0.03	0.24 ± 0.03	0.25 ± 0.03
$D_{\text{bulk}} (10^{-5} \text{ cm}^2/\text{s})$	1.85 ± 0.05	1.85 ± 0.05	1.85 ± 0.05	1.85 ± 0.05
$\tau_{\text{bulk}} (\text{ps})$	0.91 ± 0.10	1.64 ± 0.07	0.96 ± 0.09	1.45 ± 0.11
$D_{\text{hydration}} (10^{-7} \text{ cm}^2/\text{s})$	5.9 ± 0.3	4.5 ± 0.3	5.7 ± 0.3	2.9 ± 0.3
$\Gamma_{\text{proteome}} (\text{mcV})$	0.43 ± 0.01	0.43 ± 0.01	0.43 ± 0.01	0.43 ± 0.01
358K	Tba_MG		Tba_Ø	
	0.1 MPa	40 MPa	0.1 MPa	40 MPa
P_{elastic}	0.01 ± 0.01	0.01 ± 0.01	0.01 ± 0.01	0.01 ± 0.01
$P_{\text{hydration}}$	0.22 ± 0.03	0.21 ± 0.03	0.21 ± 0.03	0.21 ± 0.03
P_{bulk}	0.47 ± 0.05	0.47 ± 0.05	0.47 ± 0.05	0.46 ± 0.05
P_{proteome}	0.31 ± 0.05	0.32 ± 0.05	0.32 ± 0.05	0.33 ± 0.05
$D_{\text{bulk}} (10^{-5} \text{ cm}^2/\text{s})$	5.2 ± 0.1	5.1 ± 0.1	6.7 ± 0.1	6.6 ± 0.1
$\tau_{\text{bulk}} (\text{ps})$	0.10 ± 0.05	0.11 ± 0.05	0.46 ± 0.09	0.47 ± 0.08
$D_{\text{hydration}} (10^{-7} \text{ cm}^2/\text{s})$	5.6 ± 0.4	4.0 ± 0.4	2.7 ± 0.4	1.8 ± 0.4
$\Gamma_{\text{proteome}} (\text{mcV})$	0.61 ± 0.01	0.61 ± 0.01	0.61 ± 0.01	0.61 ± 0.01

Table 1

Fit parameter values for the two samples at different pressures (0.1 MPa and 40 MPa) and temperatures (298 K and 358 K). The fields in green show characteristic responses to high hydrostatic pressure of piezophiles. Dark green indicates similarities between samples; light green fields, differences. The fields in blue correspond to the osmolyte effects on bulk water. The fields in red indicate a different response to high temperature between samples.



Masato Matsuura, Japanese Neutron Science and Technology Centre, (CROSS), Tokai, Japan
'I am the scientist responsible for the backscattering spectrometer, DNA, installed at J-PARC MLF. I'm studying lattice and ion dynamics in condensed matter, including organic molecular materials, relaxor ferroelectrics, quasicrystals and Li-ion conductors.'

Lattice dynamics coupled to charge and spin degrees of freedom in the organic charge-transfer salt κ -(BEDT-TTF)₂Cu[N(CN)₂]Cl

Thermal neutron three-axis spectrometer IN8

Organic molecular materials, which are characterised by their softness, are considered attractive as lightweight and flexible electronic materials. They exhibit a variety of electronic states, from superconductivity to electronic ferroelectricity and insulator-metal transition, that are closely related to this 'softness'. Although inelastic neutron scattering (INS) is an ideal probe for studying potential lattice anomalies coupled to these interesting properties, the lack of sufficiently large single crystals has hampered systematic INS studies with only a few exceptions [1].

AUTHORS

Ma. Matsuura (Science and Technology Center, CROSS, Japan)
T. Sasaki (Institute for Materials Research, Tohoku University, Japan)
J. Müller and **M. Lang** (Institute of Physics, Goethe-University Frankfurt, Germany)
O. Stockert (Max Planck Institut für Chemische Physik der Festkörper, Germany)
A. Piovano (ILL)

ARTICLE FROM

Phys. Rev. Lett. (2019) — doi:10.5291/ILL-DATA.9-11-1773

REFERENCES

- [1] L. Pintschovius, H. Rietschel, T. Sasaki, H. Mori, S. Tanaka, N. Toyota, M. Lang and F. Steglich, *Europhys. Lett.* 37 (1997) 627
 [2] P. Lunkenheimer, J. Müller, S. Krohns, F. Schrettle, A. Loidl, B. Hartmann, R. Rommel, M. de Souza, C. Hotta, J.A. Schlueter and M. Lang, *Nat. Mater.* 11 (2012) 755

κ -(BEDTTF)₂Cu[N(CN)₂]Cl (κ -Cl) has been intensively studied as a typical dimer-Mott system. Recently, its electronic ferroelectricity has attracted new scientific attention [2]. However, the origin of the electric dipoles in this compound is still under debate because of the lack of direct evidence from optical spectroscopy, which is sensitive to the molecular charge. Given that the electron-lattice coupling is finite, fluctuations of the electric dipoles are expected to give rise to anomalies in the lattice dynamics that can be sensitively probed by INS. To study a phonon anomaly associated with electronic ferroelectricity, we performed an INS experiment on deuterated single crystals of κ -Cl, mainly using the three-axis spectrometer IN8 at the ILL. We succeeded in obtaining clear phonon signals with ~8 min counting, owing to the large neutron flux and low background from two co-aligned single crystals with a total mass of 7 mg (**figure 1a**).

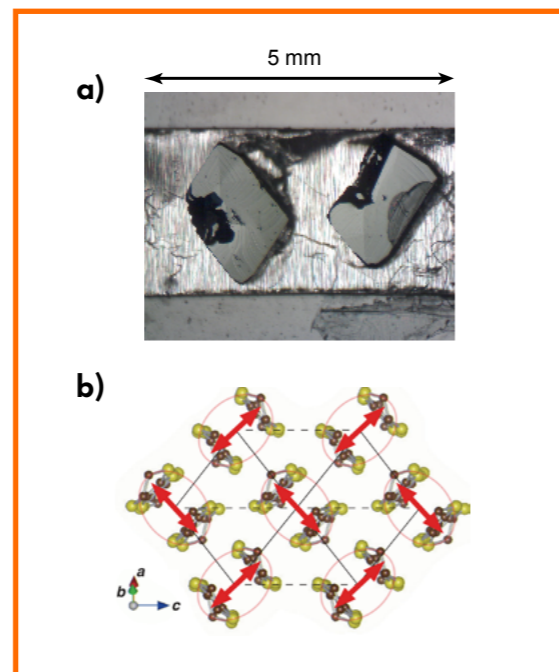


Figure 1

a) Photo of deuterated single crystals of κ -Cl.
b) Crystal structure of BEDT-TTF molecule layers in κ -Cl. Ellipses indicate BEDT-TTF dimers, while thick arrows show schematically the breathing mode of BEDT-TTF molecules mainly detected at (603).

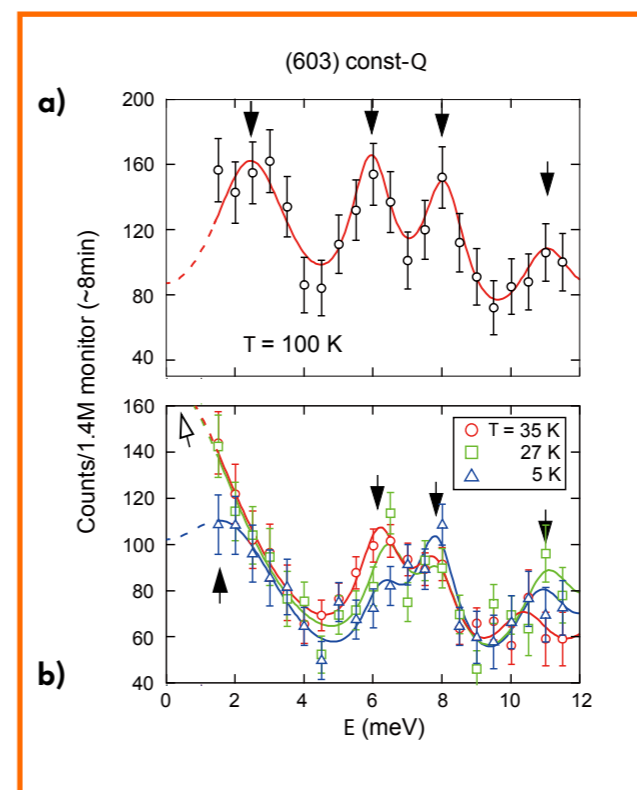


Figure 2

a) and **b)**: Temperature dependence of constant-Q cuts at (603) measured on IN8.

Figures 2a and **2b** show the temperature dependence of the constant-Q cuts at $Q = (603)$. At $T = 100$ K we observe clear phonon peaks at $E = 2.6, 6, 8$ and 11 meV, shown by the closed arrows. On cooling, the peak at 2.6 meV changes into a sloped signal whereas the three modes at $6, 8$ and 11 meV remain at almost the same energy. We associate the change in the 2.6 meV peak with an increase in the damping factor for a bond-breathing mode of the BEDTTF dimers, schematically shown in **figure 1b**. From fits of constant-Q spectra by the damped harmonic oscillator function, we clarify that the bond-breathing mode at 2.6 meV becomes overdamped between T_{ins} ($\sim 50 - 60$ K), where electrical resistivity increases rapidly, and $T_N (= T_{FE} = 27$ K), at which ferroelectric ordering and antiferromagnetic ordering occur simultaneously. The phonon anomaly, roughly coinciding with the change in electrical resistivity, ferroelectricity and magnetism, suggests close correlations between the lattice and the spin and charge degrees of freedom in the BEDTTF molecules.

We consider these INS results to represent an important step and one that may trigger further systematic studies on lattice dynamics and its coupling to the electronic degrees of freedom in the family of organic charge-transfer salts.



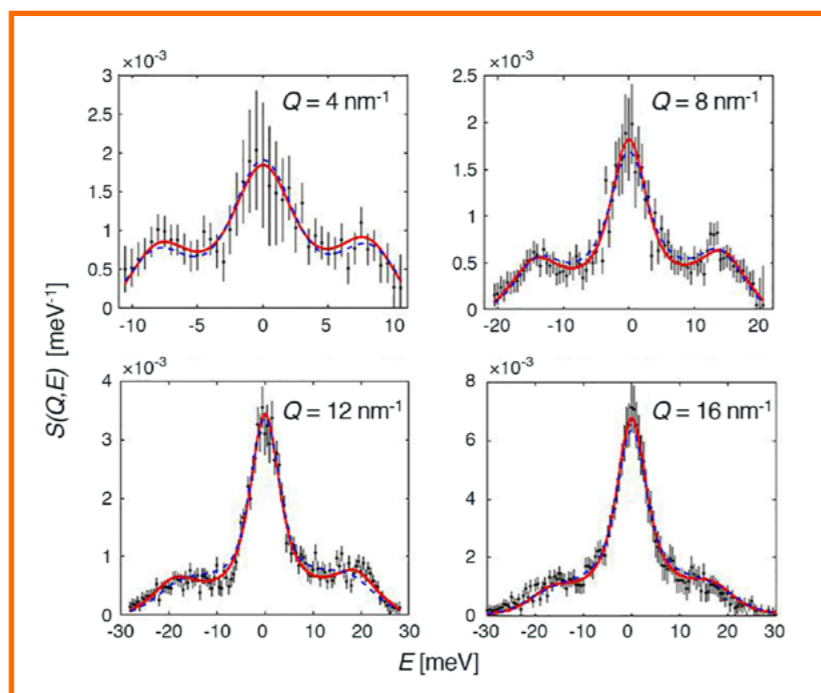
Eleonora Guarini, Italian Department of Physics and Astronomy, University of Florence, Italy
 'For 25 years my research has focused on the study of static and dynamic properties of the liquid state, through neutron scattering experiments, the analysis of molecular dynamics simulations and theoretical work on the dynamical interpretation of various classes of liquids (atomic, molecular, metallic and quantum fluids).'

Neutron scattering and *ab initio* simulation: essential and inseparable tools for studying liquids dynamics such as shear waves in silver

Brillouin scattering spectrometer BRISP

The propagation of compression waves in a liquid is a well-established phenomenon, responsible for the travelling of sound in it. More debated is the case of shear waves, which are in principle not allowed to propagate in an ideal liquid. This is an important issue relating to the innermost nature of the liquid state. We therefore decided to combine neutron and numerical techniques to examine the existence of shear excitations in liquid silver and the conditions under which it is possible to detect them.

Figure 1
 Experimental (black dots) and AIMD (blue dashes) dynamic structure factor of liquid silver. The red line is the fit to neutron data.



AUTHORS

E. Guarini and F. Barocchi (University of Florence, Italy)
 A. De Francesco and F. Formisano (IOM-CNR c/o ILL)
 A. Laloni (ESS, Lund, Sweden)
 U. Bafilo (IFAC-CNR, Florence, Italy)
 B.G. del Rio, D.J. González and L.E. González (University of Valladolid, Spain)

ARTICLE FROM

Phys. Rev. B (2020) — doi:10.1103/PhysRevB.102.054210

REFERENCES

- [1] S. Hosokawa *et al.*, J. Phys.: Condens. Matter 27 (2015) 194104
- [2] E. Guarini *et al.*, Phys. Rev. B 88 (2013) 104201
- [3] E. Guarini *et al.*, Phys. Rev. E 95 (2017) 012141

Sound waves propagate in all fluids, even in the most dilute ones such as air. These are longitudinal pressure waves. The propagation of transverse waves, on the other hand, requires that the medium is able to resist shear stresses, which is not the case for fluids in normal conditions. However, when the density is high enough, as in liquids, and the wavevector Q is above a certain threshold, a fluid also becomes able to sustain transverse waves. This is shown clearly by simulations of the transverse-current autocorrelation spectrum, which is not, however, a measurable quantity. A presently debated issue in the field of liquids dynamics is whether what is actually determined in an experiment, *i.e.* the dynamic structure factor $S(Q, \omega)$, does or does not show evidence of shear excitations. Experimental investigations, mostly focused on liquid metals, have reported contradictory results in different systems [1]. In particular, one neutron scattering and simulation study failed to reveal transverse waves in the $S(Q, \omega)$ of liquid gold [2]. This result inspired us to investigate the dynamics of another noble metal, *i.e.* silver.

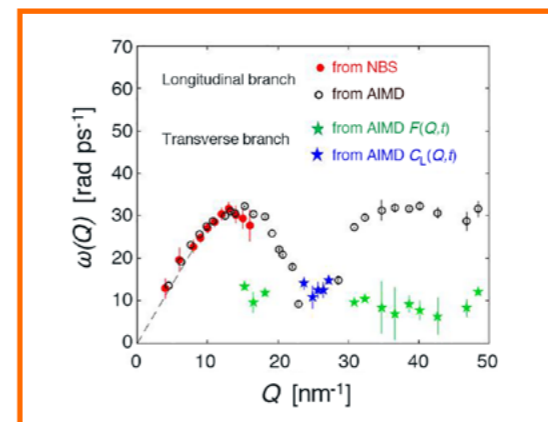


Figure 2

Longitudinal and transverse branches in the dispersion curve of liquid Ag.

Neutron Brillouin scattering at thermal wavelengths is an excellent technique for such studies because it probes relatively high frequencies ω in the low- Q range relevant to collective excitations. We measured the $S(Q, \omega)$ of liquid Ag using the dedicated spectrometer BRISP.

Figure 1 shows examples of the experimental spectra, together with a best fit of the generalised-hydrodynamics model and the results of an *ab initio* molecular dynamics (AIMD) simulation. Both visual inspection and the fact that a model containing only the contribution of sound modes provides a good fit suggest that in the experimentally accessible Q range, transverse excitations are below a detectability threshold, if present at all. In this respect, silver displays behaviour similar to that of gold.

AIMD simulations can, however, also probe the dynamics at larger Q s than those accessible experimentally, and their good agreement with neutron data at small Q s makes it possible to investigate $S(Q, \omega)$ in a broader Q range with confidence. Doing so, we found that a transverse component clearly emerges at wavevectors above the maximum reached by the measurements ($Q \sim 16 \text{ nm}^{-1}$). Thus, the appearance of shear wave propagation in $S(Q, \omega)$ in liquid Ag is established. **Figure 2** shows the frequencies of sound and shear modes as functions of Q .

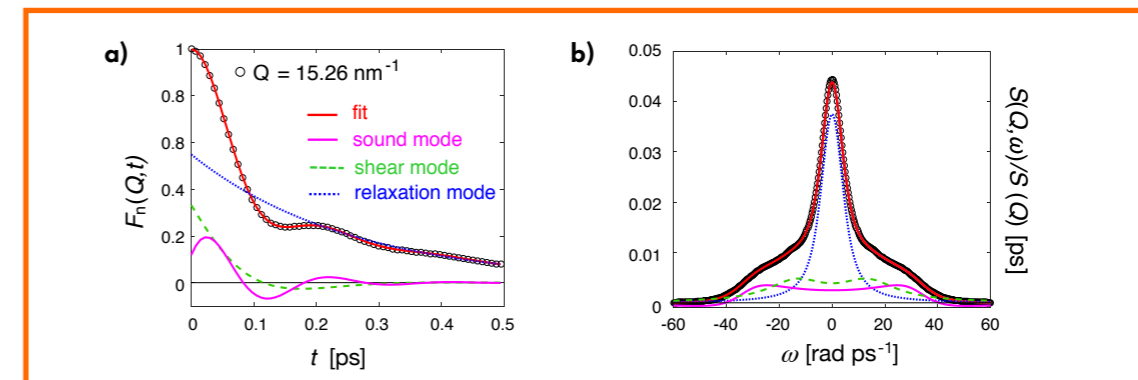
Our work also shows that a well-founded modelling of the dynamical response of the liquid is crucial for correctly interpreting both the experimental and the simulation results. This point has not always been given due consideration; indeed, model fitting is often used

as a heuristic method to simply locate lines, shoulders or other spectral features. In fact, all excitations and relaxations must be modelled in such a way that the total system response complies with a few general theoretical properties of $S(Q, \omega)$. This goal has been attained through consistent application of the well-tested and efficient multi-exponential decomposition of the corresponding time correlation function $F(Q, t)$ [3]. An example of this analysis is shown in **figure 3a**, where a perfect fit to AIMD data is displayed together with its main components, with the presence of the shear modes evident. **Figure 3b** shows the corresponding spectral contributions.

The most valuable indications coming out of this work are that: (i) more than one correlation function has to be studied, with simulations paralleling experimental work; (ii) rigorous methods of analysis need to be applied to reliably interpret the spectra; and (iii) multi-exponential analysis allows for an in-depth assessment of the dynamical processes. Future advances in our general understanding of the dynamics of disordered systems with high-energy excitations require neutron spectrometers able to probe $S(Q, \omega)$ in the low- Q range, BRISP being the first working prototype of this kind in the world.

Figure 3

a) Simulated intermediate scattering function $F(Q, t)$ (black circles) and fit result (red solid curve). The multi-exponential fit components are also shown separately, as indicated in the legend.
b) Corresponding spectrum, once again resolved into its components as per the legend in (a).





Nicolae Mărginean, Romanian Horia Hulubei National Institute of Physics and Nuclear Engineering, Romania
'I am senior scientist and recently General Director of IFIN-HH, Măgurele, Romania. I study the structure of atomic nuclei by employing different types of reaction

mechanisms and arrays based on high-purity germanium detectors, such as ROSPHERE in Măgurele and FIPPS at the ILL, in order to achieve the highest precision possible in γ -ray spectroscopy.'

The stable nucleus ^{64}Ni offers new insights into the nature of nuclear forces

Fission product prompt gamma-ray spectrometer FIPPS

Nuclear states of different ellipsoidal shapes have been identified in semi-magic ^{64}Ni using the FIPPS instrument, which provided unprecedented sensitivity in a thermal-neutron capture experiment with a radioactive ^{63}Ni (2 GBq) target. This shape coexistence phenomenon is similar to the Jahn–Teller effect in molecules, which describes the appearance of deformation in terms of symmetry breaking. Large-scale Monte Carlo shell-model calculations provide a complete microscopic understanding of these unexpected structural features and highlight the key role of the monopole tensor part of the nucleon–nucleon interaction, a component of the nuclear force that has not been properly considered until recently.

Figure 1

The FIPPS array equipped with 16 clover detectors (eight on loan from IFIN-HH) arranged in a 4π geometry, with a $\sim 3.7\%$ total efficiency at 1.3 MeV.

AUTHORS

N. Mărginean (IFIN-HH, Măgurele, Romania)
C. Michelagnoli (ILL)
S. Leoni (University of Milan and INFN, Italy)
R. Janssens (University of North Carolina and TUNL, USA)
B. Fornal (Institute of Nuclear Physics, Krakow, Poland)
T. Otsuka (University of Tokyo and RIKEN, Japan)

ARTICLE FROM

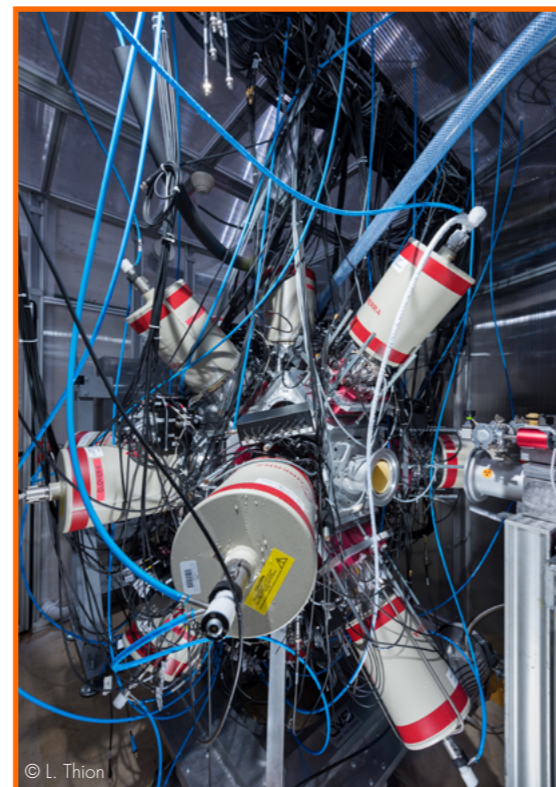
Phys. Rev. Lett. (2020) — doi.org/10.1103/1.25.102502

REFERENCES

- [1] K. Heyde and J.L.Wood, Rev. Mod. Phys. 83 (2011) 1467
- [2] H.A. Jahn and E. Teller, Proc. R. Soc. A 161 (1937) 220
- [3] A. Harder, S. Michaelsen, A. Jungclaus, K.P. Lieb, A.P. Williams, H.G. Börner, and M. Trautmannsheimer, Z. Phys. A 343 (1992) 7
- [4] T. Otsuka, Y. Tsunoda, T. Abe, N. Shimizu and P. Van Duppen, Phys. Rev. Lett. 123 (2019) 222502

The physics of atomic nuclei has revealed a number of peculiar facets of nuclear microstructure. One of these is shape coexistence: states of different shapes (like a sphere and an ellipsoid) may appear at similar excitation energies in certain nuclear species [1]. This phenomenon is similar to the Jahn–Teller effect in molecules where it describes the appearance of deformation in terms of symmetry breaking [2].

Until recently, the general text-book rule has been that by moving away from the nuclear magic numbers along isotopic chains, states with strong ellipsoidal deformation come down in excitation energy and 'intrude' into low-lying spherical states. In this study, we found a counter-example hidden deep in the nickel isotopic chain and occurring in the valley of stability where the important, relevant structure data were thought to be known.



© L. Thion

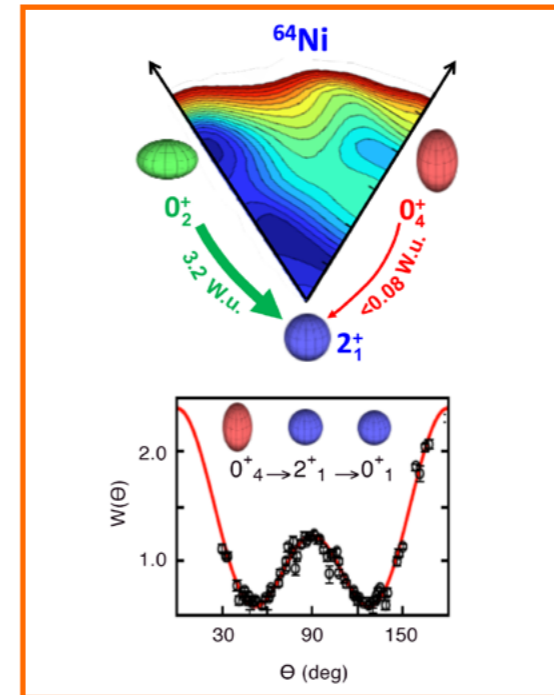


Figure 2

Top: ^{64}Ni potential-energy surface, in the deformation space, for the lowest 0^+ states. Prolate, oblate and spherical ellipsoidal shapes are in red, green and blue, respectively. Arrows indicate the decay transition probability (in Weisskopf units, W.u.) between different configurations, with an extremely small value for the prolate-to-spherical transition.

Bottom: Angular correlations measured with FIPPS for the $0^+_4 \rightarrow 2^+_1 \rightarrow 0^+_1$ γ -ray cascade showing the characteristic pattern of a pure E2 quadrupole decay, key information for identifying the prolate deformed 0^+_4 state.

In ^{64}Ni , a stable nucleus understood up to now to be purely spherical, we found evidence of an unexpectedly complex landscape of triple-shape coexistence (spherical, oblate and prolate ellipsoidal shapes) with respect to similar states in the 'magic' nucleus ^{68}Ni , with strongly deformed states going up in excitation energy by about 1 MeV.

To achieve the sensitivity required to probe the structure of ^{64}Ni , various reaction mechanisms (proton and neutron transfer, thermal-neutron capture, Coulomb excitation and nuclear-resonance fluorescence), combined with state-of-the-art γ -ray detection techniques, had to be employed in a *tour de force* involving four experiments jointly conducted at four different laboratories in Europe and the USA: the ILL, the IFIN-HH Tandem Laboratory (Romania), the Argonne National Laboratory (Chicago, USA) and the Triangle Universities Nuclear Laboratory (TUNL, North Carolina, USA). These experiments were performed by a large collaboration led by experimentalists and theorists from Romania (IFIN-HH), the ILL, Italy (University of Milan), the USA (University of North Carolina and TUNL), Poland (IFJ-PAN, Krakow) and Japan (University of Tokyo).

At the ILL, the combination of the high neutron flux, the high-performing FIPPS instrument and a long measurement time (20 days) allowed us to collate exceptionally high-quality statistical data through thermal-neutron capture. To obtain detailed information on all the quantum mechanical properties of ^{64}Ni , including the angular momentum and parity of the excited states, the FIPPS array was equipped with 16 clover detectors (eight on loan from IFIN-HH) arranged in a 4π geometry and covering a large range of angles (**figure 1**). By measuring, with high precision, the distribution of γ rays in space we clearly established the coexistence of 0^+ and 2^+ states with intrinsic spherical, oblate and prolate ellipsoidal shapes, with the prolate ones

residing in a deep, well-isolated potential well as indicated by the significantly hindered prolate-to-spherical decay (with $B(E2) \ll 1$ W.u.) (**figure 2**).

With the FIPPS instrument, the ILL is unique among the world's neutron facilities in enabling such a measurement; a measurement that is a challenge not only from the detection point of view but also because of its rare and radioactive target. Originally produced during a long experiment on the GAMS instrument at the ILL [3], the ^{63}Ni meanwhile has served in a number of investigations, including Mößbauer spectroscopy at TU Munich and astrophysical cross section measurements at LANL and CERN, while a fraction of it was used by the PSI radiochemistry group to prepare the present sample. This radioactive sample (2 GBq) required particular protection, health and safety protocols.

To interpret the data we had to employ large-scale Monte Carlo shell-model calculations, which turned out to be so complex that a computing farm in Japan employing a million processors was used to carry them out. As a result, we obtained a complete, microscopic understanding of the observed, yet unexpected, structural features of ^{64}Ni : the shape coexistence phenomenon in ^{64}Ni and the rise in excitation energy of the prolate shape clearly originate from the action of the monopole tensor force (not considered until recently), which shifts effective single-particle energies, already in the valley of stability, weakening resistance against deformation [4].

Our experimental achievement is, therefore, a crucial benchmark for theoretical models and sheds new light on nuclear forces. This is essential for gaining a thorough understanding of the microscopic structure of all nuclei, including the 'exotic' systems that power reactions in stars under conditions that cannot be reproduced in laboratories on Earth.



Santwana Dubey, Indian University of Central Florida, USA
 'In 2019 I received my PhD from the University of Mainz on isotopic fission yield measurements using CLTDs on the LOHENGRIN spectrometer. Now I am a postdoc in the USA, studying atom-light interactions with a COLTRIMS.

That's a recoil-momentum spectrometer, just like LOHENGRIN, but we induce the dissociation with photons instead of neutrons and the energy scale of the ions is seven orders of magnitude lower compared with fission.'

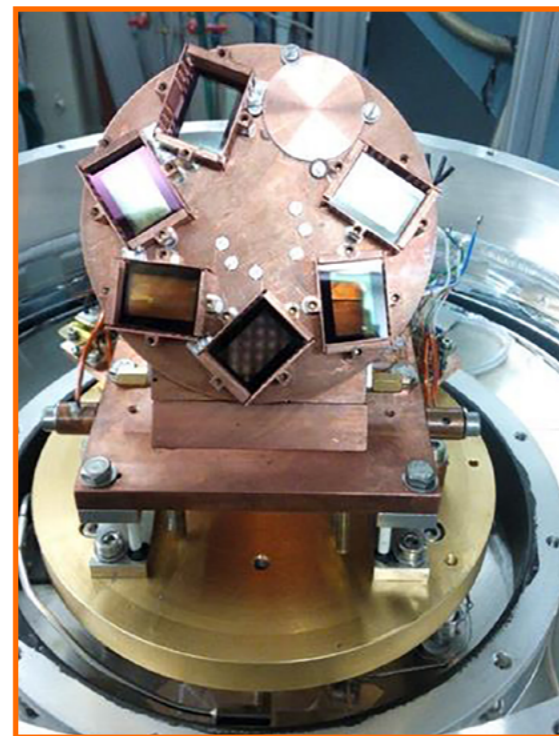
Accurate ^{92}Rb and ^{96}Y yields from thermal-neutron-induced fission of ^{235}U and $^{239,241}\text{Pu}$ determined using calorimetric low-temperature detectors

LOHENGRIN spectrometer

The novel technology of calorimetric low-temperature detectors (CLTDs) was applied to determine isotopic yields of fission fragments from thermal-neutron-induced fission on the LOHENGRIN spectrometer at the ILL. Accurate yields were determined for the dominant contributors to the high-energy portion of the reactor antineutrino spectra ^{92}Rb and ^{96}Y . Our new measurements resolve inconsistencies between previous yield measurements and fission data libraries and reduce nuclear data uncertainties in the computation of reactor antineutrino spectra using the summation method.

Figure 1

The CLTDs along with movable SiN absorber foil stacks of different thicknesses housed in the cryostat are operated at about 1.5 K.



AUTHORS

S. Dubey, A. Echler, P. Egelhof and P. Grabitz (GSI, Darmstadt; JGU Mainz, Germany)
 S. Kraft-Bermuth (Giessen University, Germany)
 U. Köster (ILL)

ARTICLE FROM

Phys. Rev. C (2020) — doi:10.1103/PhysRevC.102.044602

REFERENCES

- [1] G. Mention *et al.*, Phys. Rev. D 83 (2011) 073006
- [2] D.A. Dwyer and T.J. Langford, Phys. Rev. Lett. 114 (2015) 012502
- [3] P. Egelhof and S. Kraft-Bermuth, Top. Appl. Phys. 99 (2005) 469
- [4] S.V. Tipnis *et al.*, Phys. Rev. C 58 (1998) 905

The so-called reactor antineutrino anomaly [1]—an apparent $\approx 2.5\sigma$ deficit in antineutrino rate from the Standard Model prediction—has been derived by comparing measured antineutrino rates from nuclear reactors. The observed anomaly could be explained by particle physics through the existence of a fourth 'sterile neutrino' [1]. However, it could also originate in nuclear physics as a problem in the conversion of experimental, integral, fission-product beta energy spectra to antineutrino spectra, based on the measurement by Klaus Schreckenbach *et al.* using the BILL spectrometer at the ILL. The expected antineutrino spectra can also be computed independently using the summation method, where the contributions of antineutrino spectra from known decay branches of fission products are summed, weighted with their fission yields. Only a few fission products with a very high Q value for beta decay contribute to the high-energy part (4 ~ 6 MeV) of the antineutrino spectra, where the discrepancy is particularly pronounced. Therefore, accurate measurements of the

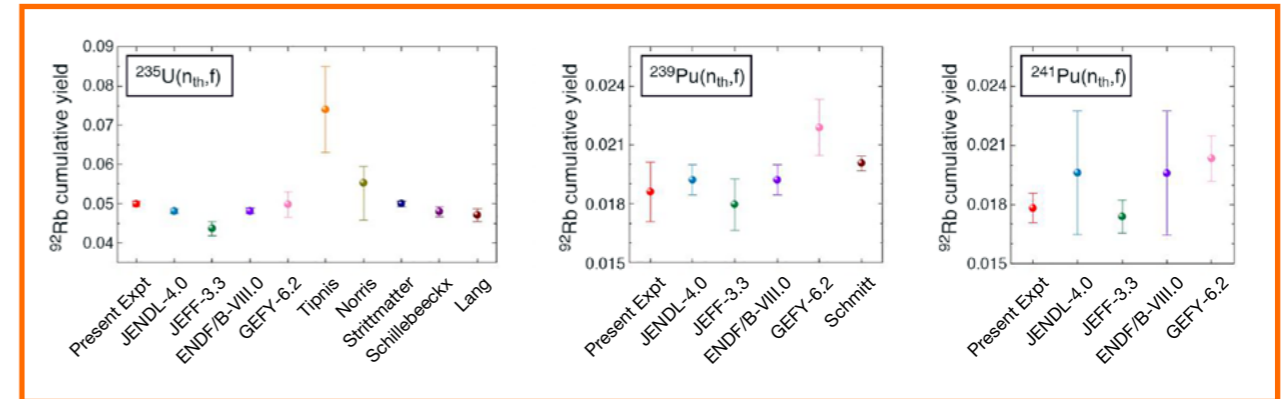


Figure 2

Cumulative yields for ^{92}Rb measured for three different targets, ^{235}U , ^{239}Pu and ^{241}Pu , compared with values reported in nuclear data libraries and prior experiments.

isotopic yield of these fission products are required in order to verify whether the antineutrino anomaly can be traced back to a nuclear physics origin.

In the following we report on new measurements of the fission yields of the two key contributors, ^{92}Rb and ^{96}Y , a measurement explicitly requested by ref. [2]. Accurate yield measurements for ^{92}Rb and ^{96}Y were achieved by applying the new technology of calorimetric low-temperature detectors (CLTDs) [3] on the LOHENGRIN spectrometer at the ILL (figure 1). To determine the isotopic fission fragment yields we used the passive absorber technique, a fairly universal method that exploits the Z-dependent energy loss of fission fragments in an energy absorber. After passing through a stack of SiN foils, the residual energy of the fission fragments is measured in the CLTDs via the temperature rise due to thermalisation of the particle's kinetic energy in the detector. Because of their principle of operation, which is independent of ionisation processes, CLTDs provide very good energy linearity and resolution for the spectroscopy of heavy ions at low energies. These advantages of CLTDs help to determine accurate yields by a new and independent method. Measurements were performed at different kinetic energy and ionic charge settings on LOHENGRIN to determine independent and cumulative fission yields. Particular effort was devoted to measuring the thermal neutron-induced fission of ^{235}U , since these results are relevant to the search for sterile neutrinos in the experiments STEREO at the ILL and PROSPECT at the HFIR (ORNL) given that both are research reactors with highly enriched ^{235}U fuel. Moreover, yields were determined for $^{239}\text{Pu}(n_{th},f)$ and $^{241}\text{Pu}(n_{th},f)$, which are additional contributors in power reactors.

Nuclear data libraries such as JEFF, ENDF and JENDL, as well as the GEF code, provide recommended fission yields based on prior experimental values combined with theoretical and/or empirical constraints (figure 2). However, how individual inputs have been weighted in these evaluations is often not traceable. For example, one measurement [4] reported a 50% higher cumulative yield for ^{92}Rb from $^{235}\text{U}(n_{th},f)$, which would further increase the anti-neutrino anomaly by 8% in the high-energy region. Ref. [4] used γ -ray spectrometric techniques, which may have a systematic bias for those fission products most relevant to the high-energy part of reactor antineutrino spectra in particular. This bias can be avoided by direct ion counting, as in the present experiment, thus leading to more reliable results. Therefore, we conclude that the value reported by ref. [4] has to be considered as a clear outlier.

The present study has demonstrated that the combination of the LOHENGRIN spectrometer with CLTDs provides isotopic fission yields of high accuracy. This reduces the nuclear physics uncertainties in investigations of the antineutrino anomaly and numerous other applications. This new technology can also be extended to other fission products, enabling more accurate fission yield libraries in the future.

**Werner Heil.** German

Institut für Physik, Johannes Gutenberg-Universität Mainz

'As an ILL Senior Fellow (1996–1999)

working on ^3He neutron spin-filters, I became fascinated by the rich and profound activities of the nuclear and particle physics group there.

Back in Mainz, the aSPECT project was launched which, after almost 20 years, ended in a successful scientific result.'

An improved determination of Standard Model parameters (a coefficient) in free neutron decay with the aSPECT spectrometer

Polarised cold-neutron beam facility PFIB

This study presents the most precise measurement to date of the electron-antineutrino angular correlation coefficient a in free neutron decay, using the 'PF1B' cold-neutron beam facility at the ILL. a is inferred from a detailed analysis of the integral proton-recoil spectrum measured with the aSPECT set-up, a MAC-E-Filter-type spectrometer with 4π acceptance. The result, which is in slight tension with recent measurements of g_A via the β -decay asymmetry in neutron decay, can be used to determine the axial-vector coupling constant g_A in the weak interaction.

Figure 1

Schematic of the aSPECT setup, a MAC-E-Filter-type spectrometer with 4π acceptance. Only the most important electrodes are shown. The whole setup is under ultra-high vacuum conditions.

AUTHOR

W. Heil (Johannes Gutenberg University, Mainz, Germany) on behalf of the aSPECT* collaboration [1]

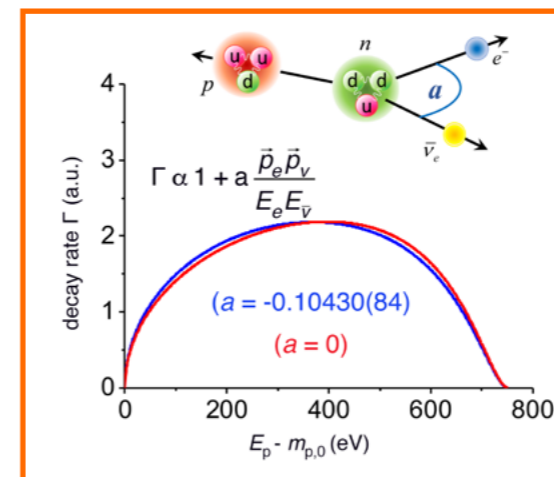
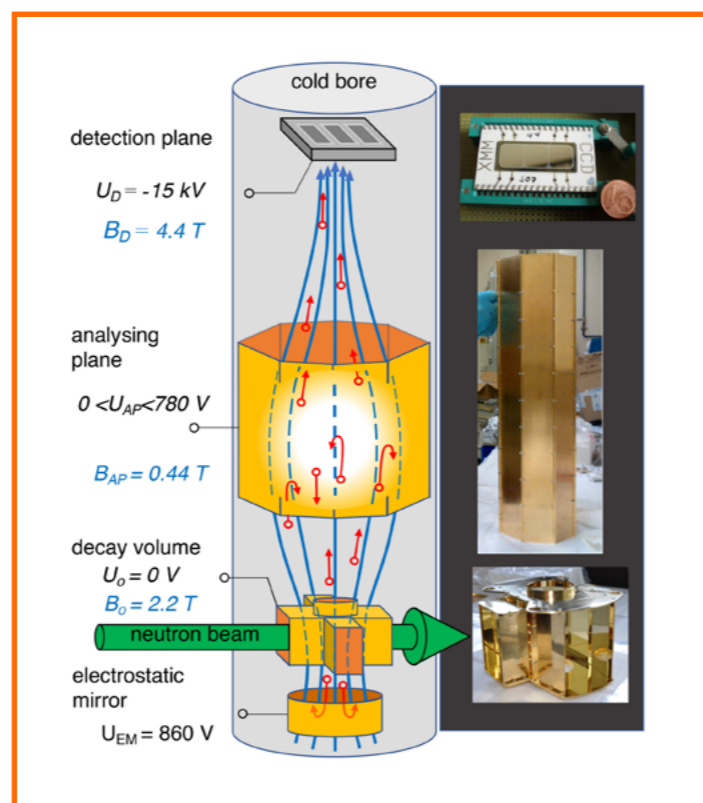
ARTICLE FROM

Phys. Rev. C (2020) — doi: <https://doi.org/10.1103/PhysRevC.101.055506>

REFERENCES

- [1] aSPECT* collaboration: M. Beck, F. Ayala Guardia, M. Borg, J. Kahlenberg, R. Muñoz Horta, C. Schmidt, A. Wunderle and W. Heil (Johannes Gutenberg University, Mainz, Germany); R. Maisonneuve, M. Simson, T. Soldner, R. Virost and O. Zimmer (ILL); M. Klopff and G. Konrad (Atominstut, Technical University of Vienna, Austria); S. Baeßler (Department of Physics, University of Virginia and Oak Ridge National Lab, USA); F. Glück (IKP and Karlsruhe Institute of Technology, Germany); and U. Schmidt (University of Heidelberg, Germany)
- [2] N. Severijns, M. Beck and O. Navliat-Cuncic, Rev. Mod. Phys. 78 (2006) 991
- [3] D. Dubbers and M.G. Schmidt, Rev. Mod. Phys. 83 (2011) 1111
- [4] J. Jackson, S. Treiman and H. Wyld, Phys. Rev. 106 (1957) 517
- [5] B. Märkisch et al. (PERKEO III Collaboration), Phys. Rev. Lett. 122 (2019) 242501

Observables in free neutron decay are abundant, *i.e.* the number of independent observables is considerably larger than the small number of parameters describing this decay in the Standard Model (SM) [2]. While the neutron lifetime gives the overall strength of the weak semileptonic decay, neutron decay correlation coefficients depend on the ratio of the coupling constants involved and hence determine its internal structure. Today, neutron β -decay provides an important input to the calculation of semileptonic charged-current weak interaction cross sections needed in cosmology, astrophysics and particle physics [3]. With the ongoing refinement of models, the growing need for more precise neutron decay data must be satisfied by new experiments.

**Figure 2**

Differential proton-recoil spectrum (decay rate Γ) for $a = -0.10430$ (83) (our result), and for comparison, for $a = 0$ (red line).

With the aSPECT experiment we determined the ratio of the weak axial-vector and vector coupling constants $\lambda = g_A/g_V$ from a measurement of the β - $\bar{\nu}_e$ angular correlation in neutron decay. The SM dependence of the beta-neutrino angular correlation coefficient a on λ is given by [4]: $a = (1 - \lambda^2)/(1 + 3\lambda^2)$. To date, the most accurate value of λ has been extracted from measurement of the β -asymmetry parameter A . However, determining λ from a yields complementary information, since the experimental systematics are different and systematic effects are relevant in these types of high-precision experiments.

A schematic of the aSPECT spectrometer is shown in **figure 1**. The longitudinal magnetic field of the MAC-E filter is created by a superconducting multi-coil system oriented in the vertical direction. The neutron beam enters horizontally in the lower part of the aSPECT spectrometer at the height of the high magnetic field B_0 and is guided through the decay volume (DV) electrode towards the beam dump further downstream. Protons and electrons from neutron decays inside the DV electrode are guided adiabatically along the magnetic field lines. Downgoing protons are converted into upgoing protons by reflection off an electrostatic mirror electrode below the DV electrode, providing a 4π acceptance of aSPECT. The protons are guided magnetically towards the analysing plane (AP) inside the main AP electrode. Protons with sufficient energy pass through the AP and are focused onto a silicon drift detector both magnetically and electrostatically. A re-acceleration voltage of $U_0 = -1.5$ kV applied to the electrode containing the detector is used to detect the protons.

Several beam times were taken with aSPECT on PF1B, the cold neutron beam facility at the ILL. The beam time of 100 days in 2013 then constituted the production measurement for a new determination of a . To determine the impact of systematic effects, measurements were made for seven different configurations of the aSPECT apparatus, with key properties of the instrument deliberately changed from their optimum settings. As a novelty in the field, a simultaneous fit to all these measurements was done, including a full simulation of the apparatus. A final result of the global fit, $a = -0.10430$ (84) was obtained, resulting in a relative uncertainty of $\Delta a/a = 0.8\%$. All values from the seven individual configurations, including systematic corrections as well as their weighted mean, are statistically in agreement with this result.

Figure 2 shows the differential proton-recoil spectrum (blue line) for the a -value extracted. Our new value is in good agreement with the present PDG value of (-0.1059 ± 0.0028) but with the overall accuracy improved by a factor of 3.3.

From a we obtain $\lambda = -1.2677$ (28). This value deviates by $\sim 3\sigma$ from the most recent λ measurement by the PERKEO III collaboration [5], which was determined via the β -asymmetry parameter A . This experimental situation calls for further improvements in measurement accuracy, in particular to that on a par with the PERKEO result. A significant deviation in the extracted λ -values from a - and A measurements may indicate contributions beyond SM in neutron decay.



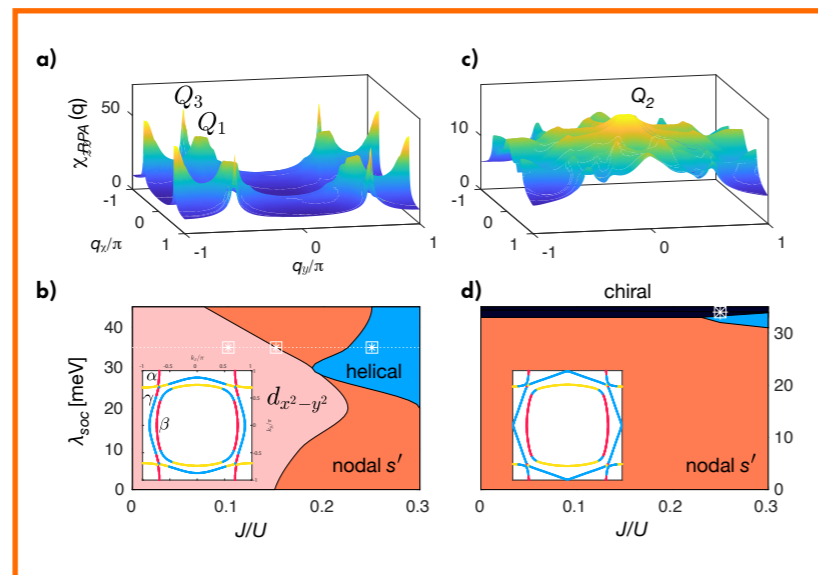
Astrid T. Rømer, Danish Niels Bohr Institute, Denmark
'I am a condensed matter theorist with a strong interest in the link between material models and experiments. A postdoctoral researcher, I am currently based at the Niels Bohr Institute. In 2018–19, I joined the ILL theory group working with models of superconducting pairing interactions in unconventional superconductors.'

Knight shift and leading superconducting instability from spin fluctuations in Sr_2RuO_4

The conductance of electrical current without resistance continues to fascinate and intrigue condensed matter physicists. Despite enormous efforts, since their discovery more than 100 years ago only the simplest superconducting materials are well understood theoretically. However, several other classes of superconductors have been discovered and classified using numerous experimental probes. Common to all of them is the existence of an electronic pairing mechanism that enables electrons to co-operate in such a way that they become impervious to small obstructions and are able to travel through the material without hindrance. We propose a model that describes how electronic pairing takes place in the superconducting system Sr_2RuO_4 .

Figure 1

Longitudinal spin susceptibility and leading superconducting instability as a function of spin-orbit coupling and Hund's coupling for two different choices of the chemical potential of the xy orbital. The Fermi surface in each case is depicted in the inset, with the dominating orbital content indicated by colour: xy orbital is blue, xz is red and yz is yellow. The susceptibility shown in (a) and the corresponding Fermi surface and phase diagram in (b) are compatible with the experimental situation, while (c, d) are not.



AUTHORS

A.T. Rømer (Niels Bohr Institut, Denmark and ILL)

ARTICLE FROM

Phys. Rev. Lett. — doi:10.1103/PhysRevLett.123.247001 (2019)

REFERENCES

- [1] A.P. Mackenzie *et al.*, npj Quantum Mater. 2 (2017) 4
- [2] A. Tamai *et al.*, Phys. Rev. X 9 (2019) 021048
- [3] P. Steffens *et al.*, Phys. Rev. Lett. 122 (2019) 047004
- [4] A. Pustogow *et al.*, Nature 574 (2019) 72

Pairing between electrons can occur as a result of a weak, effective attraction that arises due to lattice vibrations inside the crystal, as described by the celebrated BCS theory. This provides a very good model of conventional superconductors but fails to describe their unconventional cousins. Many unconventional superconductors are found in close proximity to magnetic order, in the sense that one can tune the system from a magnetic to a superconducting state by, e.g. doping or strain. This points to the relevance of magnetic fluctuations and even to the possibility that these could provide the effective electronic pairing. If the itinerant electrons themselves give rise to the pairing through magnetic fluctuations, we can construct a simple model where only electrons are at play.

We set out to construct one such model in the case of the enigmatic material Sr_2RuO_4 . This is an unconventional superconductor that has been scrutinised by almost every possible experimental probe over the past 25 years, and yet its superconducting order remains a mystery [1]. At high temperatures it is a Fermi liquid and exhibits a very well-defined Fermi surface when measured by ARPES, although correlations are relatively strong [2]. The sharp Fermi surface makes it one of the most appealing systems for investigating the problem of superconducting pairing arising from spin fluctuations of the itinerant electrons.

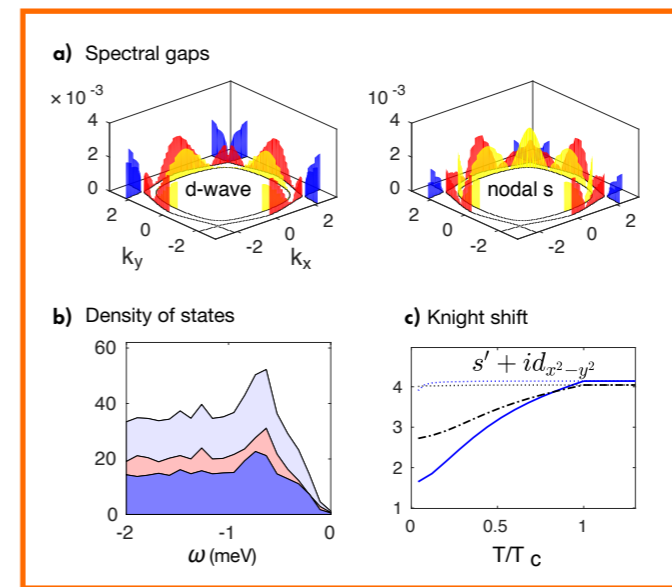


Figure 2

(a) Spectral gaps for superconducting $d_{x^2-y^2}$ and nodal s' -wave order; (b, c) density of states and Knight shift of the combined superconducting solution $d_{x^2-y^2} + is'$. In (c) the solid blue (black dashed-dotted) line is the Knight shift for in-plane (out-of-plane) fields, while dotted lines display the Knight shift results in the absence of superconductivity. Experimentally, only in-plane fields have been accessed in Ref. [4], showing a significant reduction in the Knight shift in the superconducting state.

At the same time, it is important to correctly take into account the multi-orbital nature of the electronic structure, which adds a level of complexity to the modelling.

If magnetic fluctuations are responsible for the pairing interaction they should be clearly visible from neutron scattering, and this is indeed the case. Neutron scattering experiments have provided important information about the magnetic correlations in Sr_2RuO_4 [3]. Interestingly, theoretical calculations find a similar structure arising from Fermi-surface nesting. Recent research from the ILL has established that ferromagnetic fluctuations are present, albeit much weaker [3]. In addition, strong spin anisotropy between the in-plane and out-of-plane spin components has been established through polarised neutron scattering. This points to a prominent role of the spin-orbit coupling.

What type of superconducting order parameter arises if the effective electron pairing happens through magnetic fluctuations? We answered this question by modelling Sr_2RuO_4 while paying special attention to the spin fluctuation spectrum, the presence of strong spin-orbit coupling and the multi-orbital nature of the electrons.

We found that spin-fluctuation-mediated pairing favours even-parity, singlet-like, superconducting order. Only if the ferromagnetic fluctuations are much stronger

than experimentally observed can a chiral triplet superconducting order be realised. Other triplet solutions can, however, be stabilised in the regime of strong spin-orbit and Hund's couplings. Nuclear magnetic resonance [4] reveals a substantial reduction in the Knight shift below the superconducting critical temperature, pointing to a spin-singlet type of superconducting order parameter where magnetic moments are gradually frozen out due to the formation of singlets. Other experimental probes find evidence of nodal structure in the superconducting gap, as well as evidence of time-reversal symmetry-breaking in Sr_2RuO_4 .

The combination of these experimental facts led us to propose an accidental degeneracy between two different even-parity solutions, $d_{x^2-y^2}$ and s' . The combined solution $d_{x^2-y^2} + is'$ maintains a nodal structure and break time-reversal symmetry. Therefore this proposal reconciles most but not all the experimental observations. From the perspective of spin-fluctuation-mediated superconductivity, nearly degenerate solutions appear quite naturally as a result of the large Fermi surface pockets and the number of nesting possibilities, which each favour different superconducting gap structures. This renders an exotic proposal like $d_{x^2-y^2} + is'$ plausible in the case of Sr_2RuO_4 .



Leopoldo R. Gómez, Argentinian National University IFISUR-CONICET, Argentina
'I'm a physics professor and researcher from Argentina. I'm interested in the structural and dynamical properties of soft condensed matter systems. Currently, I'm working as a George

Forster Fellow at the MSS Institute of the Friedrich-Alexander University Erlangen-Nuremberg (Germany). Since 2017 I have been involved in a fruitful collaboration with members of the ILL Theory Group which has led to this publication.'

The packing structure of elastic rings

Understanding how disordered assemblies of ring molecules pack together is key for describing polymer rings and cyclic biomolecules. Here, we study the geometrical and topological properties of these systems by imaging assemblies of macroscopic rubber bands using tomography. While short bands pack in liquid-like, untangled structures, the container forces folded configurations for longer bands, creating highly interpenetrated and entangled assemblies. These results show that tomography is a crucial tool for revealing the structure of disordered filamentary systems.

AUTHORS

L.R. Gómez (UNISUR-CONICET, Bahía Blanca, Argentina)
 N.A. García (ILL, Grenoble, France)
 Th. Pöschel (Institut MSS, University Friedrich-Alexander Erlangen-Nürnberg, Germany)

ARTICLE FROM

Proc. Nat. Acad. February 18, 2020 117 (7) 3382-3387

REFERENCES

- [1] M. Rubinstein and R.H. Colby, *Polymer Physics* (Oxford University Press, New York, NY, 2003).
- [2] M. Rubinstein, *Phys. Rev. Lett.* 57 (1986) 3023
- [3] D. Michieletto and M.S. Turner, *Proc. Natl. Acad. Sci. U.S.A.* 113 (2016) 5195
- [4] J. Smrek and A.Y. Grosberg, *ACS Macro Lett.* 5 (2016) 750

The dynamics of linear polymers is well understood in terms of chain-entanglements and the reptation model [1]. Here, a chain in the assembly is confined to moving in a tube due to the presence of surrounding chains (entanglements = obstacles to lateral motion). Thus, in order to relax and diffuse, linear chains need to move like a snake (reptation = end-directed diffusion). However, ring molecules are topologically different. The absence of free ends here avoids reptation, so that conformations and the diffusion mechanisms remain unclear and hotly debated. In addition to entanglements, in disordered assemblies of rings there can also be threadings of molecules. Although early models of fully flexible polymer rings neglected the presence of threadings [2], more recent simulations showed that threadings completely dominate the structure of semi-flexible rings, producing a very slow relaxation dynamics [3].

In order to shed light on the geometrical and topological properties of assemblies of semi-flexible rings, we imaged disordered packings of rubber bands of various lengths using X-ray and neutron tomography. Despite being athermal, these simple systems display the key features observed in circular filamentous matter and, as shown in **figure 1**, allow the detailed characterisation of the geometry and topology of structures as a function of band length.

Figure 1

- Tomogram of bands' packing.
- Our analysis allows each band in the structure to be determined.
- Highlighted band in the assembly.

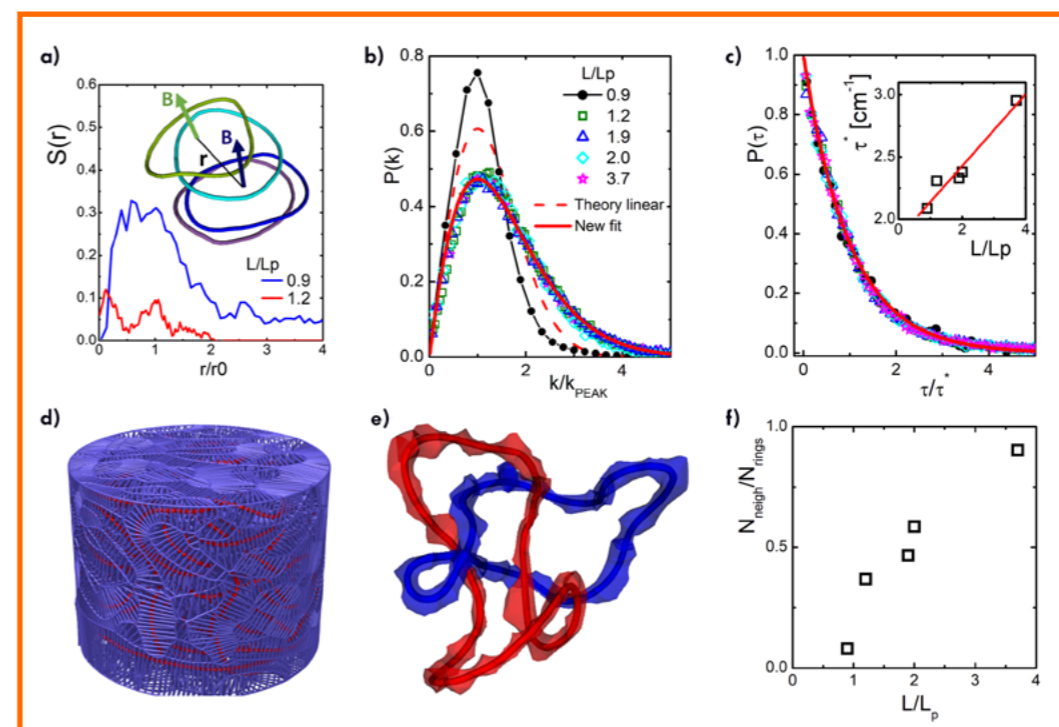
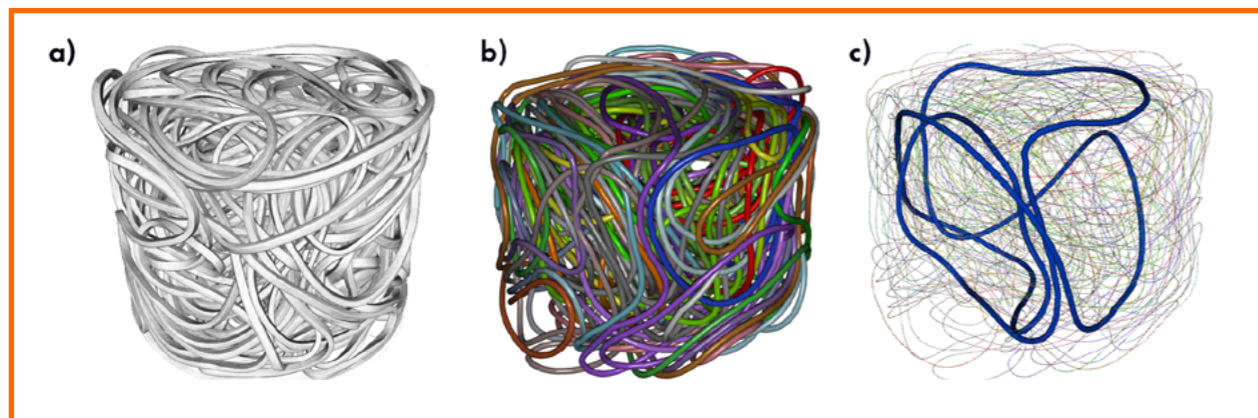


Figure 2

- Correlations of bands.
- Curvature distributions.
- Torsion distribution.
- Generalised Voronoi tessellation.
- Voronoi volume (tube-like) of two bands.
- Normalised number of neighbours of bands.

Figure 1a shows the typical tomography of a band's packing. To analyse these structures, we first developed a new method of analysing images that allowed us to obtain configurations of each band. **Figure 1b** shows the result of our analysis, with each band identified by a different colour. In **figure 1c**, a single band in the packing is highlighted in blue in order to better visualise its configuration and folding.

First, we studied the geometrical properties of the bands. For the shortest bands, we found that most pack like planar, almost undistorted, circular rings (see **inset, figure 2a**). For these short bands, an average band orientation can be obtained by averaging the binormals **B** (arrows in **figure 2a, inset**). Then, orientational correlations between close bands can be quantified using the order parameter $S(r) = \langle 3/2 \cos^2(\theta(r)) - 1 \rangle$, where $\theta(r)$ is the misorientation between the bands' binormals separated by a distance r . **Figure 2a** shows that at short distances (of the order of a band's radius) the binormals are somewhat aligned, such that short bands pack parallel with their neighbours, showing short-range, orientational correlations (blue line); for longer bands, this short-range order disappears due to chain flexibility (red line in **figure 2a**).

Next, we examined the distribution of the local curvature $P(k)$ and the local torsion $P(\tau)$ of the bands. **Figure 2b** shows $P(k)$ for the shortest bands (black line with points) and for the rest of the bands (coloured lines). The latter

nice collapse in a master curve; in contrast, the shortest (almost undistorted) rings clearly display a different, narrower, curvature distribution. In **figure 2c** we show the distribution of the absolute value of the torsion of the bands $P(\tau)$, for all the systems. In this plot, the torsion of the bands is normalised with a characteristic torsion τ^* , which scales linearly with the length of the band (**figure 2c, inset**). As can clearly be seen, after normalisation the torsion distribution for all the systems collapses in a universal master curve, which can be approximated accurately by a single, exponential decay function (red line in **figure 2c**).

To analyse the topology of the structures, we studied the threadings between bands [4]. We found these to increase linearly with band length, meaning simply that assemblies of longer bands are more entangled. To complete the characterisation of the rings' environment, we calculated the number of bands in the neighbourhood of a band in the structure using a generalised Voronoi tessellation (**figures 2d** and **2e**). Even for the smallest bands we find a co-ordination number of 26, which is approximately double that for dense liquids and solids. Remarkably, for the longest bands we observed that all the bands are first neighbours of each other, forming a complex, disordered, fully entangled structure (**figure 2f**). It is expected that thermal systems with a similar degree of entanglement will display an extremely slow dynamics.

MODERNISATION PROGRAMMES AND TECHNICAL DEVELOPMENTS

FIND US ON:   



- 72** MODERNISATION PROGRAMME AND INSTRUMENT UPGRADES
- 80** TECHNICAL AND METHODS DEVELOPMENTS

60M€
ENDURANCE
8 YEARS (2016–2023)



PANTHER
COMMISSIONED
IN
2020 

- INCREASED FLUX
- REDUCED BACKGROUND
- LARGER DETECTORS
- IMPROVED RESOLUTION
- ENHANCED CAPABILITIES
- RELIABILITY & PERFORMANCE

In 2020, the COVID-19 pandemic considerably altered our personal and professional landscapes. Despite the prevailing uncertainty and anxiety, we nevertheless adapted to major changes in our lives—total lockdown, remote working and travel restrictions. It is normal for ecosystems to spontaneously reorganise under environmental pressure in order to preserve their energy and address new challenges; thus, we have seen unexpected and innovative forms of discussion and exchange, as well as new styles of working, to emerge from this crisis.

During this extraordinary period, the ILL demonstrated exactly this potential to rapidly adapt and re-organise, thereby maintaining its international lead in neutron science. It has achieved this level of excellence by continuing to upgrade and modernise its instruments and technical facilities.

The Projects and Techniques Division continues to successfully manage the many instrument and infrastructure projects within the Endurance programme, in close collaboration with the Science Division. We have made the most of video-meeting technology to ensure, under the supervision of project managers, the ongoing follow-up and evaluation of design studies, purchasing, manufacturing, scheduling and budgeting for the instrument projects.

Staff and managers of the DPT were both efficient and reactive in maintaining activities on site, pushing the Endurance programme forward. During the first lockdown, in the spring of 2020, we were able to install both the second protein

crystallography station DALI and the liquid diffractometer D3; these were then commissioned during the summer reactor cycle. This cycle was run with a minimum number of users on site, having been prepared following a re-organisation of the teams for this purpose.

The summer cycle was, in fact, a tremendous success, given that the ILL managed to perform the usual number of experiments with only 35 % of the normal user contingent on site. This was thanks to massive efforts made by the IT and Instrument Control Services to finalise the VISA platform and remote-NOMAD facilities, enabling our users to manage their experiments and data-processing remotely. We received very positive feedback from users on this. It has given significant momentum to the extension of our remote-access solutions to other large-scale facilities as part of the European PaNOSC project.

Elsewhere, the DPT's Experimental Areas Mechanical Service and its Projects and Calculations Office worked closely with the Reactor Division on the series of complex thermal and neutronics calculations required for replacing the H1–H2 beam tube; the Detector Service and Neutron Optics continued with their development of new detectors (upgrades for the SANS D11 and D22 detectors), monitors, monochromators and supermirrors, as well as designing state-of-the-art ³He cells for neutron polarisation; and the Building and Site Maintenance Service remained heavily involved with the Reinforcement of Physical Protection project—the new security and visitor reception facilities should be operational by the summer of 2021.

The high levels of knowledge and skills developed within the DPT over many years have ensured our role in various EU-funded projects and collaborations with other large-scale facilities, on technological innovations, artificial intelligence and fuel conversion plans.

Thus, despite the pandemic situation, 2020 was a fruitful year for the ILL. It can be summarised as reflecting our considerable collective effort to prepare for the future, given the enormous challenges we face: completion of the Endurance programme, the delivery of neutrons for science and ensuring the reactor's compliance with regulations.

Given the complexity of these challenges, we have bundled the impressive list of maintenance tasks and the projects to replace the critical H1–H2 beam tube and H24 and H15 guide systems into the overarching project management programme 'ILL20/23'. Managed jointly by the DPT and the Reactor Division, the aim is to ensure the fine-grained co-ordination of upcoming reactor operations and shutdowns with the incremental installation of the Endurance instruments. This should ensure that the latter are fully commissioned and operational for the beginning of 2024. The success of ILL20/23 will mean our users are provided with a fully modernised suite of world-class instruments, together with a reliable supply of neutrons. The ILL will effectively be a brand-new installation, ready to operate for the decade to come.

Jacques Jestin
Head of the Projects and Techniques Division



KEEP UP-TO-DATE:

-  facebook.com/ILLGrenoble
-  twitter.com/ILLGrenoble
-  linkedin.com/company/institut-laue-langevin

Endurance: waiting patiently for the H1-H2 long shutdown

Endurance phases 1 & 2 encompass more than 30 new or upgraded instrument and infrastructure projects. Funded in phases and with a financial envelope of nearly 60 M€, the programme is being rolled out over eight years, between 2016 and 2023. Endurance is a massive undertaking on the part of the ILL and the ILL's Associates. Several new or upgraded instruments and infrastructure packages are already deployed and in user operation. The ILL's impending long reactor shutdowns in the next few years will see the installation of a full suite of modernised instrumentation under Endurance and associated gains in performance and capability, ultimately enabling new science.

AUTHORS

C. Dewhurst and J. Jestin (ILL)

Endurance 1 has already seen the delivery and entry into user operation of the fission-fragment gamma ray spectrometer **FIPPS** and the upgraded **INS** cold time-of-flight spectrometer and its **H16** neutron guide, as well as the delivery and commissioning of the new TOF spectrometer, **PANTHER**. **PANTHER** will be further improved with a new background chopper system and will enter the user programme early in 2021. The commissioning of a new position-sensitive area detector and polarisation components for the **D3** hot-neutron diffractometer has also begun. This will allow the efficient measurement of hydrogen-containing liquid samples using the precise discrimination of incoherent scattering. Meanwhile, the end of the long and complex construction of the **SuperSUN** source of ultra-cold-neutrons is in sight, with the successful commissioning of the ensemble of cryogenic equipment and its mounting in place anticipated in early 2021. Once the converter guide is installed inside the superfluid helium chamber, **SuperSUN** will begin to produce the highest density of UCNS in the world and will allow science to begin on the PanEDM experiment. Upgrades to the **IN20** thermal triple-axis spectrometer (TAS) have begun with the receipt and installation of a velocity selector for wavelength filtering, while the construction of new, double-focusing, graphite and Heusler monochromators and analysers is in progress for delivery in 2022.

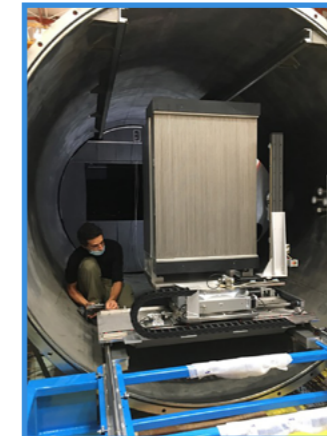
Endurance 2: In the first round of funding for Endurance 2 we were able to rapidly construct detectors for the SANS instruments **D22** and **D11**. Both detectors are being installed and commissioned during the winter 2020/2021 shutdown and will be available to users in the first cycle of 2021. **D22** is to receive an additional high-angle detector for extended q-range, while the **D11** detector replaces the ageing multidetector with a modern and increased area, efficiency and count-rate detector. The **D16** cold-neutron diffractometer is also undergoing an upgrade of the secondary spectrometer, including a new wide-angle detector.

The neutron-imaging facility at the ILL entered the user programme in 2020. Initially a part-time and private activity hosted by the 3SR group of the Université Grenoble Alpes (UGA) on the D50 instrument, a collaboration between UGA, Helmholtz Berlin and the ILL now allows for neutron-imaging activities within the regular ILL user programme. The **NeXT** project, funded within Endurance 2 and capitalising upon this collaboration, will see a full re-build of the imaging instrument backbone. This will allow for state-of-the-art imaging with advanced contrast techniques, high spatial resolution, intense neutron flux, combined X-ray imaging and even a second (monochromatic) imaging station for specific types of measurement and technique development. The **NeXT** instrument will be built during the H1-H2 long shutdown and be available again to users in 2023.

The **SuperSUN** cryogenic assembly. © Ecliptique – L. Thion



DALI – The second protein crystallography station



Additional detector for **D22** and new detector for **D11**.



The COVID-19 pandemic has by no means stopped activity at the ILL or the roll-out of Endurance projects. During the first lockdown in spring 2020, not only was the H4 beam tube replaced allowing the **D3** instrument to be re-assembled and upgrades commissioned, but also the **H141** guide was modified and the second protein crystallography instrument, **DALI**, installed in the previous IN11 position. **DALI** was commissioned with neutrons in autumn 2020 and will complement the existing LADI instrument when it welcomes users at the beginning 2021.

Endurance 1 & 2 have been waiting for H1-H2:

As well as seeing a vast amount of maintenance and upgrade work to ensure the safety and longevity of the ILL reactor, the H1-H2 shutdown from the end of 2021 to the end of 2022 will also see the installation of the new **H24** (thermal) and **H15** (cold-) neutron guides and the beginning of the installation of a large number of new and upgraded thermal- and cold-neutron instruments. The ILL 7 guide hall will undergo a significant re-modelling of instrumentation and infrastructure, including the provision of new instrument cabins providing comfortable spaces for users to work in. The **H24** project will bring dedicated thermal neutron guides to the upgraded **D10+**, **IN13** and new **XtremeD** (CRG) powder and single-crystal diffractometer, as well as providing neutrons to the test instrument CT2 and Cyclops.

H15 forms the lion's share of Endurance 2. The guide itself has a rather complex opposing curved expanding section referred to as 'the trumpet'. The trumpet serves two important purposes. The first is to spatially expand the neutron guide, thus converting the upstream high divergence to a lower divergence but extended over a greater area. This allows the guide to be split into multiple individual guide branches allowing dedicated end-of-guide beam positions for instrumentation. The second is to allow the opposing curve to leave a 'fingerprint' correlation between the divergence profile and the spatial position

at the end of the trumpet. In other words, neutrons on the left of the guide have a divergence distribution on average pointing to the left, and neutrons on the right side a divergence distribution on average pointing to the right. Importantly, this allows guide branches to be more widely separated in angle, thereby allowing space for substantially more instrumentation downstream. The final **H15** guide design took nearly two years to mature and, although complex, is now simplified compared with the original ambitious scenario. All its guide optics have now been ordered and all the instrument projects launched. **H15** will accommodate a substantially upgraded **D(00)7** instrument boasting more than x10 in neutron flux, making polarisation and spectroscopic analysis measurements realistic as well as achieving massive gains for the more usual diffuse scattering measurements. **D11** should receive an increase in neutron flux on the new **H15** guide and will be rebuilt and relocated with an optically cleaner collimation. The two additional end-of-guide positions are available for new instrumentation: the **SHARP+** (CRG) cold TOF spectrometer, with an expected neutron flux more than x10 its predecessor **IN6-SHARP** and a fourth short SANS instrument, **SAM** (CRG), with a MIEZE option. The matrix of performance and capability gains for the upgraded instruments under the Endurance project is given in **Table 1**.

The volume of work to be carried out at the ILL, and not only in delivering these extensive infrastructure and instrumentation projects, is daunting, requiring detailed planning of logistics and resources and operating within the constraints of critical reactor maintenance consolidated under the ILL 20/23 operating programme. These massive Endurance packages, **H24**, **H15** and associated instruments, will begin installation towards the end of 2021 with the first new instrumentation on **H24** coming on-line at the end of 2022 and **H15** instruments towards the end of 2023. Exciting times lie ahead.

MODERNISATION PROGRAMME AND INSTRUMENT UPGRADES

FIND US ON:   

Table 1

Matrix of performance and capability gains as a result of the Endurance project.

Instrument/Project	Flux ϕ	Background Reduction	Detector $\Delta\Omega$	Measurement Range (q, E)	Capabilities, Features, Options	Reliability, Longevity
Endurance 1 (2016-2018)						
PANTHER 1 (End.1) PANTHER 2 (CPER)	x2	x10	x3	✓ (q,E)	Multi- λ mode. Double-focusing monochromator. 2D Position-sensitive detector. Unique, high-energy TOF spectroscopy.	✓
FIPPS 1 (End. 1) FIPPS 2.1 (CPER)	–	x1.5 (anti-Compton shields)	–	✓ (γ)	New instrument, new capability – prompt γ fission.	–
SuperSUN	*UCN density x7	–	–	–	A source of ultra-cold neutrons with UCN density ~ x100 the previous record. PANEDM collaborative experiment to install on SuperSUN source for world-record measurements of the neutron electric dipole moment.	–
Rainbows	x10	–	–	–	Renewed focusing guide to maximise ‘coherent summing’ method for specular reflectivity measurements. Note: project re-scoped from the original Rainbows proposal and that defined in Endurance 2.	✓
H24	x4	✓	–	–	Crucial infrastructure renewal of ageing (1972) thermal neutron guide. High-performance, modern, multiple-branch neutron guide. x4 capacity for end-of-guide, optimised, thermal-neutron instrumentation.	✓
D10+	x5	–	x2	–	Modernisation of this ageing workhorse instrument. x5 flux on the sample due to the new H24 guide and larger, modernised monochromators. x2 gain in detector efficiency with the new detector.	✓
IN13+	x4	–	–	–	Modernisation and re-siting of IN13 onto the new H24 guide. A new thermal gradient monochromator and deflector to allow IN13 to capitalise on the increased flux of the new H24 guide.	✓
XtremeD	–	–	–	–	Spanish CRG powder and single-crystal diffractometer. Optimised for diffraction measurements under extreme conditions. Expected performance comparable with that of D20.	✓
NESSE	–	–	–	–	Stimulus and new capabilities in sample environment for neutron scattering measurements across all instruments and scientific domains.	✓
BASTILLE	–	–	–	–	Stimulus, new capabilities and maintenance of scientific software for data treatment and analysis. The ILL joins the international Mantid data treatment project.	✓
Endurance 1 extension (CPER) (2018)						
IN5+ / H16	x3	✓	–	✓ (q,E)	H16 guide & instrument focusing guide renewal. Access to shorter λ , higher E. Flagship instrument pushing the boundaries further.	✓
D3-Liquids	–	–	x10	✓	Wide-angle detector for liquids studies. Polarisation and analysis for studies of hydrogenated liquids. A novel and important extension to D3’s capabilities.	–
IN20-Upgrade	x2	✓	x10 (multiplex analyser)	✓ (q,E)	Higher order and background suppression. Improved flux and polarisation. Multiplexed analysis. Unrivalled thermal TAS spectroscopy.	–

Instrument/Project	Flux ϕ	Background Reduction	Detector $\Delta\Omega$	Measurement Range (q, E)	Capabilities, Features, Options	Reliability, Longevity
Endurance 2 – 2019						
D11 Detector	–	–	x2	✓ ($\Delta q \times 1.5$)	Large, modern, high count-rate detector. Workhorse instrument, necessary upgrade.	✓
D22++ Detector	–	–	x10	✓ ($\Delta q \times 10$)	Second large, modern, high count-rate detector for extended q-range. Flagship instrument with cutting-edge science pushing the limits of SANS.	–
D16 Detector	–	–	x4.5	✓ ($\Delta q \times 4.5$)	Modern, larger, high count-rate detector. Larger solid angle and dynamic q-range. Unique cold-neutron diffractometer.	✓
DALI	–	–	–	–	x2 protein crystallography capacity. Higher resolution mode. Best-in-the-world instrument. High-impact science.	–
NeXT/IM2020	✓	✓	✓	✓	New capability and public neutron imaging instrument. State-of-the-art capabilities and ILL neutron flux for imaging promises a world-leading instrument.	✓
Endurance 2.2 H15 (2020–2023)						
H15	x4	–	–	–	Crucial infrastructure renewal of ageing (1972), low-performance, cold-neutron guide. High-performance, modern, multiple-branch neutron guide. x7 capacity for end-of-guide, optimised, cold-neutron instrumentation.	✓
D11 collimation	x1.4	✓	–	–	Flux gain due to new H15 guide. Replace unreliable, difficult to maintain, optically poor collimation. Remove parasitic scattering and reflections.	✓
D7+	x20	✓	–	–	Dedicated H15 end-of-guide position. Full renewal of primary spectrometer: monochromator optics, polarisation components. Massive improvement to D7, realising its full potential and making TOF spectroscopic studies realistic. Unique instrument with yet-to-be-unleashed capabilities.	✓
SHARP+ / Ramses (CRG) (c.f. IN6)	x5	✓	x2	✓ (q,E)	Renewal path IN6 -> SHARP (CRG) -> SHARP+ (CRG). High-performance, cold-neutron TOF spectrometer, comparable with IN5. Massive gains over existing IN6 with increased detector area, dedicated H15 end-of-guide position.	✓
T-Gaps (CRG) (c.f. 4F1 LLB)	x5	–	–	–	Relocation of 4F1 from LLB as CRG instrument. Increased capacity for thermal, polarised TAS.	–
SAM (CRG) (c.f. Paxy LLB)	x5	–	–	–	New CRG SANS instrument. Additional capacity. MEIZE capability option. An LLB instrument with ILL flux.	–
Endurance 2.2 Independent Projects (2020–2023)						
FIPPS 2.2	–	x2 (definition of fission fragments)	✓	✓ (fission product mass)	New capability. Gas-Filled-Magnet (GFM) fission product mass spectrometer. Combine with existing γ spectrometer for precise fission-fragment identification. Unique instrumentation.	–
WASP2	✓ (TOF)	–	x2	✓ (q,E)	Complete Wasp instrument to full specification: Full detector complement, TOF spin-echo capability.	–
D20c Detector	–	–	–	–	Critical replacement of ageing detector. Workhorse, high-demand, impact instrument.	✓
MARMOT (ThALES)	–	–	x25 (multiplex analyser)	✓ (q,E)	An optimised, multiplexed analyser detector for ThALES. Simultaneous multi-channel energy analysis over a wide angular range.	–
NESSE2	–	–	–	–	Continued stimulus and new capabilities in sample environment for neutron scattering measurements across all instruments and scientific domains.	✓
BASTILLE2	–	–	–	–	Continued stimulus, new capabilities and maintenance of scientific software for data treatment and analysis.	✓



Andrea Piovano, Italian
The ILL
*'As "Instrument Co-responsible" for IN8,
I have led and contributed to several projects
aimed at improving the performance of the
instrument. My present scientific interests are
in the fields of catalysis, dynamics in
disordered oxides and superconductivity.'*

IN8 monochromator and ThermES secondary spectrometer: enhancing the performance of the thermal neutron TAS-IN8

Three-axis spectrometer IN8

Two major projects have been completed in recent years on the IN8 three-axis spectrometer. Firstly, we have redesigned and improved the entire monochromator assembly in the primary spectrometer. Secondly, we have completely rebuilt the secondary spectrometer, providing enhanced performance and reliability. The new performance levels achieved include a 50 % increase in flux at the sample and an average reduction in background of 30 %. The instrument is now fully commissioned and in use for regular experiments.

AUTHORS

A. Piovano, A. Ivanov, S. Roux and F. Charpenay (ILL)

REFERENCES

- [1] A. Hiess, M. Jimenez-Ruiz, P. Courtois, R. Currat, J. Kulda and F.J. Bermejo, *Physica B* 385–386 (2006) 1077
- [2] T. Tejsner, A. Piovano, A. Tutueanu, A. T. Römer, B.O. Wells, J. Grivel, M. Boehm and L. Udby, *Phys. Rev. B* 101 (2020) 100504(R)

To boost the performance of the IN8 primary spectrometer we have designed and implemented a new monochromator assembly, making use of the experience we have gained over the last few decades in the engineering of multi-crystal arrays with 2D variable focusing.

The new device includes four crystal faces with remotely controlled 2D variable focusing that we can alternatively set in Bragg reflection: two mosaic, PG002 and Cu200, and two elastically bent perfect, Si111 and Si311 (**figure 1**). The new monochromator significantly outperforms the previous three-crystal-face unit, which was put into operation in 2001 [1]. Adding the fourth Si311 face has allowed us to enhance instrument performance at high-energy transfers and has provided additional flexibility for high-resolution experiments [2]. We were able to include the fourth reflecting face thanks to the original design involving a back-to-back arrangement of two pairs of reflecting faces coupled to a smart lifting



Figure 1

The new IN8 monochromator unit ready for operation, showing the PG002 face. The unexposed faces are hidden by ingenious neutron shielding.

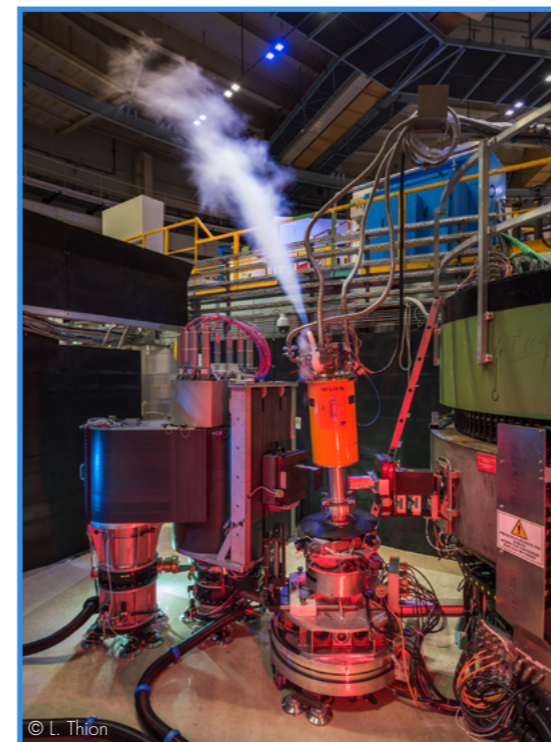


Figure 2

The brand new ThermES spectrometer in the IN8 experimental area during its first cycle of operation (© L. Thion/Ecliptique).

and face exchange system. Moreover, the new compact structure provided space to extend the lateral dimensions of each crystal face by more than 20 %, enabling better use to be made of the available white beam divergence.

Flux measurements indicate an increase in monochromatic flux at the sample position of 40 to 60 %, depending on the reflecting face and the wavelength range, compared with that achieved with the previous primary spectrometer. Furthermore, the background conditions have been improved by 20 to 40 % through the careful choice of neutron-shielding components. An additional set of Soller slit collimators with ¹⁰B-enriched coating and better stability in the intense neutron beam enhances instrument flexibility in high-resolution configurations. The monochromator performance was confirmed following the replacement of the H10 beam tube in 2019.

With the aim of maintaining the highest standards of efficiency on IN8 and preserving its position as the reference instrument among high-flux thermal TAS instruments, we have also invested considerable time and effort in developing a new single-detector secondary spectrometer called ThermES (**figure 2**).

ThermES has a compact design and optimised shielding to minimise all parasitic background not generated by the sample or found outside the main optical path. Although most of the background in an IN8 experiment typically comes from the sample and its nearest environment (cryostat, etc.), the signal-to-noise ratio can nevertheless be improved thanks to carefully arranged

neutron shielding. The new spectrometer proposes a larger dynamical range than that of the previous set-up, in particular towards high-momentum transfers. This is a major advantage for lattice dynamics studies, which are once again in high demand at IN8 along with research into magnetism.

The new compact design makes it possible to use the highest available magnetic fields, something that could not be done previously due to insufficient space to reduce the attraction forces from stray fields acting on the superconducting magnet.

In conclusion, we have optimised the IN8 spectrometer to ensure ease and comfort of operation and faster configuration changeovers and maintenance, thus minimising downtimes. Offering a performance that is more unrivalled than ever, IN8 continues to supply the highest monochromatic flux of any thermal three-axis spectrometer in the world. The instrument is optimised for inelastic neutron scattering measurements with energy transfers in the range of one to about one hundred meV, and is used to investigate the thermal spectrum range of magnetic excitations and lattice vibrations. Its high incident flux offers greater flexibility for optimising the flux and resolution conditions and allows scientists to conduct investigations of small samples and weak inelastic response that are not possible elsewhere. The enhanced performance, reliability and flexibility of IN8-ThermES will provide a major boost for user operation in the years to come.



Aleksander Petoukhov, Russian/French
The ILL

'I am interested in neutron physics, from the weak interaction in reactions induced by neutrons to the interaction of neutrons with the Earth's gravity field, with a particular emphasis on the development of high-precision neutron methods and techniques.'

Advanced solid-state polariser for PF1B

PF1B - Polarised cold-neutron beam facility

A new type of solid-state polariser has been built entirely in-house at the ILL for the PF1B cold-neutron beam facility. The polariser was installed in the PF1B casemate and tested in real conditions. The downstream polarisation averaged over the capture spectrum reached a record measured value of 0.997 for the full wavelength bandwidth of 0.3–2.0 nm, with an average transmission for the 'good' spin component of above 30%. This unprecedented performance is due to a series of design and manufacture innovations in the following areas: the choice of substrate material, the supermirror and anti-reflecting multilayer coating, the magnetising field, the assembly technique and the characterisation. This polariser has been in use for user experiments since the last reactor cycle of 2020.

AUTHORS

A.K. Petoukhov, V.V. Nesvizhevsky, T. Bigault, P. Courtois, A. Devishvili, D. Jullien and T. Soldner (ILL)

ARTICLE FROM

Rev. Sci. Instrum. (2019) — doi: <https://doi.org/10.1063/1.5114796>

REFERENCES

- [1] T. Soldner, A. Petoukhov and C. Plonka, ILL technical report ILL03SO10T (2002)
- [2] M. Kreuz, V.V. Nesvizhevsky, A. Petoukhov *et al.*, Nucl. Instr. Meth. A 547 (2005) 583
- [3] A.K. Petoukhov, V.V. Nesvizhevsky, T. Bigault *et al.*, Nucl. Instr. Meth. A 838 (2016) 33
- [4] A.K. Petoukhov, V.V. Nesvizhevsky, T. Bigault *et al.*, Rev. Sci. Instr. 90 (2019) 085112

The PF1B polarised cold-neutron beam facility at the ILL is used for experiments in elementary particle and nuclear physics. It has provided the strongest polarised and unpolarised cold-neutron beam in the world since its inception. The previous polariser, a CoTi supermirror (SM) bender built in 2002, provided up to 98.5% polarisation, the highest in the world at the time [1]. A special configuration of two polarisers in a so-called 'crossed geometry' has also been used at the ILL to achieve a record 99.7% polarisation [2]. This, however, sacrificed a major fraction of neutron intensity. After 15 years of successful service, the previous polariser was significantly damaged by radiation, resulting in degraded polarisation and transmission.

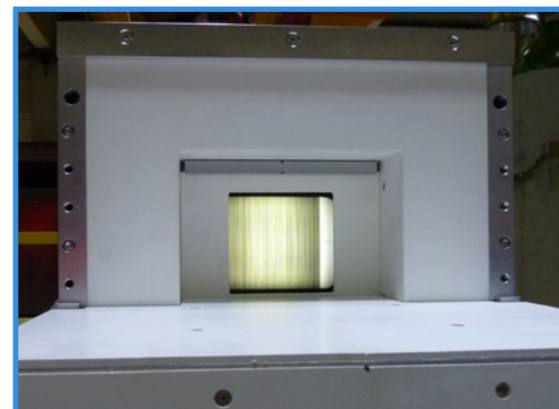
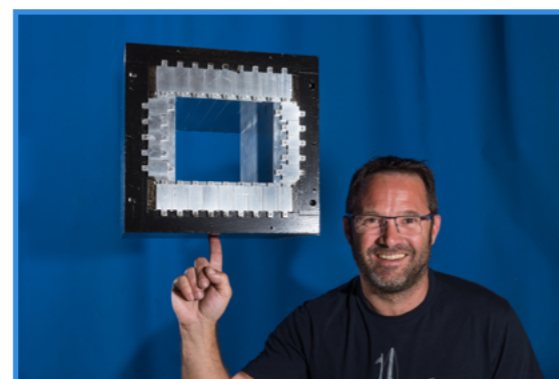


Figure 1

Top) David Jullien presents the polariser's magnetic housing, with its highly homogeneous magnetic field of 0.38 T.

Bottom) Solid-state sapphire V-bender covering a beam 80 x 80 mm² installed in its magnetic housing and neutron shielding.

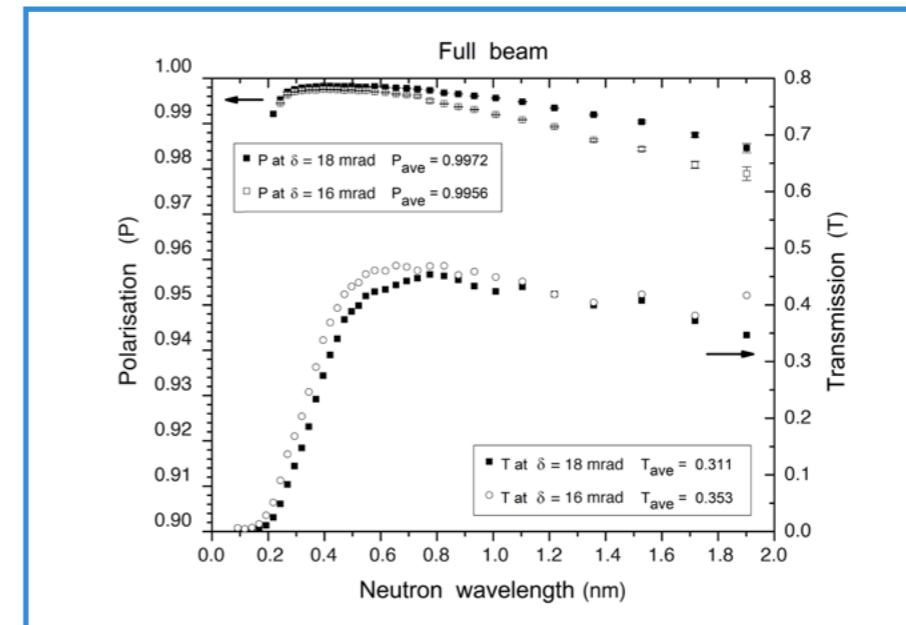


Figure 2

Measured neutron polarisation (left axis) and transmission (right axis) as a function of the wavelength for two values of the tilt angle δ . The polarisation averaged over the PF1B capture spectrum is 0.9972 for $\delta = 0.18$ mrad and 0.9956 for $\delta = 0.162$ mrad. The corresponding integral transmissions are 0.31 and 0.353, respectively.

In standard solid-state SM polarisers, neutrons propagate through the substrate and undergo spin-selective reflections from double-sided SM coatings. We presented a new polariser concept in [3, 4]. It involves the use of substrates with sufficiently large optical potential (such as sapphire, for instance) to escape the regime of spin-independent 'total' reflection at small incidence angles (a typical shortcoming of conventional FeSi SM polarisers). Two successive channel sections are kinked at a small angle, forming a V shape, which prevents a direct view through the device.

The spin-selective reflection is caused by a special, 'inverted' $m = 3.2$ Fe/SiNx supermirror, capped by an Si/Gd anti-reflecting and absorbing multilayer coated on both sides of the sapphire substrates. The coating process was iteratively refined and verified using the T3, D17 and SuperADAM reflectometers at the ILL. Two stacks, consisting of ~450 single-crystal sapphire plates each, were coated, with dimensions 80 x 25 x 0.18 mm³. The coating process took one year. A mechanical system tilts the two independent stacks at a small angle to form V-shaped channels covering a beam cross section of 80 x 80 mm².

An ideal polariser stack assembly requires perfectly parallel alignment of each SM plate, and indeed the assembly of the stacks was a major technical challenge. Even small dust particles between the plates can result in alignment errors accumulating with the rising number of plates, leading to degraded transmission and polarisation. We therefore developed a method that drastically minimises the occurrence of foreign contaminants during stack assembly and optically controls the positioning of each plate with a precision better than 0.1°. The construction process was streamlined and the final stack assemblies were verified at the SuperADAM reflectometer to ensure that the alignment of each mirror was within the tolerances. Each stack is independent and the angle between them can therefore be tuned *in situ* to adjust the polarisation and transmission to experimental requirements.

The polariser (**figure 1**) was installed in the PF1B casemate downstream of the H113 $m = 2$ ballistic guide and characterised in real conditions in February 2020. It can be used without angular collimation or filtering of the incident neutron beam wavelength. The outgoing neutron polarisation (**figure 2**) was measured using a set of 'opaque' ³He cells, which provide more than 0.999 analysing power for neutron wavelengths > 1.4, 0.8 and 0.3 nm. The time-of-flight technique was used to control the wavelength for both polarisation and transmission measurements.



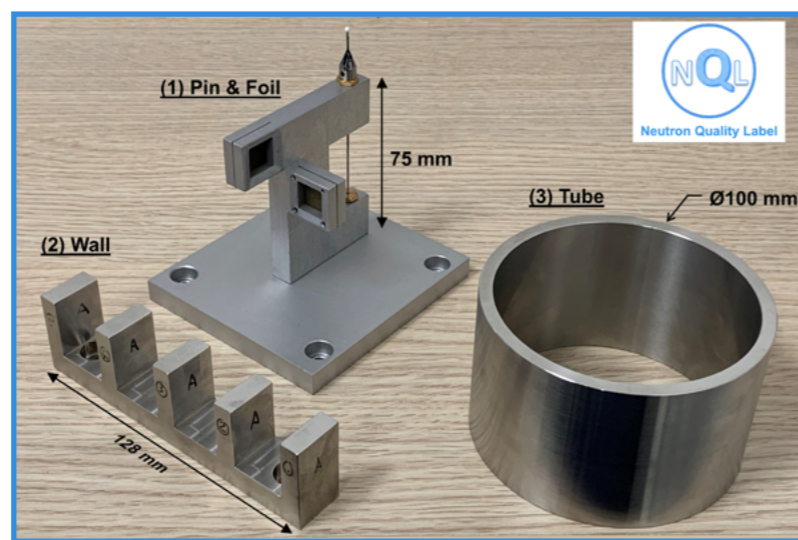
Ranggi S. Ramadhan. Indonesian The ILL
 'I am a postdoc scientist at the ILL and work on the instrument SALSA. My main research interest is neutron diffraction and neutron-imaging techniques for residual stress determination and characterisation of engineering components.'

Harmonisation of calibration protocols for neutron strain scanners

Neutron strain scanner – SALSA

Strain scanners are available in neutron facilities across the world, offering powerful capabilities for non-destructive, 3D, stress mapping. The lack of a common calibration protocol and reporting standard, however, prevents the method becoming a routine tool for industrial research. In the present study, we developed a calibration standard (samples and methods) for neutron strain scanners and applied it to four different instruments. This standard will form the basis of the 'Neutron Quality Label' (NQL), a quality standard for measurements and specific setups on neutron strain scanners. The results obtained using the new standard confirm the positional accuracy of the instruments and the efficiency of a unified protocol, while demonstrating excellent consistency between the participating facilities.

Figure 1
 The calibration samples:
 1) Pin and foil for instrument alignment and characterisation of gauge volume;
 2) Flat wall sample and
 3) Tube sample for evaluating the optical sample alignment system and entry scan method for sample surface determination.



AUTHORS

R.S. Ramadhan, S. Cabeza and T. Pirling (ILL)

REFERENCES

- [1] G.A. Webster, VAMAS Report No. 38 (2000)
- [2] A.G. Youtsos and C. Ohms, Appl. Phys. A: Mater. Sci. Process. 74 (2002)
- [3] International Organisation for Standardisation (2019)
- [4] C. Carlile *et al.*, Dipartimento di Fisica – Università degli Studi di Milano, Milan (2016)
- [5] <https://brightness.esss.se/>

Neutron strain-scanning instruments provide for the non-destructive, depth-resolved determination of the complete stress tensor on engineering components, using neutron diffraction. The VAMAS TWA20 and RESTAND programmes, amongst others, have worked on the technical development and standardisation of this method for residual stress determination [1, 2]. Their results, in conjunction with ISO 21432:2019 [3], now serve as 'best practice' guidelines. Over recent years, investigations of residual stresses have become more complex and neutron diffraction stress-determination studies more demanding. The pool of neutron strain scanners internationally has nevertheless not evolved significantly [4], and many of the instruments at large-scale research infrastructures are heavily oversubscribed. Therefore, it is important to expand the support network for the instruments available and ensure that users, including those from industry, are confident when collaborating on instruments at different institutes. Given their inherent instrumental differences, there is a clear need to ensure interchangeability between neutron strain scanners.

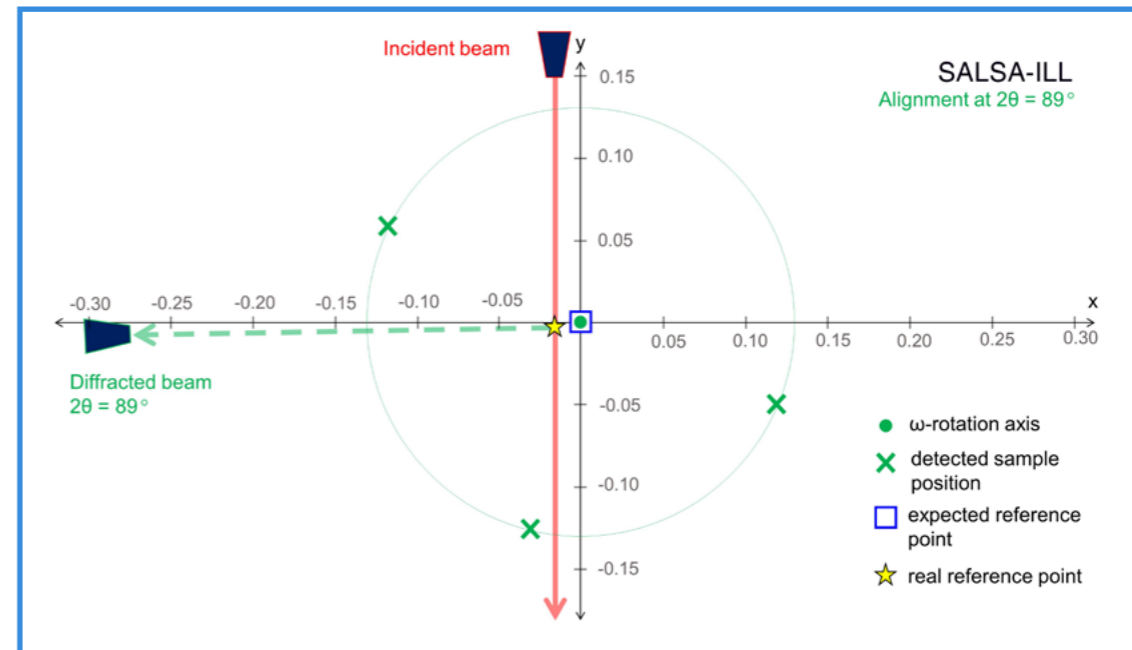


Figure 2
 Example of the accurate determination of the reference point (centroid of instrumental gauge volume) with respect to the ω -rotation axis on SALSA, showing an accuracy of $\sim 20 \mu\text{m}$ using a gauge volume width of 0.6 mm.

As part of the BrightnESS2 [5] – WP2.3 [A] Pilot Engineering task, we developed a standardised instrument calibration protocol and a unified reporting template for neutron strain scanners as part of the *Neutron Quality Label (NQL)*, with a focus on the positioning accuracy of the instrument. The development involved scientists from various instruments (SALSA, ILL, France; ENGIN-X, ISIS, UK; STRESS-SPEC, MLZ, Germany; MPISI, Necsca, South Africa). We prepared and distributed sets of calibration samples to the participating instruments. Each set contained a pin and foil calibration sample for instrument alignment and gauge volume characterisation, and a flat wall sample and a tube sample to evaluate the sample alignment system and method, and was designed with the materials and geometries required to ensure efficient calibration (figure 1). Calibration measurements were formulated taking into account the expertise and experience of each participating instrument.

The calibration results on the different instruments showed that the standardised samples and methods worked efficiently and could be harmonised for both monochromatic and time-of-flight instruments. The protocol allowed accurate determination of the reference point position (centroid of the gauge volume) with respect to the ω -rotation axis (figure 2), quantification of the accuracy of the sample alignment systems and quantification of the accuracy of the entry-scan analysis software for more accurate sample positioning. This study also demonstrated excellent agreement between the participating neutron strain scanners, where positional uncertainties better than 100 μm were attained. To conclude, a standard for calibration and reporting for neutron strain scanners is now available. We invite users of other neutron strain scanners to apply the standard and join the collaborative effort to boost industrial users' confidence in the use of neutron diffraction for stress determination.



David Jullien. French
The ILL

'I am responsible for the development of polarised ^3He optics for neutron polarisation. I am involved in the study and implementation of ^3He neutron spin filters, including their magnetostatic cavities, for the ILL instruments, and in the design, construction and operation of polarised ^3He production facilities.'

PASTIS-3: a wide-angle XYZ-polarisation analysis device using polarised ^3He for thermal neutrons

Three-axis spectrometer IN20

We have successfully designed, built and tested a new wide-angle XYZ-polarisation analysis device known as PASTIS-3. In contrast to earlier generations [1–3], PASTIS-3 uses two polarised ^3He cells to prepare and analyse the neutron beam polarisation. The device includes an optimised, in-house coil design that provides high spatial homogeneity of the magnetic field in any direction and thus ensures long ^3He polarisation lifetimes. The ^3He cell in the incident beam is equipped with a ^3He -spin flipper so that cross sections with or without neutron spin-flip at the sample can be measured. PASTIS-3 has been installed on the thermal three-axis spectrometer IN20 and successfully tested (figure 1). These tests show that constant energy scans with PASTIS-3 are at least as efficient as those conducted with a Helmholtz arrangement and single detector. PASTIS-3 will now be available to ILL users as a standard IN20 instrument configuration.

Figure 1

Installation of PASTIS-3, with its dedicated Orange cryostat, on IN20. From left to right: P. Chevalier, M. Enderle, D. Jullien, P. Mouveau and N. Thiery.

AUTHORS

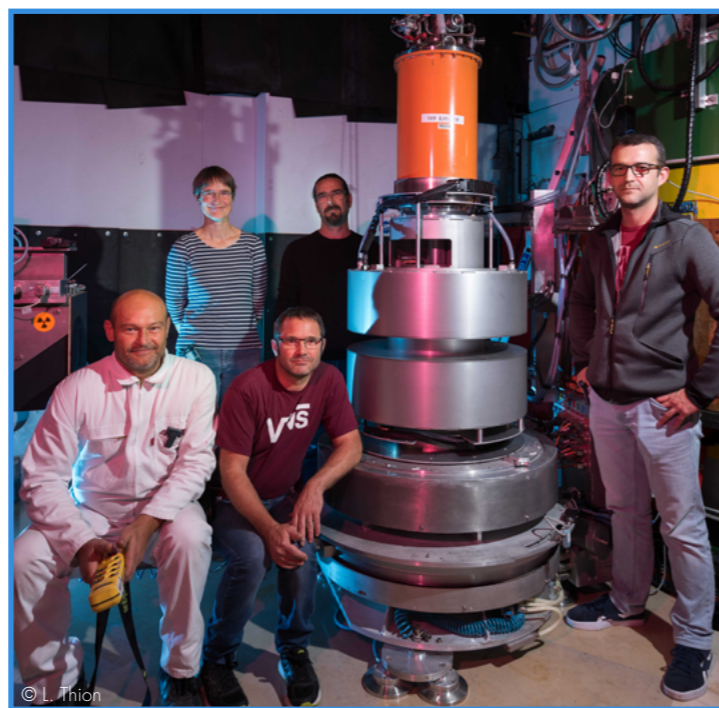
D. Jullien, A.K. Petoukhov, M. Enderle, U. Benggaard Hansen, N. Thiery, P. Mouveau, P. Chevalier, J.P. Rey, E. Lelievre-Berna and P. Courtois (ILL)

REFERENCES

- [1] J.R. Stewart *et al.*, *Physica B* 385–386 (2006) 1142
- [2] K.H. Andersen *et al.*, *Physica B* 404 (2009) 2652
- [3] M. Enderle *et al.*, *J. Phys. Conf. Ser.* 862 (2017) 012005

Neutron polarisation analysis is a powerful method for separating magnetic scattering from coherent or incoherent nuclear scattering. In inelastic neutron scattering, it makes it possible to distinguish between phonons (lattice vibrations) and local or propagating magnetic excitations (e.g. magnons, spinons, triplons, crystal-field excitations, spin transitions). Using polarised incident neutrons and polarisation analysis of the neutrons scattered after the sample, the scattering of magnetic excitations of any kind can be isolated background-free via a linear combination of suitable polarised cross sections. Moreover, it makes it possible to determine the vectorial amplitude of a magnetic excitation, including its precessional 'chiral' character.

In PASTIS-3, the technical challenge of achieving simultaneous neutron polarisation analysis in a wide range of scattering angles is met thanks to a blind-angle-free coil system. The magnetic field is sufficiently homogeneous to maintain a high degree of polarisation for a day in the two ^3He cells in two critical regions—the entrance region of the polariser cell and the wide-angle range of the banana-shaped analyser cell (both shown in figure 2)—and for any field direction at the sample, making



© L. Thiery

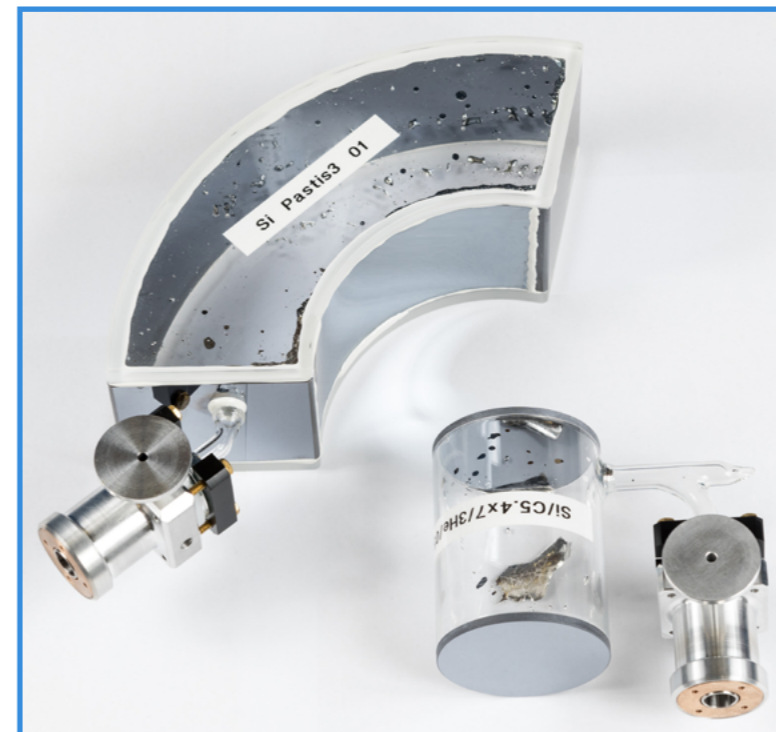


Figure 2

Coated polariser and analyser cells with silicon windows and pneumatic valves.

it possible to obtain the desired polarised cross sections. Two further field regions, above the scattering plane and above the polariser and analyser cells, are sufficiently homogeneous to host the cells with negligible polarisation loss during neutron-transmission measurements. Non-magnetic translation stages for the ^3He cells enable a convenient, automated measurement of the instantaneous ^3He -spin polarisation of the individual cells via neutron transmission. An integrated, adiabatic fast passage flipper makes it possible to invert the ^3He polarisation of the entrance cell with respect to the field, and thus to measure cross sections that either do or do not involve a neutron spin-flip at the sample. Flipping the polariser has a negligible effect on the lifetime of the two cells.

The field rotation between the horizontal scattering plane and the vertical direction is achieved by a controlled change of currents, and within the horizontal plane by mechanical rotation of the entire coil system around the ^3He cells and the sample. Averaged over all field directions, the homogeneity of the coil system results in ^3He lifetimes of over 1 000 hours for hypothetical zero-pressure cells without dipole–dipole or wall interactions of the ^3He nuclear spins. On the spectrometer, during the test experiments the overall relaxation times of the polariser and analyser cells were of the order of 100 hours, primarily due to dipole–dipole and wall

interactions of the ^3He nuclear spins. This makes it perfectly feasible to conduct experiments with daily cell-changes (a cell-change takes about half an hour). Nevertheless, we are continuing our efforts to achieve even longer lifetimes by improving the elimination of the wall interactions.

A dedicated Orange cryostat (sample space diameter of 40 mm) with a sample rotation stage at the top is inserted in the centre of the PASTIS-3 device, allowing polarisation analysis experiments to be performed at sample temperatures of between 1.9 K and 300 K.

Our tests have demonstrated that PASTIS-3 performs excellently in inelastic neutron scattering with XYZ-polarisation analysis, providing greater polarisation control than that achieved using the standard Helmholtz set-up.

A direct comparison has been carried out between PASTIS-3 and a silicon monochromator and FlatCone multi-analyser/detector and a standard Helmholtz configuration with a Heusler monochromator/analyser and single detector. The results using the same sample show that PASTIS-3 is at least as efficient if not more so than the standard Helmholtz configuration even for an individual, constant energy scan. The future IN20 PG monochromator should boost PASTIS-3 measurements even further.

PASTIS-3/FlatCone will now be made available to ILL users as a standard IN20 instrument configuration.

TECHNICAL AND METHODS DEVELOPMENTS

FIND US ON:   **Pierre Courtois**, French
The ILL

'I am head of the ILL's Neutron Optics Service. We develop and produce advanced, neutron optical components to help maintain the ILL's leading role in neutron science.'

A dedicated team of scientists and engineers provides know-how and in-house manufacturing for everything from monochromator crystals to polarising supermirrors and ^3He spin filters.'

The new, double-focusing copper monochromator for PANTHER

Time-of-flight spectrometer PANTHER

Starting from high-quality, large, single crystals grown in the laboratory, the monochromator group produces copper crystals with a well-controlled mosaic distribution using plastic deformation at high temperature. These crystals exhibit excellent neutron properties, making it possible to construct extremely efficient neutron monochromators for ILL instruments such as the newly commissioned time-of-flight spectrometer PANTHER.

AUTHORS

P. Courtois, F. Barneaud, B. Mestrallet, S. Michallat and F. Philit (ILL)

REFERENCES

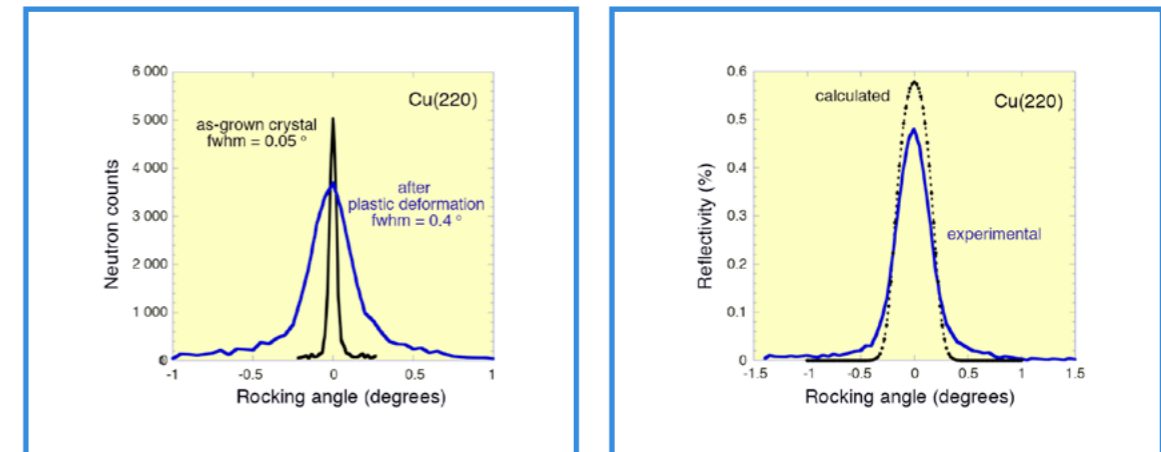
- [1] P. Courtois, B Hamelin and K.H. Andersen, Nucl. Instrum. Methods Phys. Res. A 529 (2004) 157
[2] V.F. Sears, Acta Cryst. A53 (1997) 35

Thanks to their small d-spacing and excellent neutron properties, copper mosaic single crystals provide an efficient means of producing monochromatic neutron beams in hot and thermal energy ranges where good resolution is required. In order to meet instrument requirements in terms of flux, resolution and divergence, the value of a crystal's mosaic spread must be comparable to the incoming beam divergence, which is typically in the range of 0.2 to 0.6°. Furthermore, the mosaic must be uniform in the whole crystal volume to obtain homogeneous wavelength and intensity distribution at the sample position.

Preparing a controlled and uniform mosaic spread is a difficult task. It requires the microstructure in the bulk of large monocrystalline samples to be modified because the mosaic of the as-grown crystals is generally rather small compared with the neutron beam divergence. To achieve this, we take advantage of the fact that copper is a soft and extremely malleable material. As a result, the microstructure of a Cu single crystal can be easily modified by plastic deformation at high temperature. By applying the appropriate pressure perpendicular to the surface of a crystal plate at high temperature, the mosaic spread can be increased up to the desired value while maintaining its uniformity [1]. The process also involves careful positioning in the hot-press furnace to ensure homogeneous deformation.

**Figure 1**

The new double-focusing Cu(220) monochromator for the thermal time-of-flight spectrometer PANTHER.

**Figure 2**

a) Typical neutron rocking curves from Cu(220) single crystals before and after plastic deformation at high temperature.

b) Calculated and experimental neutron peak reflectivity at $\lambda = 1.4 \text{ \AA}$ for a Cu(220) crystal with a mosaic spread of 0.4°.

This technique has been successfully used in the construction of the new, double-focusing Cu(220) monochromator for the thermal time-of-flight spectrometer PANTHER (**figure 1**). Horizontal and vertical curvatures can be varied independently in order to optimise both the neutron flux and the resolution at the sample position over a wide energy spectrum ranging from 38 to 329 meV. The monochromator comprises 165 copper pieces with dimensions of $20 \times 19.8 \times 8 \text{ mm}^3$ mounted in 15 columns and 11 lines, which corresponds to a total active area of 660 cm^2 . The Cu(220) crystals have a neutron mosaic spread of between 0.35° and 0.5°. Each piece is glued onto a precision-machined support consisting of two successive plates, one made of B_4C doped with boron-10 and the other made of aluminium. Adding a B_4C plate as neutron shielding reduces background on the instrument, leading to a better signal-to-noise ratio. We also paid particular attention to keeping the crystallographic planes parallel to the surface of the mechanical holder.

To provide the material for constructing a monochromator of this kind, two large, as-grown crystals with a mosaic spread of 3 minutes of arc were cut by spark erosion (**figure 2a**). The principal direction of cutting was parallel to the Cu(110) crystal planes. In addition, crystal orientation was chosen such that the $[-110]$ axis was along the vertical rotation axis of the monochromator. This enables all planes of the type (hhl) to be available, in particular the Cu(331) reflection, making it possible to select neutron wavelengths of between 0.5 Å and 0.9 Å.

In order to choose the best crystals, we studied the neutron properties of more than 180 copper mosaic single crystals on the test diffractometer T13C. A perfect Ge(331) monochromator crystal selected a wavelength of 1.4 Å. The effective neutron mosaic spread (FWHM) was determined as the full width at half maximum of Cu(220) rocking curves recorded in reflection geometry.

Since the double-crystal configuration was parallel and the arrangement almost dispersion-free, the width of the rocking curve directly represented the mosaic distribution of the sample under study. A typical neutron rocking curve obtained from a Cu(220) single-crystal plate used for the new monochromator is shown in **figure 2a**. The diffraction pattern indicates a symmetrical single peak with a nearly Gaussian shape, demonstrating the homogeneous mosaic structure. In addition, due to the absence of $\lambda/2$ -contamination the neutron reflectivity could be derived directly from the rocking curve. The peak reflectivity is close to 45% for a FWHM of 0.4° (**figure 2b**). This corresponds to 85% of the theoretical peak reflectivity calculated from the Darwin model for ideally imperfect mosaic crystals [2]. The origin of the lower reflectivity could be due to primary extinction processes and some crystal inhomogeneities.

The final alignment of the monochromator was performed by neutron diffraction on T13C. Each of the 165 copper crystals was oriented in both directions with an accuracy of 0.05° with respect to one another.

This new Cu monochromator will be installed on the instrument for commissioning before the first neutron cycle in 2021. Such a device offers excellent complementarity to the HOPG monochromator by extending the useful energy range to short wavelengths up to 0.5 Å. It should provide higher neutron flux and better resolution compared with the old set-up previously used on IN4.



Paolo Mutti, Italian
The ILL

'I am a nuclear astrophysicist by trade. As head of Instrument Control I also develop specific hardware and software solutions in order to carry out the scientific programme on all ILL instruments. I also develop hardware in collaboration with industrial partners. As head of Scientific Computing I support internal and external users by developing software solutions for data reduction and data analysis. I am also involved in a number of European projects and a member of several scientific collaborations.

AUTHOR
P. Mutti (ILL)

NOMAD Remote

Since the first reactor divergence in 1971 the ILL has always been the home of neutron science, welcoming users from all around the world. However, 2020 and the COVID-19 pandemic has changed not only our lives but also the way experiments are performed on our instruments. The valuable help of users in preparing and performing measurements was suddenly lost, due to travel restrictions, confinement and hygiene rules.

To allow users to continue performing their science, the SCI department has developed NOMAD Remote, an extension to the NOMAD instrument control software. With the support of the VISA virtualisation infrastructure, users are now able to connect to any ILL instrument and to pilot their experiment remotely as though they were sitting in front of the instrument computer. No need to install anything: just open your favourite web browser, create a VISA virtual machine and from there connect your NOMAD Remote from anywhere in the world (**figure 1**). Moreover, this powerful remote-access solution complies with data protection policy. Only those users registered for a given experiment are able to access the connection and only then for the duration of their beamtime.

NOMAD Remote is more than a simple graphical sharing system. Every remote session is totally configurable and all users can see and interact with the control software autonomously. For example, one member of an experimental team might be looking at a real-time data plot while another is programming the next sequence of operation to be executed by the instrument. Furthermore, thanks to the sharing ability of the VISA virtual machine, users can still fully benefit from the support and the experience of the ILL scientists.

Figure 1
NOMAD Remote within the desktop of a VISA session.

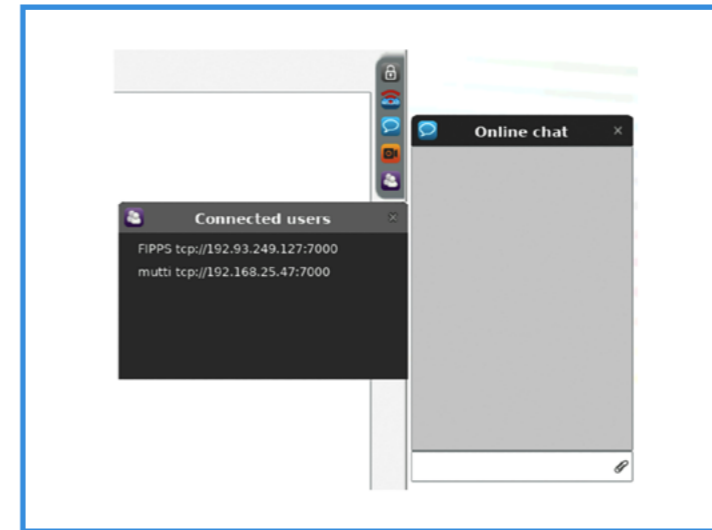
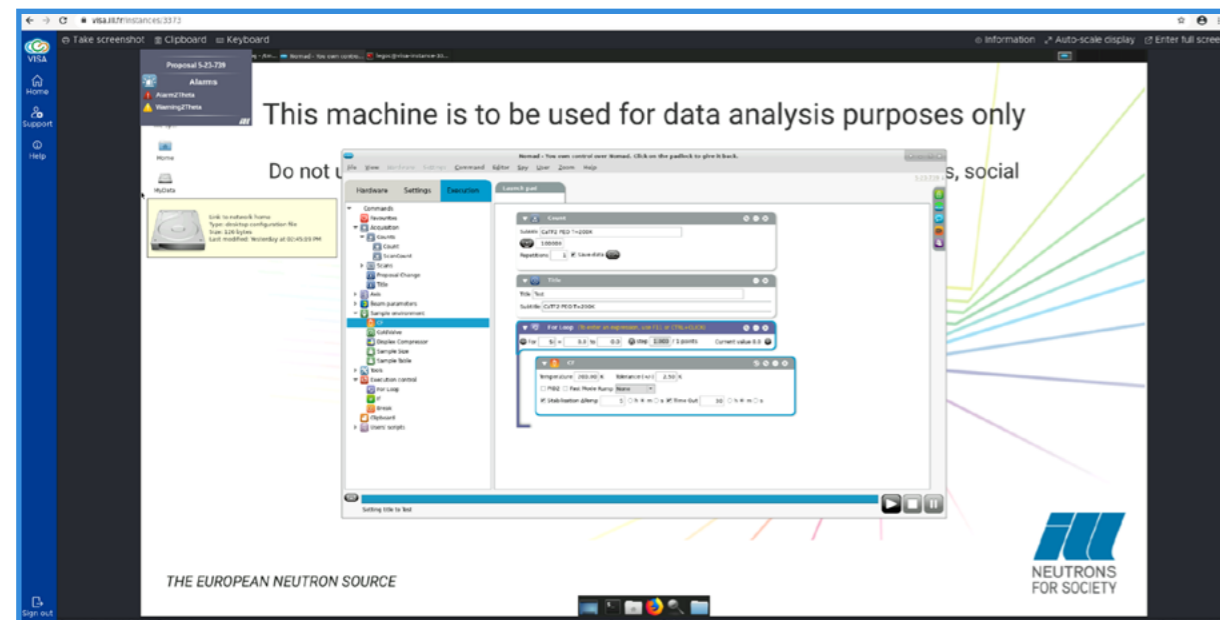


Figure 2
The dashboard of the remote connection. From top to bottom: token ownership, the status of the remote access, text chat, video chat and a list of connected users.

How does it work

The Nomad architecture was originally designed with a separate server program in C++ and a separate client program in Java SWT. These two elements can be physically located on the same computer or on machines that are far apart from each other. Communication between the client and the server is ensured through a network connection by Cameo, in-house middleware used to start and synchronise applications, and make them communicate in any language, on any platform.

The NOMAD GUI client is continuously synchronised with the NOMAD server by receiving events, e.g. a new motor position during a movement or a new detector image during data acquisition. To control an experiment with NOMAD Remote, we need to be able to run multiple GUIs (graphical user interfaces) at the same time, meaning that the workflow on different clients needs to be synchronised. Porting NOMAD GUI on a VISA instance is easy, since the only requirement is to install a Cameo server and a mechanism to automatically update the application on the virtual machine. Having multiple clients running anywhere outside the ILL requires that access to the instrument is secure. Thus, token rules have been added to prevent concurrent access, meaning that only one client can control and give orders to the instrument at any given time. To comply with data policy, all remote clients are automatically disconnected at the change of proposal thanks to Cameo, which controls the operation of remote applications.

A dashboard to control all operations

On the right side of the classic NOMAD graphical user interface, the user now has a dashboard that verifies the status of all remote operations (see **figure 2**). The main client, situated directly on the instrument, has the option of allowing or not allowing a remote connection. For security reasons this interface will always have priority over all remote clients, being able to take control of the instrument at any moment in time. All connected users can request full control from the moment remote control has been activated on the instrument, by using the token button. Every remote connection is logged in order to identify who is active during the measurement session and a list of remote users is available via the dashboard. Last but not least, a chat application is also accessible directly from the NOMAD Remote interface to facilitate exchanges between members of a team or with their local contact at the ILL. For the next release of the remote GUI, the option to access video chat will also be available through a beta test.

The perfect companion

As previously mentioned, NOMAD Remote runs on virtual machines provided by the VISA infrastructure. Within the same framework, users can access the most widely used software for data reduction and analysis, such as GRASP, Mantid, SasView and FullProf, amongst others. Controlled by the user's login, initiation of a VISA session will automatically generate appropriate links to the experimental data, which will then be available with a simple click from the VISA desktop. In this way, data reduction and analysis can be performed directly on the ILL computing infrastructure, without the need to install dedicated software or tedious sessions of data transfer.

INDUSTRIAL ACTIVITIES

The ILL provides industrial users with access to state-of-the-art neutron instrumentation and the expertise of its scientific and technical staff. The Industry Liaison Unit (ILU) is the focal point of industrial activities at the ILL. The objective of the Unit is to bridge the gap between the ILL as a facility, largely oriented towards academic research, and industry as an actor in research that is liable to benefit from neutron techniques.

Contact: industry@ill.eu

102 COMPANIES
SINCE 2011

INDIRECT INDUSTRY USE:
10 % OF TOTAL TIME

REVENUE: 190 k€

BEAM TIME SALES:



KEEP UP-TO-DATE:

[facebook.com/ILLGrenoble](https://www.facebook.com/ILLGrenoble)

twitter.com/ILLGrenoble

[linkedin.com/company/institut-langevin](https://www.linkedin.com/company/institut-langevin)

FIND US ON: [f](#) [t](#) [in](#)

Societal challenges are a major focus of research and development (R&D) activities, and industry has its own role to play when new technology is delivered. R&D ranges from pre-competitive research delivering the disruptive technology of the future, to proprietary research improving current technologies and processes. The Industry Liaison Unit operates at the interface between the ILL's science and technology teams and industry, across a range of activities to identify, develop and exploit new opportunities.

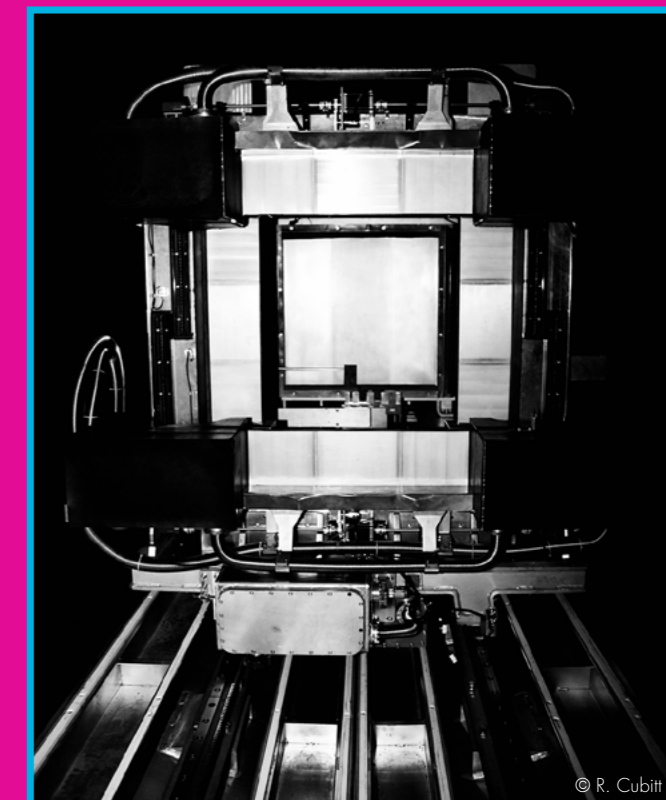
Industry is most welcome to use the ILL's state-of-the-art scientific infrastructure for its pre-competitive research, on the basis that the data are publicly available and the results published. Analysis performed in 2020 shows that this beam time use—sometimes called 'indirect industry use' because industry often works with academic groups—amounts, on average, to about 10 % of total beam time, with a peak at 16 % in 2020. While industry partners are not always visible, we have identified just over 100 companies using the ILL in this way over the last 10 years.

Another example of this type of collaboration with industry is the InnovaXN PhD programme (<https://www.innovaxn.eu/>) set up with the ESRF and Marie Skłodowska-Curie Actions-funding from the European Commission (3.3 M€). Forty PhD projects have now been selected, each with industrial and academic partners along with the ILL or the ESRF. For most of the projects, both neutrons and X-rays are required. In all, more than 35 industry partners are involved, the main industry sectors being energy storage and production, chemistry and catalysis, pharma and biotech, and metallurgy. The first wave of students started their projects in autumn 2020; a little over 20 students will be selected in spring 2021 to complete the cohort.

The need for clean energy puts considerable focus on battery research, and as such the ILU leads the ILL's involvement in the BIG-MAP (the Battery Interface Genome – Materials Acceleration Platform – <https://www.big-map.eu/>). This is a European-funded project,

with six of the 34 partners coming from industry. Along with the ESRF and the Soleil synchrotron, as well as the CEA as a local partner in Grenoble, we will develop the use of large-scale facilities for battery research, feeding our unique, experimental capability into the Battery 2030+ roadmap (<https://battery2030.eu/research/roadmap/>).

Two other European projects in which the ILU is heavily involved concern residual stress measurements of manufactured metal components and the SALSA instrument at the ILL. Additive manufacturing is currently a major application of strain scanning, and several such collaborations with industry partners have been set up (see following pages). In the BrightnESS2 project (<https://brightness.esss.se/>) the ILL leads a work package on the reproducibility of measurements, something that is essential for industry use, across multiple instruments. In addition, the so-called 'neutron quality label' is being set up as a trademark that will be readily recognised by industry. The second project, EASISTRESS, focuses precisely on deploying the stress measurements method, which has been widely used in academia, for industry.



© R. Cubitt

The ILU represents the ILL in the French IRT-Nanoelec project focusing on R&D in the micro/nano-electronics industry, which is highly developed in the Grenoble area. Funding for a new phase of this project was secured in 2020 for the period 2021–25; the ILL will work with the ESRF, LPSC-CNRS and CEA on the radiation resilience of electronic components, an obvious requirement with the massive deployment of connected devices. An additional European project in this area is RADNEXT (<https://radnext-network.web.cern.ch/main/>). To fully support irradiation activities performed on D50, equipment has been transferred to the H9 beam tube; the installation is called TENIS - Thermal and Epi-thermal Neutron irradiation Station. D50, now baptised NEXT, is a dedicated public instrument for neutron imaging for which numerous industry applications are being explored and developed.

As can be seen from this short update, the ILU, in addition to managing the ILL's beam time sales, is at the origin of activities of great societal relevance attracting considerable funding.

Neutron-diffraction stress measurements

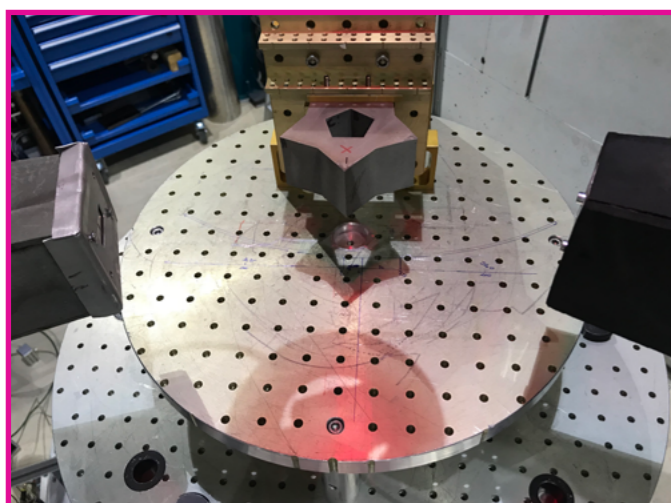
The ILL's SALSAs instrument is unique in its capacity to perform high-resolution strain scanning of engineering components in a non-destructive manner. Over the last three years, the entire SALSAs instrument team has focused on improving the instrument technically (increasing its precision), qualifying the instrument more precisely (systematic errors) and including new set-ups (*in situ* testing). At the same time, they have been extending outreach to industry and improving the projects portfolio.

In parallel, the ILL has been managing the Pilot Engineering task group of the ESS-led **BrightnESS-2** project. The group has developed a number of comprehensive calibration protocols in collaboration with other neutron centres; by producing practical guidelines and establishing a technical protocol this has provided the basis for a new *Neutron Quality Label* (see pp. 80–81) which will ensure the traceability and reproducibility (interchangeability) of neutron strain scanner configurations. This should in turn bolster the image of neutron characterisation in industry [1].

Another major step has been the harmonisation of algorithms and data processing methods, first initiated during the SINE2020 project funded by H2020. Work on the quality of experimental data for stress determination will be pursued in the three-year, H2020-funded project **EASI-STRESS**. This project is led by the **Danish Technological Institute** and is due to start in January 2021. The ILL will be responsible for the data processing and harmonisation work package.

Figure 1

The ISO-ASTM star-shaped artefact mounted on SALSAs (right). The cradle mounted on the hexapod moving stage holds the star artefact and allows the neutron probe to access any location and strain direction in the sample (left).



REFERENCES

- [1] <https://cordis.europa.eu/project/id/823867/results>
- [2] Cabeza *et al.*, Strain Monitoring During Laser Metal Deposition of Inconel 718 by Neutron Diffraction, *Superalloys 2020*, 1033–1045
- [3] DTR 52905:2019-02 - Additive manufacturing - Non-Destructive Testing and Evaluation

The ILL has also initiated collaboration on SALSAs over the last three years on additive manufacturing, and on *in situ*, direct metal deposition and standardisation in particular. We can cite four interesting examples in this context.

- In 2018, SALSAs scientists and **Fraunhofer IWS** (Dresden, Germany) performed the world's first *in situ* neutron strain scanning operation during continuous laser metal deposition [2]. Since then, following a Memorandum of Understanding, a joint PhD project has been launched with Fraunhofer on *in situ* neutron characterisation for additive manufacturing techniques. The collaboration also includes an MSc thesis by one of the ILL's students for the **European Space Agency's Athena mission**: the thesis focuses on the correlation between internal strains and the manufacturing conditions of the Ti6AlV4 optical bench.
- The ILL has also provided neutron stress scanning services on SALSAs, alongside the ESRF's synchrotron imaging, for **ISO/ASTM round-robin tests** [3]. The final report is currently being reviewed before publication. The ISO/ASTM working group is led by the **Manufacturing Technology Centre** (Coventry UK), with whom the ILL and the ESRF are currently signing a Memorandum of Understanding in order to better co-ordinate research activities in this domain.



Figure 2

Part of a launcher fuel tank manufactured by MT Aerospace AG (an OHB SE company, Germany) positioned on SALSAs for the non-destructive investigation of strains in welded areas.

- In 2020, the ILL reinforced its partnership with the **OHB space systems group**, establishing an InnovaXN PhD on the characterisation of lunar regolith. In addition, OHB and its affiliate **MT Aerospace** obtained valuable results following measurements performed on SALSAs to investigate, for example, the residual stress induced by welding a flange on a launcher tank (**figure 2**), the asymmetric stress distribution in a satellite frame structure and the distribution of forces and stress in an optomechanical interface for optical lenses. OHB has since joined **EASISTRESS** to represent the interests of the space industry.
- Finally, there have been a number of developments between the SALSAs team and **ArcelorMittal's R&D department** in Spain. This collaboration started when AM-R&D research engineers accepted the proposal available under SINE2020 to conduct a feasibility study at the ILL on in-depth stress determination. Their results, comparing SALSAs strain mapping with modelling, are about to be published. AM-R&D has also been designing other projects with SALSAs scientists, including a PhD project. Their scientists in Spain are now examining options to extend this partnership further.

The year 2020 should have seen the second edition of the *neutron synchrotron workshop on additive manufacturing*, after the successful WAM2018. The COVID-19 pandemic has obliged us to postpone the event until June 2021 (<https://workshops.ill.fr/event/276/>). It will involve 17 external speakers and provide plenty of space for discussion over two and a half days. The aim is to discuss expectations in non-destructive stress determination and identify priorities for instrumentation, methodologies and quality.

EXPERIMENTAL AND USER PROGRAMME

- 93 USER PROGRAMME
- 94 USER AND BEAMTIME STATISTICS
- 98 INSTRUMENT LIST

The **User Guide** contains all the practical information required to prepare a visit
<https://www.ill.eu/users/user-guide/>

Detailed information on the experimental programme can be found at
<http://www.ill.eu/users>



KEEP UP-TO-DATE:

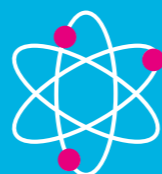
-  [facebook.com/ILLGrenoble](https://www.facebook.com/ILLGrenoble)
-  twitter.com/ILLGrenoble
-  [linkedin.com/company/institut-langevin](https://www.linkedin.com/company/institut-langevin)

884

ILL and CRG EXPERIMENTS

including **26 DDT**,
162 EASY and
31 internal
research experiments

96 DAYS OF NEUTRONS
2 254 DAYS FOR SCIENCE



791
DISTINCT USERS

1 042
USER VISITS
FROM 31 COUNTRIES

USER SATISFACTION
ABOVE
93 %*

* feedback participation rate 74 %

FIND US ON:   

User programme

PROPOSAL SUBMISSION FOR ACADEMIC RESEARCH

Neutrons beams and instrument facilities are free of charge for academic users of accepted proposals. There are various ways of submitting a proposal to the ILL, as summarised in the following table.

Detailed information can be found at





<https://www.ill.eu/users/applying-for-beamtime/>.

INDUSTRY-SPONSORED ACADEMIC RESEARCH AND INDUSTRIAL USERS

Neutrons have significant, specific applications for industry. Beamtime can be sold directly for proprietary research, in which case the experimental data are not made publicly available. The Industry Liaison Unit (ILU) is the single point of contact for industry looking to use the ILL's facilities (see p.88). However, around 25 % of industry's use of the ILL is made via academia. The data from these experiments are publicly available and the results may be published. The ILL is now measuring the number and nature of industry-via-academia experiments more accurately, with a view to promoting this use of neutrons and potentially enhancing it in the future. In 2020, **13 experiments were sponsored by industry**.

Table 1

Mechanisms for submitting a proposal to the ILL. All type of access (except DDT) are reserved for users from ILL member countries or for collaborations between non-member and member teams. The stopwatch symbol indicates quick access. Most types of proposals are submitted via the User Club interface at <https://userclub.ill.eu/userclub/>.

TYPE	APPLIES TO	WHEN	WHO FOR	RESPONSE TIME
External peer review				
Standard	All experiments, all instruments, all conditions	Deadlines twice a year, spring and autumn	All users from member countries (and non-members via 2/3 rule)	4 to 8 months after deadline
BAGs	College 8 proposals on D22	Deadlines twice a year, spring and autumn	All users from member countries (and non-members via 2/3 rule)	4 to 8 months after deadline
CRG	All experiments, CRG instruments, all conditions	Depends on CRG policy	All users from CRG collaboration	Depends on CRG policy
D-Lab	Access to the ILL sample deuteration lab	All year	All users from member countries	
Internal peer review				
DDT	Urgent experiments, hot topics, excellent science from non-member countries, all instruments, all conditions	All year	All users	ASAP 
EASY	A small amount of beamtime, not a full experiment (must be very simple measurements), all instruments, limited number of configurations	All year	All users from member countries	From one to a few weeks 
LTP	All instruments, for projects over several cycles if it can be demonstrated that they bring extra resources or capabilities that are of benefit to all users	Once a year, autumn round	All users from member countries	4 to 8 months after deadline
No peer review				
TEST	Test of sample, equipment, instrument configuration, all instruments	All year	All users from member countries	Usually on same day 
INDU	Proprietary beamtime	All year	Contact the Industrial Liaison Office	ASAP 

USER AND BEAMTIME STATISTICS

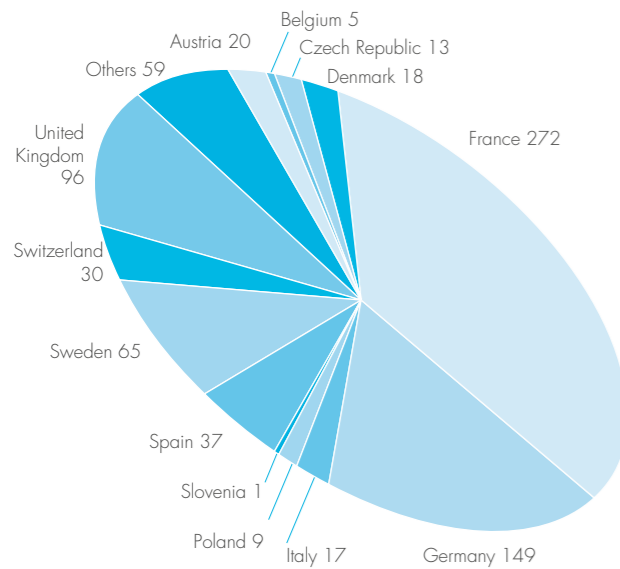
FIND US ON:   

94-95

USER AND BEAMTIME STATISTICS

Figure 1

National affiliation of ILL users in 2020.



The ILL welcomed 791 users in 2020, including 272 from France, 149 from Germany and 96 from the UK. Many of our visitors were received more than once (giving a total of 1 042 user visits).

PUMA is new ILL software, developed in the FILL2030 project. It combines the ILL's databases for proposals and publications with Web of Science, in order to develop a comprehensive understanding of beam time use based on a wide range of analyses. It should also allow us to identify laboratories and countries that might be interested in working with us at the ILL in the future. One feature of PUMA is the ability to match proposals with publications, thereby tracking the scientific process from idea to experiment to outcome. This is a continuous, ongoing process that we will extend to ILL users in the next few months.

Overall, the panel meetings in the November 2019 and April 2020 rounds examined 1 287 proposals requesting 6 885 days. Of these, 583 proposals received beamtime, requiring the allocation of 2 455 days of beamtime on the various instruments and corresponding to 636 experiments.

These experiments were to be performed in 2020. Because of the COVID-19 pandemic the ILL was able to operate only two of the three cycles originally planned for 2020, and so a number of the experiments had to be scheduled for the first cycle in 2021. During the August–September cycle, ILL scientists ran around 470 ILL and CRG experiments (including 20 DDT, 22 internal and 86 EASY experiments). Around 270 users physically travelled to the Institute, which is significantly fewer than usual; because user visits were possible only where they were essential, the ILL operated by requesting users to send in their samples.

Figure 2

Chart—obtained with the PUMA software—showing the origin of the authors of ILL publications in Europe (taken from the addresses of their associated institutes). Authors associated with the ILL have been removed from the figures.

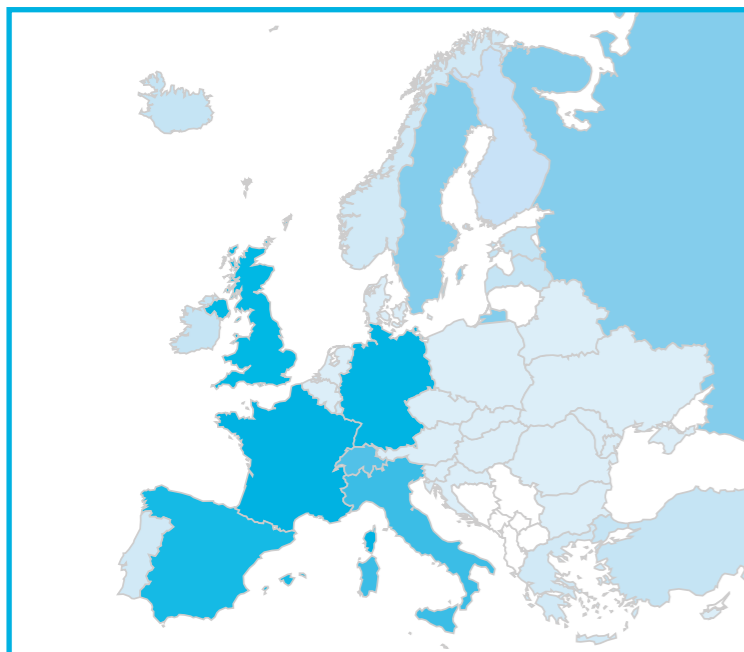


Figure 3

Proposals are divided amongst the colleges. The figure shows the distribution of accepted proposals amongst the various colleges.

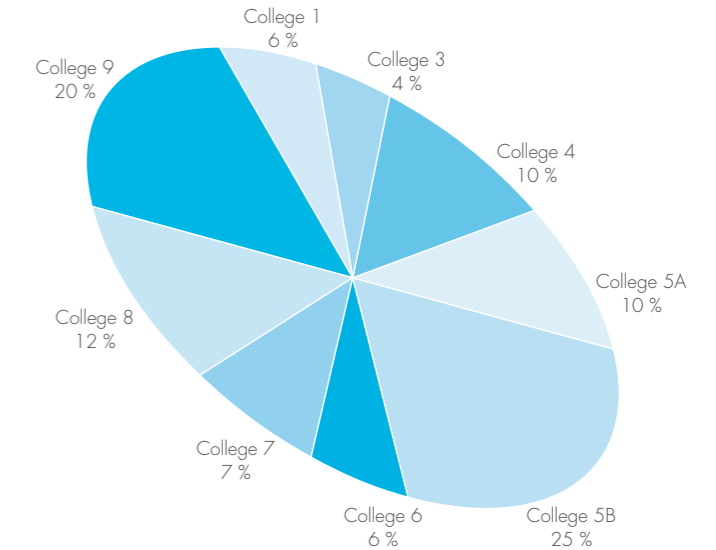


Table 1

Distribution amongst the ILL member countries of beamtime requests and allocation in the November 2019 and April 2020 panel meetings. Proposals from purely non-member countries do not appear in this table and therefore the total request and allocation is different in Table 2.

	Request days	Request %	Allocation days	Allocation %	Allocation days	Allocation %
	Without non-member countries and ILL and EU facilities redistributed			After national balance		
AT	215.03	3.08	66.45	2.68	66.81	2.72
BE	34.36	0.51	12.90	0.52	14.99	0.62
CH	292.70	4.20	94.90	3.83	74.92	3.05
CZ	75.49	1.09	19.34	0.78	19.45	0.79
DE	1 604.74	23.20	586.14	23.66	607.02	24.73
DK	202.30	2.88	52.87	2.14	44.10	1.80
ES	387.68	5.64	127.93	5.17	131.59	5.37
FR	1 638.07	23.96	588.00	23.78	599.94	24.49
GB	1 647.46	24.02	632.81	25.59	670.93	27.37
IT	312.13	4.56	110.82	4.49	55.71	2.27
PL	68.74	0.99	32.91	1.32	21.03	0.86
SE	374.45	5.40	138.56	5.60	138.11	5.64
SK	31.92	0.47	10.53	0.43	7.58	0.31
Total	6 885.07	100.00	2 474.16	100.00	2 452.18	100.00

In calculating the statistics for beamtime per country shown in **Table 1**, attribution is based on the location of the laboratory of the proposers, not their individual nationality. For a proposal involving laboratories from more than one member country, the total number of days is divided amongst the collaborating countries and weighted by the number of people from each. Local contacts are not counted as proposers. The beamtime requested by and allocated to scientists from the ILL is allocated to the member countries according to a weighting system based on the fractional membership of the country of the institute concerned. When a proposal involves collaboration with a non-member country, the allocated time is attributed entirely to the collaborating member countries. Proposals in which all proposers are from non-member countries therefore do not appear in this Table.

USER AND BEAMTIME STATISTICS

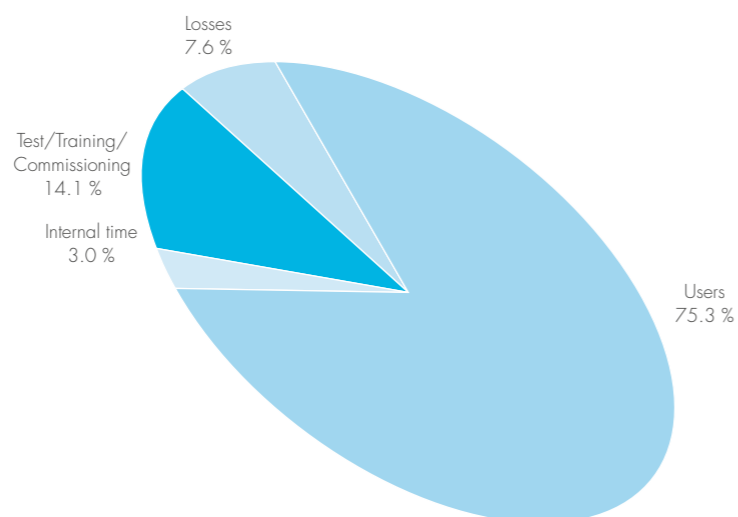
FIND US ON:   

96-97

Table 2 gives a summary of instrument performance for 2020. Around 2 167 days were made available to our users in 2020 on ILL and CRG instruments (via either standard request or the EASY and DDT routes), representing about 75 % of the beamtime available; a total of 87 days were used by ILL scientists to carry out their own scientific research; and about 14 % of the total beamtime available on the ILL instruments was allowed for tests, calibrations, scheduling flexibility, recuperation from minor breakdowns and student training. In all, 219 days were lost as a result of various malfunctions, accounting for around 7 % of the total beamtime available.

In 2020 the reactor operated for two of the originally planned three cycles, representing 96 days of neutrons. During this time, **a total of 884 ILL and CRG experiments were performed** (including 26 DDT, 162 EASY and 31 internal research experiments). **Beam days given to science (used for users, EASY, DDT and internal research) in 2020 amounted to 2 254 (78 % of the total available).**

Figure 4
Use of ILL beamtime



ILL Users in the Time of Covid.



Table 2

Beamtime request/allocation (via standard subcommittees and Director Discretion Time (DDT) together) by instrument and instrument performance. CRG instruments are in blue.

- * 'days allocated' refers to only those days reviewed by the subcommittees (i.e. excluding CRG days and DDT)
- ** 'days available' are the days of reactor operation
- *** 'days used' refers to the total number of days given to users (i.e. including CRG days for CRGs and DDT)

PF2 consists of different set-ups where several experiments are running simultaneously. The values given are averages for these positions (and normalised by a factor of 5).

D4 and IN1 share the same beam port and cannot be run simultaneously. D3 was not available to users during the two cycles in 2020.

Instrument	Days requested	Days allocated *	Number of accepted experiments	Available days **	Days used for users ***	Days lost	Days for test/ commissioning /training	Days for internal research	Days for EASY/ DDT
D10	242	96	16	96	83	3	0	0	10
D11	222	91	45	96	73	5	5	1	12
D16	146	87	18	96	74	3	3	16	0
D17	270	81	30	96	54	5	25	5	7
D19	245	95	13	96	71	8	2	1	14
D1B	159	50	27	96	78	7	7	0	4
D20	267	95	44	96	77	6	2	2	9
D22	248	105	43	96	67	4	17	4	4
D23	183	36	7	96	83	8	5	0	0
D2B	195	86	43	96	77	3	3	2	11
D33	275	101	39	96	70	4	8	5	9
D3	237	0	0	5	0	0	5	0	0
D4	159	29	9	30	26	2	1	1	0
D7	190	86	18	96	75	6	9	2	4
D9	118	76	12	96	88	3	2	3	0
FIGARO	231	84	34	96	65	5	10	8	8
FIPPS	297	156	9	96	53	20	11	0	12
IN12	101	22	4	96	66	2	22	6	0
IN13	79	40	6	96	86	3	7	0	0
IN15	191	58	15	96	61	8	17	2	8
IN16B	270	77	27	96	80	3	6	1	6
IN1	57	29	10	66	25	35	5	0	1
IN20	235	95	16	96	68	6	22	0	0
IN22	100	25	4	96	66	8	22	0	0
IN5	449	89	27	96	82	2	4	0	8
IN6-SHARP	120	37	13	96	84	3	6	0	3
IN8	139	70	13	96	55	3	36	0	2
LADI	253	85	10	96	87	3	4	1	1
NEXT	146	40	13	48	13	0	35	0	0
PANTHER	59	14	5	48	3	4	38	3	0
PFIB	65	28	3	89	79	4	6	0	0
PF2 normalised	52	52	3	96	68	27	0	1	0
PNI	172	90	7	96	80	14	2	0	0
S18	167	38	4	96	80	8	0	8	0
SALSA	194	43	14	96	44	8	14	24	6
SUPERADAM	81	36	9	96	80	2	10	3	1
THALES	202	86	17	96	74	5	14	3	0
WASP	69	50	9	96	25	3	55	8	5
Total	6 885	2 455	636	2 878	2 065	219	405	87	102
Percentage					72.0 %	7.6 %	14.0 %	3.0 %	3.4 %
					Days for science	2 254	78 %		
						2 065 + 87 + 102			

INSTRUMENT LIST

INSTRUMENT LIST – JANUARY 2021

ILL INSTRUMENTS		
D2B	powder diffractometer	operational
D3	single crystal diffractometer	operational
D4 (50 % with IN1-LAGRANGE)	liquids diffractometer	operational
D7	diffuse-scattering spectrometer	operational
D9	single crystal diffractometer	operational
D10	single crystal diffractometer	operational
D11	small-angle scattering diffractometer	operational
D16	small momentum-transfer diffractometer	operational
D17	vertical reflectometer	operational
D19	single crystal diffractometer	operational
D20	powder diffractometer	operational
D22	small-angle scattering diffractometer	operational
D33	small-angle scattering diffractometer	operational
DALI	quasi-laué diffractometer for biological macromolecule	commissioning
FIGARO	horizontal reflectometer	operational
FIPPS	fission product prompt gamma-ray spectrometer	operational
IN1-LAGRANGE (50 % with D4)	three-axis spectrometer	operational
IN5	time-of-flight spectrometer	operational
IN8	three-axis spectrometer	operational
IN16B	backscattering spectrometer	operational
IN20	three-axis spectrometer	operational
LADI (50 %)	laue diffractometer	operational
PANTHER	time-of-flight spectrometer	commissioned in 2020
PF1	neutron beam for fundamental physics	operational
PF2	ultra-cold neutron source for fundamental physics	operational
PN1	fission product mass-spectrometer	operational
SALSA	strain analyser for engineering application	operational
SuperSUN	ultra-cold neutron source for fundamental physics	operational
ThALES	three-axis spectrometer	operational
WASP	wide-angle spin-echo spectrometer	operational

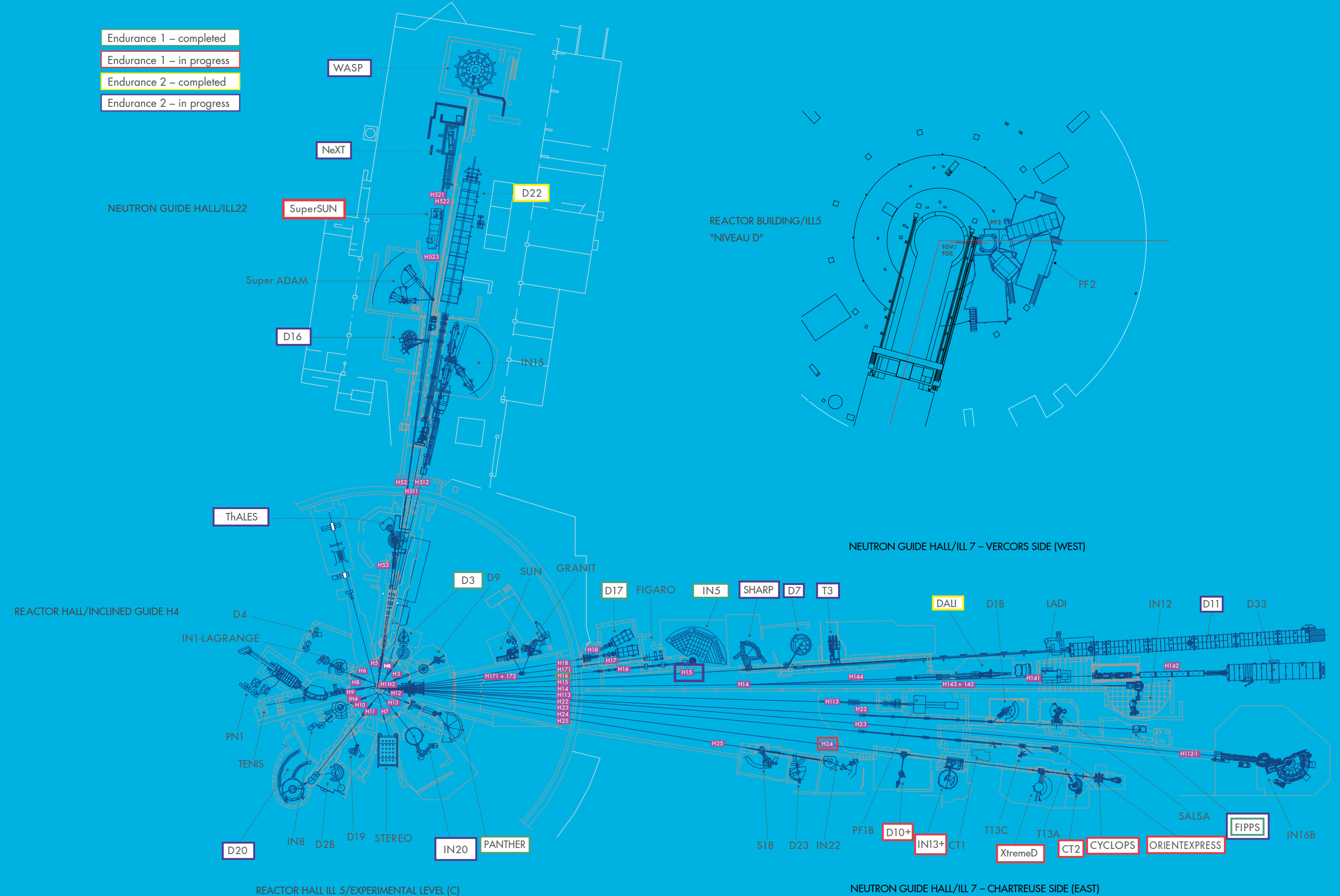
CRG INSTRUMENTS		
D1B	powder diffractometer	CRG-A operational
D23	single crystal diffractometer	CRG-B operational
IN12	three-axis spectrometer	CRG-B operational
IN13	backscattering spectrometer	CRG-A operational
IN22	three-axis spectrometer	CRG-B operational
SHARP	time-of-flight spectrometer	commissioning
SuperADAM	reflectometer	CRG-B operational
S18	interferometer	CRG-B operational

JOINTLY FUNDED INSTRUMENTS		
IN15	spin-echo spectrometer	operated with FZ Jülich
NeXT (75 %)	imaging instrument	operated with Ni-Matters composed of HZB, UGA and ILL
GRANIT	gravitation state measurement	operated with LPSC (UJF, CNRS)

TEST AND CHARACTERISATION BEAMS	
CT1, CT2	detector test facilities
CYCLOPS	laue diffractometer
TOMOGRAPHY	neutrography
OrientExpress	laue diffractometer
T3	neutron optics test facility
T13A, C	monochromator test facility

Details of the instruments can be found at <http://www.ill.eu/users/instruments/>.

FIND US ON:   



The instrument facilities at the ILL are listed in the Table on the left, and shown in the plan on p. 99. In addition to the 28 operational ILL instruments, there are 10 Collaborative Research Group (CRG) instruments. CRGs can build and manage instruments at the ILL to carry out their own research programmes. These instruments are made available to the ILL's scientific user programme at a level of 50 % (CRG-A) or 30 % (CRG-B). CRG-C external groups have exclusive use of the beam. Details about the framework of operation for CRGs can be found at <https://www.ill.eu/users/instruments/crgs/>

All current CRGs are either A- or B-type, the only exception being GRANIT which is a CRG-C instrument and therefore not available as a 'user' instrument. IN15 has special status because it is a joint venture between the ILL and FZ Jülich. The instrument STEREO is jointly funded by the ILL and CEA Saclay, LAPP Annecy, LPSC Grenoble and MPIK Heidelberg.

INSTRUMENT LAYOUT

REACTOR OPERATION

102 REACTOR OPERATION IN 2020



KEEP UP-TO-DATE:

-  facebook.com/ILLGrenoble
-  twitter.com/ILLGrenoble
-  linkedin.com/company/institut-laue-langevin

FIND US ON:   



THE ILL'S high-flux reactor produces the most intense neutron flux in the world: 1.5×10^{15} neutrons per second per cm^2 , with a thermal power of 58.3 MW. It normally operates four reactor cycles per year. At the end of each cycle there is a shutdown period, during which the fuel element is changed and checks are carried out. Occasional longer shutdowns are scheduled to allow for maintenance or refurbishment operations.


The reactor's fuel element can provide 46 days of operation per cycle at maximum power. Furthermore, the ILL's Millennium and Endurance programmes have improved the performance of our instruments by a factor of 20 to 50 over the years. However, the current beam tube replacement programme and the installation of more powerful instruments is now preventing us from providing the nominal programme of 200 days per year. We are currently scheduling the maximum number of days of operation possible in the context of the upgrades. We can also adapt the power of the reactor to experimental requirements, providing slightly lower power but beamtime over a longer period for experimentalists.

Following the nuclear disaster at Fukushima in 2011, the French nuclear safety authority (ASN) ordered additional safety assessments on all French basic nuclear installations (INBs) including the ILL. Our post-Fukushima programme has now ended; the safety of the reactor is now guaranteed even in the event of an extreme earthquake-and-flood combination following rupture of the dams upstream, which goes well beyond previous dimensioning standards.

The ASN has also asked the ILL to reorganise its technical procedures via the introduction of an Integrated Management System ('SMI' – INB Decree of 2012), to be incorporated into all our essential operating practices. ASN requests are extremely demanding and generate a significant workload. They are, nevertheless, necessary and have been given top priority by the ILL.

In addition to the above, the ILL has been working since November 2017 on another safety authority requirement: the 10-yearly reactor safety assessment. The results of this examination have just been received and are very positive. This means that the ILL is authorised to continue its operations for a further ten years, as long as it continues to modernise as required by the authorities.

Jérôme Estrade
Head of Reactor Division

TWO CYCLES AND
94
DAYS OF
OPERATION
IN
2020 

 **58.3 MW**
 $1.5 \times 10^{15} \text{ n/s cm}^2$

 A SINGLE,
HIGHLY
ENRICHED
URANIUM
FUEL ELEMENT

Three reactor cycles were planned in 2020. However, in light of the ongoing public health crisis the reactor operating schedule for 2020 was adapted to optimise, on the one hand the shutdown periods used to carry out regulatory maintenance operations and facility upgrades; and on the other, the neutron delivery periods, during which we host our scientific users.

A first cycle ran from 9 January 2020 to 26 February 2020. At the beginning of February the reactor suffered an unscheduled shutdown of two days, due to the unusually low level of the river Drac. The second cycle began on 11 August and ran until 28 September. Although the reactor shutdown between the two cycles had to be extended due to the lockdown restrictions imposed by the COVID-19 crisis, we were able to take advantage of this by reinstalling the H4 guide.

Cycle n°	Start of cycle	End of cycle	Number of days of operation	Number of days scheduled	Power in MW	Number of unscheduled shutdowns
187	09.01.20	26.02.20	46	48	56	1
188	11.08.20	28.09.20	48	48	56	0
Total			94	96	56	0

RELATIONS WITH THE FRENCH NUCLEAR SAFETY AUTHORITY (ASN)

Recent ASN inspections have gone reasonably well. It is thanks to the efforts of all our staff over the last few years that we have been able to regain the ASN's confidence as regards our regulatory compliance. We must prove that we can maintain this by intensifying our efforts and being extremely vigilant.

THE REINFORCEMENT OF PHYSICAL PROTECTION (RPP) PROJECT

The RPP project was launched in early 2017. Work on the new perimeter fence and the ILL reception building started in September 2019. We have now also provided updated security studies. It is extremely important that we adhere to the timetable established for the project. However, the COVID-19 pandemic has created a delay of six months. A technical inspection by the Security Authority took place in September and noted substantial progress.

EXAMINATION OF THE RESULTS OF THE 10-YEAR SAFETY REVIEW

The *Groupe Permanent's* examination of the review officially began on 11 February. A large number of on-line meetings were held with IRSN (Technical Support Organisation for Regulatory Body) experts during the spring COVID-19 lockdown in order to finalise the documentation. Further meetings were held in September. The decisive meeting with the *Groupe Permanent* took place in November 2020 and delivered universally positive conclusions. The ILL is now authorised to operate for the next ten years whilst working on a list of commitments to ensure continued safety standards. We now have a timeline for fulfilling these commitments over the 2020–2025 period, taking into consideration all the other technical operations scheduled. A final meeting will be held with the ASN to finalise the reactor schedule for the next five years.

REQUALIFICATION OF THE REACTOR VESSEL

At the beginning of October the reactor was shut down to allow for work to requalify the reactor vessel. This crucial obligation was successfully completed in January 2021. The vessel passed the tests and has been approved for ten more years of operation. This shutdown was also used to start work on the commitments made to the *Groupe Permanent*.

FIRE PROTECTION

Following changes in the regulations, the operations below will have to be completed by the end of 2021:

- Replacement of old fire detectors with ion smoke detectors (currently 60 % complete)
- Protection of the three remaining pillars on reactor level C supporting the concrete floor slab of level D (authorisation for this work is internal and the necessary assessment has been finalised).

The reactor shutdowns were used for a host of important maintenance and other operations:

- Fire protection of the pillars on reactor level C
- Replacement of the H4 beam tubes
- Control rod maintenance.

THE KEY REACTOR COMPONENTS (KRC) PROGRAMME

The aim of the KRC programme is to ensure the upgrade and maintenance of the reactor's most important components, thereby guaranteeing the reliability of reactor operations for the future. The main components concerned are the cold-neutron sources, the fire protection equipment and the physical protection equipment.

CLEAN-UP OF THE DETRITIATION FACILITY AND REFURBISHMENT OF SOURCE EQUIPMENT

A project plan has been produced and the costs calculated. The project is therefore well underway. The plan is first, to rapidly reduce the pressure in the last four tanks containing tritium and deuterium in order to avoid breaching nuclear high-pressure regulations. We have received ASN authorisation for this operation, to be carried out early in 2021. We will then use a recombiner unit to combine the tritium and deuterium with oxygen at very low concentration to produce heavy water. This heavy water will be injected into the primary circuit. The recombiner unit will also be used to treat the deuterium from the cold sources and clean the facility's tanks and circuits. The huge advantage of this solution is that it does not create a volatile atmosphere, which the current burner does, and it produces less waste.

RADIOACTIVE WASTE AND EFFLUENTS

The ILL's activities in 2020 generated waste and effluents in respect of the regulatory limits applicable to our installation, as follows:

Evacuation of radioactive waste	Quantity
Decay bin (60 L)*	0
5 m ³ pre-concreted crate (low- and intermediate-level waste)	0
5 m ³ crate (low- and intermediate-level waste)	6
HDPE 200 L drums of 'incinerable' waste	144
HDPE 120 L drums (laboratory waste)	0
30 L cylinders (liquid)	0
Radioactive organic liquid from the reactor	0.6 m ³

*The decay bins contain very active waste. They will be transferred to ANDRA's new storage centre CIGEO after an interim period in special storage.

Gaseous effluents	Released in 2020 (TBq)
Tritium	12
Rare gas	0.85
Carbon-14	0.32
Iodine	6,8 10 ⁻⁷
Aerosols	2 10 ⁻⁷

Liquid effluents	Released in 2020 (TBq)
Tritium	0.18
Carbon-14	2 10 ⁻⁴
Iodine	2,3 10 ⁻⁷
Other activation products	2,8 10 ⁻⁵



From top:
Getting ready for the replacement of the H4 beam tube.
The outcome of the 10-year safety assessment authorises the ILL to operate for the next ten years.
The Reinforcement of Physical Protection (RPP) project – launched in 2017 – will be finalised in 2021.

MORE THAN SIMPLY NEUTRONS

106 SCIENTIFIC SUPPORT LABORATORIES

109 TRAINING AND OUTREACH

110 EUROPEAN PROGRAMMES

FIND US ON:   

IN ORDER to maintain their ranking at an international level, European research institutes must optimise their resources and develop synergies at every level.

The ILL is firmly committed not only to building high-performance instruments but also to offering the best scientific environment for the user community. We have also established successful collaborations with neighbouring institutes over the years and launched successful scientific and support partnerships.

European collaboration is in the DNA of the ILL, and has been since its inception. In 2020 the Institute was involved in 10 European projects funded by either the H2020 research and innovation framework programme or EURATOM, both of which are administered by the European Commission. The benefits are not merely financial; the ILL also benefits from the associated networks and resources, which improve its integration with other facilities and the user community. The ILL is also currently the co-ordinator and sole beneficiary of **FILL2030** (with a grant of 4 M€), which has been extended until June 2021 due to the pandemic.

The new research and innovation framework programme 'Horizon Europe' was discussed and defined throughout 2020. During its chairmanship of **LENS**, the ILL has done its best to promote its own contribution, as well as the relevance of the European Neutron sources (LENS) as a whole, to societal challenges. A similar level of visibility was gained through the **EIROforum** partnership, under the presidency of the ILL (July 2020–June 2021).

The ILL is also involved in international funding initiatives that link its capabilities with those of other major facility operators throughout the world. A grant from the Human Frontier Science Program (HFSP) is currently held by the ILL's Life Sciences Group, linking it with groups from Hamburg, New York and New Zealand and with Free Electron Laser (FEL) sources at Hamburg and Stanford. These awards play a crucial part in nurturing a strong and productive environment for sustainable international collaboration.

Local collaboration is equally important. The ILL and the ESRF have transformed their site into what is now the **European Photon and Neutron science campus**. The EPN Campus hosts three major



European institutes—the EMBL, ESRF and ILL—and France's IBS (<http://www.epn-campus.eu/>), providing a veritable hub of international science in the Grenoble region.

Last but not least, the ILL is committed to training and outreach, which it provides in many different forms. Whilst the ILL

Graduate School and PhD programme train future generations of neutron users, we also run neutron schools and other events for MSc and PhD students; our open days and annual contributions to the local science festival help attract young talent to science and improve the general public's understanding of the science we perform.

ACCESS

TO **13** LABORATORIES
HOSTING
38 LABORATORY
INSTRUMENTS
VIA THE **PSCM**



... NO FEWER THAN **10**
DIFFERENT EU PROJECTS



Access to **23** technology
platforms, including
biological deuteration
(macromolecular & small biomolecules),
synchrotron X-ray crystallography and
SANS/SAXS via the **PSB**



OUTREACH
40 PHD
STUDENTS
AND 61 TRAINEES

HERCULES

62 PARTICIPANTS OF
27 DIFFERENT NATIONALITIES
WORKING IN
16 DIFFERENT COUNTRIES



KEEP UP-TO-DATE:

 [facebook.com/ILLGrenoble](https://www.facebook.com/ILLGrenoble)

 twitter.com/ILLGrenoble

 [linkedin.com/company/institut-laue-langevin](https://www.linkedin.com/company/institut-laue-langevin)

SCIENTIFIC SUPPORT LABORATORIES

FIND US ON:   

106-107

PARTNERSHIP FOR SOFT CONDENSED MATTER

The Partnership for Soft Condensed Matter (PSCM) is a joint initiative established by the ILL and the ESRF on the EPN Campus. The PSCM's main mission is to provide support services to ILL and ESRF scientists tackling contemporary challenges in soft matter research (nanomaterials, environmental and energy sciences, biotechnology and related fields). The PSCM provides users with access to 13 laboratories and 37 laboratory scale equipment, such as multi-angle static and dynamic light scattering machines, rheometers, Langmuir troughs, differential scanning calorimeters, spectrophotometers, optical ellipsometers and a quartz-crystal microbalance, to mention just a few.

It is the Partnership's mission to strengthen the soft matter research community by establishing long-term collaborations to develop specialised instrumentation and sample environment facilities. Six new partnership projects will start between 2020 and 2021, selected through a competitive call for proposals.

The PSCM is located, along with the Soft Matter Science and Support group, on the 2nd floor of the EPN Campus Science Building. Neutron users wishing to use the PSCM laboratories and equipment in conjunction with their neutron measurements should indicate this when submitting their request for beamtime.

<http://www.pscm-grenoble.eu>

PARTNERSHIP FOR STRUCTURAL BIOLOGY

The Partnership for Structural Biology (PSB) operates a powerful set of technology platforms provided and managed by its partner institutes (ILL, ESRF, EMBL, IBS). It provides advanced capabilities complementing the neutron scattering facilities available to ILL users: synchrotron X-rays, cryo-electron microscopy, high-field nuclear magnetic resonance, mass spectrometry and high-throughput methods (e.g. soluble expression and crystallisation); as well as a range of biophysical techniques, such as isothermal calorimetry, surface plasmon resonance and mass photometry.

The PSB includes the Deuteration Laboratory, operated as a user platform within the ILL's Life Sciences Group, and the joint SANS/SAXS platform. There are strong links and collaboration between the ILL and ESRF life sciences/structural biology and industry groups.

The aim of the PSB is to enhance the interdisciplinary capabilities of each of the facilities located on the site and to widen the scientific scope of external user communities. The Carl-Ivar Brändén Building (CIBB) acts as home to the PSB and its partner organisations.

<http://www.psb-grenoble.eu/>.

THE DEUTERATION LABORATORY

The Deuteration Laboratory (D-Lab) is located and operated as a PSB platform within the ILL's Life Sciences Group. It was created in the 2000s with major funding from the UK Engineering and Physical Sciences Council (EPSRC), its principal missions being to provide deuterated biomolecules to the user community, innovation and development for biological neutron scattering, and training.

The Life Sciences Group works in purpose-designed laboratories in the Carl-Ivar Brändén Building, the centre of the PSB. It has always functioned as a user platform, continuously innovating for novel neutron science in biology, and is embedded in a group that has an active in-house research programme with substantial external funding. Since the D-Lab platform's inception, deuteration facilities have been set up around the world providing purpose-designed deuterated samples that have revolutionised biological neutron science. Its user programme uses *in vivo* recombinant expression approaches to provide deuterated analogues of proteins, nucleic acids and lipids for studying structure (crystallography, SANS, fibre diffraction, reflection) and dynamics using neutron scattering. The D-Lab is therefore of central importance to all the ILL instrument groups involved in biological research. In terms of development, it is involved in a broad range of activities, including novel deuteration regimes, the expression of deuterated proteins using insect and mammalian cell deuteration, and the growth of large protein crystals.

The Life Sciences Group is additionally involved in a wide variety of externally-funded programmes exploiting the capabilities of the PSB as well as promoting interdisciplinary structural biology. It has strong connections with industry. It is also involved in the operation and development of the cryo-EM capabilities being set up through the installation of Titan Krios at the ESRF, in collaboration with the ESRF, IBS and EMBL. Furthermore, through its partnership with Keele University (UK) the Life Sciences Group contributes to

the site's cryo-EM platform through a joint-appointment faculty position in cryo-EM and neutron scattering. This position is held by Dr Daouda Traore, placing the ILL as an equal partner on site in this important initiative.

The Group is also actively engaged in training. Each year it takes on a number of undergraduate placement students for training in various techniques.

Access to the D-Lab is gained through a rapid, peer-review proposal system. The facility is available to all the ILL member countries, regardless of where the neutron scattering study is carried out. It is also available to users from non-member countries, although in such cases a contribution to the costs may be requested.

<https://www.ill.eu/users/support-labs-infrastructure/deuteration-laboratory>
<https://www.ill.eu/lsg>

CHEMISTRY LABORATORIES

The Soft Matter Science and Support Group (SMSS) manages the ILL chemistry laboratories together with the PSCM laboratories. The main goal is to allow ILL users to prepare and characterise their samples during their neutron experiments, while also supporting in-house research conducted by instrument scientists and PhD students.

The main facilities are located in the Science Building. In addition, three sample preparation labs can be found in the guide halls ILL 7 and ILL 22. The laboratories are stocked with the basic equipment (glassware, consumables and chemicals) necessary to prepare samples for a variety of different neutron experiments, as well as with more specific facilities, such as high-temperature furnaces, a glovebox, or an enclosure for handling nano-powders. A laboratory dedicated to biology (class I) is also available.

Further information on the Chemistry Laboratories can be found at:

<https://www.ill.eu/users/support-labs-infrastructure/chemistry-laboratories/>

MATERIALS SCIENCE SUPPORT LABORATORY

The joint ILL-ESRF Materials Science Support Laboratory (MSSL) provides a range of support from scientists (local contacts) to our users, from advice on proposals and experiment design to assistance with preparing samples and performing experiments.

The Lab has shared equipment for load testing:

- 50 kN hydraulic INSTRON rig, also allowing for cyclic testing, and induction furnace
- 15 kN small-load rig, possible to mount on cradle
- Other INSTRON rigs at the ESRF: ETMT (combined load and heating, 3 kN, Tmax ~1500 C); 4 kN hydraulic; 25 kN hydraulic.

The ILL also provides facilities for sample polishing, hardness testing and optical microscopy. Recently we acquired a Coordinate-Measuring Machine (CMM) and a portable metrology arm, which can be used to prove or benchmark samples' surface dimensions and/or distortion before actual neutron measurements, as well as increasing the speed of aligning complex/large components directly at the beamline. Other lab equipment may also be adapted to the beamline, subject to discussion with the scientists responsible for the particular instruments and safety approval.

Local contacts are responsible for working with users before the start of an experiment to optimise their methodology. This can involve standardised specimen mounting and digitalisation of samples. We invite users when designing the experiment in their proposal to get in touch with ILL scientists well in advance and to arrive at the campus a day or two before the start of their beam time in order to enable these off-line preparations to be made.



L-LAB: A PLATFORM FOR NATURAL DEUTERATED LIPID EXTRACTION WITHIN THE PSCM

Neutron scattering techniques are ideally suited to the study of lipid bilayers, major components of cellular membranes. At the ILL, we have been working for several years to provide our users with well-characterised membrane models for physical and biological studies. These efforts have been recognised and praised by the international community, and many facilities have followed our example. The considerable interest in working with lipid bilayers and biological membranes at the ILL is confirmed by the number of such experiments performed (>200) and manuscripts published (>300) in the last five years.

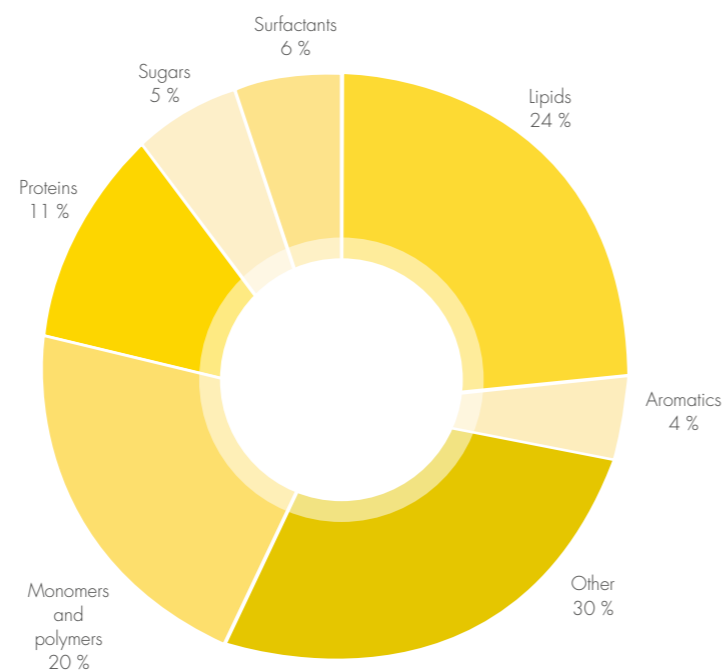
The community's interest in accessing deuterated phospholipids (PL) is confirmed by the results of a survey conducted within the DEUNET (<https://deuteration.net/>) network set up under the SINE2020 grant. From the pie chart, we can see that PLs are the species most often requested by soft- and bio-neutron scientists (targets of the survey). While PL deuteriation helps elucidate membrane structure, dynamics and function by providing selective visualisation in neutron scattering, such studies involving deuterated biomimetic membranes are currently limited by the low availability of several biologically relevant, unsaturated PL species. To overcome this, facilities such as ANSTO, ISIS and ESS have found success in chemically synthesising certain monounsaturated PLs for users (but under certain conditions of use or at high cost). An alternative, considerably cheaper, method of obtaining a wide variety of deuterated PL species (including unsaturated) is to extract them from organisms grown under deuterated conditions.

Work pioneered back in 2013 within the PSCM [de Ghellinck *et al.*, 2014], in collaboration with the Deuteration Laboratory in ILL's Life Sciences Group and Hanna Wacklin (now at ESS), has since evolved with the aim of extracting and purifying PLs from deuterated cell cultures using the following steps: (i) selection of suitable organisms for growth; (ii) optimisation of extraction protocols for PLs; (iii) development of methods for PL separation; (iv) development of protocols for characterising the prepared PLs; (v) 'Mass production' for the neutron facility's user community.

So far, we have been successful in investigating methods to characterise and quantify deuterated PLs after producing them biologically in the oleaginous yeast *P. pastoris* and the bacterium *E. coli* grown on perdeuterated medium. The PLs currently being provided to internal scientists and students in quantities suitable for neutron experiments can be found on the following website: <http://www.ill.eu/L-Lab>. Neutron characterisation of membrane mimics from these lipids include SANS from nanodiscs, diffraction from stacked bilayers, reflectometry from mono- and bilayers, and inelastic scattering and spin-echo measurements from multilamellar vesicles.

Future perspectives include: 1) the separation of PLs as a function of their chain length/unsaturation; and 2) the extraction/separation of deuterated sugars, TAGs (Triacyl Glycerols) and metabolites. The physico-chemical properties as well as the structure of membrane bilayers are characterised using techniques available in the PSCM and neutron scattering. In the short term, we will pursue such characterisation studies in two ways: 1) by producing a library of pure PLs for soft matter studies, documenting their properties and use in interactions with a variety of other molecules; and 2) by characterising contrast-matched, natural mixtures of PLs providing a very physiologically relevant environment for biology studies of membrane proteins.

At the moment, no other facility can provide this service. Nevertheless, there is strong interest in this area and scientists at universities and other neutron centres have asked to collaborate with us. Scientist Krishna Batchu has brought unique expertise on site, and since his arrival two years ago enormous progress has been made. The platform is already handling several internal requests for deuterated PLs and has been heavily involved in the preparation of samples for COVID19-related science during the lockdown and throughout the summer. The service will be offered to users for the first time in the February '21 proposal round. Finally, it is worth mentioning that this work is part of activities currently supported by LENS.

**STUDENT TRAINING**

The ILL Graduate School has grown in strength over recent years as the ILL PhD programme has evolved. The School provides training and finance for the equivalent of 40 full-time, three-year PhD students from various European countries. It also receives a number of PhD students with external funding. A total of 21 ILL PhD students began their doctoral work in 2020, eight of whom were recruited as part of the 'first wave' of the InnovaXN PhD programme financed by the EU via the Marie Curie Foundation in France. InnovaXN projects differ from the ILL's regular PhD projects in that they involve industrial partners; InnovaXN projects must have industrial applications. An important aspect of the programme is the time the PhD students spend on the industrial partner's site during their PhD.

The five-year InnovaXN programme offers three years of doctoral funding for two recruitment rounds of 10 PhD students each, and the same again for the ESRF. Thus, a total of 40 PhD students will benefit from the programme on the EPN campus. Successful InnovaXN recruitment in 2020 was accompanied by the selection of 10 ILL-based PhD projects for the second wave of recruitment, scheduled to begin in February 2021. Given the success of InnovaXN, the ongoing COVID-19 pandemic and its associated constraints on the ILL, and the imminent year-long shutdown of the ILL reactor, we decided not to have an autumn 2020 call for PhD project applications under the regular PhD programme. However, we fully anticipate resuming the yearly call for PhD projects in autumn 2021.

The **International Summer School** for undergraduate students, organised by the ILL and the ESRF every year since 2014, allows undergraduate students from all our member countries to spend a month on the site. The students follow a series of lectures and seminars on the fundamentals of X-rays and neutrons and their use in science today. The 2020 school was unfortunately cancelled because of the health crisis.

HERCULES SCHOOL

The Hercules School has been held every year since 1991. It is a one-month course on neutron and synchrotron radiation for condensed matter studies, for students and young scientists. The course includes lectures, hands-on sessions and tutorials in small groups, a poster session and visits to partner facilities.

The 2020 event took place from 2nd March to 3rd April and attracted over 110 applications. Sixty-two students, comprising 27 different nationalities and based in 16 different countries, attended; most came from Europe, while a few came from Brazil, India, Russia and Taiwan. Due to the COVID pandemic, all students had to return home after only the second week of the school; however, the last three weeks were successfully re-organised to run online and included both small-group tutorials and lectures. Thanks to both the rapid reorganisation of most of the lecturers and the support of the partner sites (ALBA, DESY, Elettra/FERMI, European XFEL, KIT, PSI, SOLEIL) and the Grenoble institutes (CEA, CNRS, ESRF, IBS, ILL, UGA), the three-week online session—consisting of about 74 hours of live video lectures and 180 hours of tutorials (with up to 12 groups working in parallel in Zoom)—was a success. All the participants (from Europe to Brazil) stayed with the course as it moved online and gave extremely positive feedback. More information is available at:

<http://hercules-school.eu/>.



Participants at the HERCULES 2020 session.

European collaborations

European collaboration has been an important part of the ILL's activities since its inception. In 2020, the Institute was involved in 10 European projects funded by either the H2020 research and innovation framework programme or EURATOM, both of which are administered by the European Commission. The benefits are not merely financial; the ILL also benefits from the associated networks and resources, which improve its integration with other facilities and the user community. **Table 1** summarises EU project activity at the ILL.

FILL2030 is a mono-beneficiary project, funded under the European Union's Horizon 2020 research and innovation programme and dedicated to ensuring the long-term sustainability of the ILL business model. Due to the pandemic, the project has been extended for six months and will hence end in June 2021. However, not only did the health crisis put a halt to several planned activities for reaching out to emerging user communities; physical meetings have now also proven to be unrealistic even within the additional six months. We have therefore adapted our means of outreach by developing more online and digital tools, such as short promotional videos and featured webpages, to promote neutron imaging, remote access (<https://youtu.be/EAVgbQXRldo>) at the ILL, and so on.

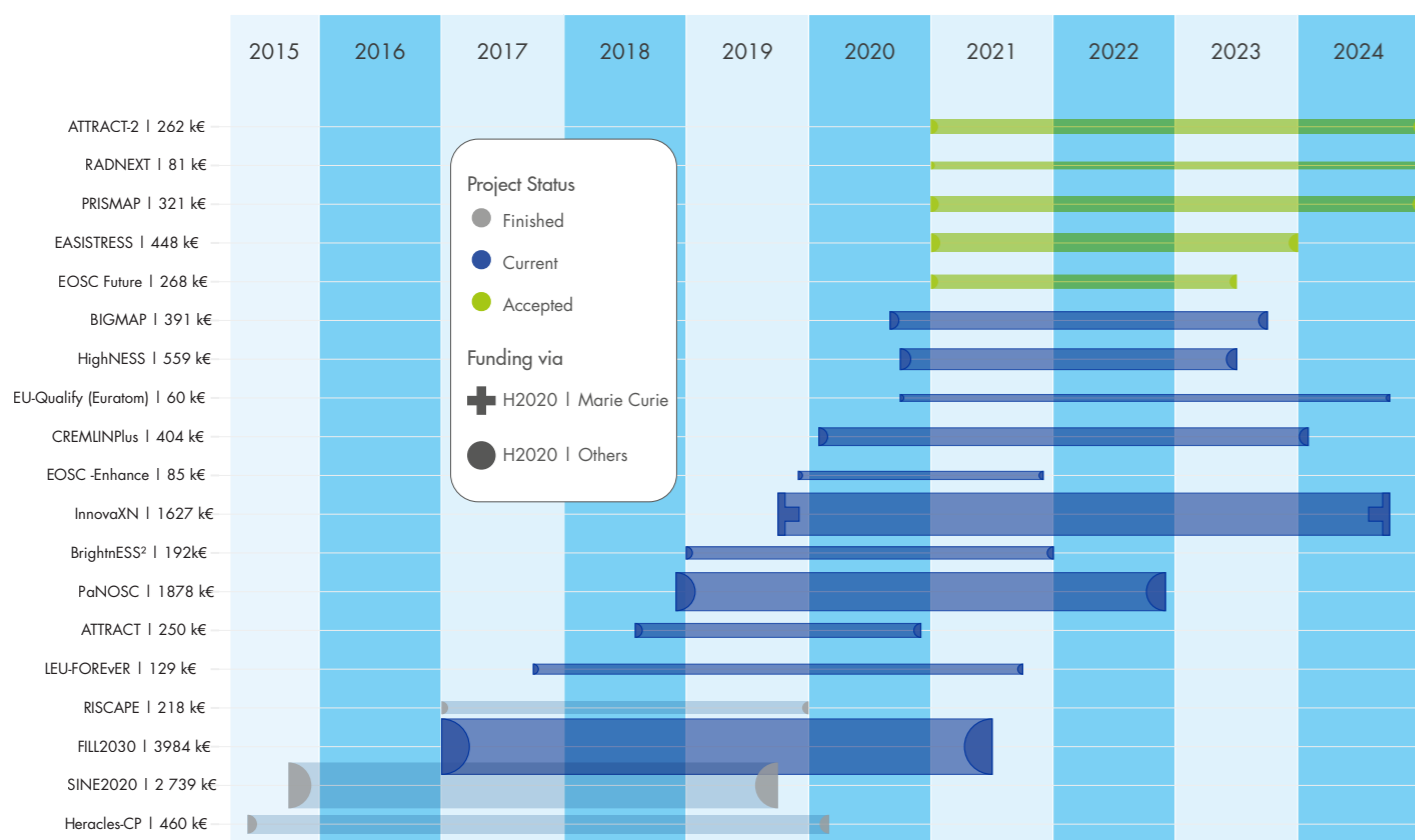
Our offer to cover open-access fees for scientific publications has been a huge success. The number of such publications has doubled, from an initial 40 to 80. This was possible due to lower fees and internal budget changes.

The newly developed bibliometric tool (PUMA) is proving a great help to the ILL's management and its scientists, allowing them to analyse the geographical and scientific spread of the user community. The initial target of matching publications linked to ILL experiments was achieved in 2020, ensuring the statistical use of the tool. PUMA has even been successfully transferred to a neighbouring institute, where it is being further developed.

The two activities mentioned above allow the ILL to identify and follow up new users in new countries and new scientific domains. This is further supported by the implementation of a continuous survey of new users.

The number of transnational access days available to users from new non-member countries will be fully exploited, thanks to the additional six months. With both the number of reactor cycles reduced and the majority of experiments conducted in remote-access mode during 2020, the extension represents a chance to achieve our original target of 50 days.

Table 1
Overview of EU project activity at the ILL.



PaNOSC (Photon and Neutron Open Science Cloud) is funded under the European Union's Horizon 2020 research and innovation programme. It provides joint policies, strategies and solutions for enabling Open Science through the adoption of FAIR principles. Since the project's start, in December 2018, six strategic European photon and neutron (PaN) sources (the ESRF, CERIC-ERIC, ELI-DL, ESS, XFEL and ILL) and the e-infrastructures EGI and GEANT have been collaborating to make FAIR data a reality at PaN facilities; this is being achieved by developing and providing services for scientific data and connecting them to the European open science cloud (EOSC).

In 2020, the PaNOSC partners agreed on the specification for a common search API (Application Programming Interface) to be implemented at all PaNOSC partner sites. This search API allows datasets to be found based on relevant domain-specific metadata and can be used by third parties to find data that has been released from any facility-imposed embargo period as well as by the original researchers. Work is now underway to implement this API and to produce a joint data catalogue encompassing search results from all the partner sites.

As well as providing a data catalogue, each facility will provide access to remote data analysis services, allowing users to analyse experimental data through remote desktops and Jupyter notebooks through a common data portal. A first iteration of the portal was deployed at all partner sites during 2020, and work has now started on the second. The current aim is to align the portal's development with that of the VISA application, which came into production in 2020. As well as providing both Remote Desktop and Jupyter notebooks for data analysis purposes, VISA provides an effective platform for performing remote experiments using the NOMAD Remote client at the ILL.

InnovaXN is a doctoral training programme, supported by the H2020 MSCA COFUND Programme, which brings together the expertise of large-scale research infrastructures and the R&D needs of European industry. In 2020, 15 PhD students of 11 different nationalities started their project within the doctoral programme InnovaXN, managed by the ILL and the ESRF. Eight of them are being co-supervised by ILL scientists, academic partners and industrial researchers in various pre-competitive research projects dealing with chemical engineering, biotechnologies and even moon exploration. A second series of 20 PhD projects has been selected by the InnovaXN scientific review board. Once recruitment has been completed, there will be around 40 students on site involved in the programme.

The League of advanced European Neutron Sources (LENS)

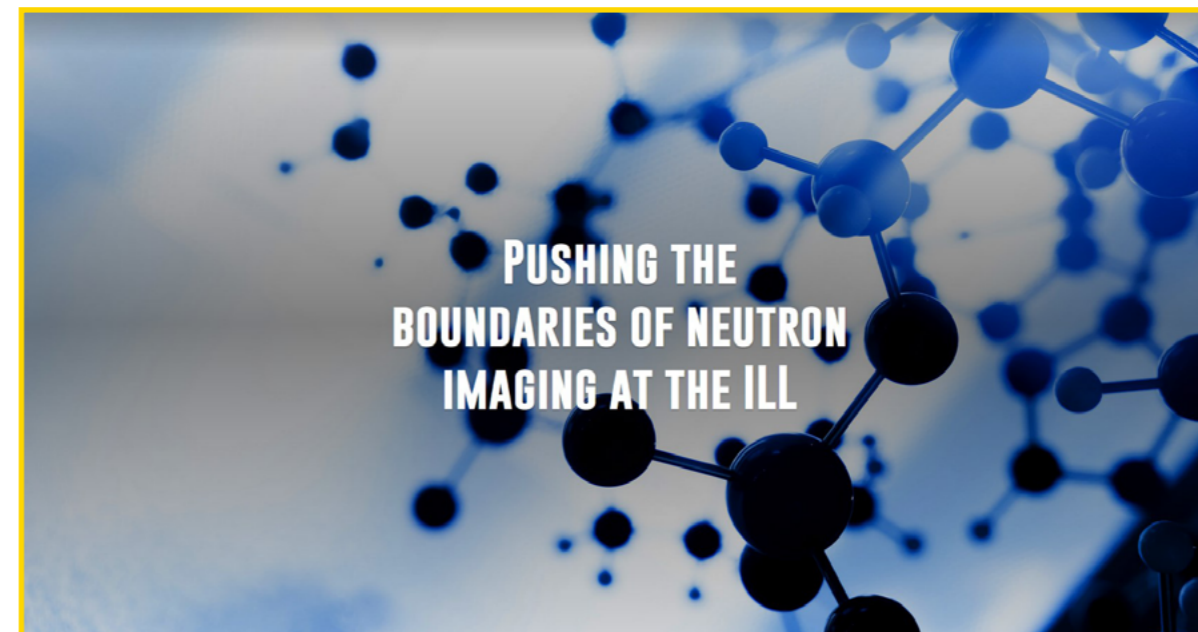
The strategic consortium of European neutron sources acts as guide and advocate for the European neutron user community. It promotes neutron science as a fundamental component of European scientific research and innovation.

The last year of the Horizon 2020 European framework programme for research and innovation has kept LENS busy writing several position papers. First there was the Green Deal, consisting of a last round of calls for the remaining budget in Horizon 2020. LENS advocated that analytical facilities could contribute to societal- and climate-relevant research, such as that directed at building a low-carbon, climate-resilient future. Its efforts were successful, as analytical research infrastructures have been issued with a call under the action ‘European Research Infrastructures capacities and services to address European Green Deal challenges’.

LENS was also involved in preparing a contribution to the five Missions for the next framework programme to be defined by the European Commission, along with six other analytical research infrastructure networks. This led to the establishment of ARIE (Analytical Research Infrastructures In Europe)

<https://arie-eu.org/> and its own position paper on the Missions. The newly established ARIE network of networks formed the consortium preparing the proposal for the Green Deal call.

The LENS general assembly validated the above-mentioned actions and acknowledged work carried out so far. LENS held its general assemblies in June and November 2019, both in a virtual format. In the latter, assembly member Caterina Biscari, chair of LEAPS, was invited to discuss how to further flesh out the mutually agreed strategic partnership. It was decided to focus on IT, where the most evident synergies between both networks lie. From now on, a LENS representative will participate in the IT working group meetings of the LEAPS. Both chairs reconfirmed their willingness to work together, which may lead to future common proposals under Horizon Europe.



EIROforum

EIROforum brings together the eight flagship institutions of large-scale, European research infrastructures. All EIROs are leaders in their field and work continuously to push back the frontiers of scientific knowledge, from the infinitely small to the infinitely large.

Created in 2002, the forum’s mission is to enable its eight member organisations—CERN, EMBL, ESA, ESO, ESRF, European XFEL, EUROfusion and the ILL—to pool their resources and expertise in support of European science. By promoting the exchange of know-how and best practice, EIROforum makes a major contribution to enhancing scientific collaboration in Europe.

In July 2020, Helmut Schober took over the presidency of EIROforum from Fabiola Gianotti from CERN. The last General Assembly was held virtually, just before Christmas, and provided the occasion to discuss the impact of the pandemic on the operation of the various facilities.

NI-Matters

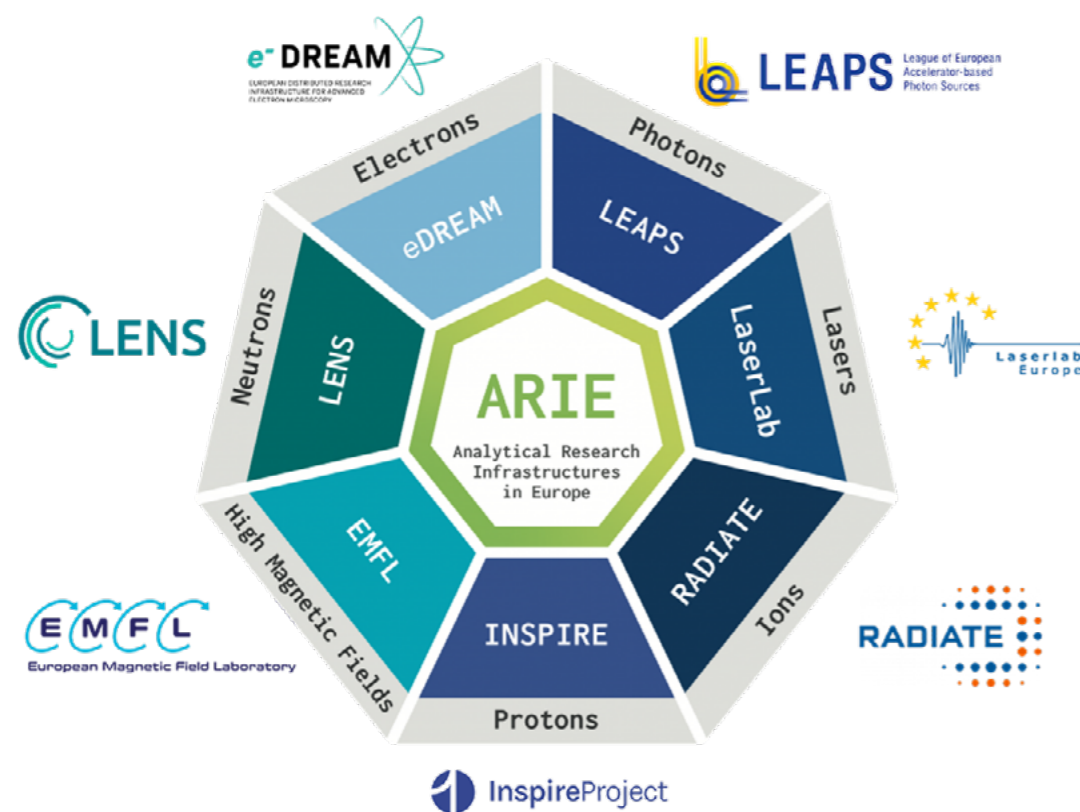
A joint research unit between the ILL, Helmholtz Berlin and Université Grenoble Alpes was created, focusing on the development and application of combined, correlative neutron and X-ray imaging in materials and energy research.

The new unit is called “NI-Matters” (Neutron Imaging for Material and Energy Research).

More information:

<https://www.ill.eu/NI-Matters>

<https://www.ill.eu/neutron-imaging>



WORKSHOPS AND EVENTS

115 CHRONICLE

116 SCIENTIFIC EVENTS

FIND US ON:   

ILL Chronicle 2020

27 JANUARY

Visit by Naohito Saito, Director of J-Parc

5 MARCH

Visit by Helen Beadman, NERC, UKRI

21–22 APRIL

Subcommittee and ILL Scientific Council virtual meetings

12–13 MAY

Meeting of the Subcommittee on Administrative Questions (SAQ)

25 JUNE

Meeting of the ILL Steering Committee

13–14 OCTOBER

Meeting of the Subcommittee on Administrative Questions (SAQ)

3–6 NOVEMBER

Subcommittee and ILL Scientific Council virtual meetings

13 NOVEMBER

Inauguration of the Joint Research Unit NI-Matters
(with signature by video conference)

17–23 NOVEMBER

Meeting of the standing group of experts
(known as the 'Groupe Permanent') for the
periodic safety review of the ILL's high-flux reactor

26–27 NOVEMBER

Meeting of the ILL Steering Committee

21
GENERAL
SEMINARS
AND
COLLOQUIA 4

 14

SCIENTIFIC
EVENTS

WORKSHOPS
SCHOOLS AND
CONFERENCES



KEEP UP-TO-DATE:

 facebook.com/ILLGrenoble

 twitter.com/ILLGrenoble

 linkedin.com/company/institut-laue-langevin



WORKSHOPS AND EVENTS

FIND US ON:   

116-117

Scientific events

In 2020, the ILL organised (or co-organised) 14 scientific events (workshops, conferences and schools). A total of 21 general seminars were also organised at the ILL in 2020, in addition to 4 colloquia. Because of the pandemic, all these events were held remotely.

2-3 MARCH

HERCULES 2020 – European School

21-22 SEPTEMBER

ESS-ILL User Meeting – Topical Workshop on Polarisation

23-25 SEPTEMBER

ESS-ILL User Meeting

13 OCTOBER

ESS-ILL User Meeting – ILL Topical Workshop on Chemistry and Magnetism

14 OCTOBER

ESS-ILL User Meeting – ILL Topical Workshop on Fundamental and Particle Physics

14-15 OCTOBER

ESS-ILL User Meeting – ILL Topical Workshop on Imaging, Materials and Engineering

13 NOVEMBER

Neutron imaging at ILL – Inauguration of the Joint Research Unit NI-Matters

9-10 DECEMBER

G-RAD Workshop – Grenoble Radiation Testing of semiconductor devices and systems

LENS WEBINARS SERIES

The LENS initiative¹ presents a live webinar roughly every month. The webinars are also streamed live to the LENS website, where they are recorded and archived.

Currently, the webinars alternate between two themes: how neutron science contributes to the fight against global health threats; and new directions in neutron instrumentation.

The complete list of webinars can be found here

<https://www.lens-initiative.org/2020/06/02/lens-webinars/>

GLOBAL HEALTH THREATS

11 JUNE 2020

Viruses: the devils who can take over our cells

10 SEPTEMBER 2020

How does the Bcl-2 protein family regulate apoptosis at the mitochondrial membrane level?

Towards the catalytic cycle of a multi-drug ABC ('ATP-binding cassette') transporter

8 OCTOBER 2020

Microbial resistance and novel antibiotics

Studying the surfaces of bacteria using neutron scattering. Finding new openings for antibiotics

Antimicrobial peptides – from membrane interactions to drug delivery

NEW DIRECTIONS IN INSTRUMENTATION

25 JUNE 2020

Neutrons for magnetic nanostructures on surfaces: beyond the specular intensity wars

20 AUGUST 2020

Polarised neutron time-of-flight spectroscopy

22 OCTOBER 2020

Neutron Diffraction Instrumentation for stress determination

26 NOVEMBER 2020

Multiplexing backends for neutron spectroscopy

¹ The League of advanced European Neutron Sources (LENS) is a not-for-profit consortium working to promote co-operation between European-level neutron infrastructure providers offering transnational user programmes to external researchers. More on p.112.

ESS-ILL User Meeting— a virtual success

For the second time the ESS and ILL held a joint user meeting, on 23 to 25 September 2020. The first joint user meeting was hosted by the ILL in Grenoble in 2018. The 2020 meeting was intended to welcome Europe's neutron users to Lund. However, pushed by the pandemic into a virtual format, the meeting took on quite a different character.

The digital format lifted restrictions on numbers, and as a result a record 777 participants registered. Over 600 unique viewers participated in the main meeting, and to date about 500 people have since watched the sessions on YouTube.

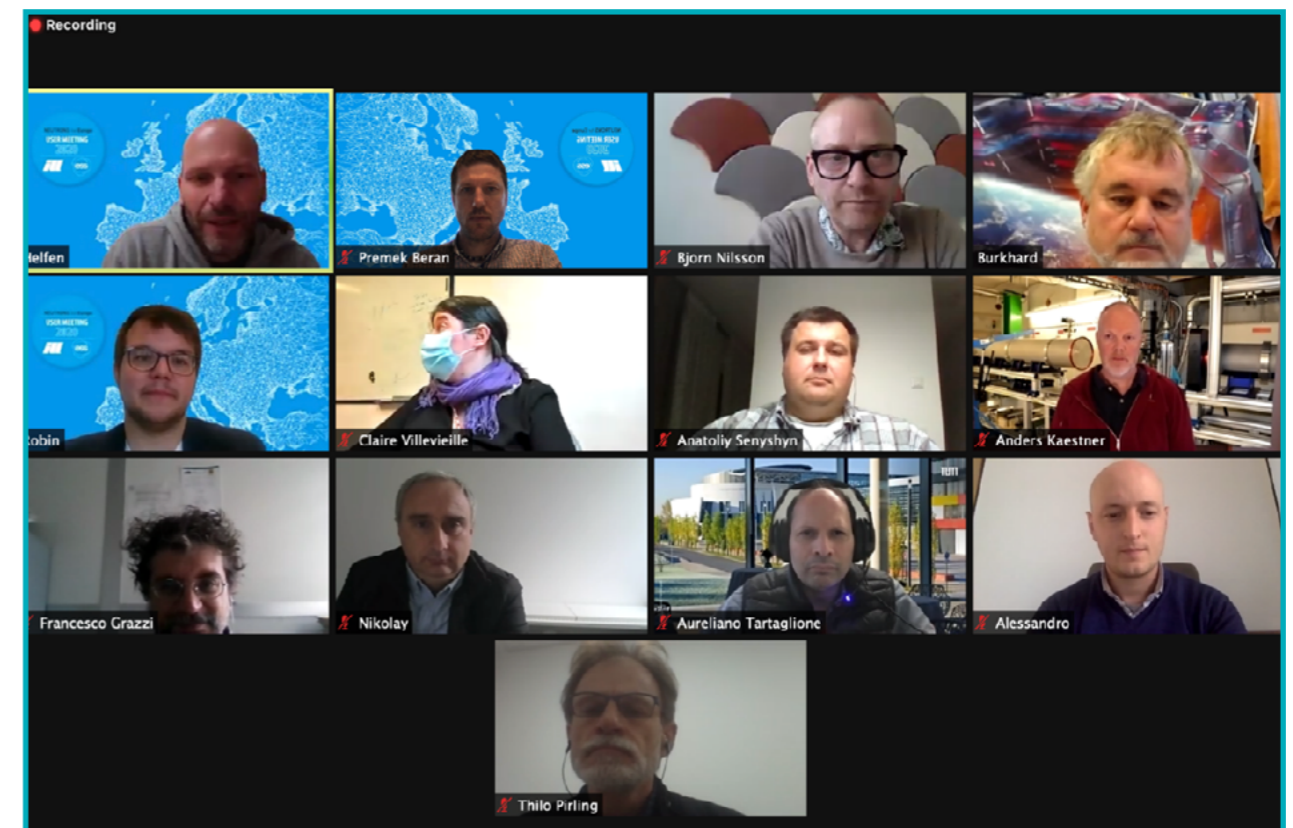
In addition to the wide range of science covered in the programme, as always a number of topical workshops were held in conjunction with the meeting. They are presented in the list on p.116.

Although the chance to catch up with participants in person was missed, the community made the best of the situation, seizing this opportunity to come together to discuss important issues and showing how much can be achieved online when necessary.

We look forward to welcoming our collaborators and friends to Lund and the ESS at the next joint user meeting, to be held in 2022.

KEY NUMBERS

Number of registrants	777
Number of unique viewers	>600 This includes 491 unique email addresses using Zoom, plus anonymous watchers on YouTube (at least 85 but more likely around 140)
Unique viewers per session	>350 This includes approximately 275 on Zoom and approximately 85 on YouTube.
Replay viewers on YouTube	appr. 500 As of January 2021. For each session: Session #1 2 800 viewers (anomaly due to YouTube push) Session #2 577 viewers Session #3 457 viewers Session #4 422 viewers



FACTS AND FIGURES

- 119 FACTS AND FIGURES
- 121 PUBLICATIONS
- 123 ORGANISATION CHART



KEEP UP-TO-DATE:

- [facebook.com/ILLGrenoble](https://www.facebook.com/ILLGrenoble)
- twitter.com/ILLGrenoble
- [linkedin.com/company/institut-laue-langevin](https://www.linkedin.com/company/institut-laue-langevin)

102 M€ ANNUAL INCOME*

* 67 % FROM THE ASSOCIATES AND 15 % FROM SCIENTIFIC MEMBER COUNTRIES



791
DISTINCT VISITORS FROM 31 COUNTRIES IN 2020

580
PUBLICATIONS RECORDED IN 2020

543
MEMBERS OF STAFF



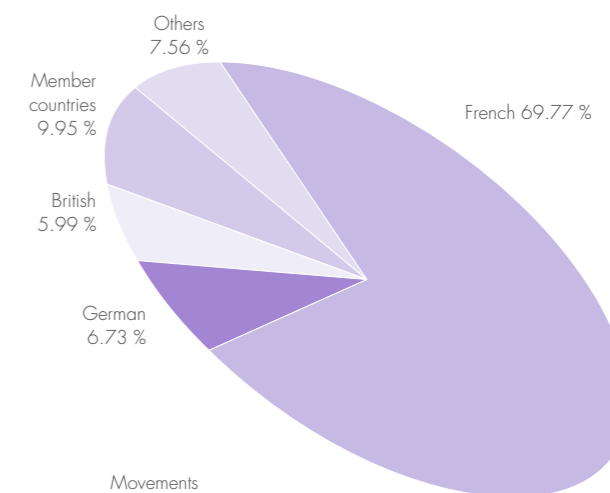
FIND US ON: [f](#) [t](#) [in](#)

STAFF ON 31/12/2020

524.5 people, including 77 experimentalists in the scientific sector and 56 thesis students.

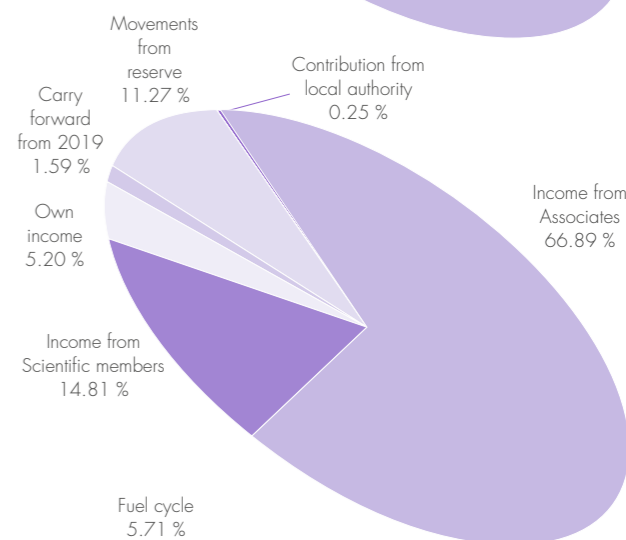
370 French; 37 German; 32 British; 52 scientific participating countries; and 32 others.

Nationality		%
French	378.5	69.77 %
German	36.5	6.73 %
British	32.5	5.99 %
Member countries	54	9.95 %
Others	41	7.56 %
Total	542.5	100 %

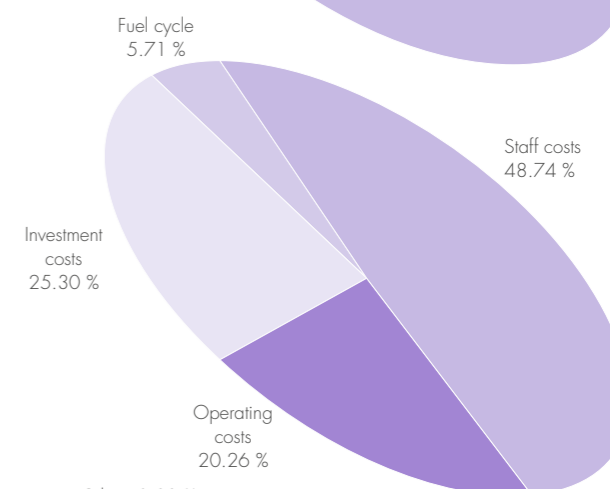


IMPLEMENTATION BUDGET 2020: 101,755 M€ (excluding taxes)

Income	M€	%
Income from Associates (incl. Endurance Programme and additional nuclear tax and insurance)	68.07	66.89 %
Income from Scientific Members	15.07	14.81 %
Own income	5.29	5.20 %
Carry forward from 2019	1.62	1.59 %
Movements from reserve	11.46	11.27 %
Contribution from local authority	0.25	0.25 %
Total	101.75	100.00 %

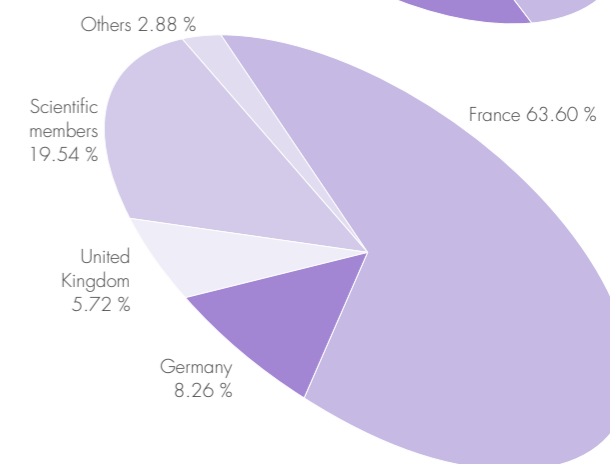


Expenditure	M€	%
Staff costs	49.59	48.74 %
Operating costs	20.62	20.26 %
Investment costs	25.74	25.30 %
Fuel cycle	5.81	5.71 %
Total	101.75	100.00 %



PURCHASING STATISTICS 2019

	M€	%
France	21.15	63.60 %
Germany	2.75	8.26 %
United Kingdom	1.90	5.72 %
Scientific Members	6.50	19.54 %
Others	0.96	2.88 %
Total	33.26	100.00 %



France captive market	10.30	23.64 %
Total captive/non-captive	43.56	0

FACTS AND FIGURES

FIND US ON:   

120-121

NAME

Institut Max von Laue-Paul Langevin (ILL)

FOUNDED

19 January 1967

Intergovernmental Convention between France, Germany and United Kingdom (19/07/1974)

ASSOCIATES

France

Commissariat à l'Énergie Atomique et aux Énergies Alternatives (CEA)

Centre National de la Recherche Scientifique (CNRS)

Germany

Forschungszentrum Jülich (FZJ)

United Kingdom

United Kingdom Research & Innovation (UKRI)

COUNTRIES WITH SCIENTIFIC MEMBERSHIP

Spain

MCIN Ministerio de Ciencia e Innovación

Switzerland

Staatssekretariat für Bildung, Forschung und Innovation (SBFI)

Italy

Consiglio Nazionale delle Ricerche (CNR)

Belgium

Belgian Federal Science Policy Office (BELSPOL)

Sweden

Swedish Research Council (VR)

Denmark

Danish Agency for Science and Higher Education

Poland

(NDPN) Consortium of Polish Scientific and Research Institutions

Slovenia

The Slovenian National Institute of Chemistry

CENI (Central European Neutron Initiative)

Consortium composed of:

Austria: Österreichische Akademie der Wissenschaften

Czech Republic: Charles University, Prague

Slovakia: Comenius University, Bratislava

CONTRACTUALLY AGREED BEAMTIME SHARE FOR MEMBER COUNTRIES

Austria	2.500 %	
Czech Republic	0.750 %	
Slovakia	0.184 %	
Belgium	0.550 %	
Sweden	4.500 %	
Denmark	1.570 %	
Italy	1.300 %	
Switzerland	2.372 %	average over 5 years
Spain	4.500 %	average over 5 years
Poland	0.800 %	
Slovenia	0.150 %	

SUPERVISORY AND ADVISORY BODIES

Steering Committee, which meets twice a year

Subcommittee on Administrative Questions, which meets twice a year

Audit Commission, which meets once a year, and statutory auditor

Scientific Council with 9 Subcommittees, which meets twice a year

REACTOR

Operating 2 cycles in 2020

96 days in total, average power (p. 102)

EXPERIMENTAL PROGRAMME

884 ILL and CRG experiments
(of which 636 accepted by the Subcommittees)

791 distinct visitors from 31 countries

Publications in 2020

In 2020, the ILL received notice of 580 publications by ILL staff and users (published at the end of 2019 or in 2020).

They are listed on the ILL website:

<https://www.ill.eu/about-the-ill/documentation/scientific-publications/scientific-publication-list>.

THE DISTRIBUTION BY SUBJECT IS AS FOLLOWS

Applied Physics, Instrumentation and Techniques	45
Biology	74
Crystallography and Chemistry	66
Liquids and Glasses	6
Magnetic Excitations	30
Magnetic Structures	88
Materials Science and Engineering	40
Medicine	8
Nuclear and Particle Physics	74
Soft Condensed Matter	92
Spectroscopy in Solid State Physics and Chemistry	35
Theory	22

ILL PHD STUDENTSHIPS

Full-time-equivalent ILL-funded PhD projects in 2020	40
PhD students working on ILL PhD projects in 2020	55-60
Successfully defended ILL PhD theses in 2020	15

REVIEW PANELS

Key

Chair/focus group Chair

ILL college secretary/focus group secretary

ILL specialist

REVIEW PANELS

APPLIED METALLURGY, INSTRUMENTATION AND TECHNIQUES

M. Strobl (PSI, Switzerland)

L. Helfen

T. Pirling/A. Wildes/L. Porcar/G. Cuello

NUCLEAR AND PARTICLE PHYSICS

M. Van der Grinten (STFC, UK)

Y.H. Kim

T. Soldner

MAGNETIC EXCITATIONS

A. Boothroyd (Oxford University, UK)

U.B. Hansen

P. Steffens

CRYSTALLOGRAPHY

K. Edkins (Manchester University, UK)

L. Cañadillas-Delgado

T. Hansen

MAGNETIC STRUCTURES

E. McCabe (Kent University, UK)/

D. Lott (GKSS Forschungszentrum; Germany)

J.A. Rodriguez-Velamazan/T. Saerbeck

C. Ritter

STRUCTURE AND DYNAMICS OF LIQUIDS AND GLASSES

P. Huber (Hamburg University of Technology, Germany)

M. Appel

M.M. Koza

SPECTROSCOPY IN SOLID STATE PHYSICS AND CHEMISTRY

F. Juranyi (PSI, Switzerland)

J. Ollivier

P. Fouquet

STRUCTURE AND DYNAMICS OF BIOLOGICAL SYSTEMS

J. Lawrence (Manchester University, UK)

O. Matsarskaia

M. Blakeley/J. Peters

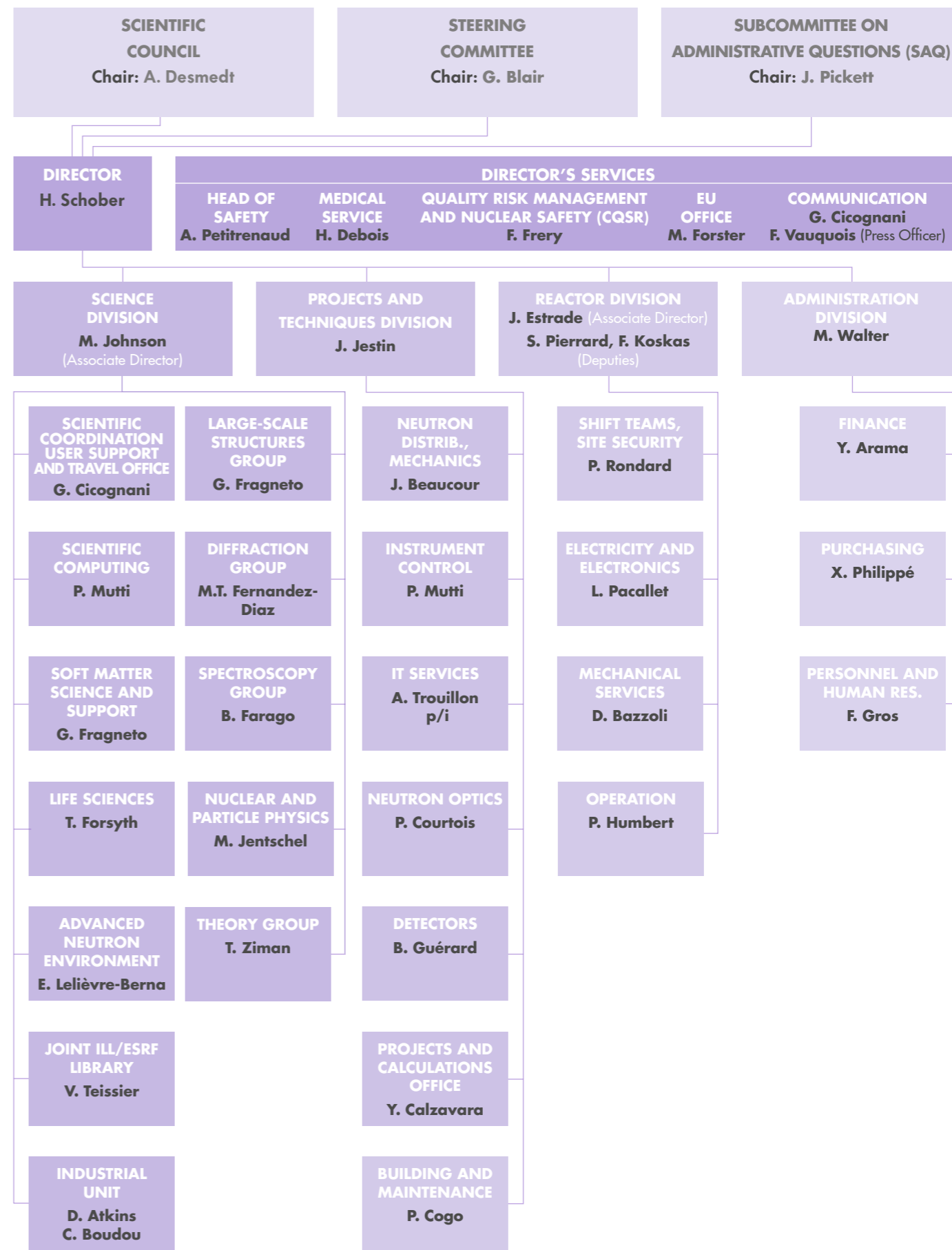
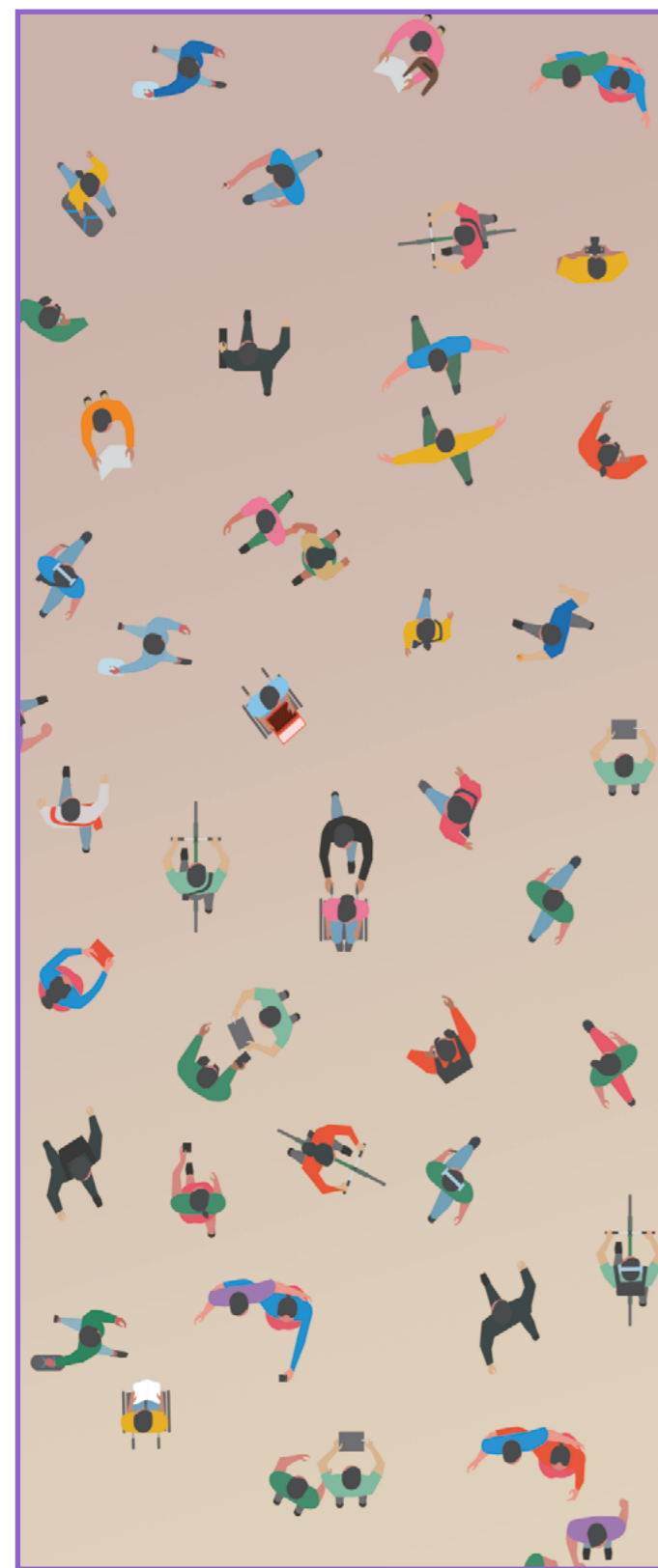
STRUCTURE AND DYNAMICS OF SOFT CONDENSED MATTER

E. Dubois (Pierre and Marie Curie University, Paris, France)/

A. Zarbakhsh (University of London, UK)

S. Prevost/A. Maestro

O. Czakkel/P. Gutfreund – R. Schweins (obs)



71, avenue des Martyrs
38000 Grenoble
France

www.ill.eu



This report has been printed using FSC certified paper www.fsc.org